Modelling the phreatic surface in regional flood defences

P.H. Dorst

TU Delft

Iv-Infra

Cover: The Duifkade near Schipluiden, a regional flood defence and one of the research cases in this thesis. Picture taken on 17-12-2018.

Modelling the phreatic surface in regional flood defences

By

P.H. Dorst

in partial fulfilment of the requirements for the degree of

Master of Science

in Civil Engineering

at the Delft University of Technology,

to be defended publicly on Wednesday April 3rd, 2019 at 14:00.

Thesis committee:	Prof. dr. ir. M. Kok	TU Delft
	Ir. S.J.H. Rikkert	TU Delft
	Dr. A. Askarinejad	TU Delft
	Ir. M. Monden	Iv-Infra
	Ir. G. Willemsen	Hoogheemraadschap van Delfland

Preface

This thesis report is the product of my graduation research completing my master Hydraulic Engineering at the Delft University of Technology. The research has been conducted in cooperation with Iv-Infra in Sliedrecht. This report presents the research method, results, and conclusions of the research.

I would like to thank Iv-Infra for providing the opportunity and resources to write this master thesis. In particular I would like to express my gratitude to my supervisor Martijn Monden for his guidance and positive feedback during the entire process of writing this thesis. I would also like to extend my appreciation to all the other colleagues at Iv-Infra for their help and making it a pleasant period.

Furthermore, I would like to express my gratitude to the other members of my thesis committee, Prof. Dr. Ir. Matthijs Kok, Ir. Stephan Rikkert, Dr. Amin Askarinejad, and Ir. Geert Willemsen, for all their advice and constructive feedback. Special thanks go out to Stephan for proposing this thesis subject, and to Geert for supplying all the information I needed from the water board of Delfland. Many thanks also to the water board for making this information available.

Finally, I would like to thank my friends and family for their help and support throughout my entire study period at TU Delft.

Pieter Hendrik Dorst
Klaaswaal, March 2019

Summary

Apart from the primary flood defences that protect the land from the sea, the big rivers, and the lakes, many smaller flood defences can be found in the Netherlands. These regional flood defences protect the land against smaller bodies of water inside the primary flood defences. The groundwater table inside these regional flood defences has an important influence on the stability and therefore the safety of these flood defences. This groundwater table, called the phreatic surface, is dependent on many factors which complicates the determination of its position in the flood defence. For stability calculations usually a schematisation of the phreatic surface is used, based on the geometry of the flood defence and the water levels. No precipitation or soil characteristics are explicitly included in these schematisations, which means they are potentially inaccurate and therefore might result in a higher or lower calculated stability than in reality is the case.

A possible method to determine the location and the fluctuations of the phreatic surface based on external factors, could be to model the phreatic surface using a numerical model. Research has been conducted with the use of such models, but in most cases the models cannot be verified due to lack of measurements of the phreatic surface. It is therefore unclear to which extent a numerical model is able to simulate the phreatic surface. Based on this problem the main research question for this thesis was composed: *Can a numerical model contribute to a more accurate estimation of the phreatic surface in a regional flood defence during extreme conditions?*

To answer the research question, a case study was performed on three regional flood defences for which the phreatic surface has been monitored for a certain period. For these flood defences a groundwater flow model was set up in which the phreatic surface was simulated. To analyse the accuracy of the simulation, the results of these models were compared to the measurements. Two of the research cases are located in the area of the water board of Delfland, and had a measurement set of 4 years available. The third research case is part of a research project in the area of the water board of Rijnland, which was ongoing during the writing of this thesis. The measurement set therefore had a length of only several months, but despite this the research case was included because the conductivity of the soil was measured, and because four measurement points were used in the cross-section. For the other locations no conductivities were measured, and only three monitoring wells were used.

To construct the three models a numerical model had to be chosen. Eventually the choice was made to use the numerical model MODFLOW in combination with a Python package called FloPy, which is able to facilitate the input and output of the model. The models were calibrated by variation of the soil parameters, most notably the hydraulic conductivity. The parameters can be variated for each soil layer, which means many combinations of parameters had to be tested to find an optimum calibration.

For all models it was possible to simulate head fluctuations similar to those in the measurements. How accurately the fluctuations were modelled was different between the research cases and between different points in the cross-section. On average the difference between the model and the measurements was about 10 cm. This difference was smaller for high phreatic surfaces and larger for low phreatic surfaces. For one of the models the effect of this error on the macro-stability was assessed, and this effect was sufficiently small. Considering the necessary simplifications needed to construct the models, it is therefore concluded that it is possible to simulate the head measurements with sufficient accuracy.

However, this sufficiently good fit of the models was only reached after extensive calibration of the models to the measurement sets. Comparison between calibrated and uncalibrated models has shown that calibration is necessary to obtain an accurate model. This means measurements are a necessary part of the construction and calibration of a numerical model. The calibration

itself can be a long-drawn process, due to the large amount of parameter variations. The large amount of required data and the difficult calibration process make it questionable whether it is always worthwhile to construct a numerical model to determine the position of the phreatic surface.

Apart from simulating the measurements sets in the numerical model, some extra simulations were carried out. Extreme precipitation events of various duration, intensities and time patterns were imposed on the models. This analysis confirmed conclusions from earlier research that precipitation with a long duration has a larger effect on the phreatic surface than short, intense events. The analysis also confirmed that the phreatic surface eventually reaches an equilibrium position, where it rises no further. The three research cases responded similarly, with differences in response time dependent on the soil characteristics. The precipitation patterns containing a single peak resulted in the most critical phreatic surface. For this pattern first the equilibrium situation is reached, and the peak then induces a small extra head rise.

Furthermore, for one of the research cases a simulation using 31 years of meteorological data was performed. From this simulation it was found that the schematisation of the phreatic surface according to the guidelines of the water board maintaining the flood defence is exceeded regularly. These exceedances only occurred near the toe and the inside drainage ditch. In the main simulation of the same model a slight exceedance in the outer crest was found as well. In the inner crest the schematisation remained well above the modelled phreatic surface. This indicates that potential improvements to the schematisation can be made in these areas.

From the long-term simulation it was also found that the probability of a certain height of the phreatic surface can be described with a lognormal distribution. The fluctuations and therefore the standard deviation of the distribution vary over the cross-section. These fluctuations are largest at the inner crest.

Several stability calculations were performed to determine the effect of a change in the phreatic surface on the stability. A change had the largest effect at the inner crest and at the toe. Stability calculations using the highest phreatic surface from the simulations lead to slightly higher stability than when using the current schematisation.

Table of contents

1 Introduction

1.1 Regional flood defences

A large part of the Netherlands is formed by the delta of the rivers Rhine and Meuse. Due the low elevation of the land in this region, it has since long been subject to flooding. From about the twelfth century onwards, the inhabitants of these lands started building dikes to protect the region against this threat. These dikes form the system of primary flood defences which protects the Netherlands from outside water like the sea and rivers.

Apart from this system of primary flood defences a system of regional flood defences was constructed. These regional flood defences are located inside of the primary flood defences and protect the land from smaller bodies of water like canals and small rivers. The loads and protected area of these regional flood defences are usually much smaller than those of primary flood defences. For this reason regional flood defences usually have smaller dimensions than their primary counterparts.

Several types of regional flood defences can be distinguished, for example compartment dikes and flood defences along regional rivers. A large part consists of the so called 'boezemkaden'. These are regional flood defences that protect low-lying areas from the water in regional canals. The low-lying areas, called polders, are constantly filled with water from precipitation and seepage, and are therefore vulnerable to flooding. To prevent this flooding, the excess water has to be pumped out. The water is pumped into a system of regional storage canals called the 'boezem', which stores the water and transports it towards the outside water. In this boezem a constant water level is maintained, which is higher than the water level in the polders. The boezemkaden are the barriers between the boezem and the polder. This specific type of regional flood defences is the subject of this study. For practical reasons it is referred to as regional flood defences in this thesis, even though it is actually just a single type of regional flood defences.

1.2 Background

By Dutch law, flood defences have to be assessed on safety in regular periods. There are several failure mechanisms that have to be assessed in order to classify a regional flood defence as safe (STOWA, 2015):

- Overflow;
- Wave overtopping;
- Piping and heave;
- Macro-stability of the inner slope;
- Macro-stability of the outer slope;
- Micro-stability;
- Cover of the slopes;
- Stability of the foreshore.

One of the most important failure mechanisms for regional flood defences is macro-instability of the inner slope. The macro-stability of a soil structure can be defined as the ability to withstand loads without loss of function due to large deformations (TAW, 2001). Usually the macro-stability is assessed using a slip plane analysis, which assumes a slide occurs along a certain slip plane. This is illustrated in figure 1.1. The slip plane is subdivided into vertical slices, for each of which the balance of forces is computed. The considered forces are usually the self-weight of the soil, the top load on the crest of the structure, and the shear force along the slip plane. The self-weight of the soil is both a driving and a resisting force. Near the crest of the structure the self-weight acts in the same direction of the sliding of the slip plane, but near the toe it is possible that the soil

is pushed upwards. In this area the self-weight is a resisting force. The location of the most critical slip plane is unknown beforehand, and therefore the stability has to be assessed for a large number of slip planes in order to find the normative slip plane. For this reason a stability analysis is usually performed using a computer program.

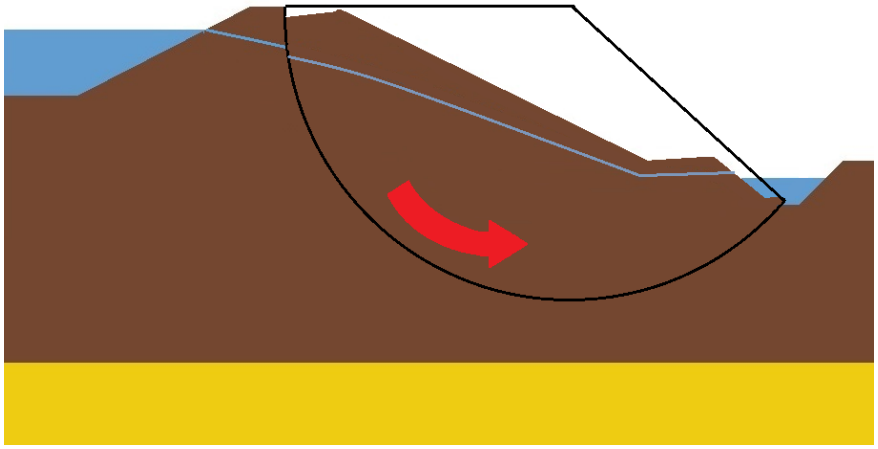

Figure 1.1: Illustration of macro-instability

The shear force that can be generated by the soil along the slip plane is an important factor in the macro-stability. It is dependent on soil characteristics and on the effective stress in the soil. The effective stress is the difference between the total stress resulting from the self-weight of the soil and the load on top of it, and the pore water pressure caused by the groundwater. As long as the volumetric weight of the soil and the top load do not change, an increase in pore pressure will cause a decrease of the effective stress and consequently the shear resistance. The magnitude of the pore pressure is therefore an important factor in the stability of the structure.

The magnitude of the pore pressures inside the structure is influenced by groundwater flow. In the Netherlands the subsoil of a dike usually consists of a permeable Pleistocene sand layer, covered by a less permeable Holocene top layer (TAW, 2004). In some cases intermediate sand layers can be present in the Holocene layer. The groundwater flow in each of these layers has different characteristics due to the differences in permeability.

In the dike profile and the Holocene layer a groundwater flow is present from the outside water towards the inside water. Along the profile the pore pressures gradually decrease from the outside water level to the inside water level. This gradient of the hydraulic head along the width of the flood defence forms the phreatic surface. It is defined as the position where the water pressure is equal to the atmospheric pressure. This definition is important, because above this surface water is also present in the soil due to capillary forces. In this capillary zone the water pressure is lower than the atmospheric pressure.

In the Pleistocene sand layer the situation is different. Due to the larger permeability the decrease in pore pressure is less over the distance, which means the pore pressures are usually different to those in the Holocene layer. Therefore in the lower part of the Holocene layer a transition zone is present, where the pore pressure varies over the depth. Often the pore pressures in the Pleistocene layer are higher than in the Holocene layer. Although this thesis is mainly concerned with the pore pressures in the Holocene layers, the pore pressures in the lower layers also influence the higher layers, and therefore these have to be considered as well.

A schematic display of the soil layers and the phreatic surface is given in figure 1.2.

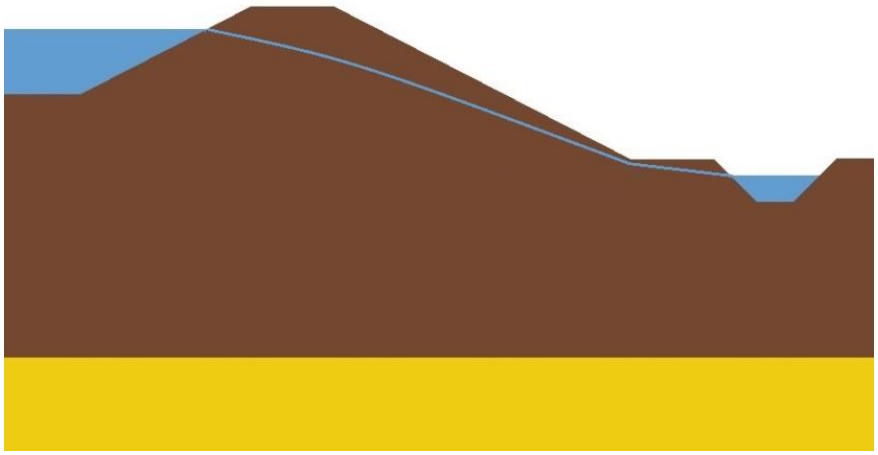

Figure 1.2: Schematic display of the soil layers and phreatic surface for a regional flood defence

The phreatic surface is more dependent on external circumstances than the hydraulic head of the sand layer. The main influences are the water levels on each side of the flood defence, the internal composition of the structure, and precipitation. Due to these factors it is difficult to predict the exact position of the phreatic surface. It is therefore an important variable in stability analyses; the uncertainties are high and the influence on the macro-stability is large.

All the factors involved make an accurate schematisation of the phreatic surface difficult when no pore pressure measurements are available. Usually a schematisation is used. The water boards managing regional flood defences often prescribe a schematisation, but differences exist between the water boards. Moreover, the justification of these schematisations is not entirely clear. The influence of precipitation is not based on soil characteristics or the amount of precipitation. Due to these aspects it is unclear how accurate the schematisations are. If the schematisations are inaccurate they result in a higher or lower calculated stability than in practice is the case.

For this reason research has been conducted on the phreatic surface in flood defences. From Ten Bokkel Huinink (2016) it was found that the pore pressures are overestimated at larger depths in the schematisation. In simulations the calculated phreatic surface is higher than the schematisation, but because the pressure distribution is non-hydrostatic the actual pore pressures are lower. In De Loor (2018) a similar result was found for a simulation in which a clay dike is subjected to long-term precipitation. However, it is not clear what causes this non-hydrostatic pressure and whether this actually occurs or whether it is a result of the used model.

Determining the position of the phreatic surface using a numerical model like in the mentioned theses could be a method to obtain a more accurate result. In this way the influence of water levels, precipitation and internal composition of the dike can be accounted for. However, currently it is not clear whether such models accurately represent reality. In De Loor (2018) and Ten Bokkel Huinink (2016) no pore pressure measurements were available to back up the results. In 2012 a study was conducted where the position of the phreatic surface was modelled after a field test with artificial precipitation, and the results were compared to measurements from this field test (Alterra, 2013). It was concluded that a numerical model is able to accurately predict the position of the phreatic surface. There are a few problems with this test, for example artificial precipitation was applied to simulate an extreme event, no dry periods were included, the simulated period was quite short and only a single cross-section was considered. Therefore the results of this test do not conclusively show it is possible to determine the position of the phreatic surface using this method for every situation.

The problems can be summarised in the following problem statement:

The position of the phreatic surface during extreme conditions is an important influence on the macro-stability and therefore the safety of a regional flood defence. It is currently unclear whether it is possible to determine this position of the phreatic surface more accurately using a numerical model.

1.3 Objective

The objective of this thesis is to extend the knowledge of modelling the phreatic surface in regional flood defences with the use of a numerical model.

1.4 Research questions

From the problem description and objective the main research question for this thesis was composed:

Can a numerical model contribute to a more accurate estimation of the phreatic surface in a regional flood defence during extreme conditions?

To answer this question the following sub-questions need to be answered:

1. *What are the main influencing factors on the phreatic surface?*
2. *How is the phreatic surface currently schematised in regional flood defences?*
3. *What are the requirements for a numerical model to model the phreatic surface in a regional flood defences?*
4. *How accurately can a numerical model simulate measured pore pressures in a regional flood defence?*
5. *How does the phreatic surface in the numerical model respond to an extreme event?*
6. *What parameters and data are at least required for an accurate determination of the phreatic surface using a numerical model?*

1.5 Research method

To answer the research questions, a case study will be performed on a number of regional flood defences for which pore pressures have been monitored during a long period. For these flood defences a groundwater flow model will be set up in which the phreatic surface is simulated. These simulated phreatic surfaces will be compared to the measurement data to analyse the accuracy of the simulation.

Literature study

Starting point for the research is a literature study. This literature study is needed to answer the first three research sub-questions and to obtain a better understanding of the subject. The following subjects are researched:

- Currently used schematisation of the phreatic surface;
- Factors that influence the position of the phreatic surface;
- Theory on groundwater flow;
- Numerical models for groundwater flow.

In the literature study an investigation is made of the numerical models that can be used for the research. Based on this a choice will be made. The chosen model is used to simulate the phreatic surface for the research cases over the period for which measurement data of the phreatic surface is available.

Research case
Regional flood defences exist in many shapes and sizes. Between cases there can be large differences in geometry, soil composition, and water level difference. This makes it difficult to provide a general answer to the research question. Therefore the research is focused on several research cases. These research cases should fulfil the following requirements:

- Pore pressure measurements from monitoring wells or pressure sensors are available for the case, so that the location of the phreatic surface over the cross-section is known. This means several measurement points are needed per cross-section. Preferably the data spans a period of least a year to have seasonal influences included.
- The case should be representative for a typical regional flood defence. What exactly classifies as typical is hard to determine, as there can be large differences between regional flood defences. At least a case should be chosen that is comparable to most other flood defences. For example, no structural elements should be present in the cross-section. Ideally the researched cases have some differences between them. If the same conclusions are found for different situations, these conclusions are more general and more likely to apply to other regional flood defences.
- Data regarding soil composition, water levels, precipitation and evapotranspiration is available or can be acquired for the case.

Construction and calibration of the model
Using the model of choice, a model is constructed for each of the three research cases. In order to do this, first a schematisation of the cross-section has to be constructed based on data from soil borings and cone penetration tests. The load data (precipitation, water levels and evaporation) are applied to the model as boundary conditions. The geotechnical parameters have to be estimated based on the soil types in the cross-section. Using this input data the model is run to simulate the period for which the measurement data is available.

To assess how accurate the model simulates the phreatic surface, the model results have to be compared to the measurement sets. If large differences are found the model has to be calibrated by adjusting the geotechnical parameters. To keep the model realistic, the parameters should be variated within a realistic range. After each simulation the effect of the adjustment can be analysed. This process should be continued until the best possible approximation of the measured phreatic surface is reached.

The process of constructing and calibrating the model is illustrated in the flow chart in figure 1.3.

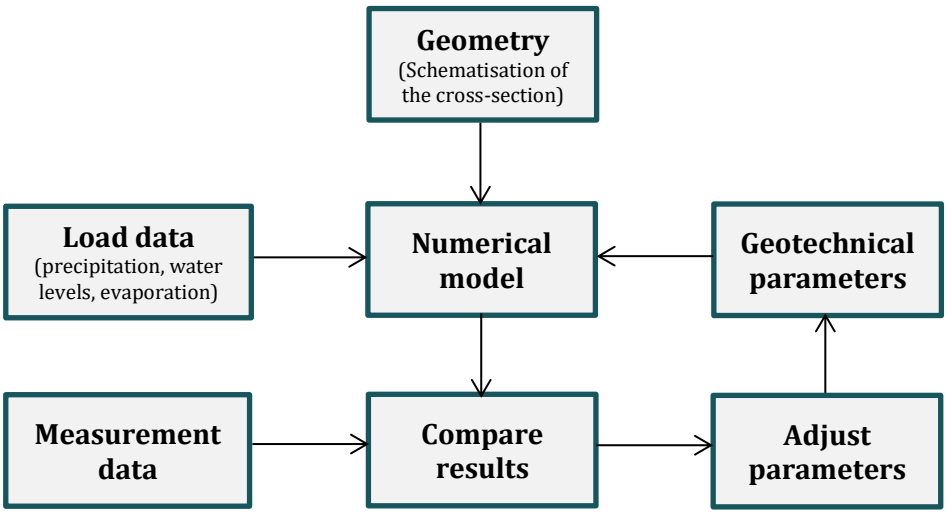

Figure 1.3: Schematisation of the proposed research methodology

Extreme events
The fifth research sub-question aims to determine how the phreatic surface in the numerical model responds to an extreme event. To answer this question, the extreme event first has to be defined. Two types of extreme events can be of relevance: an extreme precipitation event and a period of lasting drought. The extreme precipitation event will be analysed first, since this situation is usually more relevant for the stability than the drought event.

First it is investigated whether any extreme events have occurred during the measurement period, and it is determined what the return periods of those events are. For these events the simulated and measured phreatic surface are compared to investigate how accurately extreme events are simulated compared to normal conditions.

As a next step, a fictitious extreme event is simulated using the calibrated model. Regarding precipitation many variations are possible. For a fixed return period various combinations of durations and intensities can be tested. The effect of the way the precipitation is distributed over time is also investigated.

Minimum requirements for an accurate model
The last research sub-question is aimed at determining what parameters and data are required for an accurate determination of the phreatic surface using a numerical model. The way in which the answering of this question is approached depends on the result of the main simulation. If the model cannot accurately predict the position of the phreatic surface the sub-question becomes irrelevant. If the model is able to model the phreatic surface with sufficient accuracy, it can be investigated which parameters have the most influence on this result. Partly this is done already during the calibration of the model. Additionally, it can be investigated how many monitoring wells have to be placed in a cross-section, and how long these have to be monitored in order to obtain enough measurements to create a sufficiently accurate model. This can be investigated by calibrating the model for only a part of the measurement period (for example only the winter or summer period) and analyse how this calibration compares to the main model. If a research case is chosen for which measurements of the permeability are available, it can be analysed what the influence of using a measured permeability is compared to using an estimate.

2 Literature

As starting point for the research a literature study has been conducted. The aim of this literature study is to answer the first three research sub-questions, to obtain a better understanding of the factors that influence the phreatic surface and to make an assessment of the numerical models that could be used to conduct the research.

2.1 Schematisation of the phreatic surface

As described before, the phreatic surface is an important variable in the stability assessment of a flood defence. Due to the large amount of influencing factors and the uncertainties, it is usually schematised based on a number of points in the geometry. Since the stability has to be assessed for high water situations and dry periods, schematisations exist for both situations.

2.1.1 Technical report pore pressures in dikes (TAW, 2004)

In the guideline for the assessment of the safety of regional flood defences (STOWA, 2015) the approach given in the report 'Pore pressures in dikes' (TAW, 2004) is recommended for the high water situation. This schematisation is mainly directed at primary flood defences. In principle, the report only recommends this approach when no pore pressure measurements are available.

For the approach in this report four different types of dikes distinguished, based on whether the subsoil is compressible or not, and whether the dike core is constructed out of clay or out of sand. The schematisation of the phreatic surface for the types with a clay core is displayed in figure 2.1.

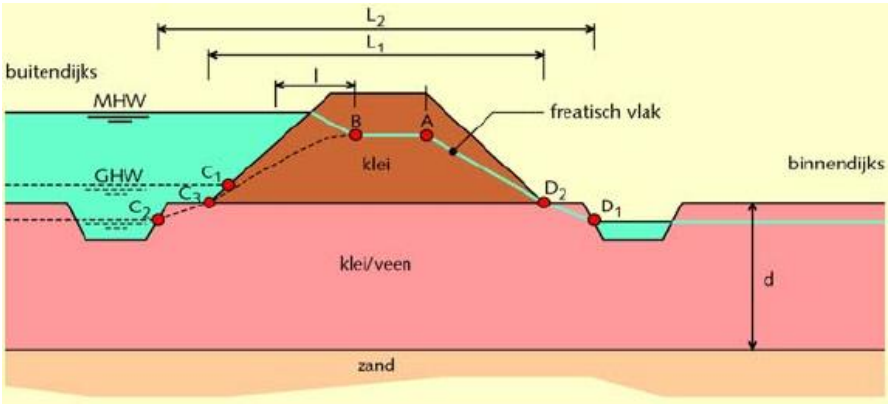

Figure 2.1: Schematisation of the phreatic surface in the report 'Pore pressures in dikes' (TAW, 2004)

The variables in this schematisation are defined as follows:

C: Point C represent the phreatic surface at the outer toe, and its location depends on the presence of a drainage ditch. For dikes permanently loaded by water the point C_1 on the slope is used, which is the case for regional flood defences.

D: Point D_1 is used in case of a drainage ditch near the inner toe, point D_2 is used when no drainage ditch is present.

L: Width of the dike base; dependent on the location of points C and D.

B: Dependent on the horizontal intrusion length I, which indicates how far into the dike the influence of a water level raise reaches. Since water level fluctuations are smaller for regional flood defences than primary flood defences, this parameter is of less relevance. Point B should thus be located close the entry point.

A: Represents the bulging of the phreatic surface due to precipitation. The horizontal location is below the inner crest. The height is dependent on points C and D, the width of the dike and the thickness of the clay sub-layer.

For types with a sand core a similar type of schematisation is used. This schematisation will not be treated here, because these types are less relevant for the research.

Pleistocene sand layer

The pore pressure schematisation of the Pleistocene sand layer is dependent on whether or not the compressible (Holocene) layer is pushed up by the water pressure. If this is not the case, the hydraulic head according to the points C_1, D_1, E_1, and G_1 in figure 2.2 applies. If the compressible layer is pushed up the points C_2, D_2, E_2, and G_2 are used instead.

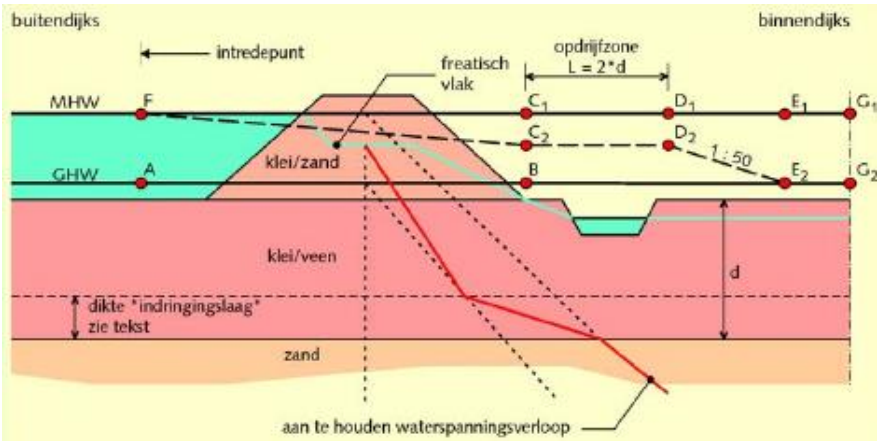

Figure 2.2: Pore pressures in the Pleistocene sand layer. Source: TAW, 2004.

The horizontal location of point F is at the so-called entry point. This entry point is the point where the outside water level is the boundary condition for the Pleistocene sand layer, i.e. the point at which the head in the sand layer is equal to the outside water level. The location of this point is dependent on the soil composition below the outside water and therefore the entry point is hard to define. Considering the small dimensions of the canals that form the outside water of regional flood defences, it is likely that this point often does not exist in reality. The height of point F (as well as points C_1, D_1, E_1, and G_1) is the design high water level.

The horizontal location of points C_1 and C_2 is at the inner toe of the dike. From this point inwards a push-up zone is defined with a length of 2*d, where d is again the thickness of the Holocene layer. Points D_1 and D_2 are located at the end of this zone. The height of points C_2 and D_2 is at the so-called boundary potential, which is the hydraulic head for which the water pressure below the compressible layer is equal to the weight of this layer. Points E_2 and G_2 are at the average high water level outside the dike. The head decline between points D_2 and E_2 is schematised as a gradient of 1:50. This inclination determines the horizontal location of point E.

Since the heads in the top- and subsoil are different, somewhere a transition has to occur between those heads. This transition zone is modelled as a so-called intrusion layer, in which the head linearly transitions between the two heads. In the report 'Pore pressures in dikes' a formula is provided to calculate the thickness of this intrusion layer, based on the permeability and thickness of the compressible layer and the head in the sand layer. However, in practice usually an intrusion layer thickness of 3,0 m us used for dikes in river and lake areas, and 1,0 m for sea dikes.

The scientific basis for the schematisations in the report 'Pore pressures in dikes' is not entirely clear. In an expert report from 2009 (Expertisenetwerk waterveiligheid, 2009) it is pointed out that the report provides no information whether the schematisation is based on expert judgement or on measurements. Furthermore, the bulging of the phreatic surface due to precipitation is

based on the geometry and the type of the dike and not on soil characteristics and the amount of precipitation. Soil characteristics are used to calculate the intrusion length, but this only accounts for water level variations and not for precipitation. For these reasons the accuracy of the schematisation can be disputed.

Another potential problem is that these schematisations are mostly aimed at river dikes, for which high water events have a water level several meters higher than the normally occurring water level. In regional flood defences the outside water level is always close to the crest of the dike, and the water level rise during high water events is no more than several decimetres.

This difference has only small consequences for the schematisation of the phreatic surface, because that schematisation is mostly based on the geometry of the dike, except for the horizontal intrusion length. However, for the transition between the phreatic surface and the head in the Pleistocene sand layer the approach using an intrusion layer this difference may lead to problems. This intrusion layer is based on the occurrence of a high-water wave, resulting in an increased head in the Pleistocene sand layer. This higher head creeps in the compressible layer, which is a slow process due to the low permeability of this layer. The thickness over which the head in the compressible layer is influenced by the increased head in the Pleistocene layer is the intrusion layer.

As mentioned, high water events for regional flood defences involve a much smaller water level rise than for river dikes, resulting in a smaller or negligible increase of the head in the sand layer. In addition to this, the head in the Pleistocene layer is often higher than the inside water levels. This means that the use of an intrusion layer, which represent a transient state of the pore pressures, is not valid for most regional flood defences. Instead, the transition between the two head will occur over the entire thickness of the compressible layers. The exact course of this transition is dependent on the conductivities of these layers.

2.1.2 Water boards

The water boards that manage regional flood defences often have their own guidelines for the schematisations of the phreatic surface, usually based on pore pressure measurements and expert judgement. Between water boards there are differences in these guidelines.

For the water board 'Hoogheemraadschap van Delfland' a schematisation was established in an expert workshop (Delfland, 2008). However, based on field measurements the schematisation for the high water situation was later adjusted to a more conservative approach. This more recently established approach is described here. This information is taken from an assessment report of a regional flood defence in the management area of this water board (RPS & Witteveen+Bos, 2016).

High water situation

In the high water situation the outside water level is the design water level with a return period of 100 years. The phreatic surface below the inner crest is assumed to be at the intended water level (the water level that is usually maintained in the boezem system). At the inner toe it is assumed that seepage occurs, meaning the phreatic surface is at ground surface level. For the inside water level it is assumed that the water level is 0,15 m above the intended water level. Between these points a linear gradient of the phreatic surface is assumed. In some cases no drainage ditch is present. If this is the case, and the polder water level is less than 0,5 m below the ground surface, the phreatic surface inside of the flood defence is schematised at ground level. When the polder water level is more than 0,5 m below the ground surface, the height of the phreatic surface is schematised at 0,5 m above the polder water at 15 m from the toe. Between this point and the toe again a linear course is used.

Dry situation

In the dry situation the intended outside water level is used. Below the outer crest a height of 1,5m below the outside water level is used. From this point onwards a slope with the same angle

as the inner slope is schematised, up to the point where the intended inside water level is reached. In case no drainage ditch is present, the inside water level is schematised at 0,7 m below the intended polder water level.

The schematisations for both situations are displayed in figure 2.3.

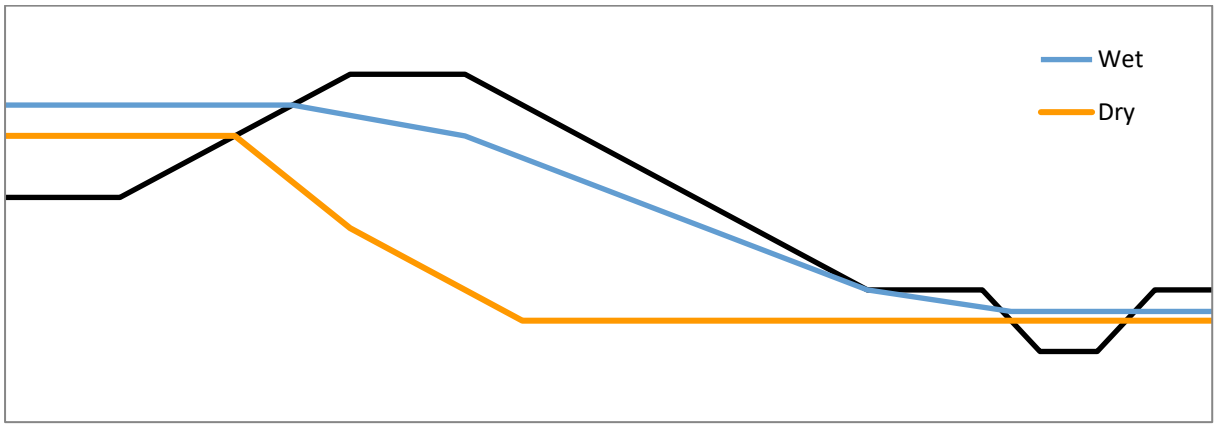

Figure 2.3: Schematisation of the phreatic surface for a dry situation.

The schematisation is not applicable to every situation. An advisor has the obligation to interpret whether or not the schematisation is realistic for a specific situation, for example when intermediate sand layers are present. If the calculated stability of a flood defence is insufficient using this schematisation, measurements of the phreatic surface are carried out over a period of 14 weeks. If the maximum measured height during this period is more than half a meter below the schematised phreatic surface, the schematisation can be adjusted to a height of 0,5 m above this maximum measured value, on the condition that precipitation has occurred during the measurement period. If the maximum measured head at the inner crest is less than 0,1 m below the intended water level, the schematisation at this location is adjusted to 0,1 m above the intended water level.

A problem that occurs for these schematisations is the applicability in practice. Most regional flood defences have an irregular geometry and have a much smoother shape than the dikes in the schematisations. This means the exact boundaries between crest, slope and toe are hard to define. Different interpretations can lead to a different schematised phreatic surface. In general it can be concluded that the schematisation of the phreatic surface is fairly subjective.

2.2 Factors of influence on the phreatic surface

This section discusses the various factors that may be of influence on the height of the phreatic surface. Various hydrological processes determine the in- and outflow of water in the dike, and therefore determine the height of the phreatic surface. These processes are:

- Water level variations (in and outside water);
- Precipitation: partly infiltrates in the dike, and partly flows away as surface runoff;
- Evaporation and transpiration by plants (together evapotranspiration).

A schematic illustration of these factors of influence is given in figure 2.4.

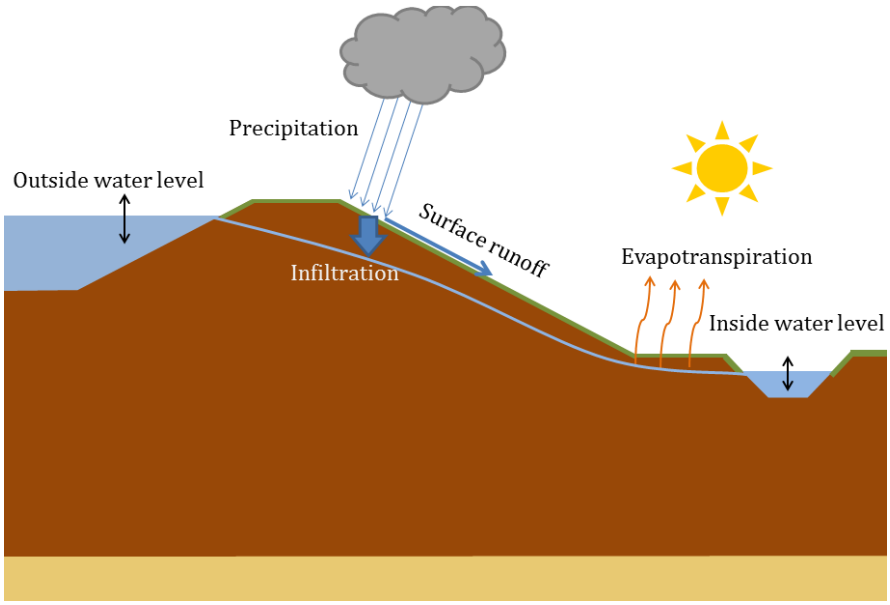

Figure 2.4: Illustration of the various hydrological processes influencing the height of the phreatic surface

2.2.1 Water level variations

One of the main influences on the position of the phreatic surface are the water levels on both sides of the flood defence. For regional flood defences the situation regarding water levels is different than for other types of flood defences. In primary flood defences the design water level is usually much higher than the normally occurring water level, but in regional flood defences the water level is at all time close to the crest.

In the technical report pore pressures in dikes (TAW, 2004) it is described that during a situation with a higher water level the pore pressures inside a flood defence follow the outside water level with a certain delay. When the high water level has passed the pore pressures will remain high for some time. This lingering effect is mostly present in river dikes, where a high water event can cause a water level raised by several meters for a multiple days. In a regional flood defence a higher water level can also last for an extended period of time, but the difference compared to normal water level is less than a meter. The rise of the phreatic surface is therefore also much smaller, which means the lingering effect has only a small influence. The effect could be of importance for a situation where the outside water level suddenly drops, which might occur when another regional flood defence nearby breaches and causes the canal to drain.

The thesis of De Loor (2018) shows that the permeability has a very large influence on the reaction of the phreatic surface to water level changes. It also shows that clay layers with soil structure deterioration have a large influence due to their larger conductivity. Therefore the conductivity and extent of clay layers with deterioration are an important factor in the change of the phreatic surface due to water level differences. This influence could be even larger in regional flood defences. These usually have smaller dimensions than primary flood defences and therefore the deteriorated top layer forms a larger part of the total structure.

In 2012 a field test was conducted by the water board 'Hoogheemraadschap Hollands Noorderkwartier' which was aimed at gaining insight in the influence of precipitation on peat dikes (Alterra, 2013). In this field test both natural and artificial precipitation was applied to two cross-sections on opposite sides of a boezem canal, and for both cross-sections the pore pressures were monitored on several locations. Furthermore two reference cross-sections were monitored to which no artificial precipitation was applied. After the first part of the test the water in the boezem canal was raised about 30 cm, to investigate the influence of precipitation in combination with a heightened outside water level. Although it was not the aim of the study, in the measurements the effect of this raise of the water level can be observed. For both sides of the

boezem canal and for both the irrigated and reference cross-sections the effect of the water level raise can be observed. The rise of the phreatic surface occurs quite fast, within the same day a more or less steady situation is reached. However, in the report it is mentioned that rubble is present in the crest of the cross-section. Rubble has a large permeability and this might be the cause for this fast rise of the phreatic surface.

Variation of water levels
In general, the variation of both the inside and outside water levels is relatively small for regional flood defences. Both water levels are regulated by pumping stations, so water level rises can only occur when the pumping capacity is temporarily lower than the inflow caused by precipitation and seepage. Another possibility could be wind set-up in the system of boezem canals. The variations that occur are small compared to the normal water level difference over the flood defence.

An event that might cause a significantly lower water level could occur if the boezem canal is drained due to a breach in another flood defence nearby.

It follows that the measure in which water level variations influence the phreatic surface is dependent on the following factors:

- Water level difference variation;
- Duration of the water level variation;
- Soil characteristics (conductivity, porosity and composition)

Especially the soil characteristics and composition are important. In the study of De Loor (2018) a homogeneous clay dike showed virtually no response to a flood wave, while a dike with a top layer with higher permeability did show a response. The test described in Alterra (2013) show a fast response to a relatively small water level rise, which is possibly caused by rubble in the crest. The extent of soil structure deterioration is hard to determine, and also variable over time. Inhomogeneity of the soil caused by for example rubble is also generally unknown. These factors make it difficult to determine the effect of water levels on the phreatic surface. However, water level differences for regional flood defences are usually small compared to difference between the inside and outside water level. Therefore the changes they cause in the phreatic surface are also comparatively small.

2.2.2 Influence of precipitation
Another main influence on the position of the phreatic surface is precipitation. Some of the precipitation that falls on a flood defence flows away over the surface (run-off), but a part of it infiltrates into the groundwater. This causes the groundwater table to rise, resulting in a flow towards the edges of the structure, mostly towards the inner toe. This will cause the phreatic surface to bulge, which in turn causes larger pore pressures and thus decreases the stability of the dike.

According to the report ‘pore pressures in dikes’ (TAW, 2004), the type of cover of the flood defence is an important factor in the influence of precipitation on the phreatic surface. A dike with an impermeable asphalt cover is less influenced by precipitation than a dike with a grass cover. A road on the crest of the flood defence causes less infiltration below the road, but near the roadsides there is more infiltration due to the water flowing away over the road. The structure below the road is also important. It usually consists of sand or other permeable materials, which can cause an increased infiltration into the dike core.

The precipitation that falls on the slope of the structure is mostly absorbed by the unsaturated zone above the phreatic surface. In clay soils, structures are present in this zone. These structures are formed by mechanical and biological processes and can be divided in two types: a coarse continuous system of cracks and tunnels and a finer, less continuous system of pores. These

structures influence the permeability of the unsaturated zone. The infiltrated water in the unsaturated zone will partly infiltrate further into the core of the dike and partly evaporate or transpire through plants.

For regional flood defences the internal structure of the dike determines the influence of precipitation on the phreatic surface. A dike with a clay core responds slower to fluctuations than a dike with a sandy core. The width is also important. For a regional flood defence with a small width there is a risk that the groundwater exits the dike on the inner slope, which may cause erosion.

TAW (2004) lists the following effects of precipitation on the phreatic surface:

- At the point of entry on the outer slope the height of the phreatic surface is equal to the outside water level;
- At the inner crest the phreatic surface rises with 0,30 m compared to a regular situation, but it never rises above the outside water level;
- At the inner toe the phreatic surface lies at ground level.

Many dikes are very dense due to traffic load over the years, which means the bulging of the phreatic surface develops very slowly, but also is very insensitive to dry periods.

The thesis of Ten Bokkel Huinink (2016) is aimed at finding a method to assess the probability distribution of the phreatic surface in regional flood defences. As a part of the research the influence of precipitation on the phreatic surface was studied, by re-analysing the data from the earlier mentioned field test described in Alterra (2013), and by using a finite element numerical model.

From the analysis of the field test data it was found that both artificial and natural precipitation have an effect on the phreatic surface, but no general method can be found to describe this influence due to the variety in the results. The measured phreatic surface reacts to a precipitation event within hours. The soil configuration has a large influence on this reaction speed. Furthermore, it was found that the permeability of the soil is very uncertain, and shows a large variability.

From the numerical study it was also found that precipitation can have a large influence on pore pressures in a dike. The following conclusions were found:

- The toe of the dike responds first to a precipitation event, and the crest responds last.
- After an infinitely long precipitation event the position of the phreatic surface is solely dependent on saturated permeability and not on the unsaturated characteristics.
- After a finite precipitation event the position of the phreatic surface depends on precipitation duration and intensity and on both the saturated and unsaturated characteristics of the soil;
- During a precipitation event pore pressures do not increase linearly with depth.
- The reaction speed of the pore pressures to a precipitation event is dependent on the unsaturated permeability.
- The phreatic surface in a dike can rise to surface level as a result of a precipitation event; this is in contradiction to the governing schematisation in (TAW, 2004).
- In the simulations, the calculated phreatic surface is higher than in the governing schematisation of (TAW, 2004), but the pore pressures are lower due to their non-hydrostatic nature. The schematisation therefore overestimates the pore pressures.

In the thesis of De Loor (2018) the effect of precipitation was also investigated for several dike types. Furthermore, some extra tests were performed: a test where the dike was subjected to measured long term precipitation for both a period of 26 years and of 52 years, and a test where extreme events were added to this precipitation data.

Regarding precipitation, the following conclusions were found (De Loor, 2018):

- In a homogeneous clay dike the phreatic surface shows no response to a precipitation event, but a clay dike with soil deterioration in the top layer has a buffering effect in the top layer. The top layer prevents run-off and slowly releases the water to the core. However, most of this water flows through the top layer towards the toe.
- The sand dike shows more response to the load events than the clay dikes.
- In none of the simulations the rise of the phreatic surface was such that a dike failure might occur.
- In clay dikes, small but regular events have a greater influence on the phreatic surface than extreme events, since most precipitation runs off the slope due to the low permeability.
- A uniform rainfall shape leads to the most infiltration; other shapes lead to more run-off.
- The core of the clay dikes becomes fully saturated when real precipitation data over a period of 26 or 52 years is applied. However, the pore pressure in the subsoil barely changes from the starting point. This means the pore pressure over the depth is not hydrostatic.

When considering all sources discussed, it can be concluded that precipitation has a definite influence on the position of the phreatic surface in a flood defence. The magnitude and speed of the reaction are dependent on several factors, mainly the soil composition and characteristics. From the studied reports the following aspects are of particular importance:

- A road on the crest of the flood defence;
- A deteriorated clay top layer with soil structures influences the infiltration;
- The distribution of pore pressures over the depth may not be hydrostatic.

Soil characteristics determine for a large amount of the influence of precipitation on the phreatic surface.

2.2.3 Influence of evapotranspiration

Evaporation of water from the surface of the flood defence is a factor that can also be of influence on the phreatic surface. Evaporation can occur directly from the surface, but loss of water also occurs via transpiration through plants. The total outward flux from these two effects is called evapotranspiration. The total evapotranspiration flux consists of three elements (GeoDelft, 2007): evaporation of interception water (precipitation stored by plants above the surface), soil evaporation and transpiration through plant leaves.

The outward flux of evapotranspiration causes the phreatic surface to become lower. This means evapotranspiration is of relevance for this research. If it is not taken into account the simulated phreatic surface could be higher than the measurements, especially in the summer months. For peat dikes evapotranspiration is also important for stability reasons. In most flood defences a lower phreatic surface has a positive effect on the macro-stability, but this is not the case for peat dikes. Peat decreases in weight and volume when it dries out, which has a negative effect on the stability. Due to this effect several regional flood defences have failed in the past, for example in Wilnis and Terbregge in 2003.

Several models exist to calculate the evapotranspiration flux, like the Penman-Monteith or the Makkink methods. However, the flux calculated using these models represents the potential evapotranspiration, which is the evapotranspiration that would occur with an unlimited water supply. In reality evapotranspiration reduces the water content of the unsaturated zone, which reduces the evapotranspiration rate. Therefore the actual amount of evapotranspiration is lower.

In 2014 a study was conducted using the model dgFlow in which the possible lowering of the phreatic surface in a peat regional flood defence due to dry circumstances was analysed (Sman, 2014). For this analysis a particular case for which pore pressure measurements were available

was used. From the analysis it was concluded that the dry period result in a significantly lower phreatic surface. The lowering mostly occurs near the toe of the structure, and remains limited near the crest. Lowering the outside water level results in an even lower phreatic surface. Adding a clay top layer has a smaller effect than expected. The clay layer seems to be diminishing the desiccation, but also to be diminishing the infiltration. It is however remarked that it is uncertain whether this effect accurately represents reality, because the model was calibrated for the situation without the clay cover.

From the sources it is clear that dry periods play an important role in the stability of peat flood defences. However, the influence of dry periods is caused by several factors apart from evapotranspiration, like lack of precipitation and a lower outside water level. It is unclear how large the influence of evapotranspiration itself is. Most likely the relative influence is smaller during dry periods, because then the top layer is fully unsaturated which means no evapotranspiration takes place.

2.2.4 Soil structures in the unsaturated zone

In clay the unsaturated zone is characterised by a soil structure, formed by cracks caused by swelling and shrinking of the clay and by biological activity, like animal digging and plant rooting. This soil structure has a large influence on the geotechnical characteristics of the soil. Clay itself has a low permeability, but the soil structure can cause the permeability to be much larger.

The technical report 'clay for dikes' (TAW, 1996) describes how the soil structure in clay is formed. Shrinking and swelling of clay is caused by drying and moisturising, which leads to formation of cracks and tears in the unsaturated zone. Larger cracks usually form vertically, while smaller tears may form in any direction. Besides cracking, the soil structure is also formed due to burrow digging by worms and moles. Below a grass cover a soil structure is formed in several years up to a depth of about 0,8 m. However, deeper in the flood defence a soil structure can also be present. In case of a strengthened dike deeper layers may have been a top layer in the past, and a soil structure can still be present. Plant and tree roots can also form structures deeper into the flood defence.

These soil structures have a strong effect on the permeability of the soil. In an initially well-compacted clay cover the permeability can increase from 10^{-6} m/s to 10^{-5} m/s in half a year due to formation of a soil structure. The permeability of clay cover layers is rarely lower than 10^{-5} m/s to 10^{-4} m/s due to soil structures.

In the earlier mentioned thesis of De Loor (2018) several simulations were performed using a top layer with soil structures (described as soil structure deterioration). It was found that this top layer is more influenced by water level changes due to the larger permeability. Furthermore, the top layer acts as a buffer zone for precipitation. Water that would normally run off over the slope is temporarily stored in the top layer and slowly released into the less permeable core of the dike.

For peat the same processes as for clay play a role, due to drying and moisturising cracks are formed (GeoDelft, 2005). Cracks play a large role for infiltration, because water that would normally run off the slope is collected in cracks and infiltrates at a larger depth. For evaporation the effect of cracks is of small influence.

From the various sources it is clear that the soil structure of the top layer of the flood defence can have a large influence on the phreatic surface. Because of its larger permeability and cracks, water is stored in the top layer and slowly released to deeper layers. This increases the amount of infiltration and therefore the rise of the phreatic surface. It is however difficult to determine the permeability when a soil structure is present.

2.3 Modelling the phreatic surface using numerical models

From literature it becomes clear that the height of the phreatic surface is mostly dependent on water levels and precipitation. The extent in which precipitation and changes of the water level influence the phreatic surface is largely determined by the soil composition and soil characteristics. Factors like soil structure deterioration, rubble, the geometry of the dike, and a road on the crest can have a large influence. This makes determining the height of the phreatic surface difficult when no measurements are available. A possible method to include all the listed factors of influences is the use of a numerical model. Several studies have been performed which involved modelling of the phreatic surface using a numerical model.

The earlier mentioned study of the field test described in Alterra (2013) also involved modelling the groundwater flow during this test, for which the model Hydrus-2D was used. For the set-up of this model, a soil survey had been executed. Several samples were taken to determine the saturated conductivity and retention characteristics of the unsaturated zone. The model showed that initially the precipitation flows downwards, but soon changes to more horizontal. By adding measurement points into the simulation at the same locations as the sensors in the field test it was possible to compare the model results to the actual measurements. The main difference occurs near the crest, near the toe the differences are smaller. At the start of the simulation the simulated phreatic surface below the crest is higher than in the measurements. Later the difference becomes smaller, but the simulated phreatic surface remains higher than the measurements. Halfway the cross-section the opposite is true; the model shows a lower phreatic surface than the measurements. In the report, the conclusion was drawn that a model like Hydrus-2D can be used to model the effect of precipitation on dikes, but to generate reliable model results it is necessary to have sufficient information about the soil. Furthermore reliable measurements of ground water level are necessary to calibrate the model.

The report of this test shows that a model can approximate the influence of precipitation on the phreatic surface, but several remarks can be made on this. In the model only extreme, artificially applied precipitation was modelled, and no dry periods were included. Additionally, the simulated period was relatively short and only one cross-section was modelled, so the experiences with the model are limited. Due to these aspects it is not evident that the model can be used in every situation. It is unclear how well the model approximates the location of the phreatic surface during dry periods, or after a precipitation event following a dry period.

As mentioned before, in Ten Bokkel Huinink (2016) the model PlaxFlow was used to determine the effect of precipitation on regional flood defences of three different soil types. However, because of the theoretical nature of the research no real measurement data of the phreatic surface was available to back up the results. Furthermore, the used models had a homogeneous cross-section which is rarely the case in practice.

In De Loor (2018) a PlaxFlow model was used as well. In this case the cross-section was modelled after a real flood defence, but no measurements of the phreatic surface were available and the simulations were not based on actual events. Furthermore, the research was aimed at river dikes and not regional flood defences. In most river dikes no continuous high water load is present, as is the case for regional flood defences.

All in all, it is unclear how accurate a numerical model simulates the position of the phreatic surface in a regional flood defence. In two of the mentioned studies (Ten Bokkel Huinink, 2016; De Loor, 2018) no actual measurement data was available to verify the results. In another study (Alterra, 2013) actual measurement data was present, but it is unclear whether the results can be applied to a longer time period or to other cases.

3 Numerical model

The central element in the research method presented in chapter 1 is a numerical model to simulate the groundwater flow in a regional flood defence. There are many such models that could potentially be used. In order to understand the theoretical background behind these models, first the basic theory on groundwater flow is described. Next, an assessment is made of the numerical models that are suitable and available for the research. Based on this assessment a choice is made between these models.

3.1 Theory on groundwater flow

Groundwater flow can be separated into flow in the saturated zone and flow in the unsaturated zone. The saturated zone is the area below the phreatic surface, where the pore water pressures are higher than the atmospheric pressure. In the unsaturated or vadose zone water can also be present due to capillary rise and infiltration of precipitation.

3.1.1 Saturated flow

The basis for calculation models of saturated flow is Darcy's law and the law of conservation of mass. According to (TAW, 2004), Darcy's law is defined as follows for homogeneous and incompressible fluids and isotropic permeability:

$$q_x = -K \frac{\partial \varphi}{\partial x}$$
$$q_y = -K \frac{\partial \varphi}{\partial y}$$
$$q_z = -K \frac{\partial \varphi}{\partial z} \qquad (3.1)$$

Where:

q	=	specific discharge	(m/s)
K	=	hydraulic conductivity	(m/s)
φ	=	hydraulic head	(m)
z	=	location height with respect to reference level	(m)
ρ	=	water density	(kg/m^3)
g	=	gravitational acceleration	(m/s^2)

The hydraulic conductivity K represents the ability of the soil to transmit fluid. It is a property of both the soil and the fluid. To exclude the effect of the viscosity of the fluid the intrinsic permeability k is defined, which is independent on the fluid characteristics. The relation between the hydraulic conductivity and intrinsic permeability is expressed as (Todd & Mays, 2005):

$$k = \frac{K\mu}{\rho g} \qquad (3.2)$$

Where:

k	=	intrinsic permeability	(m/s)
K	=	hydraulic conductivity	(m/s)
μ	=	dynamic viscosity	(N s/m^2)
ρ	=	fluid density	(kg/m^3)
g	=	gravitational acceleration	(m/s^2)

Since water is the only relevant fluid for the flow in regional flood defences, the hydraulic conductivity is used in this thesis.

In the equations 3.1 it was also assumed that the hydraulic conductivity was isotropic, i.e. equal in all directions. For anisotropic soils the conductivity can be divided in an x, y, and z direction. Often the conductivity in vertical (z) direction is smaller than in the horizontal (x, y) directions. Therefore often a horizontal (K_h) and (K_v) vertical conductivity are used to specify the hydraulic properties of a soil.

Law of conservation of mass

For stationary flow the hydraulic conductivity and the geometry of the soil are sufficient to calculate the groundwater flow. In these conditions the continuity equation applies (TAW, 2004):

$$\frac{\partial q_x}{\partial x} + \frac{\partial q_y}{\partial y} + \frac{\partial q_z}{\partial z} = 0 \tag{3.3}$$

This means the total amount of fluid in the soil does not change. The inflow of water is equal to the outflow of water.

For non-stationary flow the amount of water changes and therefore equation 3.3 does not hold. In order to comply to the law of conservation of mass storage has to occur. There are two types of storage (TAW, 2004):

- Phreatic storage: occurs when the rising groundwater table fills the pore space in the soil. The storage capacity is therefore dependent on the porosity.
- Elastic storage: occurs when the effective stress in the soil changes. This happens if the pore pressure changes while the total stress remains the same. This changes the pore space and therefore the amount of water that can be stored. The water itself may also be compressed when gases are present in the pore space. The elastic storage capacity is dependent on the stiffness of the soil. Clay and peat have a larger elastic storage capacity than sand. The amount of elastic storage is significantly smaller than the phreatic storage.

For phreatic storage the continuity equation is defined as:

$$n\,\frac{\partial h}{\partial t} + \frac{\partial (h q_x)}{\partial x} + \frac{\partial (h q_y)}{\partial y} = N \tag{3.4}$$

Where:

h	=	hydraulic head with respect to the base of the considered soil layer	(m)
N	=	net infiltration due to precipitation	(m/s)
n	=	effective phreatic porosity	(-)

For elastic storage the continuity equation is defined as:

$$(m_v + n\beta)\frac{\partial u}{\partial t} = \frac{\partial q_x}{\partial x} + \frac{\partial q_y}{\partial y} + \frac{\partial q_z}{\partial z} \tag{3.5}$$

Where:

m_v	=	compressibility of the soil	(m^2/N)
β	=	compressibility of the water	(m^2/N)

Combining Darcy's law and the continuity equation, a differential equation describing the ground water follows. In order to solve this equation initial- and boundary conditions are required.

This equation can be solved using an analytical or a numerical model. Analytical models are more transparent and need less input parameters than numerical models. However, a strong schematisation of the geometry is necessary and therefore an analytical model is only suited for relatively simple situations. This means an this type of model is not suited for this research, a numerical model needs to be used.

Several types of numerical models can be distinguished (TAW, 2004):

- Finite difference method (implicit or explicit);
- Finite element method;
- Analytical function method;
- Boundary integral method.

The last two methods are not commonly used. Most models use the finite element method (FEM), since it allows the most freedom in modelling complex geometry.

3.1.2 Flow in the unsaturated zone

Apart from the flow in the saturated zone, the flow in the unsaturated zone can also be important. Groundwater recharge by precipitation first has to flow through the unsaturated zone before the saturated zone is reached. The flow in the unsaturated zone has different characteristics than the flow in the saturated zone. The pores are partially filled with air and therefore the permeability is lower. The unsaturated permeability is dependent on the water content of the soil, and therefore on the saturation. The saturation is in turn dependent on the pore pressure, which is negative due to capillary rise (suction). The relation between this suction and the saturation is described by a so-called water retention curve. The shape of this curve can be hysteretic. This means that the curve follows a different path when the suction pressure increases than it does when it decreases. Several models are available to describe the water retention curve. A commonly used model is the Brooks and Corey model. However, the Van Genuchten model (1980) includes more soil parameters and is therefore a more accurate representation of reality. The Van Genuchten model defined as follow:

$$S_{eff} = \begin{cases} 1, & p_c \leq 0 \\ [1 + (\alpha p_c)^n]^{-m}, & p_c > 0 \end{cases} \tag{3.6}$$

Where:

$$S_{eff} = \frac{\theta - \theta_{res}}{\theta_{sat} - \theta_{res}} \tag{3.7}$$

S_{eff} = effective saturation
θ = water content
θ_{res} = residual water content, the amount of water that always remains in the soil
θ_{sat} = saturated water content, water content in saturated conditions

p_c = capillary suction pressure
α = parameter related to air entry suction
n = parameter related to pore size distribution
m = 1 – (1/n)

The parameters α and n are dependent on soil characteristics. From the effective permeability the relative permeability can be calculated:

$$k_r = (S_{eff})^{1/2}\left[1-\left(1-(S_{eff})^{\frac{1}{m}}\right)^{m}\right]^2 \tag{3.8}$$

The relative permeability is the ratio of the unsaturated permeability to the saturated permeability:

$$k_r = \frac{k_{unsat}}{k_{sat}} \tag{3.9}$$

3.2 Possibly suitable models

Various groundwater flow models exist that might potentially be suitable for this research. In order to be suitable the model has to fulfil at least the following requirements:

- It should be able to compute transient groundwater flow;
- It should be able to include precipitation and evapotranspiration;
- It should be able to model the sometimes complex geometry of the subsoil of regional flood defences.

There are several models or programs that fulfil these requirements and therefore could be suitable for the research. The models found to meet the requirements are described in the following paragraphs.

3.2.1 D-Geo Flow

D-Geo Flow is a Deltares software module used to calculate 2D groundwater flow. It uses the finite element model DgFlow, and also includes module for piping. Several types of boundary conditions can be applied to the model: these are head, flux, seepage, submerging and no-flow boundary conditions. Furthermore the program has the ability to model the unsaturated zone using the Van Genuchten model to calculate the relative permeability (Deltares, 2018).

D-Geo Flow is a relatively new program, as of 2018 it has not been fully released yet. This means not much experience in using the software has been gained yet, and some issues are still present in the program. In addition to this, the user manual is relatively short and seems to be unfished. These aspects could lead to some problems if D-Geo Flow is used for the research.

3.2.2 COMSOL

COMSOL Multiphysics is a finite-element analysis simulation software for multiple fields in physics. Several modules are available for electrical, mechanical, fluid and chemical applications. One of these modules is the subsurface flow module, which is used to simulate flow in porous media. This module allows for simulation of flow in unsaturated porous media and water retention using the Van Genuchten and Brooks and Corey formulations. Additionally, it is possible to simulate flow in fractures (COMSOL, 2013). COMSOL has the possibility to run models via MATLAB files. A disadvantage is that it appears that no boundary condition can be applied to include evapotranspiration dependent on the saturation of the soil.

3.2.3 PlaxFlow

PlaxFlow is an add-on module to the finite element program PLAXIS 2D. PLAXIS by default has options to model stationary groundwater flow, but the PlaxFlow addon enables the option to model transient groundwater flow. Several options are available to model the unsaturated soil behaviour, like Mualem-Van Genuchten, approximate Van Genuchten and user-defined soil water retention curves. Furthermore, various pre-defined data sets are included for common soil types. The program allows for time dependent boundary conditions, which means precipitation can be modelled. It is also possible to include an evaporation flux. The evaporation flux is only applied when the top of the soil is not fully unsaturated (PLAXIS, 2018).

3.2.4 HYDRUS 2D/3D

Hydrus is a software package for simulating water, heat and solute movement in 2- and 3-dimensional variably saturated media. The program can handle several types of boundaries, which can vary over time. The unsaturated soil properties are described using various functions, among which Van Genuchten, Durner, and Brooks and Corey. Hysteresis of the water retention curve can also be implemented. Furthermore, add-on modules are available to model complicated phenomena like dual permeability, which can be used when cracks are present in the soil. However, these modules are only recommended for experienced users. Evapotranspiration can be modelled by using input data for potential evapotranspiration. HYDRUS adds this as outward flux dependent on water availability (Šimůnek, Van Genuchten, & Šejna, 2018).

3.2.5 MODFLOW + FloPy

MODFLOW is a modular finite-difference flow model from the U.S. Geological Survey. It is considered an international standard in groundwater flow modelling. The source code is in the public domain and therefore free to use (USGS, 2018). Due to this, numerous commercial and non-commercial interfaces exist. FloPy is an interface that uses the programming language Python to run MODFLOW models. It includes many of the available MODFLOW packages (Bakker, et al., 2018).

Modflow also includes a package to model the flow in the unsaturated zone. However, this package uses the Brook and Corey model and has no option to use the van Genuchten model, which is more commonly used. However, this package does include options to model groundwater recharge and evapotranspiration dependent on the saturation of the soil. Furthermore, packages are included to include these effects without modelling the unsaturated zone.

An advantage of using FloPy to write input for the model is that there are various Python packages available to facilitate the input and output of the model. This means input and output can directly be processed without transferring the data to another program.

The advantages and disadvantages of each program/model are summarised in table 3.1.

Table 3.1: Advantages and disadvantages of several numerical models

Model	Advantages	Disadvantages
D-Geo Flow	• Specifically aimed at flood defences • Same software series as commonly used software for stability analyses	• New program, so not much experience to build on • No possibility to run via scripting tool • No possibility to include evapotranspiration dependent on water availability
COMSOL	• Two possible formulations for the unsaturated zone • Possibility to use with MATLAB	• No possibility to include evapotranspiration dependent on water availability
PlaxFlow	• Several formulations available for the unsaturated zone, including user defined • Predefined data sets included • Evaporation flux dependent on water availability	• No possibility to run via scripting tool
HYDRUS	• Several formulations available for the unsaturated zone • Possibility to include hysteresis • Evaporation flux dependent on water availability	• No possibility to run via scripting tool
MODFLOW + FloPy	• In Python, so broad possibilities to facilitate in- and output • MODFLOW is an international standard • Evaporation flux dependent on water availability	• Works with rectangular elements, so slope cannot be modelled as smooth surface • Unsaturated zone can only be modelled using Brooks and Corey.

3.3 Model choice

From the models in table 3.1 the choice was made to use MODFLOW 6 in combination with FloPy. This choice was made for the following reasons:

- With the use of FloPy the input and output of the Modflow model can be controlled using Python. This means there are no limitations imposed by a graphical user interface, which enables various possibilities, like reading the desired precipitation values from a csv file for a specified period, to use Python libraries to plot the output of the models, and many other options.
- Modflow is an international standard in groundwater modelling.
- Completely open source, so no licenses are required.

A disadvantage is that the unsaturated zone can only be modelled using the Brooks and Corey formulation, which uses less parameters than the more recent Van Genuchten formulation. On the other hand, modelling of the unsaturated zone also requires extra parameters to be specified, which induces uncertainties to the input of the model. Therefore an option worth considering could be to exclude the unsaturated zone in the model. Both these options will be investigated.

3.3.1 Model grid

In Modflow 6 there are two possible types of grid to construct the model (Langevin, et al., 2017):

- Regular grid: a rectilinear grid consisting of layers, rows and columns;
- Unstructured grid: The cells need not be rectangular in the horizontal direction, and the number of connections between cells may vary per cell. Unstructured grids offer more flexibility in constructing models with complex geometry.

These grids only are different in the horizontal direction. Both grids use cells with a horizontal top and bottom. Since the model is constructed in 2 dimensions, the grid choice is irrelevant. A regular grid is easier to use because the cells in a regular grid are specified by the indices of the layer, row, and column, which makes it easy to specify input and to obtain output for the cells. For this reasons a regular grid is chosen for the model.

In a regular grid, the rows and columns represent the horizontal dimensions and the layers represent the vertical dimension. The width and length of the cells has to be constant, but the height can vary per cell. This makes it possible to specify one model layer for each layer of soil. Another possibility is to keep the grid rectilinear in vertical direction, so that all cells in a layer have the same top and bottom elevation. The soil type is then specified for each cell. These two options are illustrated in figure 3.1.

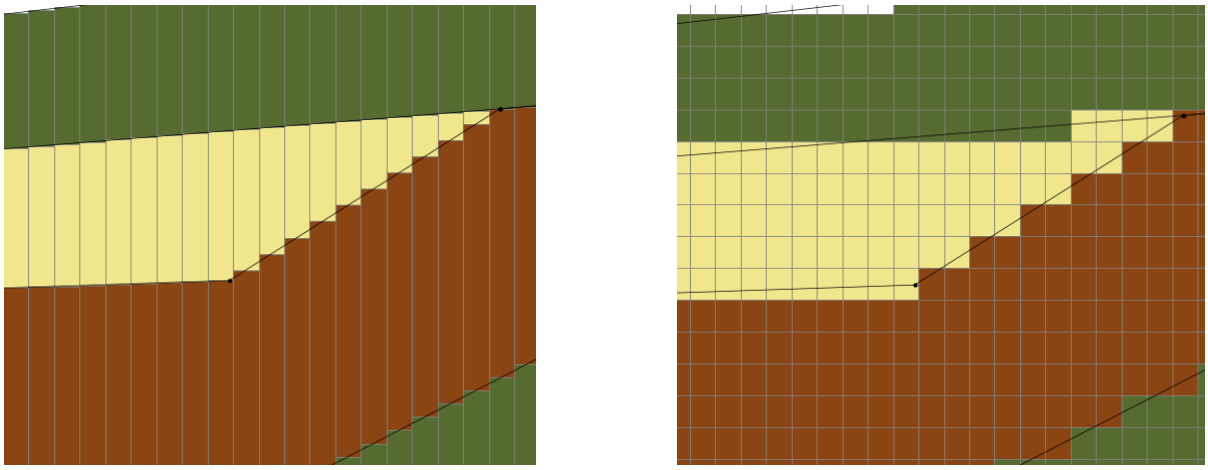

Figure 3.1: Options to construct a regular grid in Modflow. Left: using different elevations in a single layer. Right: using strictly horizontal layers. The number of columns in horizontal direction is the same for both options.

It can be observed that the possibility to use different elevations for each layer allows for a much finer resolution in vertical direction. The boundaries between layers are much smoother than when strictly horizontal layers are utilised, while the number of columns in horizontal direction is the same. Furthermore, the first option uses only 4 layers in the example, while the second options uses 21 layers. The calculation times using option 1 are therefore shorter. A disadvantage of using only one layer per soil type is that only one pore pressure is calculated for the entire height of the layer, meaning a variation of the hydraulic head over the head of the layer cannot be observed. However, this research considers the phreatic surface and therefore one head per layer is sufficient. For this reason, and the comparatively faster computation time, the choice was made to use the first option.

Using this method a difficulty arises for layers that do not extend along the entire width of the model, like the intermediate (yellow) layer in figure 3.1. On the left boundary of the model 4 layers exist, while on the right boundary only three layers exist. However, the number of layers cannot vary in the horizontal directions of the model. To overcome this problem the following method from the Modflow manual is used (Langevin, et al., 2017): The height of the cells on the locations where the layer does not exist is set to a very small number, and these cells are specified to be non-existent in the model. For a non-existent cell Modflow directly connects the cells above and below the non-existent cell.

Another consequence of choosing this grid type is that layer boundaries under a steep angle have to be treated with care. At steep angles the vertical shift between the cells is large, resulting in vertical staggering of the grid. This concept is illustrated in figure 3.2. Due to the large vertical shift combined with the small height of the middle layer, the cell of the middle layer in the right column is not bordering the cell of the middle layer in the adjacent column. Since a Modflow cell

only has horizontal connections to cells in the same layer, this leads to inaccurate flows between the cells.

Since the research only a considers a cross-section, the model is two dimensional. In longitudinal direction the model only spans a single cell. For the resolution a row and column width of 0,25 m is chosen. If the results show this is too small or too large, this value can be adjusted.

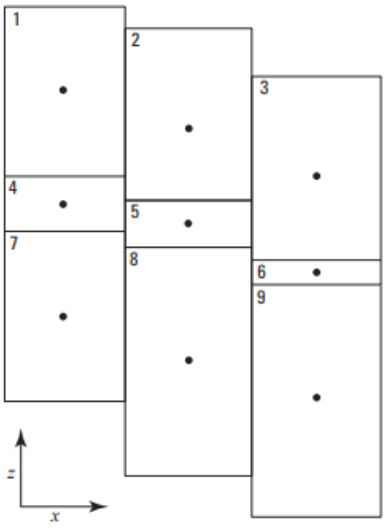

Figure 3.2: Vertical staggering of a Modflow grid. Source: Langevin, et al., 2017

Construction of the grid

The model grid has to be constructed based on a schematisation of the profile of the flood defence. In order to easily modify the resolution of the grid, the choice was made to define the schematisation as a number of connected points, and to write a Python script to construct a grid from these points and a specified resolution. The script was built such that a schematisation can be drawn in the program D-Geo stability. This program, used for stability analyses of flood defences, offers the option to export a schematisation. This export is written in the form of a text file and can be read by a Python script. In this file the schematisation is defined in soil layers, which can be converted to layers in Modflow. Layers that pinch-out in the cross-section are assigned a layer height of 1 mm for the length along which the layer does not exist, and the cells along this length are automatically specified as non-existent. This method using D-Geo Stability to draw a schematisation makes it possible to easily adjust the schematisation, or to construct a new model.

3.3.2 Time discretisation

The timing of a simulation in Modflow is subdivided in two units: stress periods and time steps (Langevin, et al., 2017). Stress periods are used to make a change in the boundary conditions of a model. Stress periods are subdivided into time steps. The number of time steps can be specified for each stress period separately, and it is also possible to vary the length of the time step over the duration of the stress period. Parameters of the boundary conditions, for example water levels and recharge rates, can be specified for each time step. Since the boundary conditions themselves do not change, one single stress period is sufficient for the simulations in this research. The measurement and precipitation data are available for hourly intervals, so a time step of hour is used for the simulations.

3.3.3 Initial conditions

For the start of the model initial conditions have to be specified, in the form of a groundwater head for each cell in the model. For the upper layers the measurements of the phreatic surface could be used, but these only provide information at a few points along the cross-sections. This means the initial conditions for the other cells have to be estimated by interpolation, which is unlikely to represent an equilibrium situation of the model.

Another option is to start the simulation with a steady-state stress period. The results of this stress period are than automatically used as initial conditions for the next, transient, stress period, in which the actual simulation is performed. For the steady-state stress period initial conditions still have to be provided, but these have no effect on the outcome because an equilibrium situation is calculated. The initial conditions only determine the amount of time steps required in the simulation to reach this equilibrium. The outcome of the steady-state simulation will probably not match the first the first measurements of the monitoring wells. The first measurements are influenced by the precipitation and evapotranspiration in the period before. Therefore the transient part of the simulation has to start at an earlier point in time than the start of the measurements, so that the model can adjust to the transient conditions.

4 Research cases

The research is centred around a number of case studies. In chapter 1 several requirements for the research cases were listed:

- Pore pressure data is available from monitoring wells or pressure sensors;
- The case should be representative for a typical regional flood defence;
- Data for water levels, precipitation and evapotranspiration can be acquired for the case.

Three research cases from two different research projects were chosen to be analysed. Two of these cases are located in the management area of the water board of Delfland, and the third research case is located in the management area of the water board of Rijnland. In figure 4.1 the geographical locations of the research cases are displayed.

Figure 4.1: Locations of the research cases

4.1 Vlaardingsekade (Delfland location 24)

In the period 2010-2014 the water board of Delfland has conducted a programme in which monitoring wells were placed in nine regional flood defences. The hydraulic head in these monitoring wells was measured over a period of about 4 years (Delfland, 2016). Due to this long measurement period the seasonal influences of several years are included.

From these nine locations two locations are chosen as research cases: the locations 24 and 25 near the village of Schipluiden, close to Delft. These locations are situated relatively close to each other (about 500 m apart) on the same storage channel. The proximity of the two locations gives the advantage that the same precipitation can be used for both research cases. At both locations

three monitoring wells were installed, while at most other locations only two monitoring wells were used. These considerations have led to the choice for these two locations.

Location 24, the Vlaardingsekade, is located on the eastern side of the Vlaardingsevaart, a canal which is part of the boezem-system of Delfland. The dike contains two pavement structures: a footpath on the crest and a road on the berm. At the toe of the dike formerly a drainage ditch was located; however, this ditch was filled in sometime between 2005 and 2010. Enquiry at the water board made clear that this ditch had been filled in before the monitoring wells were placed. A new drainage ditch was excavated in 2017, which means during the measurements no drainage ditch was present.

Three monitoring wells were installed in the flood defence: one in the crest, one in the slope, and one near the toe. However, the monitoring well near the toe was placed on the opposite side of the former drainage ditch. Since the ditch was filled with sand, it can be expected that most of the groundwater flow will take place through this former ditch, in which case the monitoring well provides no meaningful information about the phreatic surface in the dike. On the other hand it still provides information about the groundwater table on the inside of the dike, which is useful to determine the boundary condition at the polder side of the model.

A drawing of the cross-section of location 24, including the locations of the monitoring wells, is included in appendix E. The locations of the three monitoring wells are also indicated in figure 4.2.

Figure 4.2: Location of the monitoring wells at location 24.

4.2 Duifkade (Delfland location 25)

The second research case within Delfland is located about 500 m to the south of location 24, on the western bank of the same Vlaardingsevaart. The main difference between the dike at this location and location 24 is the lack of pavement: the dike is completely covered with grass. This means the infiltration characteristics are different to location 24, which could result in a different response of the phreatic surface to precipitation.

Inland of the dike a drainage ditch is present. This ditch located about 5 m removed from the toe. Three monitoring wells were placed in the cross-section: one in the crest, one in the slope near the toe and one near the drainage ditch.

The locations of the three monitoring wells are indicated in figure 4.3. A drawing of the cross-section of the dike is included in appendix E.

Figure 4.3: Locations of the monitoring wells at location 25.

4.3 Hogedijk (Rijnland)

The third research case in this thesis is located in the management area of the water board of Rijnland. The companies Iv-Infra and Nectaerra are conducting a research project on several regional flood defences of this water board with the aim to investigate whether it is possible to determine the position of the phreatic surface by hydrological analysis and modelling based on field measurements (Nectaerra, 2018). During the writing of this thesis, initially measurements from August until October 2018 were available, but after a new readout this period was extended to January 2019. In most of the cross-sections in this project four monitoring wells were placed, and in addition to that field measurements of the conductivity were carried out. Although the measurement period is much shorter than for the other two locations in Delfland, more information is available thanks to the extra monitoring well and the conductivity measurements. For this reason a case from this research project was used as the third research case for this thesis.

The research project involves four regional flood defences, in some of which monitoring wells were placed in two cross-sections. The dike chosen for analysis in this thesis is the Hogedijk near Aarlanderveen. This dike was chosen for the following reasons:

- The dike is also subject of a reinforcement project. The design for this reinforcement is drafted by Iv-Infra, which means a lot of information on the dike can readily be obtained.
- In the measurement period a precipitation event has occurred with a volume of about 95 mm; at some of the other locations this occurred as well, but the precipitation volume at the Hogedijk was the highest. It could be interesting to investigate how accurate this extreme event can be simulated in the model.

A disadvantage of choosing this location is that the measurements started about a month later than at the other locations. However, the amount of precipitation during that month was small, so no interesting events are excluded due to the later start of the measurements.

Like Delfland, Rijnland has a boezem-system, but the Hogedijk is not located directly on this boezem. The outside water is part of a polder with a much higher water level than the polder behind the dike. This slightly different situation compared to the other research cases has no influence on the modelling of the phreatic surface. The main difference between the Hogedijk and the two cases in Delfland is the composition of the dike: the Hogedijk consists primarily of peat, which is not present in the dike body for the two cases in Delfland, only in the subsoil.

Monitoring wells were placed in two cross-sections of the Hogedijk. The main difference between these cross-sections is the inside water level; one of the cross-sections is located at an area with a locally higher water level. This cross-section was not chosen for this thesis. The locally higher water level is not included in the documentation of Rijnland, and therefore the exact water level is unknown and it could also be subject to fluctuations. Furthermore, the other cross-section showed more interesting fluctuations in the measured heads.

Figure 4.4: Location of the monitoring wells and the rain gauge (blue square) at the Hogedijk.

The chosen cross-section (indicated as HGD-1) contains four monitoring wells. All are located on the inner slope, with the furthest outward well near the inner crest, and the furthest inward well located about 10 m removed from the drainage ditch. Furthermore, a rain gauge was installed about 70 m removed from the cross-section. The

locations of these objects are displayed in figure 4.4. A drawing of the cross-section of the dike is included in appendix E.

4.4 Measurement data

4.4.1 Location 24

The cross-section of location 24 including the monitoring wells is displayed in figure 4.5. The filters of the monitoring wells are indicated as a lighter colour.

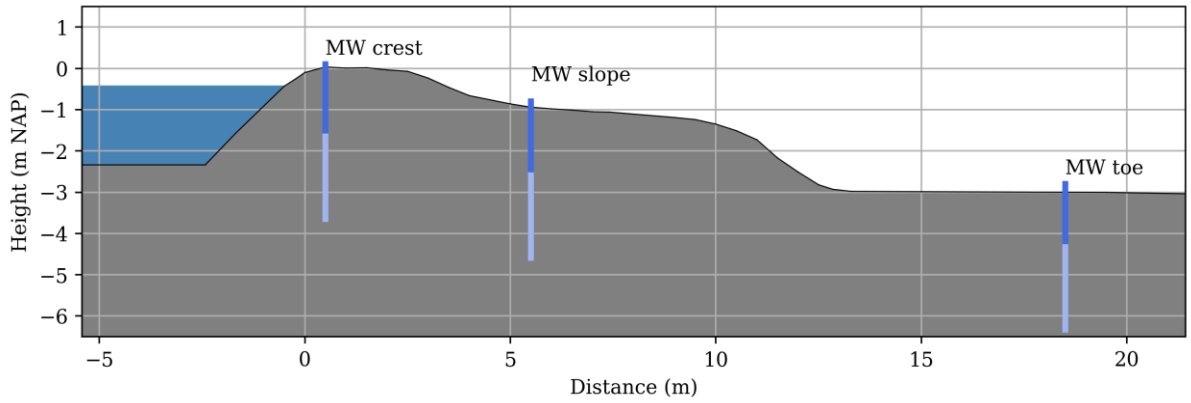

Figure 4.5: Cross-section and location monitoring wells (MW) Delfland location 24

The head measurements of the three monitoring wells are displayed in figure 4.6. The total measurement period for location 24 runs from 02-06-2010 until 07-07-2014, which is a period of just over 4 years. Three manual measurements were carried out during the measurement period, which are displayed as crosses. Larger plots of the measurements are included in appendix D.

Figure 4.6: Monitoring well measurements Delfland location 24, from 01-06-2010 until 07-07-2014

For only a part of the total period measurements are available from all three monitoring wells. Due to changes in the filters and errors of the data loggers large parts of the data are missing. At some points shifts in the measurements can be observed, where the average level of the head changes. An example of this can be seen in July 2011, in the monitoring well in the toe. The reason is probably a readout of the logger. After a readout the baseline of the measurement has to be reset based on a manual measurement. If this measurement is incorrect, this will lead to a shift of

the baseline of the data. In appendix D all holes and discrepancies in the measurement set are listed.

4.4.2 Location 25

The cross-section and locations of the monitoring wells for location 25 are displayed in figure 4.7.

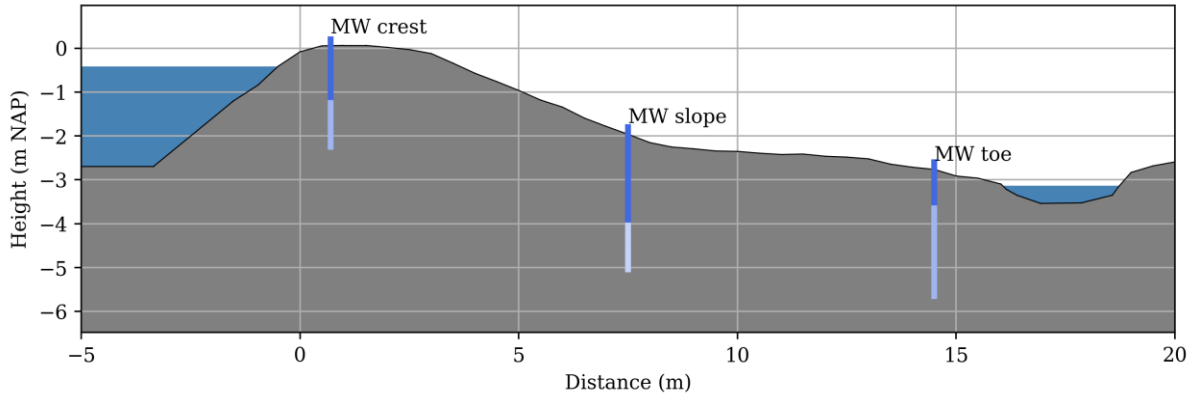

Figure 4.7: Cross-section and location monitoring wells (MW) Delfland location 25

The total measurement period for location 25 runs from 01-06-2010 until 22-10-2014. In this period four manual measurements have been carried out. The measurements are displayed in figure 4.8, larger plots are included in appendix D.

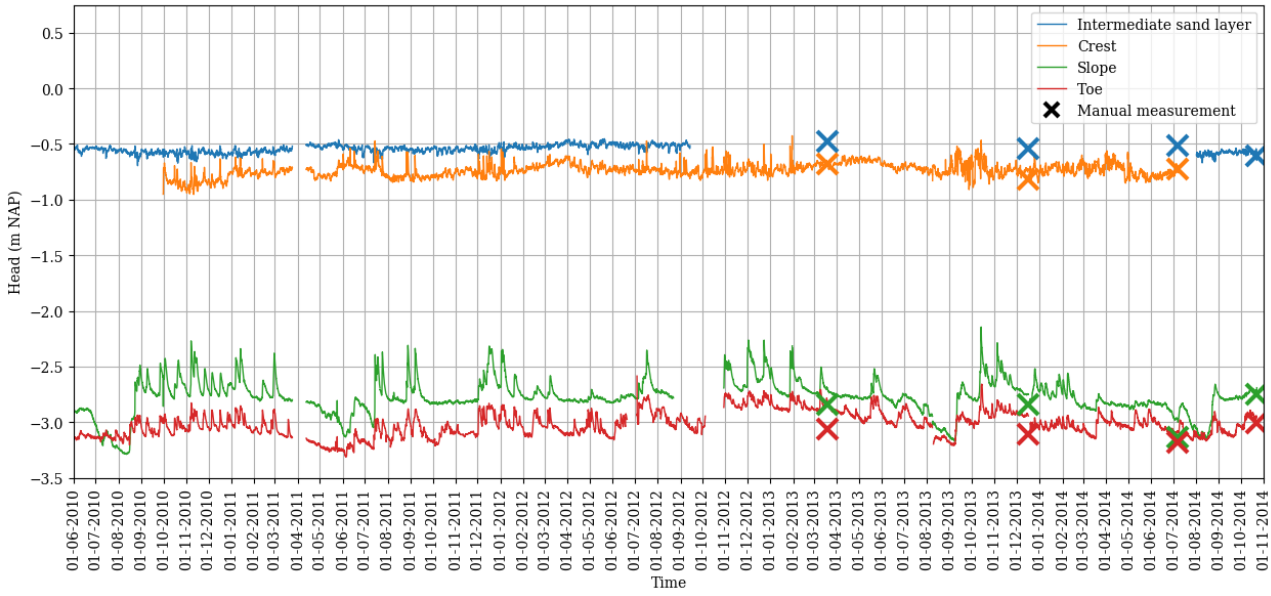

Figure 4.8: Monitoring well measurements Delfland location 25, from 01-06-2010 until 22-10-2014

The monitoring well in the crest was placed in an intermediate sand layer, which had the result that the phreatic surface was not measured. Therefore later another monitoring well was placed with a higher filter. The first monitoring well was not removed, and provides information on the head in the intermediate sand layer. Several gaps are present in the data set, but these are smaller than for location 24. Like location 24, several shifts in the baseline of the data can be observed. In appendix D all holes and discrepancies in the measurement set are listed.

The several shifts recorded in the data for both locations indicate that not all parts of the data are equally reliable. It is unclear how reliable the manual measurements are. Since the jumps in the data have a magnitude of about 10 to 15 cm, it can be argued that on average the height of the

phreatic surface is known with an accuracy of about 15 cm. The magnitude of the fluctuations compared to the baseline is likely to be more accurate.

Measurements Hogedijk
The locations of the four monitoring wells in the Hogedijk are displayed in the cross-section in figure 4.9.

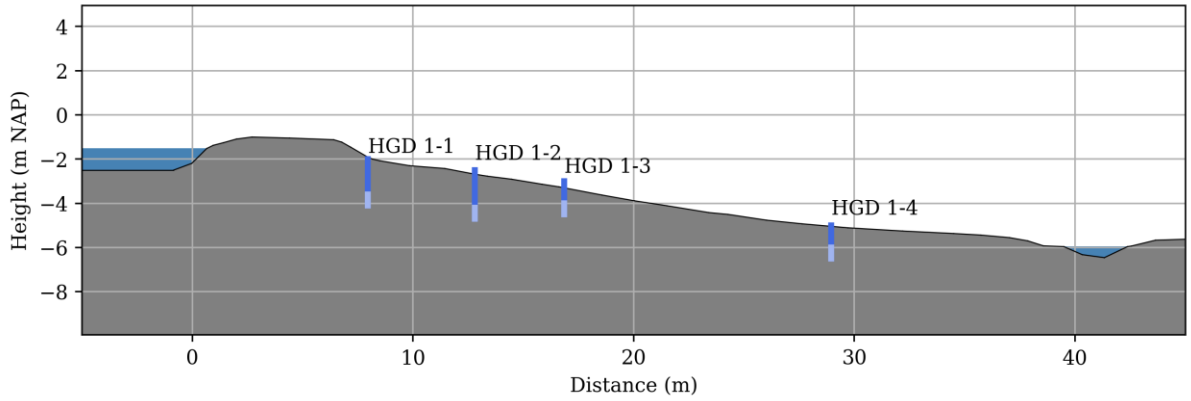

Figure 4.9: Cross-section and location monitoring wells Hogedijk

The research project including the Hogedijk was ongoing during the writing of this thesis. During the set-up and calibration of the model only measurements from 23-08-2018 until 12-10-2018 were available. Later a new readout was performed, which extended the available measurement set to 07-01-2019. This full measurement set is displayed in figure 4.10. No gaps are present in the measurements. No failures have occurred during the so far relatively short measurement period, and no measurements were removed from the data set. Notable is that the heads show a gradual increase until about December 2018. This increase is caused by the dry summer of 2018, after which it took several months for the phreatic surface to return to a more normal level. The gradual increase is therefore not a discrepancy in the measurements.

Some other phenomena can be observed in the data for which no clear explanation could be found. These phenomena were discussed in a meeting with Nectaerra, the company that carries out the measurements. From this meeting more insights were obtained regarding the discrepancies found in the data.

One of the phenomena can be observed in the measurements of the monitoring well at the inner crest (HGD 1-1). For several periods, the head is at an increased level, after which it suddenly drops back to baseline level. Outside of these periods the head fluctuations are quite small. The elevated periods are caused by submerging of the pressure logger. When this occurs the air pressure cannot be measured, and since the head is determined by subtracting the air pressure from the water pressure this results in unreliable measurements. The measurements even exceed the top of the monitoring well, which is physically impossible. The data was therefore topped off at this level, which is at NAP -2,15 m, which results in the plateaus observed in figure 4.10. Due to their unreliability, the elevated periods should be removed from the data when the measurements are analysed.

Another remarkable observation is that the measurements of HGD 1-2 and HGD 1-3 show different fluctuations, despite being placed relatively close to one another. HGD 1-2 shows a very small and damped reaction to precipitation events, whereas HGD 1-3 shows much larger peaks, which are more comparable to the peaks observed for the research locations in Delfland. This difference is most likely a results of cracks in the dike. Many large cracks are present in the dike, some of which are several centimetres wide. HGD 1-3 is probably connected to such a crack. Runoff water from the surface can reach the monitoring well through the crack, resulting in a

more direct and larger head rise. Another factor of influence causing large peaks is rise of the pore pressures due to the increased weight of the topsoil when it becomes saturated by precipitation.

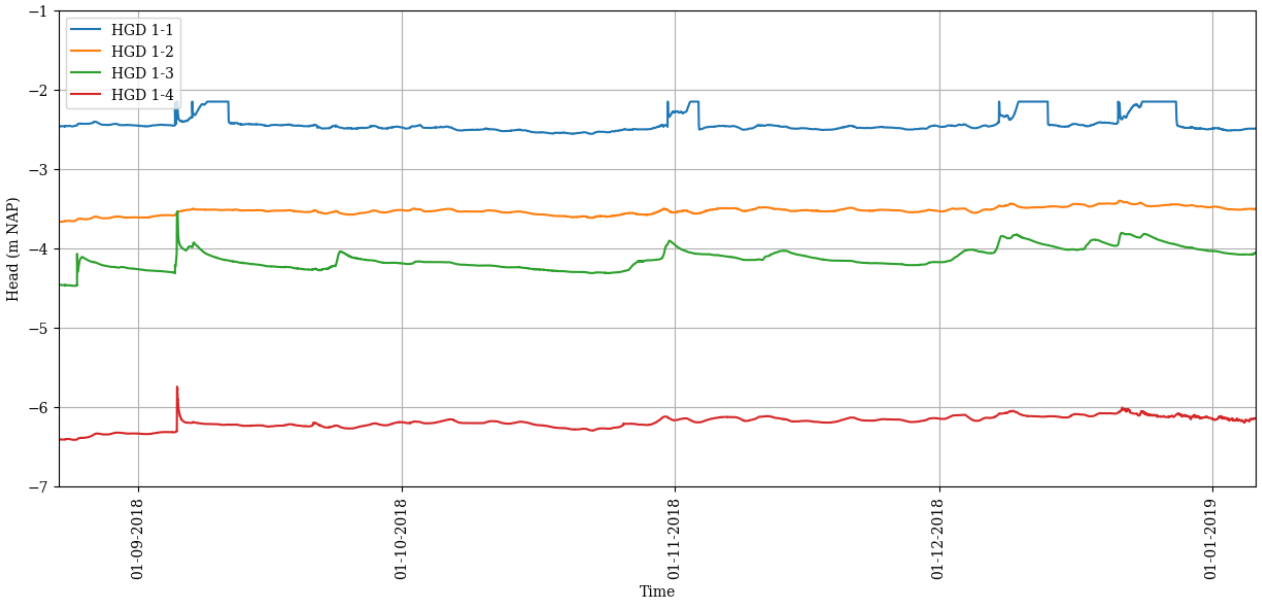

Figure 4.10: Monitoring well measurements Hogedijk, from 23-08-2018 until 12-10-2018

4.5 Influence of precipitation on the phreatic surface

To analyse the reaction of the phreatic surface to precipitation, the heads in the monitoring wells were plotted together with the precipitation and potential evapotranspiration data. These plots are included in appendix D. In chapter 5 the source of this evapotranspiration and precipitation data is discussed.

In the plots of the measurements the precipitation events can easily be recognised: the heads suddenly rise, and then slowly return towards the initial water level. To analyse the speed and the magnitude of these responses of the heads, the precipitation events for the research locations in Delfland were analysed. This analysis was not performed for the Hogedijk because of the small number of precipitation events included in the dataset.

First the precipitation events had to be identified from the precipitation data. A period of precipitation had to meet several criteria to be marked as a precipitation event in order to keep the number of events at a manageable level. These criteria were the following:

- A minimal precipitation rate of 0,1 mm per hour to start the event; this criterion was needed to exclude hours of very low intensity precipitation from the event.
- An event can have a maximum of 6 consecutive hours in which the precipitation is lower than the specified minimal precipitation rate of 0.1 mm/hour.
- The total amount of precipitation over the event is more than 20 mm.

Using a Python script, the precipitation events were identified based on these criteria. Over the period from 01-06-2010 until 22-10-2014 37 precipitation events were identified. To analyse the effect of each event on the heads in the monitoring wells a plot was made for each event. These plots included the precipitation and the head in each of the monitoring wells over the duration of the precipitation event plus an additional 24 hours. For each event the time after which the monitoring wells responded to the precipitation was determined manually, since this could not be automated properly. The total rise of the head for each event was determined using the Python script.

4.5.1 Location 24

For location 24, it was observed that the response of the heads is dependent on the shape of the precipitation. If the event starts with a high intensity of several mm per hour, the response of the heads can be observed quite clearly. However, if the event starts with several hours of lower intensity the response time is much harder to define. When the event is preceded by another precipitation event the heads can even still be declining for several hours after the start of the new event, before a new rise is observed.

The heads at the crest, slope and toe show no clear order in the time between the start of the precipitation and the response. Generally, the response starts in the same hour for all three locations. If there is a consistent sequence in which the monitoring wells respond, this occurs on a timescale smaller than an hour. On average the three wells respond after 4-5 hours after the start of the precipitation.

For the peak of the head rise a more clear sequence can be observed. For most events the toe reaches the peak of the head rise first, then the slope, and finally the crest. An example of this is given in figure 4.11. All three heads start to rise at the same time, but the toe reaches its peak earlier than the crest and the slope.

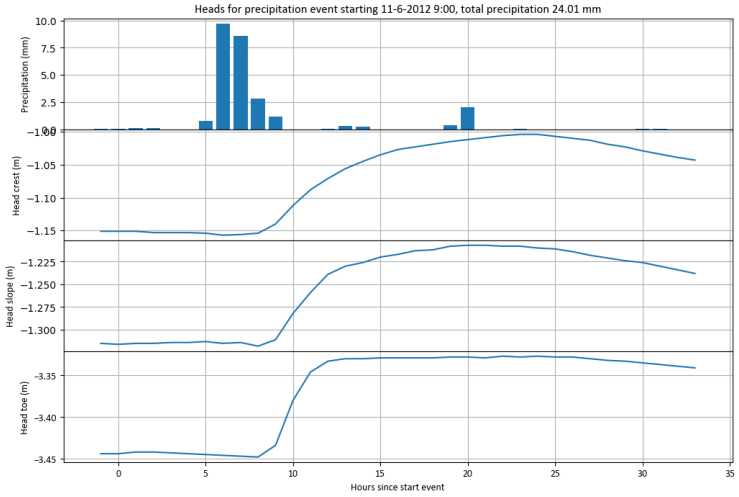

Figure 4.11: Response of the heads in the monitoring wells at location 24 for a precipitation event on

To analyse whether the order in which the peaks are reached is related to the precipitation intensity, several precipitation events are displayed in figure 4.12. On the x-axis the rank of the events is displayed, where 1 corresponds to the event with the highest volume of precipitation. The amount of precipitation is displayed on the y-axis. The colour of the bars indicates the sequence order in which the peak head rise was reached. The bars of the events for which no data was available for all three monitoring wells are left blank. For only 7 of the 33 events with a volume larger than 20 mm the heads for all three monitoring wells were measured.

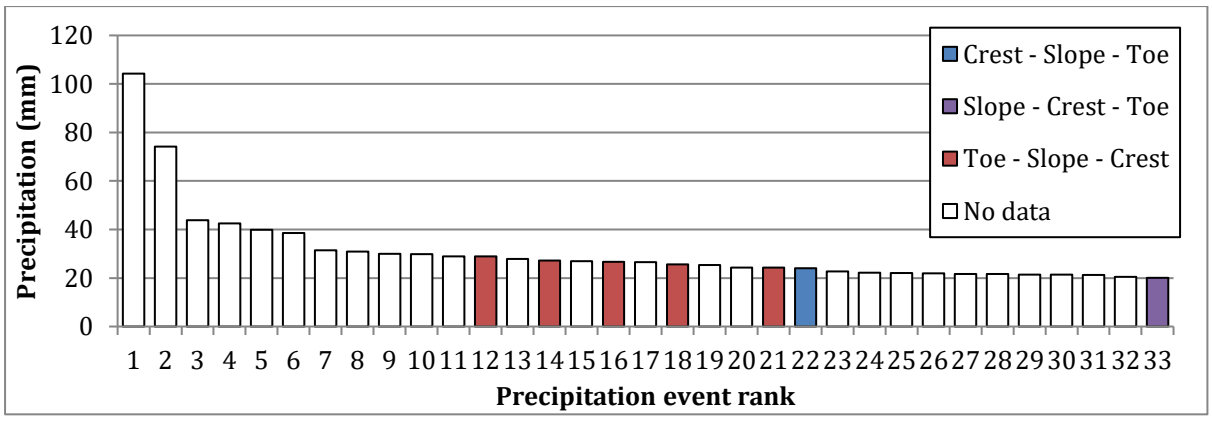

Figure 4.12: Order in which the peak head rise is reached after a precipitation event, for location 24

As was observed earlier, the most common sequence is toe-slope-crest. It appears that other sequence orders only occur at lower intensity precipitation events, but since only seven events are included no clear conclusions can be drawn. The precipitation amount of the included events

only ranges from 20 to about 27 mm, so all events have approximately the same precipitation volume. This makes it difficult to identify any relation between the precipitation volume and the sequence order.

Another aspect that was analysed is the relation between the amount of precipitation and the head rise in the monitoring wells. Again this was done by isolating the precipitation events using the Python script. For each precipitation event the head rise compared to the head at the start of the event was calculated. Since this analysis could be done automatically, more precipitation events are included. The threshold to classify a precipitation event was lowered from 20 to 2 mm, which resulted in 413 precipitation events. For these events the amount of precipitation was plotted against the head rise; this plot is displayed in figure 4.13.

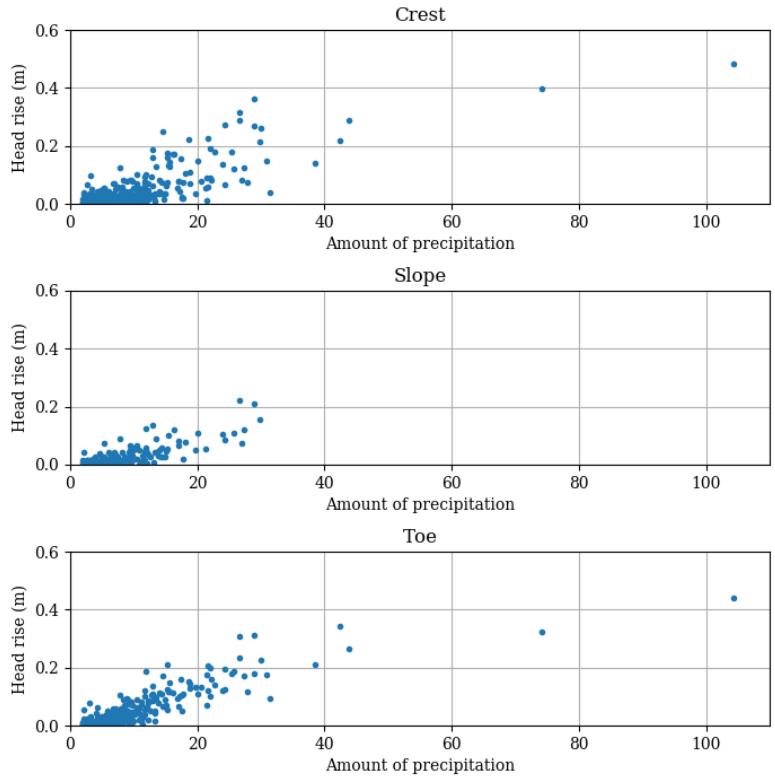

Figure 4.13: Head rise against amount of precipitation for location 24

As expected, a larger amount of precipitation leads to a larger head rise. The head rise at the crest shows more spread than the slope and the toe. Furthermore the slope shows less head rise for the same amount of precipitation compared to the other monitoring wells. This could be a result of reduced infiltration caused by the road located on the slope. However, it must be noted that the slope has less data points due to the large gap in the measurement series. Several of the largest precipitation events of the total measurement period took place during this gap.

4.5.2 Location 25

The same analyses were conducted on the measurements from location 25. Just like at location 24 the heads respond 4 to 5 hours after the start of the precipitation, and all three respond at approximately the same moment. However, regarding the peaks of the head rise no clear result was found. For several precipitation periods the sequence in which the peak was reached was exactly opposite to what was observed at location 24: the crest responded first, then the slope and finally the toe. However, in some cases the slope responded last. To analyse this is the peak sequence of the monitoring wells was analysed again. For location 25 the measurement data is more complete, and therefore more events could be analysed, including the most extreme event. The measurement period was also slightly longer, which means four more precipitation events larger than 20 mm have occurred in the measurement period.

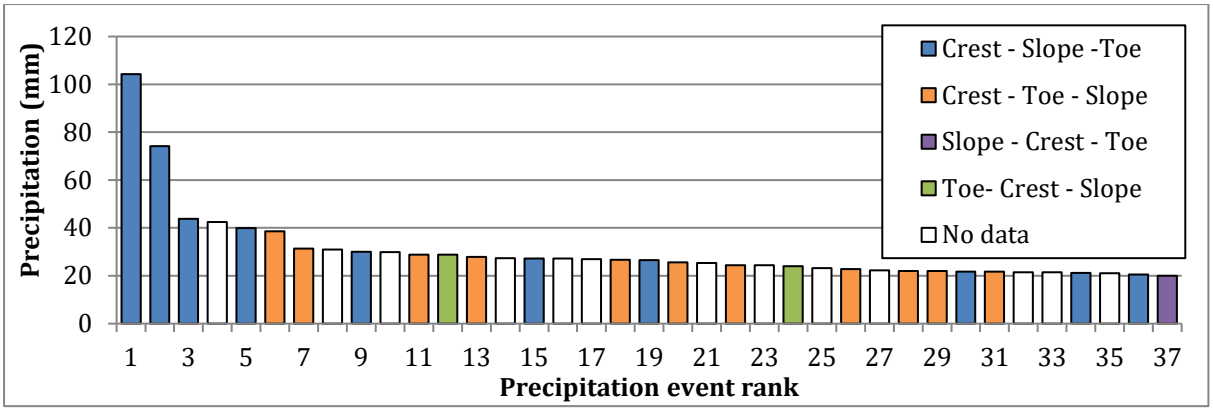

Figure 4.14: Order in which the peak head rise is reached after a precipitation event, for location 25

From figure 4.14 it is clear that for almost all events the crest responds first. Which monitoring well responds second varies; for 10 of the 24 considered events the slope responds second, and for 11 events the toe responds second. However, the four largest events all show the order crest – slope –toe. Therefore it seems like the slope responds second for larger intensity precipitation. On the other hand, this sequence also occurs for the lowest intensity events.

Another phenomenon that can be observed is a dip in the peak of the crest for some of the events. First the head rises, then declines a little, and then rises again. This is probably caused by the so called pre-draining of the boezem. When a large volume of precipitation is forecast, the water board lowers the water level in anticipation of the water level rise caused by the precipitation. This would also explain why this dip is not observed for every precipitation event.

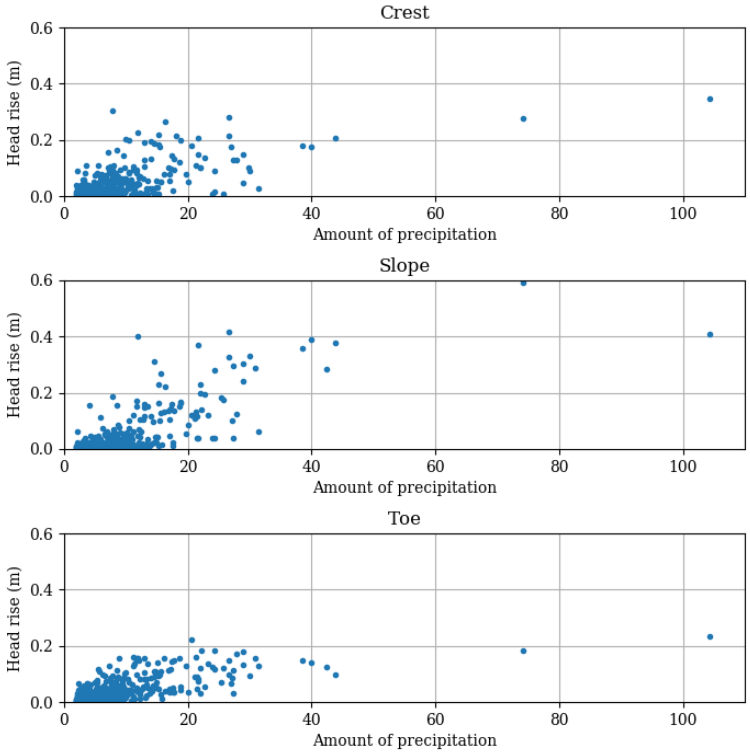

Figure 4.15: Head rise against amount of precipitation for location 25

When the head rise is plotted against the amount of precipitation, again a different result is found compared to location 24. In figure 4.15 it can be observed that that the head rise is smallest for the toe, and largest for the slope. This difference may partially be caused by the measurements: for location 24 the head at the slope was measured for a limited time, while at location 25 the

head at the slope was measured almost continuously. Furthermore, the location of the monitoring wells plays a role: the monitoring well at the toe is located quite close to the inside drainage ditch, which might explain the smaller head rise.

4.5.3 Hogedijk

During the period for which measurements from the Hogedijk are available six precipitation events of significance have occurred. The precipitation event of 05-09-2018 was the largest of these, with a daily volume of 95,6 mm. Monitoring wells 1 , 3, and 4 showed a clear response to this event, but monitoring well 2 showed only a very small and gradual increase in head. The other precipitation events lead to very small responses in the monitoring wells: only monitoring well 3 shows a clear response for the events, while the other wells only show a small and gradual increase of the heads.

The more comprehensive analyses conducted on the cases from Delfland were not conducted for the Hogedijk, since the amount of data is too limited to draw any meaningful conclusions.

4.6 Histograms

Another method to visualise the measurement data is the use of a histogram. In a histogram the range between the minimum and maximum of the measurements is divided into a number of bins. Each bin can then be plotted in a barplot, with the height of the bar representing the number of measurements included in the bin. This provides a method to visualise how often a certain head elevation has occurred in the measurement period.

Histograms with 25 bins were plotted for the measurements of the locations in Delfland. The measurement period of the Hogedijk shows an upward trend due to the short measurement period, which distorts the histogram.

The histogram for location 24 is displayed in figure 4.16. The three histograms show an approximatly equal variation range of about 0,5 m. The histogram for the slope is much lower than the other two; the reason for this is the large gap in the measurements for this location.

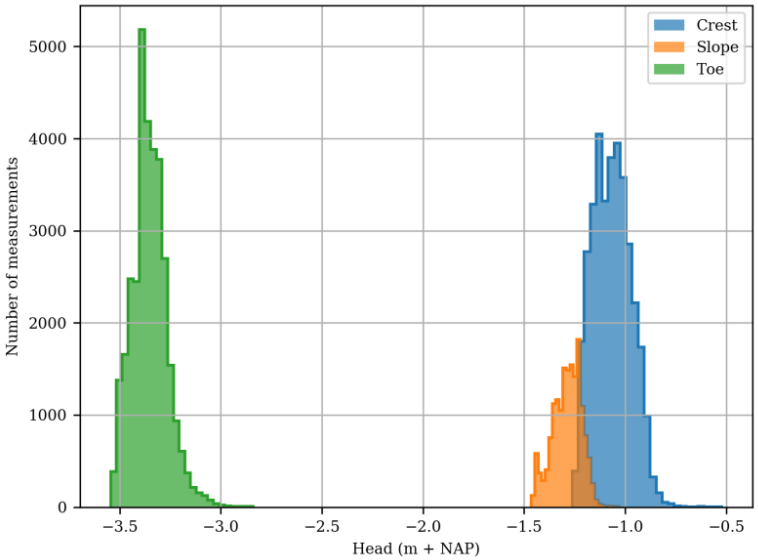

Figure 4.16: Histogram of the measurement data from location 24

The histograms for location 25 are displayed in figure 4.17. The difference between the three monitoring wells is larger here: the variation range of the crest is relatively small, whereas it is relatively large for the slope.

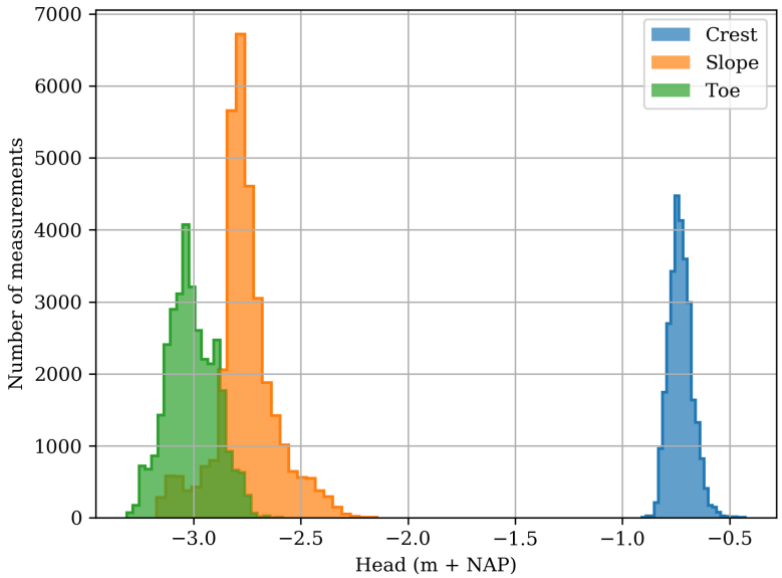

Figure 4.17: Histogram of the measurement data from location 25

Most histograms show a shape with a slightly heavier tail on the right-hand side. This indicates that higher than average heads occur more frequently than lower than average heads.

The histograms only show the frequency of a certain head in the monitoring well, but provide no information about the correlation between the monitoring wells. Therefore the correlation coefficients are calculated for each combination of monitoring wells. The hours for which either of the two monitoring wells considered had no measurement were excluded from the data. The calculated correlation coefficients are displayed in table 4.1. The numbers for the two research locations in Delfland are placed in separate columns, but no correlation coefficients between the two cross-sections were calculated. A correlation coefficient of 1 means that both monitoring wells show identical fluctuations; a value of 0 means that there is no correlation between the two monitoring wells.

Table 4.1: Correlation coefficients between the monitoring wells for the locations in Delfland

Location	Location 24	Location 25
Crest - Slope	0,831	0,007
Slope - Toe	0,204	0,716
Toe - Crest	0,416	0,230

For location 24, the fluctuations of the monitoring wells in the crest and slope are closely correlated. The correlation coefficient of either of these two monitoring wells to the well in the toe is smaller. Remarkable is that the correlation between the toe and crest is larger than the correlation between the toe and the slope. However, it should be noted that the number of measurements in the slope is much smaller than for the other two locations.

For location 25, the correlation between the crest and the two other monitoring wells is small, whereas the correlation coefficient between the slope and the toe is relatively large. A possible explanation is that the crest is more influenced by fluctuations of the outside water than the toe and the slope.

5 Model set-up

This chapter describes the set-up of the Modflow models for the three research locations. This involved determining or estimating the various required input parameters, and the schematisation of the various soil layers in the cross-sections. Furthermore, a grid had to be constructed from the soil schematisation, and the boundary conditions had to be applied to the model. When the models were completed, calibration was required to fit the models to the measurements.

5.1 Input data

The required input data for the model can be divided into two groups: hydraulic loads and geotechnical parameters. The hydraulic loads consist of the in- and outside water levels, precipitation and evapotranspiration. The geotechnical parameters encompass parameters of the soil types, like the conductivity in horizontal and vertical direction, and storage parameters.

5.1.1 Precipitation and evapotranspiration data

At the Hogedijk a rain gauge was installed, so for this location precipitation data is directly available. For the locations in Delfland this is not the case, so for those locations the data has to be obtained via other means. One available source for precipitation data is the Dutch meteorological institute (KNMI). However, for all of the research locations the closest weather station is quite far away. For the evapotranspiration this is probably not a problem, but for the precipitation data this could lead to large errors due to its large local variability. A better option is the use of a service that combines data from radar images and weather stations to estimate area-specific precipitation. One such service is the online archive Meteobase. This website is a project of STOWA, the knowledge centre of the Dutch water boards. From Meteobase precipitation and evapotranspiration data are available in grid format in a resolution of 1 by 1 km. The precipitation data is provided in hourly intervals, and is calculated by combining radar imagery and precipitation measurements from the KNMI (STOWA, 2013). The evapotranspiration data is available in daily intervals, and is calculated from weather station data using both the Makkink and Penman-Monteith methods. The Makkink method is used by the KNMI, but use of the Penman-Monteith method is more common internationally.

Due to the use of both precipitation measurements and radar imagery as well as its availability, the use of Meteobase data is the best choice for this research. In appendix C it is described how the data from Meteobase was downloaded and processed for use in the model. Because no actual precipitation was measured at the research locations in Delfland, small differences may exist between the data and the actual precipitation. However, there is no way to identify and quantify these differences. These uncertainties are likely small compared to the uncertainties in soil characteristics and are therefore disregarded.

For the location Hogedijk no Meteobase data could be obtained. The data was only available up to the date of 31-12-2016, and for the Hogedijk data for 2018 was required. Precipitation data is available from the rain gauge for the measurement period, but for the preceding period no data is available. For the potential evapotranspiration no local data is available at all. The closest KNMI weather stations to the Hogedijk are Schiphol (16,9 km), Valkenburg (21,1 km), and Cabauw (24,1 km) (KNMI, 2018). The potential evapotranspiration rate is calculated for each station, and the average of the three stations weighted by distance is used as input data for the model. This potential evapotranspiration rate was calculated using the Penman-Monteith formulation, using the same method as used for the Meteobase data (STOWA, 2013) & (Schuurman & Droogers, 2010). This method is described more elaborately in appendix C.

The locally measured precipitation was measured in 10-minute intervals. The recharge boundary condition (described in paragraph 5.3.3) is calculated for hourly intervals. To maintain consistency between the models the 10-minute data is converted to hourly data for use in the model. In order to model the period preceding the measurements, precipitation data from the weather station at Schiphol was used. Due to the local variability of precipitation, taking the average of three stations for each hour could lead to underestimation of the precipitation intensity.

5.1.2 Water levels

For each model two water levels have to be applied as boundary conditions: the outside water level in the boezem canal and the inside water level in the polder.

Location 24

The boezem canal location 24 is located on, the Vlaardingsevaart, is part of the boezem-system of Delfland, on which a water level of NAP -0,43 is maintained. (Delfland, 2018). This level is the intended water level; during and after periods of heavy precipitation the actual water level may vary. When heavy precipitation is forecast the water level is lowered in anticipation, with a maximum of 20 cm below normal level. During dry periods water is let into the boezem-system to keep the water at the intended level. This means the lowest possible water level is NAP -0,63 m. In extreme situations with heavy precipitation the water level might rise slightly above the intended water level despite the lowering of the water level beforehand. The extreme water level for these conditions was determined by the water board using a model of the boezem-system for several return periods. For a return period of 100 years the water level rise is 0,06 m, which means the water level would be NAP -0,35 m. This is the design water level used in stability calculations.

It can be concluded that the outside water level variations are quite small. The water will usually be at the intended level of NAP -0,43 m. It slightly varies in extreme situations and even then only for a short period. In addition to that, the exact variations during the measurements period are unknown. Therefore the choice is made to keep the outside water level in the model at the intended level of NAP -0,43 m.

Similar to the outside water, the inside water levels also have an intended water level. This water level is different for each polder. For location 24 the intended water level is NAP -3,63 m (Delfland, 2018). This water level applies to a small part of the polder behind the flood defence: the rest of the polder has a water level of NAP -3,42 m. Location 24 is located at an area where a slightly lower water level is maintained. From communication with the waterboard it was found that the variations in the polder water level are in the order of several centimetres. For this reason the choice is made to also keep the inside water level constant in the model. However, the drainage ditch at location 24 is filled in, meaning there is no direct inside water level present. This has to be taken into account in the application of the boundary conditions to the model.

Another parameter of importance is the head in the Pleistocene sand layer, the bottom layer in the model. The head in the layer was found in an assessment report for the flood defences along the Vlaardingsevaart, which includes location 24 (RPS BCC B.V. & Witteveen + Bos, 2010). In this report a head of NAP -1,61 m is given for location 24.

Location 25

Since location 25 is on the same boezem canal as location 24 the outside water level is the same, so at NAP -0,43 m. For the inside water level the situation is slightly more complicated: the drainage ditch has a flexible water level that can vary between NAP -3,00 m and -2,30 m. This ditch is separated from the water system in the rest of the polder, and the water level is allowed to fluctuate. However, when observing the measurement data of the monitoring well located closest to this ditch it appears that the groundwater table at this point is on average around NAP -3,15 m. This indicates that the water level in the ditch is very regularly below the intended -3,00

m. About 5 m inland of the drainage ditch is another drainage ditch, which has a water level of NAP -3,10 in summer and NAP -3,15 in the winter. Probably the ditches are so close that the groundwater flow causes the flexible water level to be constantly near the polder water level. Therefore the polder water level is used for the inside water level. For this the winter water level of NAP -3,15 m is used.

The head in the Pleistocene sand layer was obtained from the same report as for location 24 (RPS BCC B.V. & Witteveen + Bos, 2010). For a location on the opposite the canal from location 25 a head of NAP -1,55 m is given, so this head is used in the model.

Hogedijk
The water levels in- and outside of the dike are specified in the legger of Rijnland (Hoogheemraadschap van Rijnland, 2018). The polder outside the dike has an intended water level of NAP -1,54 m, and the polder inside the dike has an intended water level of NAP -5,98 m. Again these water levels are assumed to be constant over time.

The head in the Pleistocene sand layer is taken from an Iv-Infra report concerning the Hogedijk (Iv-Infra, 2018) and is NAP -5 m.

5.1.3 Soil parameters
For all three research locations soil borings at the locations the monitoring wells are available. Using this information the soil composition can roughly be determined. For the location Hogedijk measurements of the hydraulic conductivity are available as well. For the locations in Delfland this is not the case, these soil parameters have to be estimated based on the type of soil. Water boards usually have parameters sets of the local soil types based on laboratory analysis, but these sets normally only include parameters concerning strength and settlement. Therefore standardised conductivity values have to be used.

Hydraulic conductivity
For the locations in Delfland, the choice was made to use values from the Staring set as a first estimate for the hydraulic conductivity. The Staring set is a data set from the research institute Alterra containing geohydrological parameters for 36 soil types (Wösten, Veerman, De Groot, & Stolte, 2001). These soil types are divided in two groups: top-soils and sub-soils. The top-soils are soil near the surface, where the influence of plant roots is still noticeable, and the sub-soils are the soils below this zone. Each of these two groups includes several types of sand, loam, clay and peat.

Due to the nature of soils the conductivity can vary greatly, and therefore calibration is almost always necessary for geohydrological models. Because of the large amount of samples (about 800) contained in it, the choice is made to use values from the Staring set as an initial estimate for the hydraulic conductivity. During the calibration of the model these values will be altered to fit the measurements. Care must be taken that the conductivity values remain within a realistic range for the considered soil type. To define these ranges, conductivity values from several sources are compared. This includes values found in literature, but also the measurements from the research project in Rijnland. The measurements are included in appendix E. While they provide some insight in the hydraulic conductivity in regional flood defences, the number of samples is limited. Therefore literature was consulted to obtain information regarding common conductivity values for clay, peat and sand.

Clay
Comparing the values of the hydraulic conductivity of clay in the Staring set values to the other sources, the values appear to be quite large. The smallest value is larger than the largest value in some of the other sources. However, these conductivity values apply to clay as a solid material. As discussed in chapter 2 , clay soils often exhibit a soil structure which causes the conductivity to be much larger. The values in the Staring set are aimed at geohydrological modelling of large

areas of soil, and thus take this soil structure into account. This results in comparatively high values. In a report assessing whether the Staring-values are applicable to dikes (Van den Akker, 2001), it was found that the Staring set actually even underestimates the conductivity of clay soils in dikes. Compared to agricultural soils (which the Staring set is based on), soils in dikes are not tilled or ploughed, which means the soil structure is more developed and therefore the conductivity is higher.

The influence of the soil structure is also illustrated by the values given in Oosterbaan & Nijland (1994). For well-structured clay and loam a range of 0,5 – 2 m/day is given, for poorly structured clay a range of 0,002 – 0,2 m/day, and for dense clay a conductivity smaller than 0,002 m/day. Since it was established in chapter 2 that soil structure has a significant influence on the phreatic surface, the range of 0,002 to 2 m/day is considered the most realistic for use in the model, where the values above 0,1 are only allowed for top layers.

Peat
The conductivity of peat is dependent on many factors, one of which is its degree of decomposition. Decomposed (amorphous) peat has a lower conductivity than fibrous peat (Wong, Hashim, & Ali, 2009). The compression of the peat also has a large influence on the conductivity. The conductivity can vary from comparable to sand in its initial state to comparable to soft intact clay. Due to this influence of compression the distinction must be made in the model between peat layers near the surface and deeper peat layers. A similar range as for clay is used, which was 0,002 to 2 m/day, and values above 0,2 are only applicable for top layers.

Sand
The conductivity range for sand in the Staring set is lower than the values found in other sources. The sand types in the Staring set all contain loam in some measure, which probably causes this lower conductivity. Since the sand found in the research cases also often contains loam and clay, this lower range could be realistic. However, the largest Staring conductivity is just above 1 m/day, while other sources give values up to 50 m/day. Therefore a slightly larger range from 0,1 to 5 m/day is used for the calibration of the model.

The conductivity ranges for sand, clay and peat found in these sources are displayed in table 5.1.

Table 5.1: Values of the hydraulic conductivity for different soil types, found in literature

Conductivity range (m/day)		Staring	Verruijt & Broere (2011)	Wong et al. (2009)	Morris & Johnson (1967)	Oosterbaan & Nijland (1994)	Nectaerra (2018)
Clay	min	0,007 -	$8{,}7*10^{6}$ -	-	$8{,}15*10^{-6}$	< 0,002	0.22
	max	0,14	$8{,}7*10^{-4}$	-	$1{,}22*10^{-3}$	2	31.2
Peat	min	0,011 -	-	0,001	0,12	-	0,002
	max	0,81	-	1	11,4	-	0,064
Sand	min	0,099 -	0,087	-	2,5	1	1.25
	max	1,07	87	-	45	50	

Hydraulic anisotropy
The conductivities discussed thus far are the conductivities in horizontal direction. Dependent on the soil type, the vertical conductivity may vary considerably from the horizontal conductivity. This anisotropy is especially present in clay and peat due to the orientation of the soil particles or fibres. In general, the horizontal conductivity is larger than the vertical conductivity. The ratio between the horizontal and vertical conductivity is called the hydraulic conductivity anisotropy ratio and can be defined as:

$$a = \frac{K_v}{K_h} \tag{5.1}$$

Where:

a	=	hydraulic conductivity anisotropy ratio	(-)
K_v	=	vertical conductivity	(m/day)
K_h	=	horizontal conductivity	(m/day)

In order to make calibration of the model more straightforward, the anisotropy ratio is assumed to be constant for a single soil type. In the calibration the horizontal conductivity is variated, and the corresponding vertical conductivity is determined using the anisotropy ratio. Like the conductivity itself, the anisotropy ratio has a large variability. Few sources could be found regarding the relationship between the horizontal and vertical conductivity, but using the information that was available an estimate could be made for each soil type.

Clay
In Morris & Johnson (1967) average conductivities for clay in both directions are given: 0,000204 m/day in horizontal direction and 0,0000815 in vertical direction. These values result in an anisotropy ratio of 0,4. However, as said before these conductivities disregard the presence of a soil structure. A soil structure may have a different effect on the vertical than on the horizontal conductivity. The technical report 'pore pressures in dikes' (TAW, 2004) gives 0,33 as a conventional anisotropy ratio for clay. De Loor (2018) uses different anisotropy ratios for the top clay layer and the clay of the dike core in his research. For the core he uses a ratio of 0,33, which is probably derived from TAW (2004). For the top layer he uses a ratio of 2, meaning the vertical conductivity is higher than the horizontal conductivity. The explanation for this is that the soil structure in the clay top layer mainly enlarges the vertical conductivity. Especially cracks are vertically oriented, thus enlarging mainly the vertical conductivity.

As a first estimate, the value of 0,33 from TAW (2004) is used for the hydraulic anisotropy ratio. This value might be altered in the calibration process. Especially for top layers it can be necessary to use a larger value due to the soil structure.

Peat
The hydraulic anisotropy of peat is generally larger than for inorganic soil; values of about 300 have been found in tests (Wong, Hashim, & Ali, 2009). The technical report 'pore pressures in dikes' (TAW, 2004) gives the same value as for clay (0,33) as a conventional value. In engineering practice often a value of 0,1 is used; given the small number of sources and the differences between them this value will be used in the model as well.

Sand
For sand TAW (2004) gives an anisotropy ratio of 0,66. Sand itself is relatively isotropic, but since loam and clay is present in the sand of the research cases, the value of 0,66 will be used.

Specific yield
In steady-state simulations the groundwater flow is only determined by the hydraulic conductivity. When transient conditions are considered storage of the groundwater occurs. As described in paragraph 3.1, there are two storage mechanisms: elastic and phreatic storage. Phreatic storage occurs when the soil is not fully saturated and is caused by a rise of the groundwater table. The phreatic storage capacity is determined by the specific yield (S_y). The specific yield is defined as the ratio of volume of water that can be drained by gravity from a volume of soil (Todd & Mays, 2005). In the model, values from Todd & Mays (2005) will be used as a first estimate. These values are specified in table 5.2.

Table 5.2: Specific yield. Source: (Todd & Mays, 2005)

Material	S_y (-)
Clay	0,03
Peat	0,44
Sand	0,23

Specific storage
The specific storage (S_s) determines the amount of elastic storage that occurs per unit of head rise (Todd & Mays, 2005). Often the elastic storage is considered for the entire thickness of an aquifer, and is then called the storativity (S). The storativity is equal to the specific storage multiplied by the thickness of the soil layer. According TAW (2004), the specific storage of sand layers in the Netherlands varies between 10^{-4} and $3*10^{-3}$. The specific storage is a property mainly applicable to aquifers; for a small-scale model as used in this thesis the influence is probably small. As initial value 10^{-4} will be used for all soils.

5.2 Model grid and soil composition

For all three locations soil borings and profiles of the cross-section were available, which are included in appendix E. Based on this information the soil composition in the cross-section was determined, from which the model grids were constructed. Sometimes assumptions had to be made for the soil composition because of the limited information available, and sometimes adjustments had to be made due to the limitations of the Modflow grid. For each soil type an estimate of the conductivity was made based on the Staring set; the motivation for the chosen Staring soil types is included in appendix F.

Location 24
In the provided profiles of the cross-sections, the geometry below the water line is not displayed, which means the water depth is unknown. To determine the water depth the so-called 'legger' from the water board of Delfland is used (Delfland, 2018). In the legger all flood defences, canals, and other structures within the management area of the water board are included. For all these objects the required dimensions are defined, for instance the required depth for canals. For the canal outside the flood defence two depths are defined: a minimum depth of 1,55 m and a legger-depth of 1,9 m. This means that once the depth has become lower than the minimum depth, the canal is dredged out to the legger-depth. For the schematisation of the cross-section the legger-depth is used, because this is the largest depth. This gives the largest amount of interface area between the flood defence and the water. Based on the chosen depth the profile was extended: the outer slope was continued under the same angle as in the cross-section, until the legger depth is reached. From this point further outwards the canal bottom is assumed to be horizontal.

For the construction of the schematisation of the subsoil the provided soil borings are used. At the locations of each of the monitoring wells a soil boring was carried out. Additionally, several extra borings and cone penetration tests were provided by Delfland for two cress sections close to the research location. For these two cross-section soil schematisations were available as well.

Based on all the information a soil schematisation could be constructed, which is displayed in figure 5.1. In this schematisation several vertical boundaries between the soil types can be observed. This was necessary to prevent vertical staggering of the grid, as described in chapter 3 The cunets of the road and footpath, as well as the sand fill of the former drainage have layer boundaries that cannot be directly translated into a grid. For this reason the top layer is split in five parts, which are modelled as a single Modflow layer with different conductivities. Three of these parts represent the clay cover of the dike, and the other two parts represent the cunets of the footpath and the road on the dike. In reality the edges of these cunets are angled, but modelling this using the chosen grid type would result in vertical staggering. The less permeable asphalt cover of the road is not explicitly modelled in the schematisation, but is taken into account in the boundary condition.

Furthermore, there are several uncertainties in the soil schematisation. The soil borings only provide information for the exact location of the boring; between the borings an assumption has to be made. This has the result that the soil composition is open to different interpretations, and it is uncertain what interpretation is closest to reality. To account for this uncertainty several soil

scenarios were constructed, which are described in appendix F. The schematisation in figure 5.1 is the base scenario.

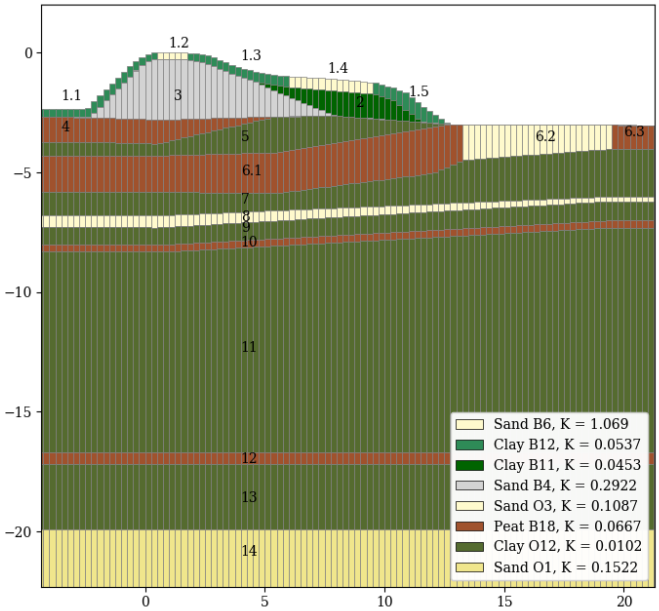

Figure 5.1: Model grid for location 24 with assigned Staring soil types

For each soil type in the schematisation a Staring soil type was chosen to make an estimation for the conductivity. These soil types and the corresponding conductivity for each layer are also included in appendix F.

Location 25

The canal on the outside of location 25 is the same as for location 24, and the depth of the outside water is the same. The profile is extended outwards in similar fashion to location 24. There are two drainage ditches located close to each other. Since it was decided to use a constant inside water level, only the drainage ditch closest to the flood defence is considered in the model. For the depth of this ditch a minimum depth of 0,25 m is defined, and a legger-depth of 0,15 m. Again, the legger-depth is used for the schematisation. The schematisation is displayed in figure 5.2.

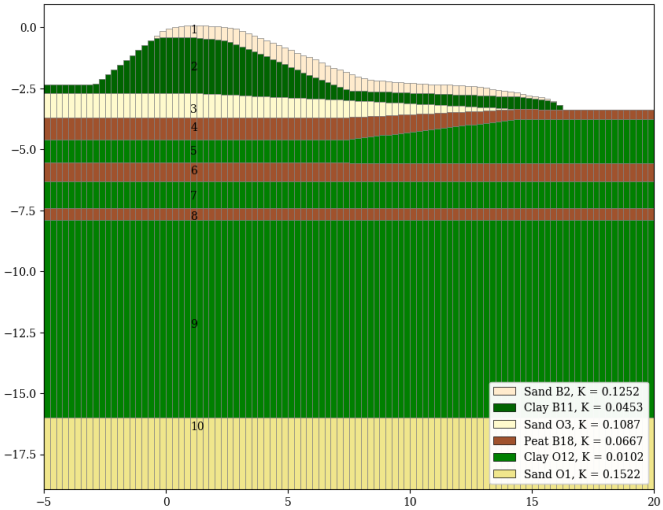

Figure 5.2: Model grid for location 25 with assigned Staring soil types

The composition of the subsoil is based on three soil borings performed at the locations of the monitoring wells. The composition of the deeper soil layers is based on different soil borings close to the cross-section obtained from DINOloket (TNO Geologische Dienst Nederland, 2018). These

borings are also included in appendix E . Again, several soils scenarios were constructed. To each soil layer a Staring soil type was assigned. These soil types and the soil scenarios are described in appendix F.

Hogedijk
The required depth of the outside water at the measurement location is not specified in the legger of Rijnland. However, it is specified for the same canal several hundreds of meters to the north and to the south of the location as 1 m. This depth of 1 m is also assumed for the research location. The legger-depth of the drainage ditch inside the dike is 0,50 m. The profile of this ditch is also included in the drawing of the cross-section of this location, and this corresponds to the legger-depth. Therefore the profile from drawing of the cross-section is used in the model.

Several soil borings as well as a cone penetration test were available at or close to the research location. These are included in appendix E. At each of the four monitoring wells a soil boring was executed, and in addition two borings and a cone penetration test were performed about 50 m to the south. Compared to the other locations, this information gives a relatively consistent picture of the soil composition. Therefore it was not necessary to construct soil scenarios.

Another difference with the other locations is that conductivity measurements are available. These conductivities are measured using the monitoring wells, and therefore represent the conductivity around the filters. These are located in a single peat layer, with the exception of monitoring well 4, for which the filter is partly in the clay layer below the peat. Since the conductivity was measured at those four locations, the peat layer is divided into four parts with the separations halfway between the monitoring wells. For each of these four parts the corresponding conductivity is assigned. For the remaining soil layers no measurements are available, the conductivity of these layers is estimated using values from the Staring set. The motivation for these values and a summary of the conductivities are included in appendix F. The soil schematisation converted to the model grid is displayed in figure 5.3.

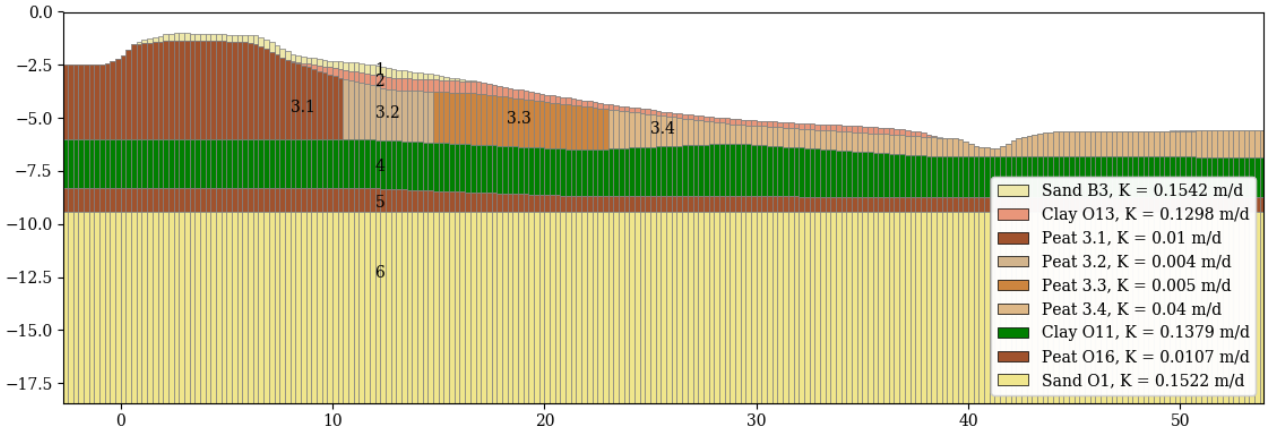

Figure 5.3: Model grid for Hogedijk with assigned conductivities

5.3 Boundary conditions

To model the inflow and outflow of water into and from the model boundary conditions need to be applied. Boundary conditions in Modflow are applied by adding packages to the model, in which the boundary conditions and the cells they are apply to are specified. Modflow includes a large amount of packages to model various types of boundary conditions.

5.3.1 Water levels

To model the outside and inside water level the river (RIV) package is used. The purpose of this package is to simulate the interaction between surface features like rivers and groundwater systems (Langevin, et al., 2017). The package allows for both flow from the river to the

groundwater and vice versa. As input variables, the river package requires the cell index, water level in the river, elevation of the river bed, and the conductance of the river bottom. The cells the river package is applied to are the cells that directly border the outside or inside water. Only the cells for which the top is above the water level are included. Since the water levels are assumed to be constant, the number of cells to which the river package is applied remains constant throughout the simulation. The water level is specified separately for each cell to which the river package is applied. For the cells bordering the outside water the outside water level is used, and for the cells bordering the inside water the inside water level. The elevation of the river bed is more difficult to define. The river package is mostly aimed at modelling rivers in large-scale regional models. For these models, often the entire width of the river is located in a single cell. The bottom of the river is then below the top of the cell and is assumed to be horizontal. However, for the model in this thesis the outside water spans several cells, and the bottom is not horizontal. Since the river package is only applied to cells below the water surface, in this case the river bottom corresponds to the cell top. The river bottom elevation for each cell is therefore specified as the cell top elevation. Finally, the river bed conductance needs to be specified. In the river package, the water in the river is separated from the groundwater system by a layer of riverbed material with low permeability. The conductance of the layer can be computed with:

$$C_{riv} = K * \frac{A}{b} \tag{5.2}$$

Where C_{riv} is the riverbed conductance, A the area of the riverbed, b the thickness of the riverbed and K the hydraulic conductivity of the riverbed material.

As discussed, in this model the cells are completely covered by the water. This makes the modelling of a riverbed is unnecessary, so a large conductance value is chosen to obtain a head equal to the water level in the cells. Test runs with the model have shown that a conductance of 0,2 produces the desired result.

At location 24 no inside water is present, which means the boundary condition had to be applied to the sand fill of the former drainage ditch. This boundary is modelled using the general head boundary (GHB) package. This package is similar to the river package, but no bottom elevation is specified. The sand ditch is connected to the polder water at some distance from the research location. This means the boundary should not always correspond to the polder level: during high precipitation rates the water has to flow through the sand towards the polder water, which will result in a head rise in the sand, and thus a higher head at the boundary. This can be modelled by using a lower conductance of the GHB package. This value of the conductance has to be calibrated to obtain a correct result.

5.3.2 Pleistocene sand layer

The head in the Pleistocene sand layer is simplified as being constant, which is modelled using the constant head boundary (CHD) package in Modflow. This is one of the simpler packages: a head is specified for a cell, and this head does not change throughout the simulation. This package is applied to all cells of the Pleistocene sand layer.

5.3.3 Ground surface

The surface of the flood defence forms the most complex boundary of the model; on this boundary the recharge by precipitation and loss by evapotranspiration has to be applied. Furthermore the seepage through this boundary has to be considered: the heads in the topmost layer cannot be higher than the ground surface, since the water seeps out of the surface if this were to occur. Since under normal circumstances the phreatic surface is below the ground surface, the top layers of the model are only partially saturated, which means precipitation has to travel through the unsaturated zone before reaching the groundwater table. There are two options for the modelling of the surface boundary: the use of the Modflow unsaturated zone flow (UZF) package, which

accounts for the behaviour of the soil in the unsaturated zone, groundwater infiltration and evaporation, and seepage. This means extra soil parameters are required for the unsaturated zone.

The second option is to apply precipitation, evapotranspiration and seepage as separate boundary conditions. The advantage of this option is that due to the simplification less parameters are required, which makes calibration of the model more straightforward. On the other hand, recharge is directly applied to the specified cells, which means the delay of the head rise caused by the travel time through the unsaturated zone is not modelled.

Both options were applied to the model for location 25 in order to assess the differences in the model results. It was found that the UZF package may cause the model to be unstable. The simulation only converged when a relatively time period was simulated. The two options to model the surface boundary could only be compared for a small portion of the total simulation period. In this small period the response to precipitation in the model made a slightly better match to the measurements when the UZF package was used, but the effect of evapotranspiration could hardly be discerned. When using the separate packages the evapotranspiration was clearly visible which also matched with the measurements. Considering the difficulties in the simulation using the UZF package it was decided to apply the boundary conditions of the ground surface as separate packages, and to not use the UZF package. This means the flow in the unsaturated zone is not modelled.

Precipitation

The precipitation is applied to the model using the recharge (RCH) package. The input to this package is relatively simple: the cells the package is applied to and the amount of recharge. The package is only applied to the topmost layer. If the cell the recharge is applied to is dry, the recharge is routed downwards until an active cell is reached (Langevin, et al., 2017). The amount of recharge is more difficult to determine; it is not realistic to directly use the amount of precipitation, since only part of the precipitation infiltrates into the soil and reaches the groundwater. The exact amount of recharge is dependent on many factors: the hydraulic conductivity of the topsoil, the amount of cracks and pores in the soil, the vegetation on the ground surface, the geometry of the dike, etc. The recharge also varies along the cross-section: on the slope water cannot collect in puddles, which leads to a smaller infiltration rate than near the toe, where puddles can form. Al these unknown variables make an exact quantification of the recharge impossible. For this reason a simplified method is used to estimate the recharge.

To include the variance of the recharge over the cross-section, the dike profile was split into four sections: the outer slope, crest, inner slope and toe. This division applied to a generic dike profile is displayed in figure 5.4. For each section a different recharge rate is applied.

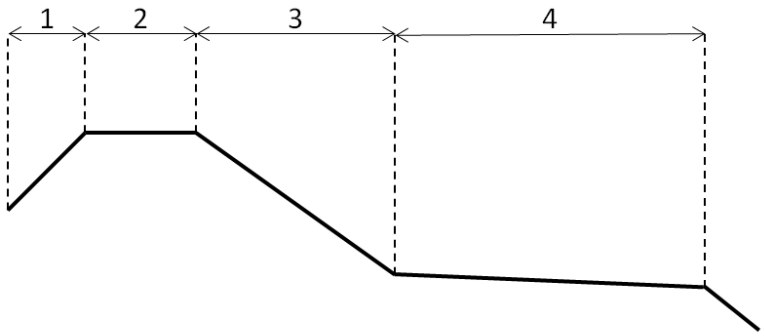

Figure 5.4: Division of a dike profile into sections to estimate recharge

For location 24 two extra sections were added, since this cross-section has a berm. One section is added to model the slope of the berm, and another to model the recharge in the hinterland. For location 25 the hinterland was not considered, since the inner boundary condition had a fixed

water level as boundary condition. For location 24 the inner boundary condition is dependent on precipitation, and therefore the recharge is also applied to the hinterland. The berm slope (section 5) is treated the same as section 3, and the hinterland (section 6) the same as section 2.

The recharge capacity for a section is calculated based on a recharge threshold and a recharge capacity. When the precipitation is below the threshold, no recharge is applied. This threshold represents the absorption of small amounts of precipitation by the grass cover. The recharge capacity poses an upper limit to the recharge: if the precipitation rate is higher than the recharge capacity, this capacity is applied as the recharge. The remaining precipitation is assumed to run off. To model the differences between the dike sections, the recharge capacity and the applied precipitation are multiplied by a section-specific multiplier. The recharge threshold is not multiplied by this multiplier so that the minimum required precipitation is the same for all sections. Finally, the recharge for each section is multiplied by a general multiplier for calibration purposes. The recharge is thus calculated as follows:

$$R_s = 0{,}024 * m_{tot} \begin{cases} 0, & ps < R_{min} \\ m_s * p_s, & R_{min} \leq p_s < m_s * R_{cap} \\ m_s * R_{cap}, & p_s \geq m_s * R_{cap} \end{cases}$$

(5.3)

Where:

Rs	=	recharge rate for section s	(m/day)
Rcap	=	recharge capacity of the soil	(mm/hour)
Rmin	=	recharge threshold	(mm/hour)
p_s	=	precipitation rate for section s	(mm/hour)
m_s	=	recharge multiplier for section s	(-)
m_{tot}	=	recharge multiplier for entire model	(-)

The recharge is multiplied by a factor of 0,024 to convert the values from mm/hour to m/day. This was done because the values are supplied in mm for each hour, whereas the model uses units of days and meters.

For most sections the precipitation data is directly used as the precipitation rate p_s. However, for location 24 and the Hogedijk, the presence of the road on the berm and the footpath on the crest must be taken into account. These structures have a low infiltration capacity. The water flows over the structures towards the edges, where it infiltrates or runs off. The infiltration rate on the surface is therefore nearly zero at the pavement of the road, and relatively high near the edges. This infiltration behaviour is modelled by changing the precipitation rate for the sections containing a road. The precipitation rate is set to zero for the largest part of the section, only on the cells at the edges of the section precipitation is applied. The precipitation rate for these cells is calculated by multiplying the input precipitation by the width of the road, dividing this by two (since the precipitation flows towards both sides of the road) and finally dividing this by the width of the cell. The width of the cell is dependent on the chosen grid resolution. This can be formulated as follows:

$$p_{s,r} = \frac{p * w}{2 * drow}$$

(5.4)

Where:

$p_{s,r}$	=	precipitation rate for section containing a road	(mm/hour)
p_s	=	input precipitation rate	(mm/hour)
w	=	width of the section considered	(m)
drow	=	width of the cell (dependent on grid resolution)	(m)

This calculated precipitation rate is much higher than the input precipitation rate. For many of the precipitation events the value will be higher than the recharge capacity. However, since the substructure of the road consist of sand and/or rubble, the infiltration capacity is larger than for the other sections. To model this, a large value is chosen for the multiplier m_p,

As initial estimates a recharge capacity of 5 mm/hour and a recharge threshold of 0,2 mm/hour are assumed. The total multiplier is set to 1, and the section multipliers are set to 0,5 for section 1 and 3 (the slopes), to 0,7 for section 2 (the crest) and to 1 for section 4 (the berm). For the sections containing a road the multiplier is set at a value of 2, due to the mentioned larger infiltration capacity.

For the crest and toe a larger multiplier is used, since these surfaces are nearly horizontal. If the amount of precipitation is larger than the infiltration capacity, the excess water can store in puddles, from which the infiltration can continue if the precipitation rate decreases. Because the crest is less wide than the toe area, it is assumed that the puddles there are less developed than near the toe. Therefore the multiplier for the crest is taken smaller than for the toe. The slope infiltration also has to be corrected for the angle: assuming the precipitation is applied vertically, the amount is dependent on the horizontal length of the slope. This precipitation is spread out over the total length of the slope, meaning the precipitation per meter of slope is smaller than the precipitation per meter on a horizontal surface. This correction was made by multiplying the precipitation with the cosine of the slope angle.

The recharge is calculated for every hour; the data is only available in hourly intervals and for simplicity it is assumed that the precipitation cannot be stored in puddles for longer than an hour. For the inner slope (section 3) the amount of rejected precipitation is calculated and added to the precipitation for the toe section (section 4). This intends to simulate the collection of slope run-off water at the toe of the dike. The distribution of the precipitation over the dike is displayed in figure 5.5.

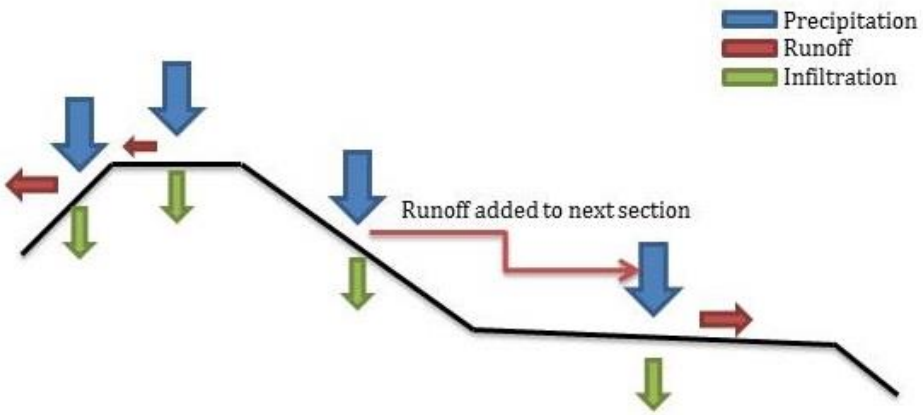

Figure 5.5: Distribution of total precipitation volume over the cross-section

The blue arrows represent the total amount of precipitation, directly taken from the input data. The green arrows represent the infiltration, and this amount is added as recharge rate for the boundary condition. The red arrows represent the rejected precipitation, the runoff. This amount is removed from the model. These calculated recharge rates are added to the model as a time series. For this time series a stepwise interpolation mode is specified, meaning that between one value and the next the value is kept constant. This ensures that the total amount of recharge over the simulation period is correct, which is not the case if linear extrapolation would be used.

Evapotranspiration
For the modelling of water loss by evapotranspiration, Modflow includes the evapotranspiration (EVT) package. This package is only used to model evapotranspiration from the saturated zone, but since the unsaturated zone is not modelled this is no problem. The EVT package uses several assumptions to calculate the evapotranspiration rate (Langevin, et al., 2017). Firstly, it is assumed that when the water table is above a certain elevation, the evapotranspiration rate is equal to the user specified rate. This elevation is called the ET surface. Secondly, when the water table is below another certain elevation, the extinction depth, the evapotranspiration is zero. Between the extinction depth and the ET surface the evapotranspiration rate is a fraction of the user specified rate, dependent on the water level. The relation between the water level and the evapotranspiration rate in this region can be specified using a curve consisting of several linear segments. If the extinction depth is lower than the cell bottom, the evapotranspiration is extended to the cell below. Therefore the package only has to be applied to the topmost layer.

Because these input parameters are a schematisation of the process for which no parameters are known, assumptions have to be made. It is assumed that the evapotranspiration rate is equal to the potential evapotranspiration rate if the water table is at the ground surface, and that it decreases immediately when the water table becomes lower than the ground surface. This is modelled by placing the ET surface at ground surface level. For the extinction depth a assumption of 2 m is used as initial estimate. The interpolation between the extinction depth and the ET surface is simply assumed to be linear. For the potential evapotranspiration input the daily values from Meteobase are used.

Seepage
Modflow has no dedicated package to simulate seepage. To simulate seepage often the drain (DRN) package is used which is used for modelling drainage pipes, but its functionality can also be applied to seepage through the ground surface. For each cell the package is applied to, two values need to be specified: the elevation of the drain and the drain conductance. If the water table is above the drain elevation, water is discharged from the cell. The magnitude of the discharge is proportional to the difference between the water table and the drain elevation, and the constant of proportionality is defined be the drain conductance (Langevin, et al., 2017). This conductance is similar to the conductance for the river package. To simulate seepage, the drain elevation is simply defined as the surface elevation. The drain conductance is more difficult to define. If the drain conductance is taken too low this might lead to a calculated water table above the ground surface. The value should not be set too high either, since there is some resistance to seepage caused by the vegetation on the surface. A value of 1 m^2/day is used as an initial estimate.

5.3.4 Model edges
At the left and right edges of the model no flow should occur. Modflow automatically models the edges of the model as no-flow boundaries, so no boundary conditions need to be applied.

5.3.5 Application to the model
With the exception of the boundary for the Pleistocene sand layer, all boundary conditions are applied to the topmost active cells in the model. Since not all layers span the entire width of the model, this means some boundary conditions are applied to multiple layers, albeit not in the same rows. In figure 5.6 it can be seen which boundary conditions are applied to which cell.

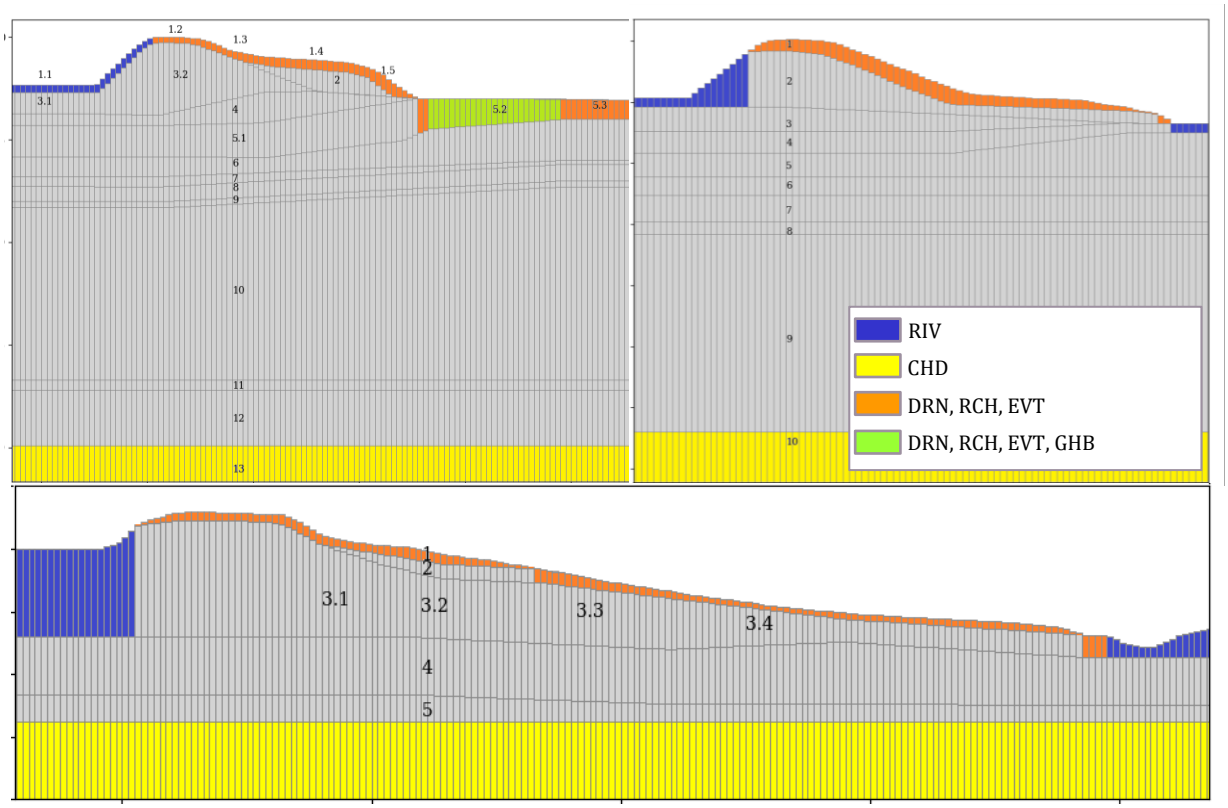

Figure 5.6: Applied boundary conditions to location 24 (top left), location 25 (top right) and the Hogedijk (bottom). RIV = river package, used to model the in- and outside water, CHD = constant head boundary to model the head in the Pleistocene sand layer, DRN = drain package, used to model seepage, RCH = recharge package to model infiltration of precipitation, EVT = evapotranspiration package, GHB = general head boundary package, used to model the inner boundary of location 24.

5.3.6 Processing of the output

The output of a Modflow model is written to a binary file, containing the head for each model cell for each time step. When the simulation has finished, this file can be read using FloPy to access the information. It is possible to extract more information from the model, for example flow velocities, but since this research is concerned with the phreatic surface the heads are sufficient.

To interpret the output of the model, the data has to be visualised. Due to the large amount of data choices have to be made: to show the variation of the head over the width of the flood defence for a certain time step, or to show the variation of the head for a single point in the cross-section over the duration of the simulation. Furthermore, there is variation over the depth in the cross-section. The variation of the heads along the width of the model is different for each soil layer.

To assess the fit of the model to the measurements, a simple plot is used showing the head fluctuations over time for the points in the cross-section corresponding to the monitoring wells. The measurements are plotted in the same figure, to compare the results to the measurements.

When the heads in the cross-section have to be visualised, a plot can only be made for a single time step simultaneously. Only by making an animation the heads in the cross-section varying over time can be visualised. This was done to analyse the fluctuations, but these animations cannot be included in this thesis report.

5.3.7 Tests

Before and during the calibration some tests were executed to assess the sensitivity of some of the variables in the model. The following observations were made:

- For time steps smaller than 24 hours, the time step has small influence on the shape and magnitude of the precipitation peaks. Smaller time steps provide more detail in the peaks, for instance smaller sub-peaks. For time steps larger than 24 hours errors can occur sometimes, for instance the head may not return to base level after precipitation.
- Within a certain range, the grid resolution also has small influence. A finer resolution provides a smoother, more detailed phreatic surface. However, for a column width smaller than 10 cm the running times of the model increase drastically, errors occur and in some cases the model becomes unstable. The initial column width of 0,25 m gives a good balance between detail and stability, and is therefore maintained.
- After the start of the transient part of the simulation, the model needs less than two simulated weeks to adjust to the precipitation. In these two weeks, the model might give slightly lower or higher heads, dependent on how close the result of the steady-state is to the phreatic surface at the start of the model. The steady-state simulation provides an average level of the phreatic surface, so if the transient simulation starts shortly after a dry or wet period the model needs to adjust.
- The influence of the specific storage is negligible. Values ranging between 10^{-2} and 10^{-6} were used, but no discernible difference could be observed in the resulting heads. The initially assumed value of 10^{-4} is therefore used for all soil types. Most likely the specific storage is more important for large models with thick aquifers.
- Another parameter that influences the results of the transient simulation is the specific yield. The specific yield influences the phreatic storage and therefore only has an effect on not fully saturated layers. A lower specific yield results in a larger response to precipitation, and thus larger fluctuations of the heads. This can be explained by the influence of the specific yield on the phreatic storage: a lower specific yield results in a smaller phreatic storage capacity, which means that the same volume of recharge results in a greater head rise.
- Changing the recharge parameters can lead to unexpected results. Increasing the recharge capacity generally leads to larger peaks, but individual peaks sometimes decrease, and increase again when the recharge capacity is increased further. Above about 15 to 20 mm the influence of the parameter diminishes. The reason for this is that an hourly precipitation volume of this magnitude rarely occurs, meaning the full recharge volume is applied to the model for nearly every hour. The recharge threshold behaves similarly: increasing the value leads to smaller peaks and less detail in the peaks, but individual peaks may increase. The section multipliers only have a very small influence on the model. The recharge is probably quickly redistributed in the cross-section, resulting in a small influence of the initial distribution over the cross-section. The overall multiplier behaves as expected: decreasing the value decreases the magnitude of all recharge peaks.

5.4 Calibration

For none of the three models the initially assumed parameters directly resulted in a well-fitting model. Calibration of the models is therefore necessary . To adjust the model in a meaningful way, an assessment was made of the variables that can be adjusted. Some of the variables have little effect on the outcome, and can be neglected.

The adjustable variables can be divided in two groups: variables that can be adjusted for the steady state simulation, and variables that can only be adjusted in the transient simulation. The former group is easier to adjust, since a steady state simulation only takes several seconds to run. In addition to that the result can directly be observed, since they are not variable in time. For these reasons the choice is made to calibrate the variables for which it is possible under steady state conditions, and to calibrate the other parameters subsequently in a transient simulation. In the steady-state simulation a constant recharge rate is applied to the model, to represent the long-term influence of precipitation. The rate of this recharge is set to 525 mm per year, which is approximately a yearly average precipitation. The calibration is based on comparing the model

to the average of the measurements. The measurement period of approximately 4 years is considered to be long enough for the average to represent steady-state conditions.

Steady state
The variables that can be calibrated for steady state conditions are the following:

- Soil composition;
- Hydraulic conductivity;
- Conductance of the boundary conditions;
- Steady state recharge rate.

The conductance of the boundary conditions is for most situations set to a large value, since no resistance is present in reality. This is with the exception of location 24, for which is the only boundary condition that has to be calibrated.

Transient
Once the steady-state simulations match the measurements, transient conditions can be considered. The steady-state parameters mainly influence the average height of the phreatic surface, the parameters variated for the transient simulation influence the magnitude of the fluctuations of the phreatic surface over time. Therefore the simulation results and the measurements have to be compared for a time interval, preferably the entire measurement period.

The variables that can be adjusted for transient conditions are:

- Hydraulic conductivity;
- Specific yield;
- Specific storage;
- Time period that has to be simulated before the start of the measurements;
- Infiltration parameters

It was already determined that the time period required before the start of the measurements is about two weeks, and that the influence of the specific storage is negligible. These variables are therefore not used in the calibration. The specific yield only has to be adjusted for the upper layers, since the parameter has no influence on the storage in fully submerged cells.

The calibration of the transient part of the simulation is more complicated than the calibration for the steady-state part for two reasons. Firstly, when the full measurement period is simulated using a time step of one hour the total runtime of the simulation is about 5 minutes. This means that changing a variable and assessing the influence is a lengthy process. Secondly, no clear measure can be used to quantify how well the model results fit the measurements. Since the simulation period spans multiple years the model may fit well for some parts of this period while it does not for other parts.

There are two possible solutions to speed up the calibration process: simulate only a part of the total period, or use a larger time step or grid resolution. Comparison between simulations using a time step of 1 hour and of 12 hours shows that a time step of 12 hours is sufficient when the total measurement period is considered. The use of this larger time step results in less detail, but does not lead to large differences in the results. Therefore the choice was made to use a time step of 12 hours to calibrate the model, and perform a simulation using the calibrated values afterwards for which a time step of 1 hour is used. The difference between model and measurements is assessed by plotting the measurements and the model results in a single plot. The fit of the model can be determined by comparing the two graphs.

5.4.1 Location 25

The first research location that was modelled is Delfland location 25. The choice was made to start with this location because the soil composition is simpler than for the other locations, which

makes it easier to set up this model. In this paragraph the calibration process is summarised; a more elaborate description and the resulting parameters are found in appendix F.

During the steady-state calibration some difficulties were encountered. A well-fitting model could be obtained, but the resulting calibrated conductivities were not realistic. The values were within the range of what is possible for the respective soil types, but relative to each other the values were unrealistic. The intermediate sand layer in the cross-section was assigned a lower conductivity than an adjacent peat layer. Since the conductivity is the only defining characteristic of a soil type in this model, this means that in reality the sand layer is modelled as peat and vice versa.

Further tests confirmed that the only soil composition resulting in a well-fitting model and realistic parameters was a schematisation where the intermediate sand layer starts below the slope of the dike, and extends inwards to the polder. The problem with this schematisation is that it is in contradiction to the soil borings performed at the locations of the monitoring wells. Other soil borings along the same flood defence were available, some of which contradict the other soil borings. The borings show that the position of the sand layer varies along the length of the flood defence. Two possible causes were identified to explain the contradiction between the model calibration and the soil borings:

- Information uncertainty regarding the soil composition: available soil borings are in contradiction to each other, and provide no information for locations between the borings.
- Flow in the longitudinal direction occurs in the sand layer, which cannot be modelled using the two-dimensional model.

Eventually the choice was made to use a model with the intermediate sand layer below the toe. This was the only soil composition for which the measurements could be matched, and for which the conductivities had realistic values. This position of the sand layer can be seen as a simplification of the variation in longitudinal direction, which is not modelled.

This schematisation, along with the results of the calibrated steady-state simulation are displayed in figure 5.7. The model calculates the head for each cell. These heads are visualised as a line plotted for each model layer. To avoid clutter, only the heads of the topmost seven layers are plotted. The monitoring wells are displayed as well, with the filter represented by a lighter colour. The average head of the measurements for each monitoring well is indicated by a white bar.

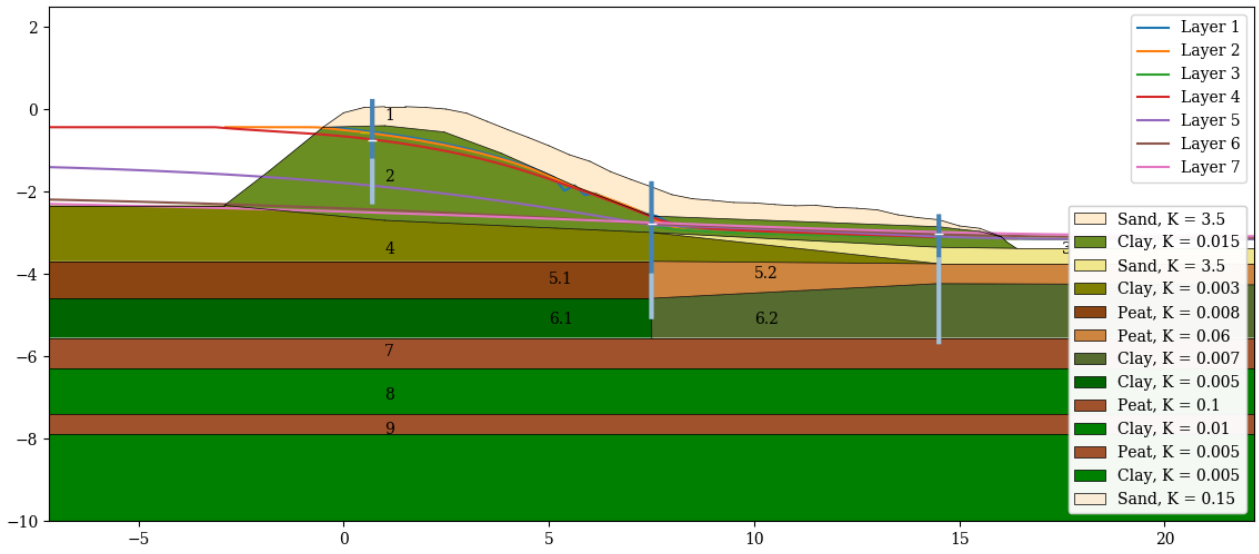

Figure 5.7: Delfland location 25, results calibrated steady state simulation using the adjusted soil schematisation.

Using this updated schematisation the model was calibrated further in the transient simulation. Regarding soil parameters, this mainly involved the two topmost layers. The sand layer was given a larger conductivity and a smaller specific yield to increase the magnitude of the precipitation peaks. The clay core was given a larger anisotropy ratio for the same reason. This ratio was set to a value larger than 1, meaning the vertical conductivity is larger than the horizontal conductivity. This is unusual, since in most soils the opposite is the case. The explanation for this is that the cracks and pores in the clay mainly enlarge the vertical conductivity. De Loor (2018) also uses a larger vertical than horizontal conductivity for the top part of clay layers in his research.

Additionally, some adjustments were made to the recharge parameters. These changes, the calibrated soil parameters, and a more elaborate description of the calibration process can all be found in appendix F.

The evapotranspiration parameters were left unchanged; changing these did not result in a better fit. However, by varying the parameter it did become clear that evapotranspiration was a necessary process to include for this model. When the evapotranspiration was set to zero, the shape and magnitude of the dips in the head were not matched correctly. This means that for location 25 evapotranspiration is a necessary boundary condition to include in the model.

5.4.2 Location 24

The next model that was calibrated was Delfland location 24. The full description of the calibration process is included in appendix F.

Like location 25, the constructed soil scenarios were compared in a steady-state simulation to determine the most probable of the six scenarios. Even though the results found in scenario 2 showed a slightly better fit to the measurements, scenario 1 was chosen for the soil schematisation used for the further analyses. By changing the conductivity of the clay cover, similar results to scenario 2 could be reached. The difference between the scenarios was therefore too small to choose one over the other based on the model results. Scenario 1 is based on soil borings directly at the measurement location, whereas scenario 2 is based on soil borings further away. Scenario 1 is therefore preferable, and is used in the further calibration.

The steady-state calibration process was started by matching the measurements at the monitoring well near the sand-filled drainage ditch. Although this monitoring well does not provide information about the phreatic surface in the actual cross-section, it could be used to calibrate the groundwater table inside of the dike. This was mainly done by varying the conductance of the general head boundary package. Furthermore the conductivity of the deepest clay layers had to be adjusted: the head in the Pleistocene resulted in too high heads near the toe. The heads of the other two monitoring wells could easily be calibrated by changing the conductivity of the rubble core of the dike and the clay cover.

The model still showed the phreatic surface exiting at the inner slope and the toe resulting in seepage. Unfortunately no monitoring well was placed at the inner crest of the berm, so no measurements are available to either prove or disprove whether this is correct. However, it is not likely that seepage would continuously occur. With some further calibration a model could be obtained with no seepage, and which still matched the measurements. The heads resulting from this calibration are displayed in figure 5.8.

The transient calibration of the model was similar to location 25. The anisotropy ratio of the clay top layer was increased to a value of 2, and the specific yields of the topmost layers was decreased to increases the precipitation peak heights. The reaction of the recharge parameters was different: the section multipliers had some influence, and this was used to increase the recharge peaks near the toe.

Conversely to what was observed for location 25, the evapotranspiration for location 24 had a negative effect on the fit of the model. The multiplier was reduced to 0,5 and the extinction depth

from 2 m to 1 m, to reduce the dips in the head. Apparently evapotranspiration has a smaller influence on this flood defence than on location 25.

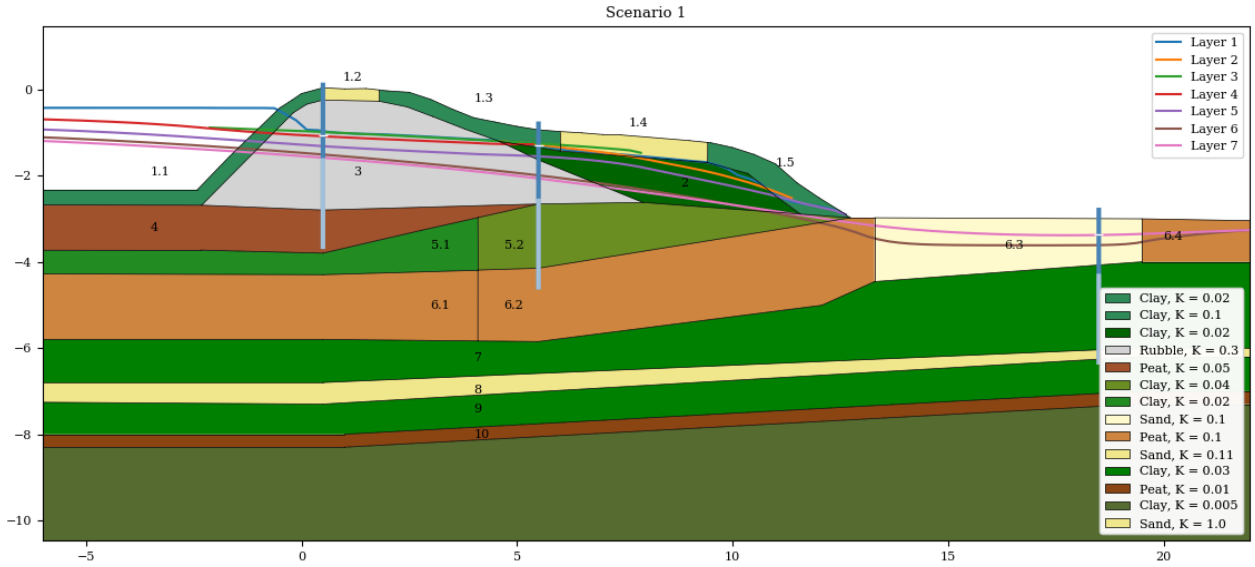

Figure 5.8: Delfland location 24, results steady state simulation using calibrated values

5.4.3 Hogedijk

The calibration process for the Hogedijk was performed using a different method than the two other research cases. Calibrating the model in a steady-state simulation is not meaningful in this case, since only two months of measurements are available. This measurement period was preceded by the dry summer of 2018, and the average of the measurements can therefore not be said to represent the average position of the phreatic surface. For this reason the model was calibrated directly in a transient simulation.

Running the model using the initially assumed parameters did not result in a good fit. For monitoring wells 1, 2, and 3 the model result was lower than the measurements, while for monitoring well 4 the simulated head was too high. For this monitoring well the head is almost continuously lower than the polder water level, except for one peak caused by a precipitation event. The monitoring well is placed in the slope 9 m removed from the drainage ditch, so a measured head lower than the polder water level is unexpected. According to the available information the polder water level is correct. Since there is no explanation why the measured head is so low, the model is calibrated using the other three monitoring wells.

The modelled head at monitoring well 4 was slightly lowered by reducing the conductivity of the deepest layers covering the Pleistocene sand layer. Due to the low elevation of the polder the Pleistocene sand layer is relatively close to the surface, resulting in a large influence of its head.

To fit the model to the measurements, some changes were made to the schematisation:

- Below the crest, an extra section was created in the peat layer to obtain a correct head in the monitoring well at the inner crest. This section was assigned a higher conductivity, which can be explained by the sand and rubble of the road cunet.
- The transitions between the different sections of the peat layer were too sudden. At a transition between two monitoring wells the phreatic surface was too close to the surface. To prevent this, a linear gradient was assumed between the measured conductivities. This is more in accordance to reality as well: the conductivity does not change from one value to another at a vertical separation.

After these modifications the general height of the phreatic surface was in accordance to the measurements, but the shape and magnitude of the precipitation peaks were not. One of the

parameters that was of influence for this was the conductivity of layer 2, the loam top layer. Assigning this layer a lower conductivity resulted in higher peaks near the crest. This is contrary to the observations made in the other two models: a larger (vertical) conductivity of the top layer resulted in higher peaks. The explanation for this is seepage. During precipitation events seepage occurs near the toe through the loam layer, so a low conductivity of this layer provides more resistance to seepage. Since the water cannot flow away as easily, the head upstream in the cross-section will rise more. Since the loam layer does not extend fully towards the crest, the lower conductivity has no influence on the resistance to recharge in the crest.

A strange phenomenon that could not be modelled properly was the difference in reaction between monitoring wells 2 and 3. In the measurements, monitoring well 2 shows a damped response to precipitation, whereas monitoring well 3 shows a much more peaked response. This is strange, since these wells are located close to each other, and both are placed in the slope of the dike. In the model this different response could not be reached. It was possible to approximately match the damped response or the peaked response for both points simultaneously, but not for each point individually. Changing recharge multipliers slightly increased the difference between the two points, but not enough to match the measurements.

Eventually the model was calibrated by changing the specific yields such that both monitoring wells 2 and 3 are matched approximately. At neither location the peaks could be matched exactly. The fast, almost direct response of monitoring well 3 to a large precipitation event in early September could not be modelled. The model responds more slowly, and reaches the peak after a few days. The height of the peak could be matched, but if this was done the phreatic surface remained too high for weeks after the precipitation. The choice was made to calibrate so that the model result is close to the measurements most of the time, even though the peak height is not matched.

In figure 5.9 the heads calculated in a steady-state simulation using the calibrated parameters are displayed. The model was not calibrated using the steady-state simulation, the figure is only intended to display the general position of the phreatic surface in the cross-section. Notable is that for the steady-state to reach equilibrium, 100 time steps were required instead of the 20 that were used in the other models.

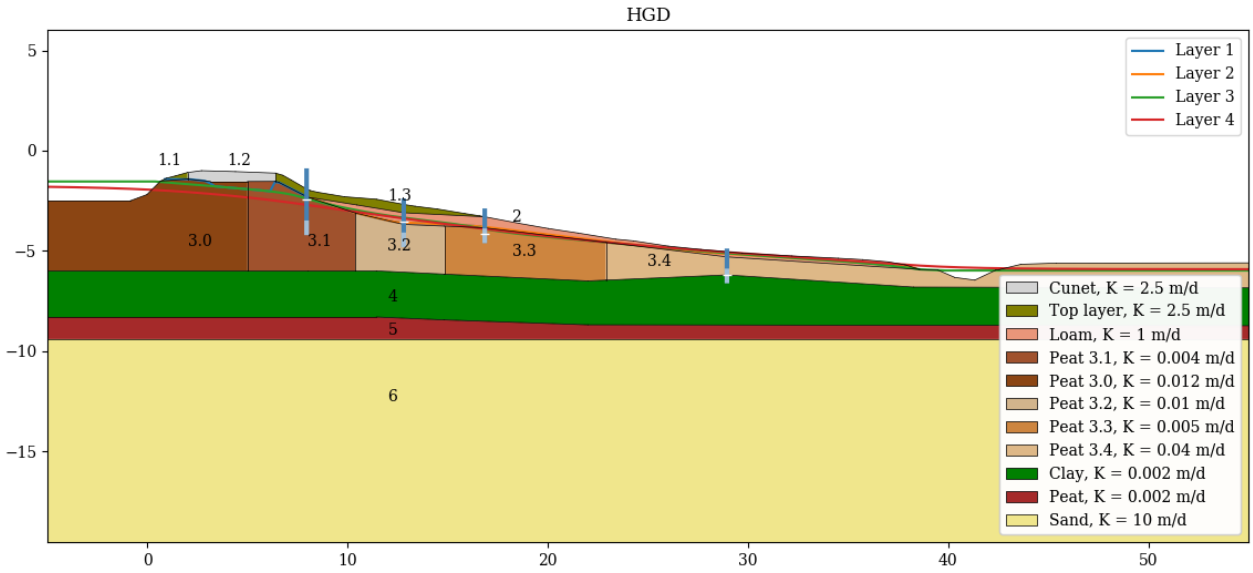

Figure 5.9: Steady-state simulated heads in the Hogedijk

6 Results

In this chapter the results of the simulations are presented. The simulated heads from the model are compared to the measurements to assess the accuracy of the model. To check the fit of the model under extreme circumstances, and in order to compare the phreatic surface during these circumstances to the schematisation, the highest and lowest simulated phreatic surfaces were identified from the results and analysed. To further analyse extreme precipitation events, precipitation with different combinations of duration and intensity were applied to the calibrated models. An extra analysis was performed using the calibrated model from Delfland location 25. In this analysis meteorological data from a longer period of 31 years was applied to the model to analyse the long term fluctuations of the phreatic surface. Finally, some stability calculations were carried out to assess the influence of variations of the phreatic surface on the macro-stability of the flood defence.

In most of the analyses the model results are compared to a schematisation of the phreatic surface, in order to assess whether the schematisation is a good approximation of the phreatic surface under design conditions. For the two cases in Delfland, the schematisation from the water board is used, which was described in paragraph 2.1.2. For the Hogedijk the schematisation constructed by Iv-Infra was used (Iv-Infra, 2018). This schematisation was based on the guidelines from the water board of Rijnland, which are nearly identical to those of Delfland.

6.1 Main simulation

The main simulation for this research is the simulation of the measurement period of the monitoring wells. In chapter 5 the models were calibrated as good as possible for this period. To analyse the fit of the model results, the measurements were plotted along with the head fluctuations in the model cell closest to the corresponding monitoring well.

General

In all three models, it could be observed that the heads were different for each soil layer. When looking at multiple soil layers, this means that the heads in the cross-section are non-hydrostatic. This non-hydrostatic gradient of the pore pressures over the depth was also observed by Ten Bokkel Huinink (2016) and De Loor (2018). For the models in this thesis, this gradient is related to flow in vertical direction. Vertical flow occurs during precipitation events, but also in dry conditions it is present due to the head in the Pleistocene sand layer. If this head is higher than the phreatic surface, the vertical flow is upwards and the head increases with depth. When the head in the Pleistocene layer is lower the opposite happens. Both situations can simultaneously occur in the same flood defence, when the head in the Pleistocene layer is somewhere between the inside and the outside water level.

The gradient of the of the pore pressures over depth is dependent on the relative conductivity of the soil layers. In a multi-layered system, the head gradient over the less conductive layers is larger than over the more conductive layers. In the models, the height of the phreatic surface could sometimes be manipulated by changing the conductivity of the soil layers relative to each other. This indicates that the conductivity of deeper soil layers, in conjunction with the head in the Pleistocene sand layer, influences the height of the phreatic surface.

The response of the pore pressures is also variable over depth. The topmost (partially) saturated layer shows the largest response, while deeper layers exhibit smaller and slower head fluctuations.

The topmost layer in the models sometimes responded in an unexpected and unrealistic way. During a precipitation event the layer was often filled up to the ground surface, while the layer below still had a much lower head. During periods with a large evapotranspiration flux, the layer was completely dry. In that case Modflow modelled the head of this layer as being on the level of the extinction depth of the evapotranspiration package. This had the result that the head of this layer in the model was often below the heads of the deeper layers. The cause of this is the way in which the recharge and evapotranspiration are modelled. The choice was made to not take the effect of the unsaturated zone of the model into account, which means said effects are modelled in a simplified way. The top layer is normally unsaturated, and since unsaturated effects are not modelled the heads in this layer are not accurate. This is not a problem, since the phreatic surface is by definition the point where the saturated zone starts. However, it has the consequence that the heads in this layer should not be used to determine the phreatic surface in the model as long as the layer below it is not fully saturated.

6.1.1 Delfland 25

The model results and the measured heads for Delfland location 25 are displayed in figure 6.1. The plot consists of four parts: the model results and measurements for each of the three monitoring wells, and the daily precipitation and evapotranspiration volumes as bar plots in a single graph.

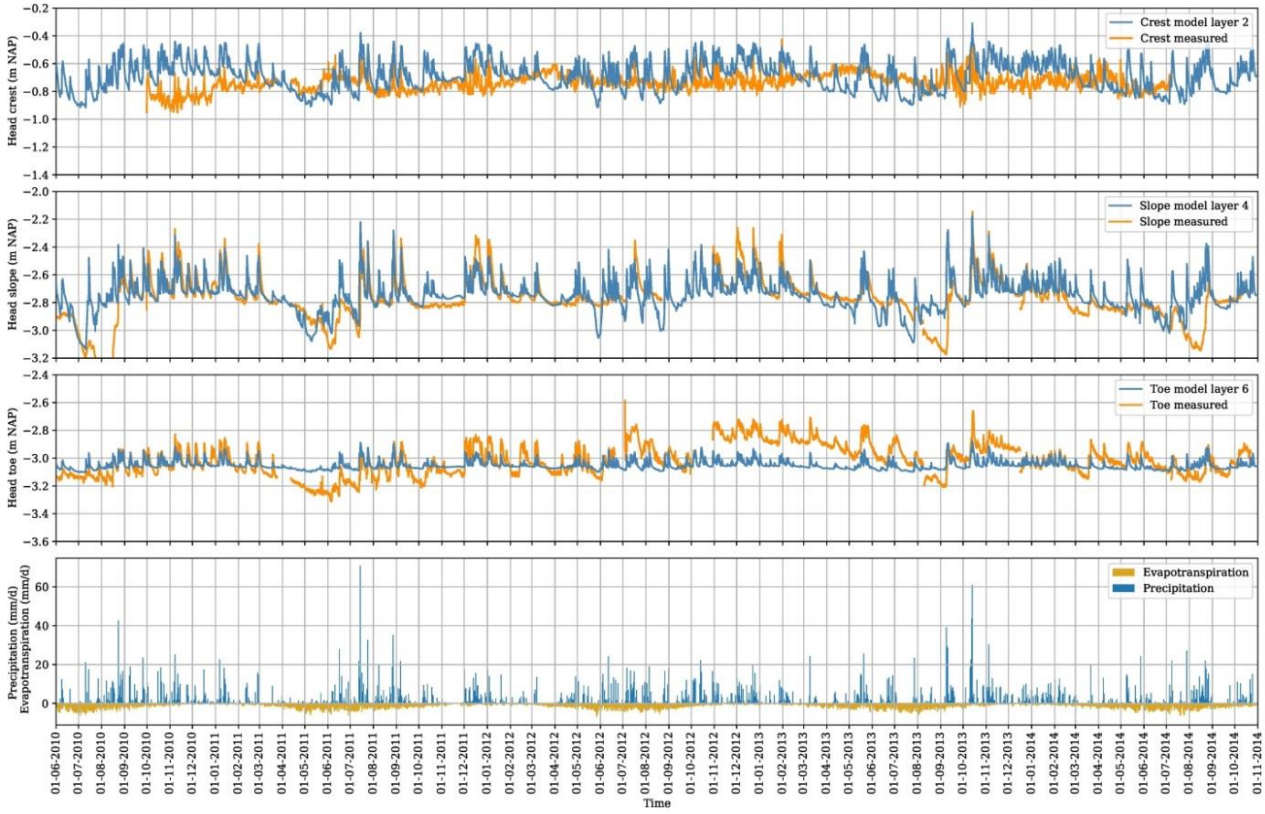

Figure 6.1: Model results Delfland location 25

Differences can be observed in the fit of the model for the different locations in the cross-section: in the crest the model fits better than for the other two locations. For a single monitoring well differences can be observed between the peaks, some are modelled better than others.

In the crest, the fluctuations of the heads in the model are larger than what is observed in the measurements. A possible explanation for this could be that the local conductivity is slightly different than in the rest of the flood defence. In the model the dike core is schematised as one homogeneous layer, while in reality the conductivity is probably more variable.

In the measurements long-term variations can be observed that are not present in the model. This variation does not correspond to the seasonal variation caused by evapotranspiration, which can be observed for the slope and the toe. A possible explanation could be variations of the outside water level. From the water board of Delfland has water level measurements for the outside water are available, but the overlap of these measurements with the measurements of the phreatic surface only spans several months. This is not enough to determine whether water level variations could be the origin of this long-term variation.

For the monitoring well in the slope the best fit between the model and the measurements is observed. Most precipitation peaks reach the same height as in the model, but some peaks are modelled too low. Comparing these peaks to the precipitation data, this mostly occurs for precipitation events with a longer duration and lower intensity. This points to the model being more suited to model high intensity precipitation than low intensity precipitation. Several dips in the head caused by evapotranspiration can be observed that are not present in the measurements. On the other hand, some of the dips in the measurements are not seen in the model results.

For the toe some sections can be observed where the modelled head is lower or higher than the measurements. This is mostly caused by the jumps in the measurements discussed in chapter 4 . These jumps are probably errors in the measurements, which would explain the difference. When the general height of the heads is disregarded and only the peaks are observed, the peaks match the measurements quite well in shape, but are slightly smaller in magnitude.

To compare the frequency of occurrence of a certain head in the model and in the measurements, histograms are plotted of the measurements and the model results. These are displayed in figure 6.2. On the horizontal axis the head elevation is displayed, and the vertical axis provides a measure of the frequency of occurrence of a head elevation. Because the number of measurement points is smaller than the number of time steps (due to gaps in the measurements), the histograms are normalised to make comparison easier. Some of the histograms have a very narrow tail which makes it unclear what the extreme values in the data are. For this reason the extremes are indicated with a triangle. Furthermore, the height of the schematisation at the locations of the monitoring wells is displayed in each of the plots.

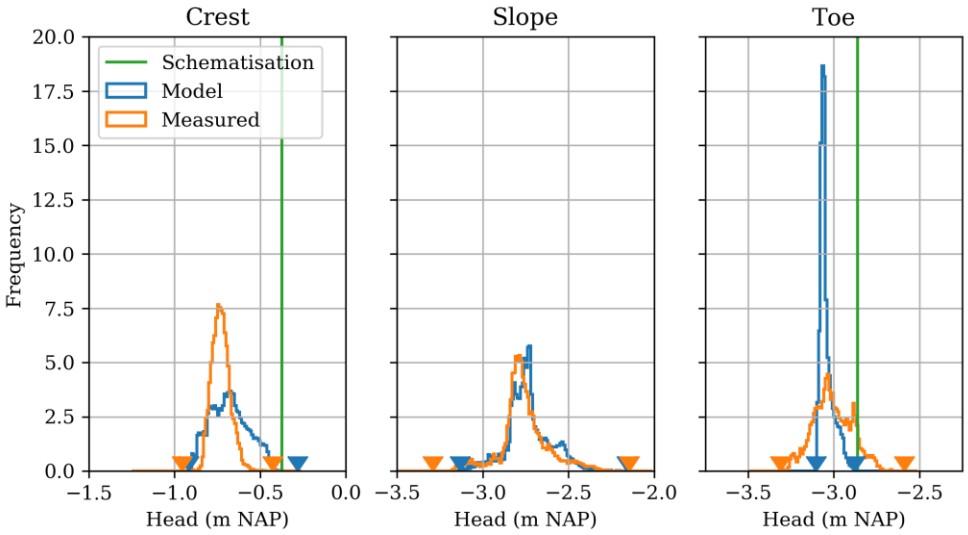

Figure 6.2: Histograms of the measurements and model results of Delfland location 25

The histograms confirm the observation that the model is fitted best to the measurements in the slope. The height of the schematisation in the slope is removed some distance from the highest head in both model and measurements, indicating that the schematisation is not exceeded at this

point in the cross-section. For the head in the crest the histogram of the model is somewhat wider on the right-hand side than it is for the measurements. This means relatively high heads occur more often in the model than in the measurements. The heads are also closer to the schematisation. In the model the schematisation height is exceeded for 10 consecutive hours on 13-10-2013, but in the measurements this is not the case. At the toe, the histogram for the model is taller than for the measurements. This means the variation range of the modelled heads is smaller. As discussed earlier, this can in part be explained by the shifted parts in the measurements. This would also explain the second peak that can be observed in the histogram of the measurements, which would be the mean of the shifted measurements in that case. In the measurements the schematised phreatic surface is regularly exceeded, but in the model this does not occur.

As a last assessment of the fit of the model, the difference between the measured head and the modelled head was calculated for each time step, with the exclusion of time steps for which no corresponding measurement existed. From these values the mean and standard deviations were calculated.

Calculating the mean error is not necessarily a good indicator for the fit of the model; a mean error close to zero only means that the model results are approximately equally often lower as they are higher than the measurements. The mean only shows if the model consistently over- or underestimates the heads. To provide another indication of the model fit, the Nash-Sutcliffe model efficiency coefficient is calculated. This coefficient is used to determine the predictive power of hydrological models, but can also be used for other types of models. The coefficient can be calculated using (Nash & Sutcliffe, 1970):

$$NSE = 1 - \frac{\sum_{t=1}^{T} (h_m^t - h_o^t)^2}{\sum_{t=1}^{T} (h_o^t - \overline{h_o})^2} \tag{6.1}$$

Where:

NSE	=	Nash-Sutcliffe model efficiency coefficient	(-)
T	=	number of timesteps	(-)
h^t_m	=	modelled head for timestep t	(m NAP)
h^t_o	=	observed (measured) head for timestep t	(m NAP)
$\overline{h_o}$	=	mean of observed heads	(m NAP)

A value of NSE smaller than 0 means the mean of the measurements is a better predictor of the head than the model results. A value of 1 means the model results are identical to the measurements.

Table 6.1: Errors between the model and the measurements per time step

Error	Crest	Slope	Toe
Mean (m)	0,06	-0,04	0,03
Standard deviation (m)	0,12	0,13	0,1
Maximum error (m)	0,25	0,31	0,50
Minimum error (m)	-0,45	-0,84	-0,27
Nash-Sutcliffe (-)	-4,35	0,25	0,18

The mean error is relatively low for all three monitoring wells. The minima and maxima show that large errors are present for some time steps. These are mostly caused by the dips and peaks that are modelled too high or too low. The slope, which showed the best fit, remarkably has the largest standard deviation for the error per time step. It also has the largest minimum error. The

cause of this is that for most time steps the model fits very well, but some of the largest errors also occur at this location. The errors are mainly overestimations, underestimations are much rarer and smaller. The overestimations are mainly caused by periods with large dips in the measurements, which were not properly modelled.

The Nash-Sutcliffe model efficiency coefficients are above 0 for the slope and the toe, but for the crest the value is below zero. This means that the fit of the model is less good in the crest, as was observed earlier. The long-term variations in the measurement not being present in the model has the result that the modelled head is almost always slightly higher or lower. This results in a low model efficiency coefficient. On the other hand, many of the fluctuation patterns in the measurements in the measurements can also be observed in the model, but at a slightly different height. This shows that using a single indicator only shows limited information on the fit of the model.

6.1.2 Delfland 24

For Delfland location 24, the model results are displayed in figure 6.3. The data for the monitoring well in the toe is displayed as well, although it has no meaning for the phreatic surface in the cross-section. As discussed earlier, this monitoring well is placed on the polder side of the sand fill in the former drainage ditch, and the boundary condition is applied to this sand fill. The measurements were only used to calibrate the boundary condition such that the inside groundwater table was matched approximately.

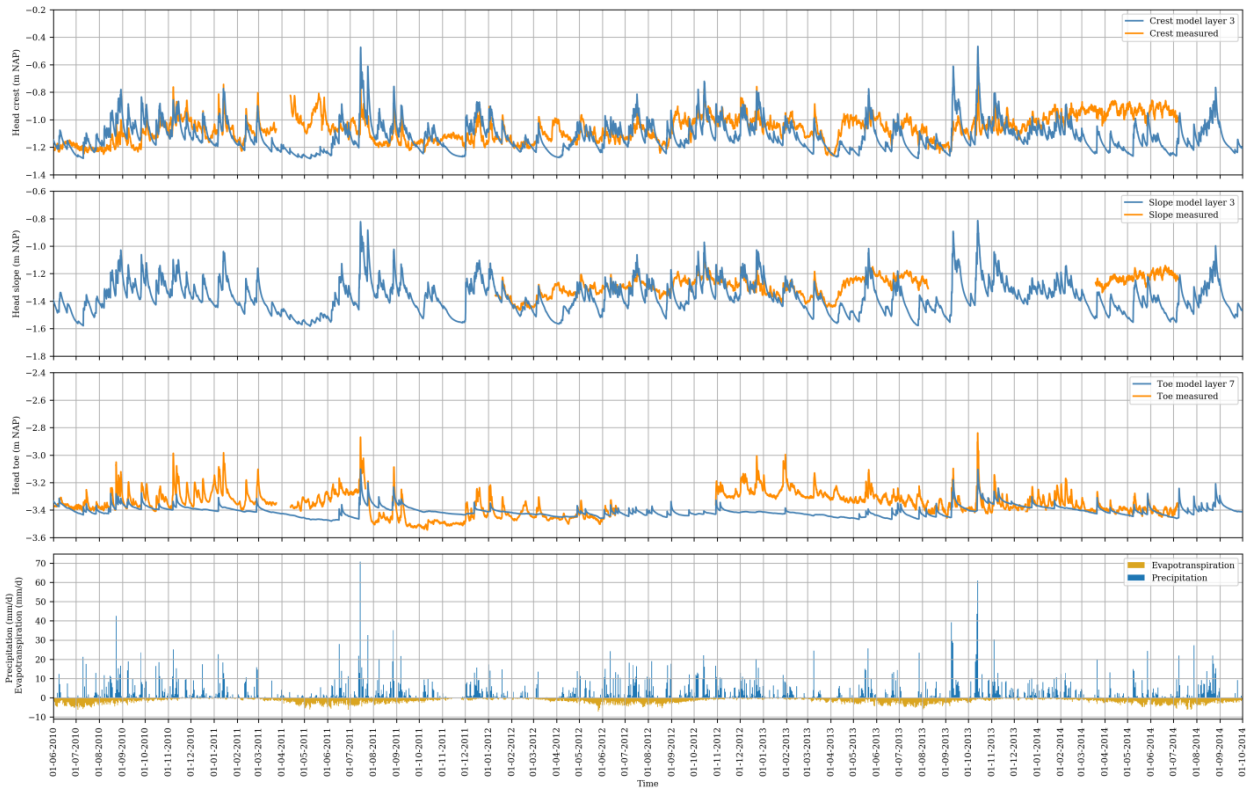

Figure 6.3: Model results Delfland location 24

On first sight, the fit to the measurements is less good than for location 25. When taking a closer look, it is mainly the dips in the model results that show a difference to the measurements. During precipitation peaks the model fits quite well, but when the precipitation stops the modelled heads decrease, whereas the measurements remain more stable.

This is illustrated in figure 6.4, which shows one of these dips in more detail. Up until the dry period of several weeks, the model fits well, but then the heads decrease while the measured heads remain constant. The measurements even show a head rise in the middle of the dry period, which does not correspond to any precipitation event. This is probably caused by fluctuations in the outside water level. During dry periods water is let into the boezem to maintain the water level. This could be the explanation for this head rise.

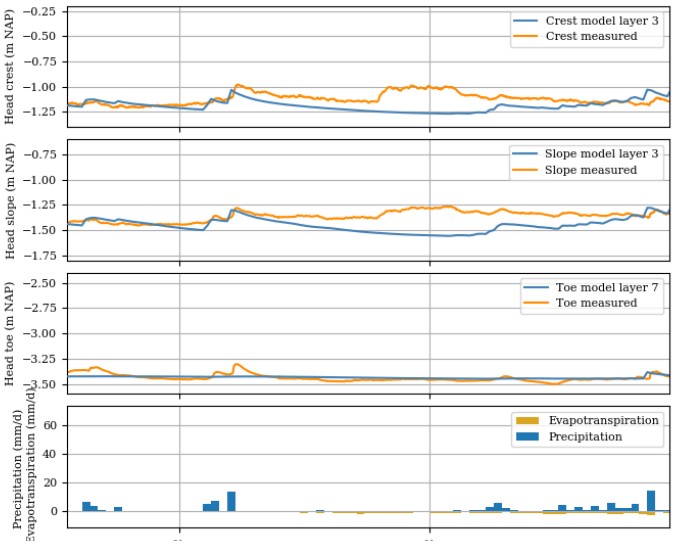

Figure 6.4: Detail of model results location 24

However, fluctuations do not fully explain this difference between the model and the measurements. The outside water level is kept constant in the model, so if the outside water level slowly decreases during a dry period, the measured heads would decrease whereas the model results would not. The soil parameters could not be calibrated such that both the precipitation peaks and these dry periods are modelled correctly. The explanation is probably found in the soil schematisation. The rubble core is modelled as a single, homogeneous layer with a clear boundary, but in reality the transition to the clay cover is probably more gradual.

This difference between the model and the measurements is reminiscent of the monitoring well in the crest of location 25, which heads could also not be fully modelled. For location 24, the monitoring wells are both in the crest, because of the permeable rubble core the heads of the two locations are very close to each other. Both wells are therefore affected by the outside water level, like the well in the crest of location 25. Neglecting the variation of the outside water level might thus be part of the reason why the heads in the crest are modelled less accurately than in other parts of the cross-section.

Again, histograms were plotted to compare the model results to the measurements. These are displayed in figure 6.5.

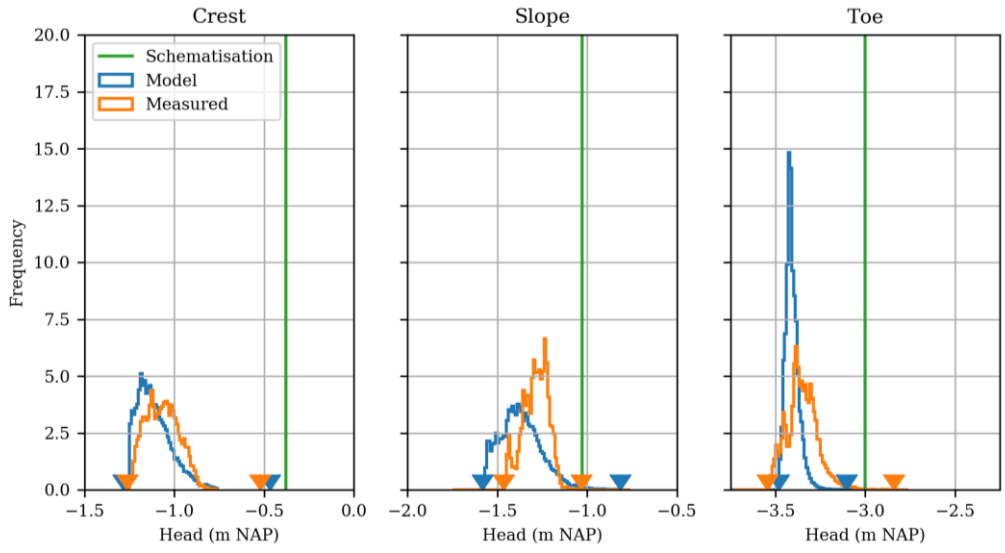

Figure 6.5: Histograms of the measurements and model results of Delfland location 24

Large parts are missing in the measurements, especially for the slope. Some of the differences between the histograms may be caused by these gaps rather than actual differences between the model and measurements. For example, the two largest precipitation events are excluded from the measurements which might partially explain why the higher heads in the slope occur more regularly in the model than in the measurements. It can also be observed that lower heads are also more present in the model, which corresponds to the observation that during dry periods the modelled heads are too low.

In the slope, the schematisation is exceeded regularly, during 294 time steps. Many of these time steps are consecutive and should be counted as single event. When this is done the schematisation was exceeded during 9 events. The schematisation is never exceeded in the slope. In the toe the schematisation is exceeded by the measurements a few times, but never by the model.

Once again, the error between the simulated and measured head was calculated for each time step. The means, standard deviations, maxima and minima of these errors are displayed in table 6.2. The Nash-Sutcliffe model efficiency coefficient is also included.

Table 6.2: Errors between the model and the measurements per time step

Error	Crest	Slope	Toe
Mean	0,05	0,1	0,05
Standard deviation	0,12	0,11	0,09
Maximum error	0,44	0,37	0,56
Minimum error	-0,46	-0,22	-0,15
Nash-Sutcliffe	-1,09	-3,34	-0,43

The mean error is in the same order as for location 25. The standard deviations are somewhat smaller. Based on this information it would seem that the fit of this model is better than for location 25. This is not the case, for location 25 the largest errors are larger, but the most common magnitudes of error are smaller for location 25 than for 24. The Nash-Sutcliffe model efficiency coefficient is below zero for all three locations, indicating a poor fit. The earlier discussed dips are the main cause of this, since the errors are large for these sections.

6.1.3 Hogedijk

For the Hogedijk, the model results are displayed in figure 6.4. In contradiction to the other models, the model for the Hogedijk was calibrated using only a part of the measurement period, since this was the only part available at the time. In january 2019 new measurements became available. Extending the precipitation and evapotranspiration data for this extended period the model was runned again, without performing a new calibration. This way the fit of the model can be assessed by comparing the results to measurements outside of the calibration set.

It can be observed that with the exception of the peaks, the model fits the measurements of monitoring wells 1,2, and 3 quite well. As described in chapter 4, monitoring well 1 exhibits several periods with unreliable measurements. For these periods the model does therefore not match the measurements.

For monitoring well 2 the peaks in the model are too high compared to the measurements. It was possible to calibrate the model such that the measurements were matched, but this resulted in a less good fit for monitoring well 3. For that well the fit is quite good, except for the peaks: the simulated head rises much slower. The fast response as observed in the measurements could not be reproduced. However, after a meeting with Nectaerra, the company that executes the measurements it was determined that the large fluctuations for monitoring well 3 are most likely caused by cracks in the dike, which allow runoff water to flow into the well. This could explain the inability to reproduce these measurements.

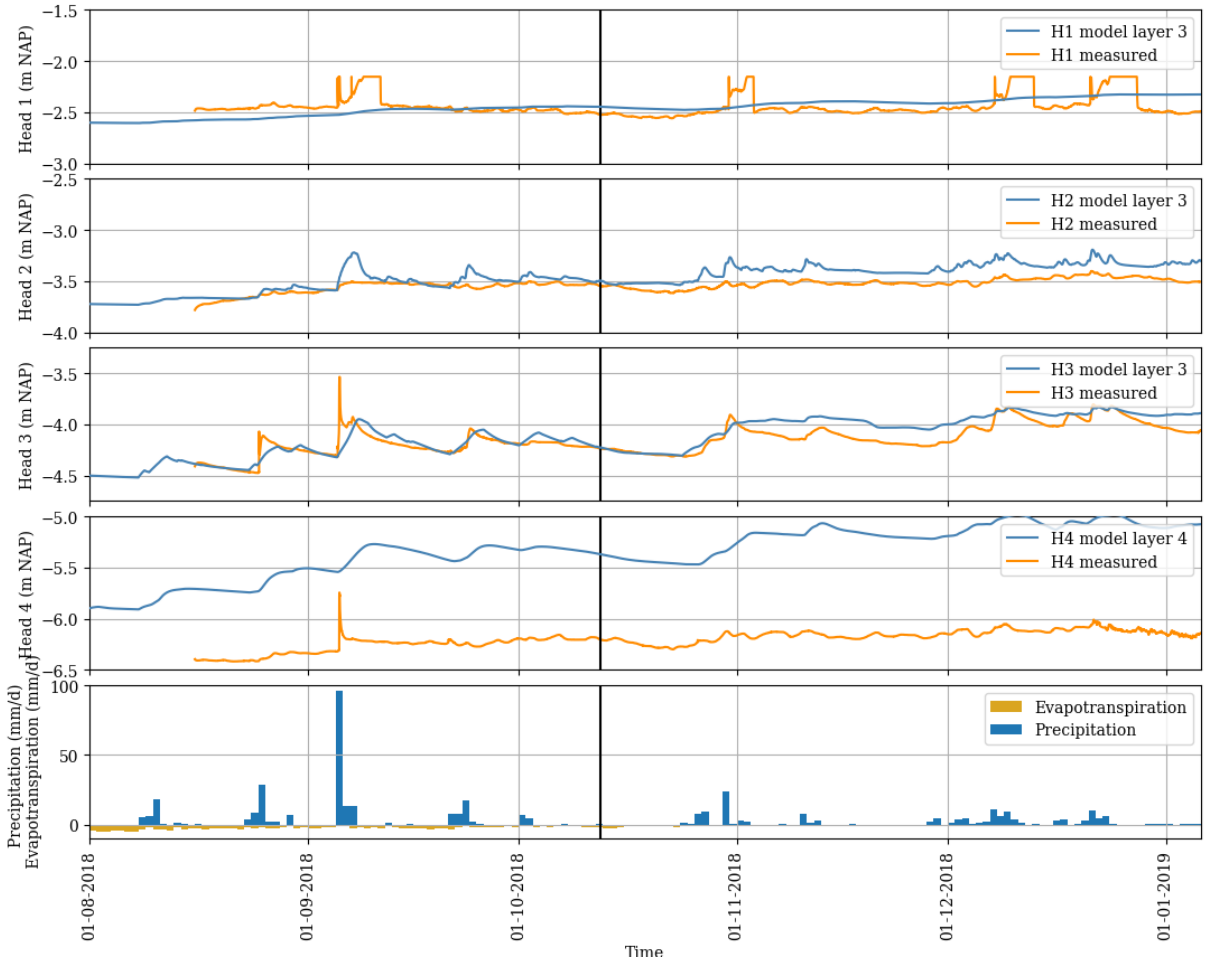

Figure 6.6: Model results Hogedijk. The black line indicates the end of the original measurement series the model was calibrated on.

In the extended measurement period the modelled heads become about 10 cm higher than the measurements, but the shape of the peaks still matched the measurements. It can be observed that both the model and the measurements still show a gradual increase of the heads after the dry summer period. In the model this increase is slightly larger than in the measurements, resulting in a small deviation. Considering that the calibration period was shorter than the extended period, and directly following the dry summer months, this deviation of 10 cm is relatively small. With a longer calibration period better results would probably be obtained.

As discussed earlier, the measurements of monitoring well 4 are rather remarkable since the heads are lower than the polder water level, although the well is placed in the slope of the flood defence 9 m removed from the drainage ditch. In the extended measurement period the head approaches the polder level of NAP -5,98 m closer, but still remains below it. The model could not be fitted to this head. A better match was possible by locally increasing the conductivity of the peat layer greatly, but this would result in an unrealistic conductivity that would deviate considerably from the conductivity in the rest of the peat layer and from the measured value. During the meeting with Nectaerra no clear cause could be determined for these low measurements. Possibly the polder level is different in reality, since many different water levels are present along the dike.

For the Hogedijk no histogram is presented. Due to the short measurement period an upward trend is observed in the heads, which distorts the histograms. The error per time step was calculated, and the characteristics of these errors are displayed in table 6.3.

Table 6.3: Errors between the model and the measurements per time step

Error (m)	HGD 1-1	HGD 1-2	HGD 1-3	HGD 1-4
Mean	0,01	-0,09	-0,06	-0,91
Standard deviation	0,11	0,06	0,08	0,13
Maximum error	0,38	0,05	0,74	-0,22
Minimum error	-0,18	-0,28	-0,21	-1,13
Nash-Sutcliffe	-0,19	-2,44	0,50	-108,58

As could be expected, the error for monitoring well 4 are very large. For the other three monitoring wells the mean errors are slightly smaller than those observed for the other two research locations in Delfland. The large maximum error for HGD 1-3 was caused by the large peak that could not be matched by the model. The Nash-Sutcliffe coefficient is only above 0 for HGD 1-3. The errors for HGD 1-1 and 1-2 are mainly caused by the structural difference in the uncalibrated period. It is likely that a better fit would be obtained when the model were to be calibrated over the entire measurement period.

6.2 Extreme simulated phreatic surfaces

The fifth research question established in chapter 1 was '*How does the phreatic surface in the numerical model respond to an extreme event?'.* To answer this question, first the extreme events that have occurred during the measurement period are investigated.

6.2.1 Extreme meteorological events in the simulation period

To assess the model results for the extreme events during the measurement period, the most extreme precipitation events are identified. For the locations in Delfland, the precipitation events during the measurement period were identified in chapter 4 . For the largest of those events an estimate was made for the return period. These return periods are based on precipitation statistics from STOWA (2015). These statistics are obtained from historical data, which was corrected for changes in the measurement method. This data was detrended to represent the climate around 2014. To include regional variations, the data was corrected for four different precipitation regimes in the Netherlands. For each of these regimes a generalised extreme value (GEV) distribution was fitted to the data, using which the relation between duration, intensity and return period is described.

Statistics from the report are published on the website Meteobase.nl in the form of tables, from which the return period can be obtained for a given duration and precipitation volume. These tables are provided for each of the four precipitation regimes. All research locations are situated in regime H. The exact values for the duration and volume of the precipitation events are not included in the tables, but by interpolating between the given values the return periods could be estimated. For the locations in Delfland three events with a return period larger than 10 years have occurred during the measurement period: these are displayed in table 6.4.

Table 6.4: Three largest precipitation events during the measurement period in Delfland

Date	Duration (hours)	Volume (mm)	Return period (years)
12-10-2013 19:00	22	102,8	250
13-7-2011 19:00	28	73,9	20
23-8-2010 1:00	9	42,4	10

At the Hogedijk, the measurement period was much shorter, so fewer extreme events have occurred. Two events with a total volume larger than 20 mm have occurred, but by coincidence one event with a very large return period of about 700 years was included. However, some remarks need to be made for the large return period found for this event. The used statistics are valid for precipitation events with durations of more than two hours. More recently the statistics

were extended for durations as short as 10 minutes, but longer durations up to 12 hours were included as well in this newer report (STOWA, 2018). Some large differences are found for these longer durations between the new and the older statistics in STOWA (2015). The return period for the event according to these newer statistics is 150 years. It is not entirely clear which of the two statistics should be used for durations between 2 and 12 hours, and therefore both return periods are displayed in table 6.5.

Table 6.5: Precipitation events with a volume larger than 20 mm during the measurements at the Hogedijk

Date	Duration (hours)	Volume (mm)	Return period (years)
5-9-2018 6:00	8	95,6	700/150
24-8-2018 21:00	13	32,4	1

The STOWA report also provides a detrended evapotranspiration series. However, no distribution was fitted to this series. Furthermore the series is based on the Makkink method whereas in the models the Penman-Monteith method was used. To be able to identify the dry periods the precipitation deficit was calculated for each year in the measurement period in Delfland. This is the sum of the potential evapotranspiration rate minus the sum of the precipitation, for the months April to September. For 2011 and 2012 there was a precipitation surplus, and for the remaining years the precipitation deficit is displayed in table 6.7.

Table 6.6: Years with a precipitation deficit for Delfland

Year	Precipitation deficit (mm)
2014	110,0
2013	73,6
2010	24,9

The measurement period of the Hogedijk was less than a year, so only one dry period is partially included in the measurements. However, 2018 was one of the driest years on record which has probably resulted in a lower than average phreatic surface at the start of the measurements.

6.2.2 Highest and lowest phreatic surface

As a next step, the highest and lowest simulated phreatic surfaces in the simulation were identified. For each column in the cross-section the highest head was taken, for each time step. In these columns the top layer was excluded, because as mentioned the simulated heads in this layer do not represent reality. The deepest layers were also excluded because these are influenced by the head in the Pleistocene sand layer. This maximum head represents the phreatic surface for that slice. From all slices in the cross-section the mean was calculated, to obtain the average height of the phreatic surface for the considered time step.

By identifying the peaks of this average head over time, the highest simulated phreatic surfaces could be obtained. Between these peaks a minimum distance of 216 hours was specified, because a single precipitation event may lead to multiple peaks.

Similarly, the lowest dips in the average head were identified to obtain the lowest phreatic surface. Between the dips a minimum distance of 672 hours (4 weeks) was used, since dry periods span a longer time period than precipitation events.

6.2.3 Delfland 25

The five highest simulated phreatic surfaces for location 25 are displayed in table 6.7. For reference, the mean of the average phreatic surface over the simulation period is NAP -1,99 m.

Table 6.7: Five highest phreatic surfaces location 25

Rank model	Date	Average phreatic surface (m +NAP)
1	13-10-2013	-1,46
2	14-7-2011	-1,52
3	10-9-2013	-1,57
4	27-8-2011	-1,60
5	4-11-2013	-1,61

The highest and second highest phreatic surfaces correspond to the two most extreme precipitation events. For rank 1 the model fits the measurements quite well. In the crest the model is slightly higher than the measurements, but in the measurements a dip can be observed before the precipitation peak. This dip could be the result of pre-pumping of the boezem, which is not taken into account in the model. For rank 2 the heads in the model are slightly higher than the measurements of all monitoring wells. For rank 3 the model fits well for the crest and toe, but in the slope the heads are almost 0,5 m higher than the measurements. The peak in the measurements is preceded by a gap and an inexplicable dip, so there might be an error in the measurements for this precipitation event. For rank 4 and 5 the model fits the measurements well.

The highest phreatic surface of the simulation is displayed in figure 6.7. In this figure the phreatic surface is displayed, along with the measured heads in the monitoring wells which are displayed as red crosses. Additionally, the schematisation of the phreatic surface is displayed for reference.

The schematisation is very similar to the simulated phreatic surface for this situation. Below the inner slope the schematisation is slightly more conservative than the model, but near the crest and the toe the simulated heads are a few centimetres higher than the schematisation.

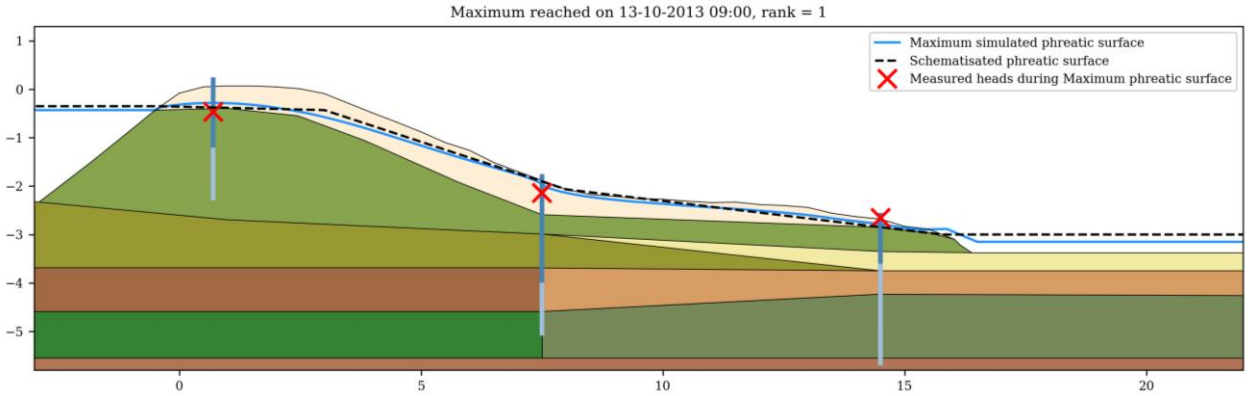

Figure 6.7: Highest simulated phreatic surface for Delfland location 25

The five lowest phreatic surface are displayed in table 6.8.

Table 6.8: Five lowest phreatic surfaces location 25

Rank model	Date	Average phreatic surface (m +NAP)
1	10-7-2010	-2,27
2	24-7-2013	-2,25
3	28-5-2012	-2,25
4	8-5-2011	-2,25
5	5-6-2011	-2,23

It stands out that the average height of the phreatic surface is almost the same for all five dates. This is the lowest phreatic surface that can be reached by the model, only a large peak in the

evapotranspiration rate can lead to a slightly lower phreatic surface. There is no clear correspondence to the years with the largest precipitation deficit; in fact 2014, the year with the largest precipitation deficit, is not present in the lowest five phreatic surfaces.

For these five lowest phreatic surfaces, the measureed heads are about 5-10 cm higher than in the model. However, there are some dips at different points in time where the measurements are 5-10 cm lower than the lowest heads in the model. This indicates the model is less accurate for the prediction of low extremes than it is for high extremes.

In figure 6.8 the lowest simulated phreatic surface is displayed. For this point in time no measurement in the crest was available, but the other four lowest phreatic surfaces are very similar, and for those the measurement corresponds well to the model.

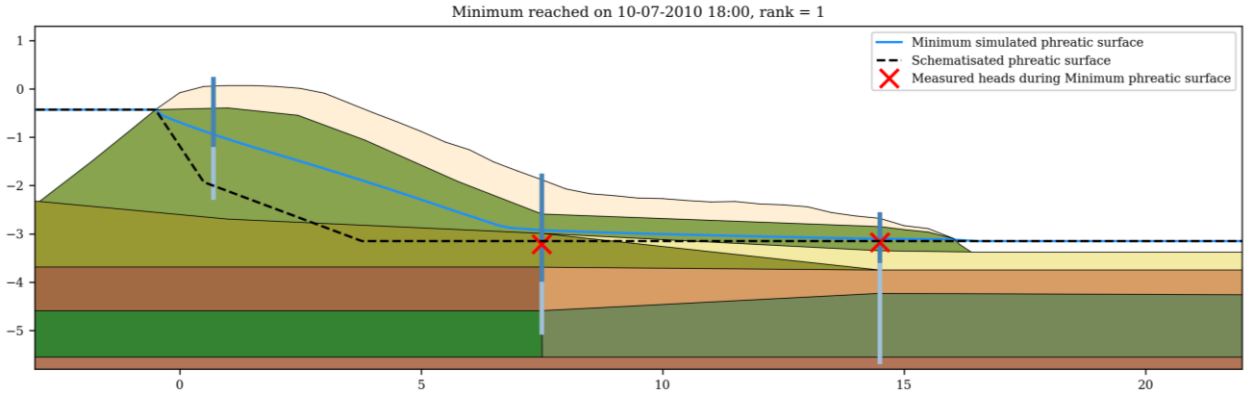

Figure 6.8: Lowest simulated phreatic surface for Delfland location 25

In the middle of the cross-section a strange dip in the heads of soil layers 2 and 3 can be observed. This is most likely a result of the way the intermediate sand layer was schematised. In this area the bottom of these two layers is slightly above the phreatic surface, which means the cells in these layers are unsaturated. When the cells are unsaturated, the head is modelled at the extinction depth of the evapotranspiration package, resulting in this dip. The phreatic surface in this area is represented by the layer below, layer 4.

For this situation, the schematisation is lower than the simulated phreatic surface. The schematisation accounts for the situation where the soil below the crest is more permeable, which results in a lower phreatic surface. Both the measurements and the model point to this not being the case for this particular flood defence.

6.2.4 Delfland 24

For the model of Delfland location 24, the five highest phreatic surfaces are displayed in table 6.9. The mean of the average phreatic surface for all time steps is NAP -1,61 m.

Table 6.9: Five highest phreatic surfaces location 24

Rank model	Date	Average phreatic surface (m +NAP)
1	14-10-2013	-1,08
2	14-7-2011	-1,10
3	24-7-2011	-1,15
4	11-9-2013	-1,18
5	14-10-2012	-1,23

Again, the two highest phreatic surfaces correspond to the two largest precipitation events. The third highest phreatic surface occurs only 10 days after the second highest phreatic surface. Between these peaks some minor precipitation had occurred, and therefore the phreatic surface was still raised when another precipitation event occurred on 23-07-2011. This shows that a

small precipitation event can still lead to a high phreatic surface, depending on the initial situation.

The highest phreatic surface in the model corresponds well to the measurement, although no measurement was available for the monitoring well in the slope. For the second and third highest phreatic surfaces the model results are slightly higher, but a dip in the measurements seems to point again to pre-pumping of the boezem being the cause of this. For the event with rank 4, the simulated phreatic surface is almost 40 cm too high, for which no clear cause can be identified. Remarkable is that the same precipitation event resulted in a similarly high phreatic surface for location 25. This might mean that the model does not respond correctly to this particular precipitation event, or that there is an error in the precipitation data for this event. For the event of 14-10-2012 the model fits well. This is the only one of the five events for which measurements were available for the monitoring well in the slope. In figure 6.9 the cross-section is displayed for the time step with the highest phreatic surface.

Remarkable is the elevated plateau in the phreatic surface. This is a result of the way the rubble core is schematised. At its right-hand edge, the core material continues below the clay of the berm. During the extreme event, the head in the permeable core rises fast, which leads to overpressure of the water below the berm material, which has a lower permeability. This causes the head in the core to rise above the ground surface. In the model, the edge of the core material is sudden, leading to a jump in the phreatic surface. In reality the change in conductivity from the core to the berm is likely to be more gradual.

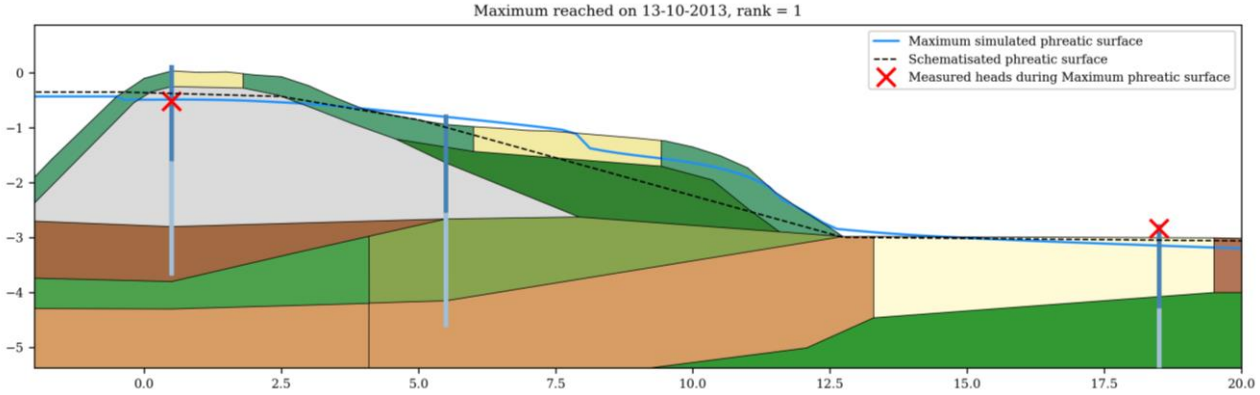

Figure 6.9: Highest simulated phreatic surface for Delfland location 24

In the crest, the phreatic surface remains below the schematisation. However, in the berm the schematisation is exceeded by a large margin. The reason for this is that there is a second inner crest at the berm. For a correct schematisation, below the crest of the berm a nearly horizontal course of the phreatic surface should be schematised to take precipitation into account.

The five lowest phreatic surfaces in the simulation are ranked in table 6.10. Again, there is almost no variation in the average height, indicating that these minima are at the lowest possible phreatic surface for the model. It also stand out that the year with the largest precipitation deficit, 2014, is not present in the top 5 for this location either.

Table 6.10: Five lowest phreatic surfaces location 24

Rank model	Date	Average phreatic surface (m +NAP)
1	8-5-2011	-1,83
2	10-7-2010	-1,83
3	26-7-2013	-1,83
4	4-4-2012	-1,81
5	9-4-2013	-1,81

For most of these five events the phreatic surface in the model is about 10 cm lower than the measured heads in the monitoring wells. The dips encountered in the model results are in general less pronounced than in the measurements.

The lowest phreatic surface in the simulation is displayed in figure 6.10. The schematised phreatic surface is much lower than the simulation. This is mainly caused by the head inside the dike, which is schematised at 0,7 m below polder water level because no drainage ditch is present.

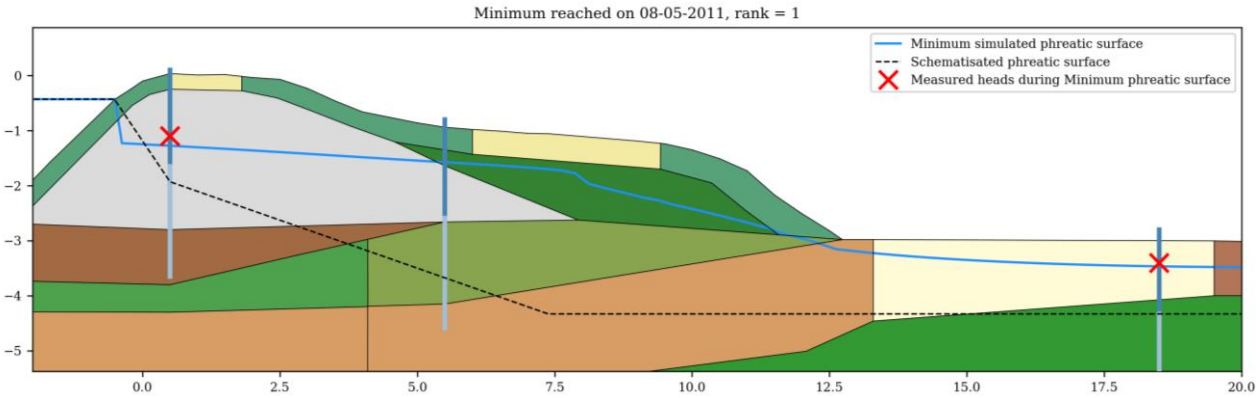

Figure 6.10: Lowest simulated phreatic surface for Delfland location 24

6.2.5 Hogedijk

For the Hogedijk the measurement period only spans several months, and therefore the highest and lowest phreatic surfaces are statistically less relevant than for the other research cases. However, by coincidence a large precipitation event has occurred in September 2018, which makes it interesting to compare the head rise caused by this event to other maxima.

The five highest phreatic surfaces during the measurements are displayed in table 6.12. The total period average of the average phreatic surface is NAP -4,16 m.

Table 6.11: Five highest phreatic surfaces Hogedijk

Rank model	Date	Average phreatic surface (m +NAP)
1	24-12-2018	-3,93
2	09-12-2018	-3,93
3	05-01-2019	-3,99
4	12-11-2018	-4,01
5	29-11-2018	-4,05

Remarkable in this top 5 is that the extreme precipitation event from 05-09-2018 is not present. When looking at the results in figure 6.4 it can be seen why: although the event leads to one of the largest peaks, the general level of the phreatic surface is still recovering from the dry summer. Only around November the heads have stabilised. Because the general level of the heads is higher, the top 5 peaks all have occurred in November or later. Furthermore the event had a very high intensity, leading to a large run-off volume and a comparitively low infiltration.

When observing the measurements, the event of 05-09-2018 shows the largest measured head for monitoring wells 3 and 4, but for monitoring well 1 and 2 higher heads are reached in November and December, like in the model. The cause of this are the sharp peaks observed in monitoring wells 3 and 4. It is unclear how accurate those peaks are: they might be caused by filling of the wells by run-off water. The quick subsidence after the maximum is reached makes the peaks different to the other peaks in the series.

In figure 6.11 the highest simulated phreatic surface is displayed.

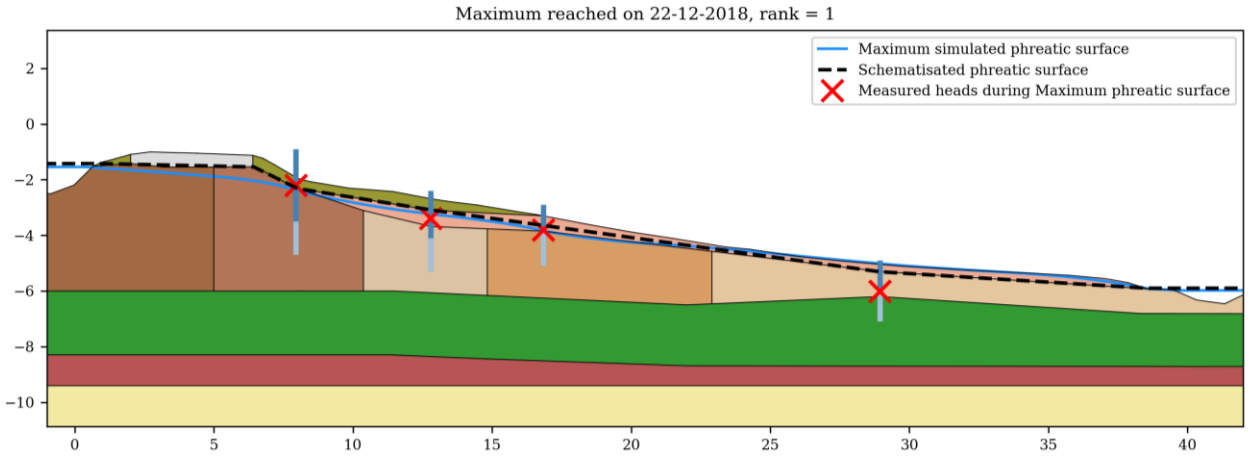

Figure 6.11: Highest simulated phreatic surface Hogedijk

At the toe and the lower regions of the slope the phreatic surface is at ground level, which indicates seepage occurs. This is not only the case for this highest phreatic surface: from about November onwards seepage nearly constantly occurs. Said region is also the region where the schematised phreatic surface is exceeded: in the rest of the cross-section the phreatic surface remains below the schematisation.

The lowest simulated phreatic surface in the measurement period is displayed in figure 6.12. The minimum is taken from the part of the simulation for which measurements are available. A lower phreatic surface might have occurred before the measurements started, but since the phreatic surface is compared to the measurements only the measurement period is considered.

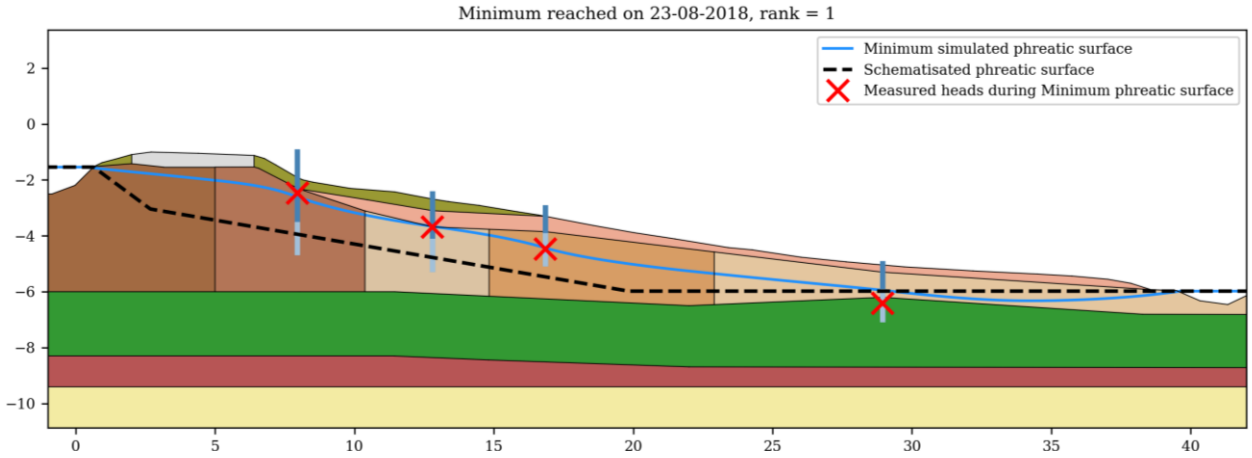

Figure 6.12: Lowest simulated phreatic surface Hogedijk

This lowest phreatic surface shows a good fit to the measurements. The low head of monitoring well 4 is still not reached, although evapotranspiration has caused the phreatic surface to be lower than the polder water level. This also means that in the regions near the toe the phreatic surface is lower than the schematisation. In the rest of the cross-section the phreatic surface remains above the schematisation.

6.3 Fictitious precipitation event

Regarding precipitation, only two events with a return period larger than 10 years have occurred during the measurement period. An extreme precipitation event can be characterised by various aspects, which may lead to a different responses of the model. To obtain a more complete picture of the response of the model to precipitation, fictitious events are imposed on the model.

6.3.1 Definition event

For the definition of the precipitation, the precipitation statistics from paragraph 6.2 (STOWA, 2015) are used again. A precipitation event for a given return period is defined by the duration of the event and the total volume of precipitation. To investigate what combination of volume and duration leads to the largest rise of the phreatic surface, several combinations are tested.

In general, the precipitation intensity is not constant over the duration of an event. Usually one or more peaks are observed, and in the longer duration events short dry periods might even occur. To model this variability of the intensity over time, STOWA has defined seven standard patterns (STOWA, 2004). For a duration of 24 hours, these patterns are displayed in figure 6.13.

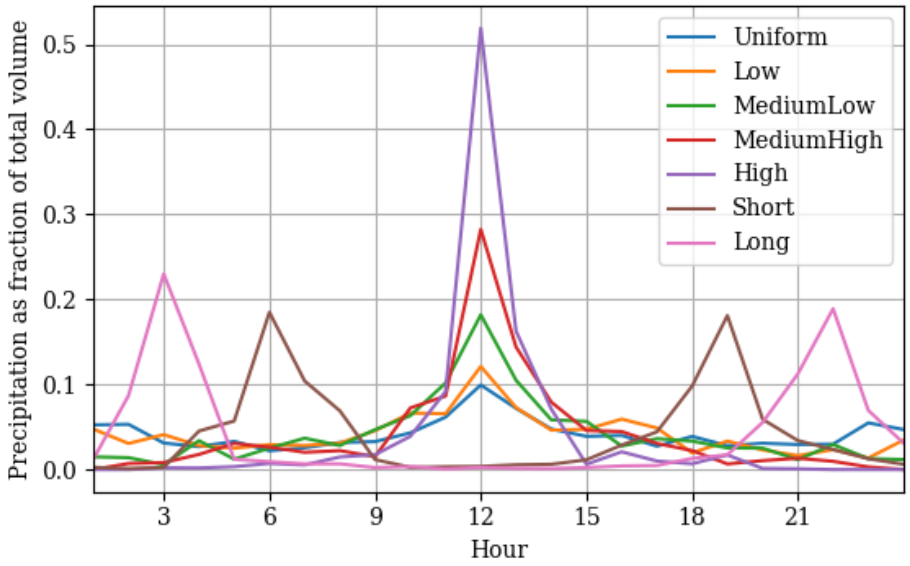

Figure 6.13: STOWA precipitation patterns

One pattern is nearly uniform with only a small peak, two patterns have two peaks, and the other four patterns have one single peak with different intensities. The patterns for longer durations are similar, but have more fluctuations. The precipitation patterns are only a for durations longer than 24 hours. Since the information on precipitation patterns for durations shorter than 24 hours is limited, patterns were generated by scaling the 24 hours pattern to shorter durations.

Initially, a constant return period of 100 years is chosen to compare the different durations and patterns. This return period is chosen based on the safety class of the flood defences. The return period of the loads used for the safety assessment of regional flood defences is dependent on the so-called IPO-class of the flood defence. This class is determined based on the economic damage in case of failure (STOWA, 2015). All three research cases have the IPO-class III, which corresponds to a return period of 100 years for the hydraulic loads.

Nine durations varying between 2 and 216 hours were simulated. Possibly the earlier mentioned statistics from STOWA (2018) should be used for the durations between 2 and 12 hours, but since this is unclear, and to maintain consistency, all data is taken from STOWA (2015). The response of the model is assessed at four points in the cross-section. For location 25 the three locations of the monitoring wells are used, with an additional point at the inner crest. For location 24 the locations of the monitoring wells in the slope and crest are used, with two additional points in the crest of the berm and at the toe. Due to its large width, six points are used for the Hogedijk. These are the four points of the monitoring wells, plus to additional points in the inner and outer crest. The phreatic surface is determined again by taking the maximum head of the upper layers, with the exclusion of the topmost layer.

Another factor of influence is the starting point of the simulations. The initial height of the phreatic surface determines the magnitude of the head rise. Several test simulations have shown

that this initial height has only a small on the maximum reached height of the phreatic surface. The head rise compared to the situation before the precipitation event is therefore dependent on the head in the initial situation. To prevent this, a steady-state simulation without precipitation was used as initial condition. After the precipitation event the model will return to steady-state conditions, and therefore the situation before and after the event are identical. Evapotranspiration was not applied to the model.

6.3.2 Response for return period 100 years

Nine duration/volume combinations with each seven precipitation patterns were applied to the models. For each duration the head variation at the four assessment points was plotted for the seven patterns. These plots are included in appendix H. For each duration it was determined which of the seven patterns resulted in the greatest head rise by calculating the maximum average head over the width of the cross-section. The normative patterns are summarised in table 6.12.

Table 6.12: Normative pattern for event durations

Duration	2	4	8	12	24	48	96	192	216
Delfland 25	Uniform	Uniform	Uniform	Uniform	Medium High	Long	High	High	High
Delfland 24	Uniform	Uniform	Uniform	Low	Uniform	Uniform	Uniform	Medium High	Medium High
Hogedijk	Uniform	Uniform	Uniform	Uniform	Low	Medium High	Medium High	High	High

Delfland 25

For location 25 there is a clear difference in the normative pattern between the shorter and longer durations. For durations shorter than 24 hours the uniform pattern is normative, whereas for longer durations the patterns including a peak lead to a larger head rise. The duration of 48 hours is an outlier being the only duration for which a two-peaked pattern is normative. This indicates that a certain intensity of precipitation is needed to reach the maximum head rise. The short events have a large intensity for all patterns. Since the model is set up such that the soil has a certain infiltration capacity, the largest infiltration is reached when this capacity is reached during the entire event. This explain why the uniform pattern is normative for the short durations. For the longer duration events the intensity is lower, especially when the uniform pattern occurs. This results in a quick rise of the head shortly after the start of the event, after which it remains approximately constant. An equilibrium situation is reached where the infiltration of precipitation is equal to the outflow to the inside water and the seepage. A higher head is only reached when the intensity increases, and therefore the peaked patterns are normative for the longer durations. The occurrence of an equilibrium situation was also observed by Ten Bokkel Huinink (2016).

To investigate the influence of the duration independent of the pattern, the response to the normative pattern for each duration was plotted in a single figure, which is displayed as figure 6.14. The four subplots show the response at the four chosen points in the cross-section.

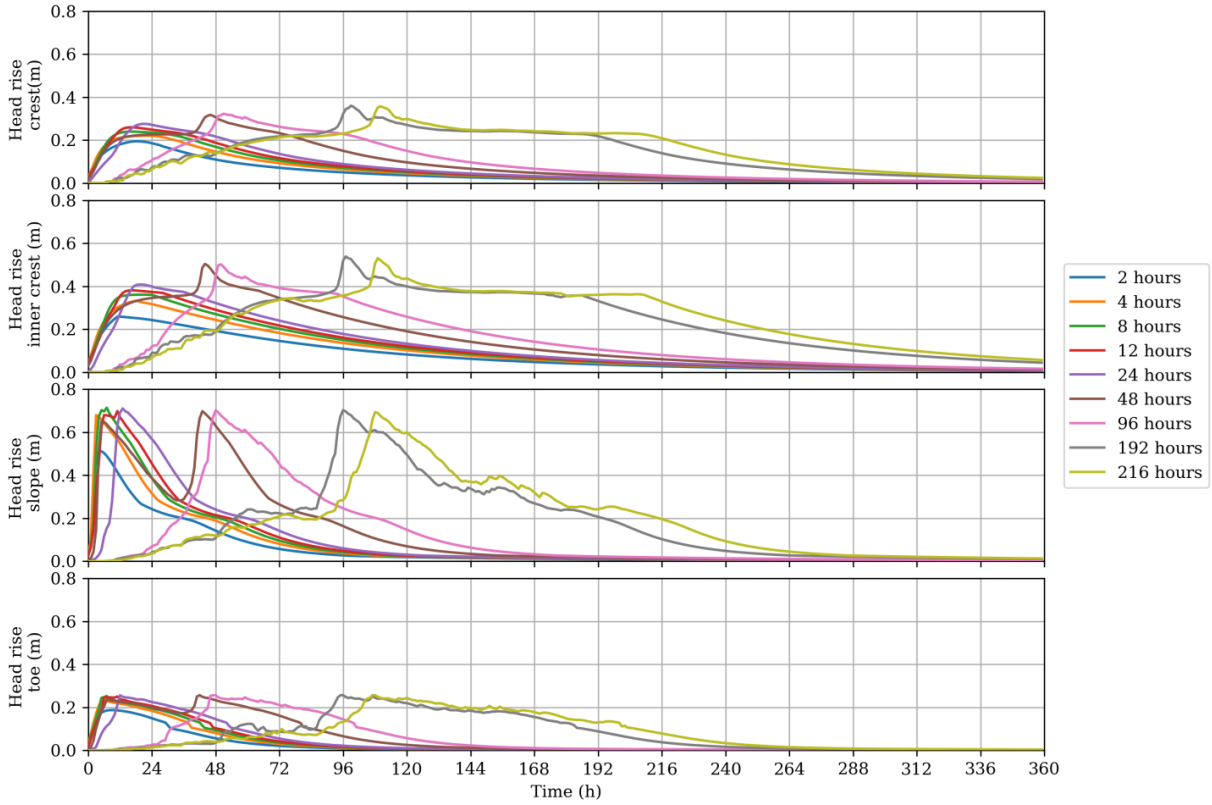

Figure 6.14: Response of the phreatic surface at location 25 to precipitation with various duration, using normative patterns

It can be observed that the durations below 24 hours lead to a smaller head rise than the longer durations, while the difference between the longer durations is very small. No larger head rise is reached than about 70 cm. At the toe and the slope the difference in maximum head rise is smaller between the durations than at the crest. At a certain height the head cannot rise any further at these points, since seepage occurs. Near the toe the initial phreatic surface is relatively close to the surface, and therefore the maximum head rise is limited.

Although the maximum head rise is nearly the same for the longer durations, a duration of 192 hours results in a slightly larger head rise than the other durations.

Delfland 24

For location 24 the relation between the normative pattern and the event duration was less clear. All durations below 96 hours have the uniform as normative pattern, with the exception of the duration of 12 hours. However, for that duration the response to the uniform pattern is almost identical to that to the low pattern. The only real difference is observed for the two longest durations, for which medium high is the normative pattern.

This difference compared to location 25 can be explained by the equilibrium situation. At location 25, an equilibrium was reached during the longer events preceding the peak of the event. Location 24 responds much slower: the equilibrium situation is not reached when the peak occurs. Only for the longest durations the effect described at location 25 occurs. The slower response can also be observed in the time it takes to return to the initial head: location 25 returns much faster. A possible explanation for this is the intermediate sand layer at location 25, which allows the flood defence to drain towards the polder.

Again the different durations with their normative patterns are displayed in a single graph, which is displayed in figure 6.15.

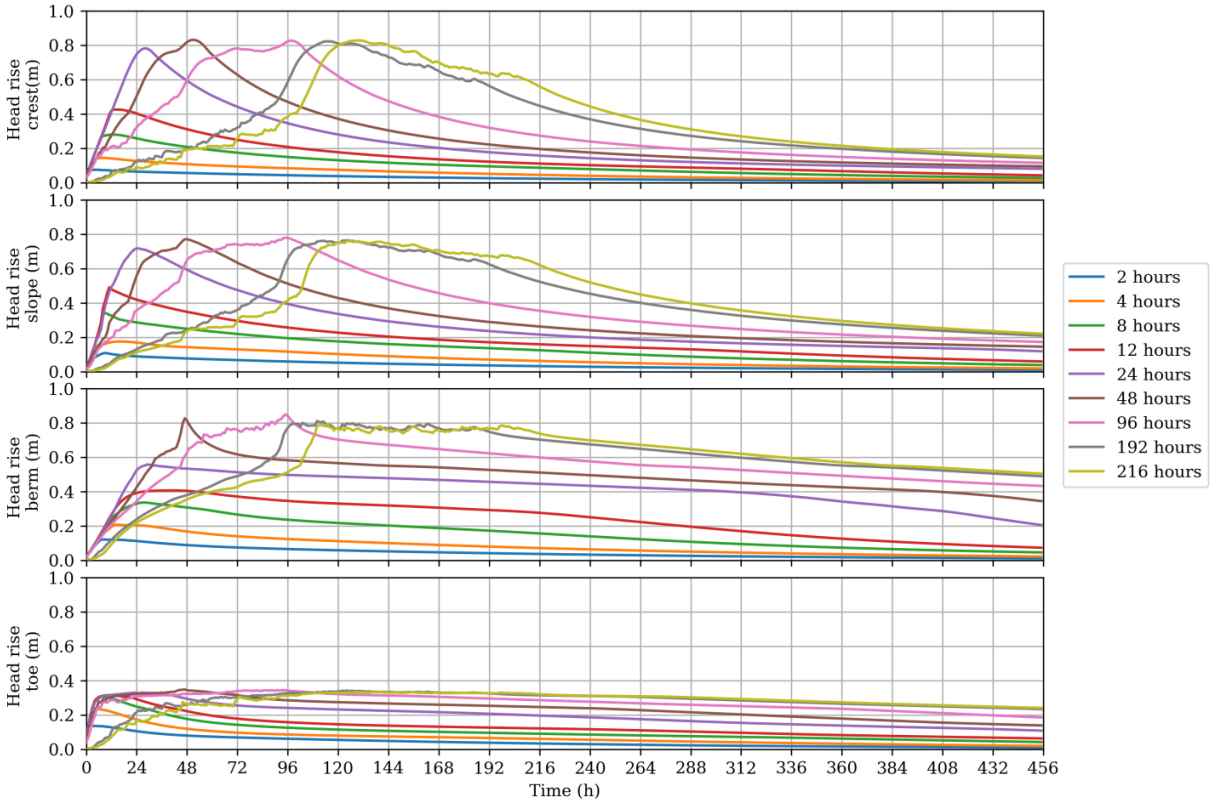

Figure 6.15: Response of the phreatic surface at location 24 to precipitation with various duration, using normative patterns

Compared to location 25, the difference in maximum head rise between the durations is more pronounced. From 48 hours onwards, the maximum head rise reaches its limit. This limit is probably an equilibrium situation where outflow and seepage balance the infiltration. In the berm this can be observed for the durations of 192 and 216 hours: at 0,8 m the head rises no further and remains constant. A duration of 96 hours results in the largest head rise, although the difference to the other durations longer than 48 hours is small.

Hogedijk

The normative patterns for the Hogedijk show a similarity to location 25: the uniform pattern is normative for the short durations, and a single-peaked pattern is normative for longer durations. For the size of this peak a trend can be observed as well: the longer the duration, the higher the peak of the normative pattern. This behaviour can be explained in similar way to location 25.

The different durations with their normative patterns are displayed in figure 6.16.

The equilibrium situation is reached quickly for the slope and the toe. As was observed earlier, seepage occurs quickly in this region, since the phreatic surface is close to ground level. The crest region of the flood defence show the opposite: the equilibrium situation is not even reached during the longest precipitation event. The head rise is also much smaller, and it takes a longer time for the head tor return to the original level. This difference in response between the higher and lower regions is caused by the differences in properties of the different parts of the peat layer. Near the toe the conductivity is larger, leading to a faster response. Another factor of influence is the specific yield of part 3 of the peat layer. In an attempt to model the quick response of the monitroing well in this section, the specific yield was set to a smaller value than the other parts of the layer. This also results in a larger response for the slope of the model.

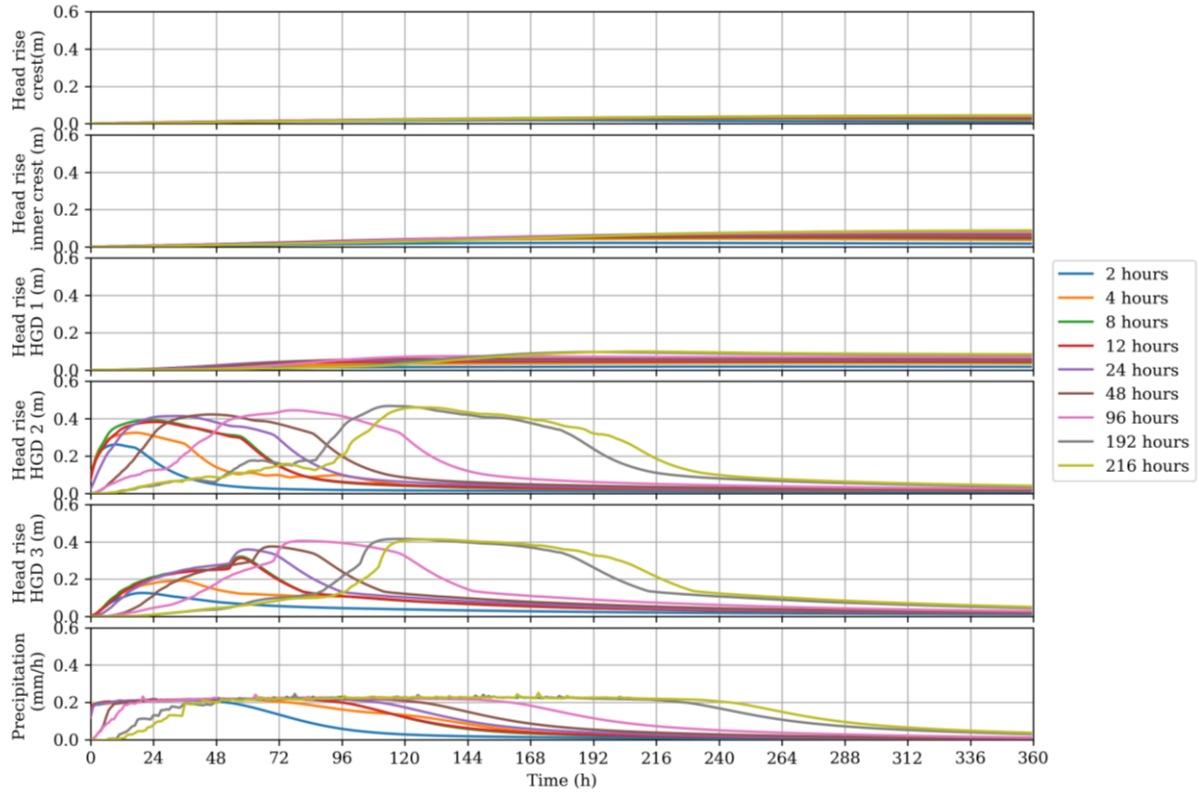

Figure 6.16: Response of the phreatic surface at the Hogedijk to precipitation with various duration, using normative patterns

Like also observed at location 24, a relation between the event duration and the maximum head rise is visible for most locations in the cross-section. Only for the toe the maximum head rise is the same for all duration, but this is caused by seepage. The maximum head rise was observed for a precipitation event with a duration of 192 hours.

6.3.3 Response for varying return periods

So far, all the precipitation events applied to the model were based on a return period of 100 years. To investigate the effect of events with a larger or smaller return period, simulations were carried out for return periods between 1 and 1000 years. The maximum reached phreatic surface for the duration and pattern resulting in the highest maximum are displayed for each return period. Note that this is not the phreatic surface for the given return period: the pattern and duration resulting in the greatest head rise are used, which have a probability of occurrence themselves. Furthermore, only the influence of precipitation is taken into account, the water levels are kept constant. The analysis is only intended to show the influence of precipitation events with various probability of occurrence.

The highest phreatic phreatic surface was determined in a similar way as in paragraph 6.2, by taking the highest head the columns of cells spanning the cross-section. The top layer is excluded because it is affected by the boundary condition.

Delfland 25

For location 25, the results of this analysis are displayed in figure 6.17. For reference, the phreatic surface in the initial situation and the schematisation are displayed as well. The difference between the various return periods is small. Below the crest and near the toe the phreatic surfaces are almost equal, and below the slope the difference between the highest and lowest is about 30 cm. This corresponds to the equilibrium situation discussed earlier: at a certain level the phreatic surface will not rise any further due to seepage. Near the toe this equilibrium

situation is reached earlier than in the slope, and therefore there is no difference between the precipitation events.

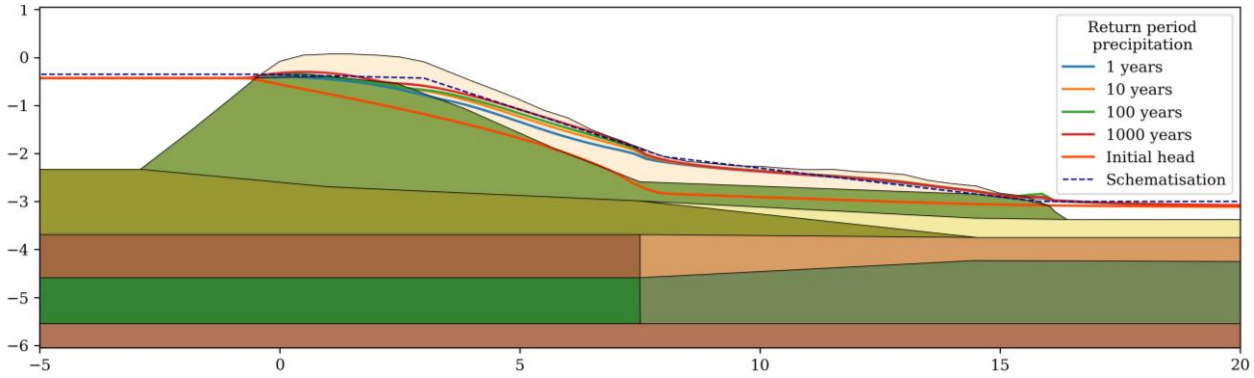

Figure 6.17: Phreatic surfaces location 25 for precipitation events with various return periods

Near the outer crest, the phreatic surface rises to above the outer water level. For return periods above 100 years, the schematisation is slightly exceeded. However, the schematisation assumes a higher than normal water level occurs, while the model does not.

Delfland 24

The results for Delfland location 24 are displayed in figure 6.18. As was earlier discussed in paragraph 6.2, the schematisation in the berm is lower than the simulated phreatic surface. The difference between the return periods is small in the berm, and larger near the crest, which is in accordance to the observations at location 25.

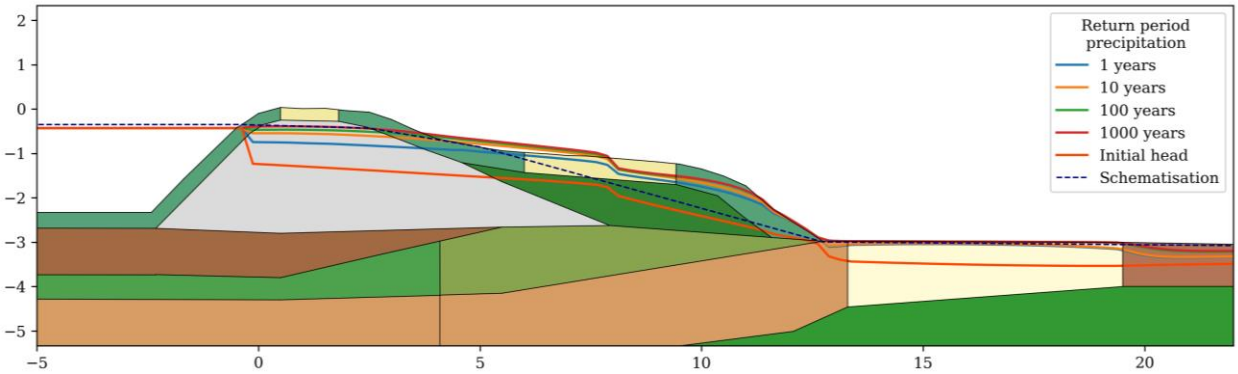

Figure 6.18: Phreatic surfaces location 24 for precipitation events with various return periods,

Hogedijk

The analysis was also performed for the Hogedijk. The results are displayed in figure 6.19.

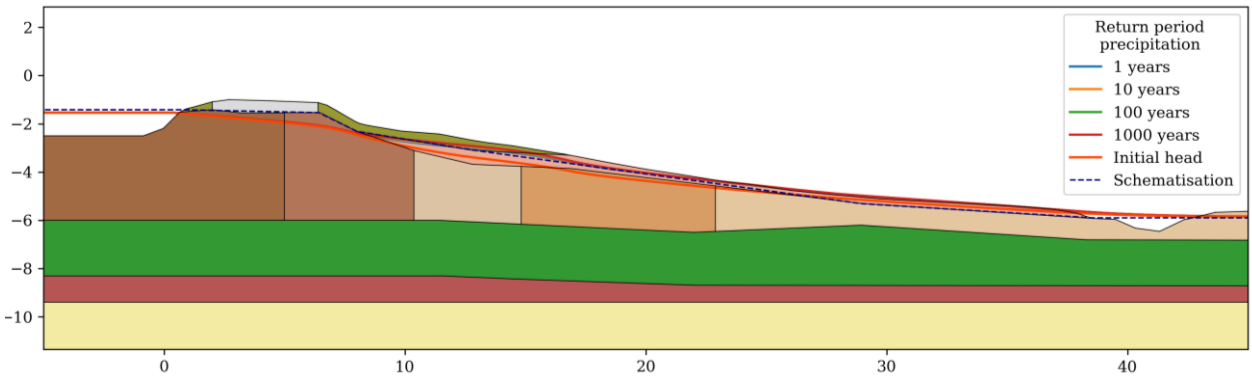

Figure 6.19: Phreatic surfaces Hogedijk for precipitation events with various return periods

The difference between the different return periods is so small that it can hardly be discerned in the figure. The maximum difference between the return periods of 1 year and 1000 years is about 10 cm. Below the berm and near the toe there is hardly even any head rise at all. Near the toe this can be explained again by seepage. Below the crest the infiltration rate is reduced due to the road on top. The small response reflects the measurements of the monitoring wells: apart from some peaks the validity of which can be disputed, the head fluctuations are relatively small. The model is calibrated to mirror this.

6.4 Long term precipitation

The simulations executed thus far had a simulation period of about 4,5 years. While this is a long period for monitoring well measurements, from a statistics point of view it is a relatively short period. By running a longer simulation using one of the calibrated models, an artificial dataset of the phreatic surface over a much longer period can be generated, which is more suitable for a statistical analysis. This simulation was performed for period of 31 years. The basis for this period is the availability of meteorological data. The closest KNMI weather station with hourly data is at Rotterdam, about 9 km removed from the locations in Delfland (KNMI, 2019). Because both precipitation and evapotranspiration data are required for the model, radiation measurements are needed. Radiation measurements at this station have started in December 1987. When the data was downloaded it was available up to the 24th of January 2019, which gives a simulation period of approximately 31 years. With this data, the daily Penman-Monteith potential evapotranspiration rate was calculated using the same method as used for the Hogedijk (described in appendix C).

Due to the simulation time and the large amount of output data, this long-term simulation was performed using just one of the three research cases. The model of the Hogedijk was calibrated on just a few months of data, and is therefore not considered reliable enough to simulate a period of 31 years. Location Delfland 24 has a permeable core, which results in an atypical phreatic surface for a regional flood defence. For location 25 some problems were encountered in determining the correct soil composition, but of the three models it resulted in the best fit to the measurements. For these reasons the choice was made to use this model for the long term simulation.

To simplify the analysis of the model results, the phreatic surface was determined again by taking for every time step the highest head of the layers for each grid column, with the exclusion of the top layer and the deepest layer.

6.4.1 Exceedance of the schematisation

In order to investigate how often the phreatic surface exceeds the schematisation, the phreatic surface for each time steps was compared to the schematisations for both the dry and the wet situation. If the head in a single cell is below the dry schematisation, or above the wet schematisation for a certain time step, the schematisation is exceeded. For the dry situation no such events have occurred: in the 31 years the phreatic surface has never been below the dry schematisation.

For the wet situation, the schematisation was exceeded for 1645 of the one-hour time steps. The total number of time steps in the simulation was 272304, which means the schematisation was exceeded for about 0,6% of the time. The 1645 exceedances are not all separate events, sometimes the exceedance occurs for several consecutive time steps. When consecutive exceedances are counted as a single event, 376 exceedances have occurred during the 31 years.

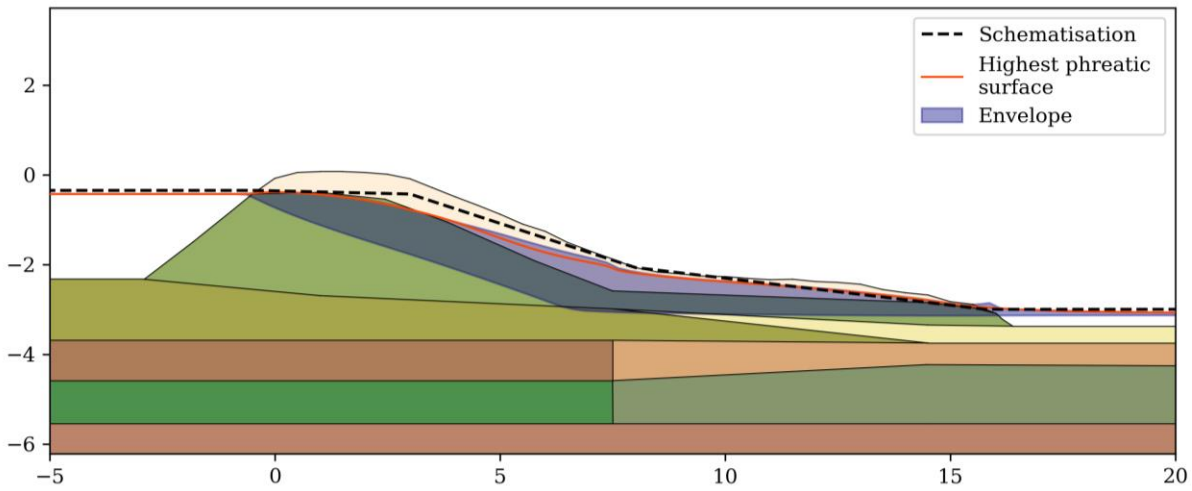

For each of the exceedances it was determined at which cell column in the cross-section it occurred. This makes it possible to determine at what point in the cross-section the schematisation is exceeded most frequently. To visualise this information, a histogram was plotted over the cross-section. This histogram is displayed in figure 6.20.

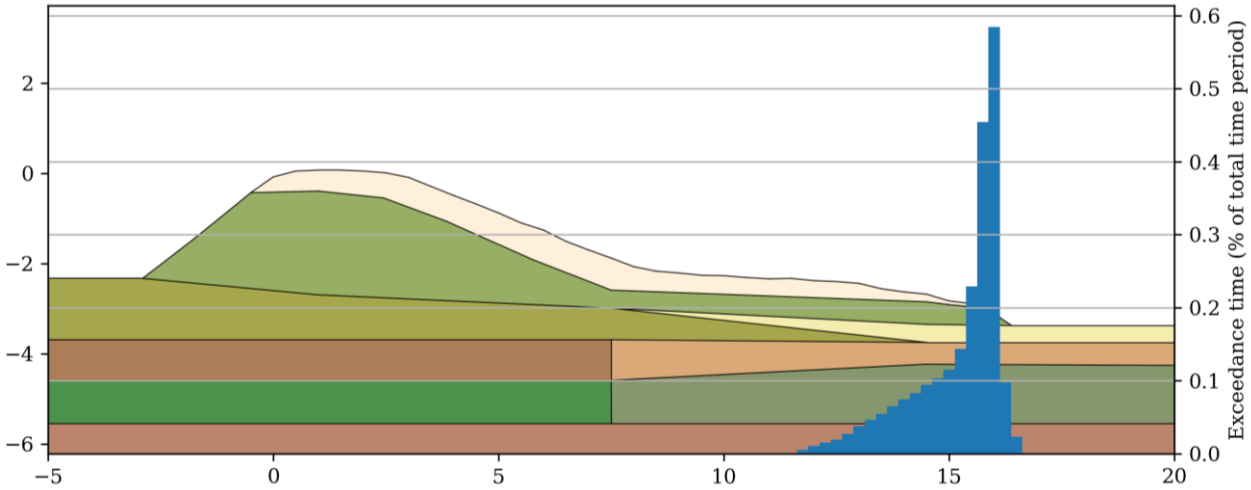

Figure 6.20: Histogram of exceedances of the schematised phreatic surface

Each bar in the histogram represents a column of cells in the model grid. It stands out that all exceedances have occurred near the toe, especially at the edge of the drainage ditch. No exceedances have occurred at the crest or the slope. The exceedances probably have occurred when seepage at the toe took place: in that situation the phreatic surface is locally at ground level, while the schematisation is mostly below ground level. The schematisation and the highest found phreatic surface are also displayed in the figure. This highest phreatic surface exceeds the schematisation by just a few centimetres. Different interpretations of the guidelines for the schematisation might therefore result in less or even no exceedances.

In addition to the histogram and the highest phreatic surface, the envelope of the found heads is included. This indicates the area in which the phreatic surface varies. For the most part, the highest phreatic surface lies on the upper boundary of the envelope. Only in the slope the boundary of the envelope is slightly higher, which means in that area slightly higher heads have occurred on some other point in time.

The highest phreatic surface was found by taking the time step with the highest average phreatic surface over the cross-section. This maximum occurred on 13-10-2013. Notable is that this is also

the day with the highest phreatic surface during the main simulation of 4,5 years. When examining the precipitation data it is found that this day indeed has the largest precipitation volume in the 31 year period.

This raises another question: why was the schematised phreatic surface exceeded in the crest in the main simulation, but not in this long-term simulation? The answer to this is the use of different precipitation data. The localised Meteobase data shows that the precipitation event had a volume of 103 mm, while in the data from the KNMI station the precipitation volume is only 63 mm. The most extreme precipitation event is therefore less extreme in the long-term model, and therefore the schematisation is not exceeded in this case. The cause for this difference in precipitation volume is most likely local variation.

6.4.2 Histogram

For this long-term simulation again a histogram was plotted of the data. The long simulation period has the result that a lot more data is included, leading to a more complete image of the distribution of the heads.

In figure 6.21 these histograms are displayed. Like in paragraph 6.1, the histograms are plotted for the locations of the three monitoring wells, but with an extra point added at the inner crest. The maximum and minimum values are displayed as triangles. The heights of the schematised phreatic surface at these points are included as vertical lines.

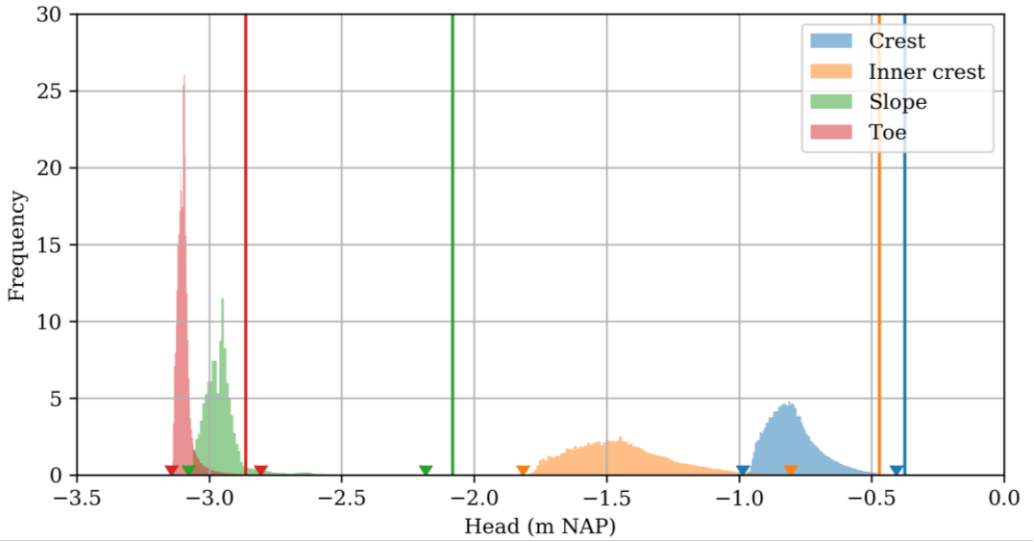

Figure 6.21: Histograms of the head at four points in the cross-section

It stands out that the shape of the histograms is smoother than of those in paragraph 6.1. The four points show a similar shape with a convex shape on the left side, and a concave shape on the right side. This shape is more pronounced near the crest than near the toe. At the toe, the histogram is very narrow and tall, indicating that the head variations are relatively small. This is probably caused by the proximity to the drainage ditch and the intermediate sand layer, which allows precipitation to flow away easily. The largest variations are observed at the inner crest.

The schematisation is exceeded at the toe, which corresponds to the earlier observations. The schematisation is almost reached at the crest, but no actual exceedances have occurred in this model. In the slope the most common fluctuations are far removed from the crest, but the highest heads are far removed from the mean and almost reach the schematisation. This histogram has a very long and thin tail. At the inner crest the distance between the histogram and the schematisation is the largest. Even the maximum value is about 30 cm removed from the schematisation.

The skewed shape of the histograms is reminiscent of the lognormal distribution. This distribution was fit to the data, and the result is displayed in figure 6.22. The distribution fits the data quite well, although the concave-convex shape of the histogram is not as pronounced in the distribution.

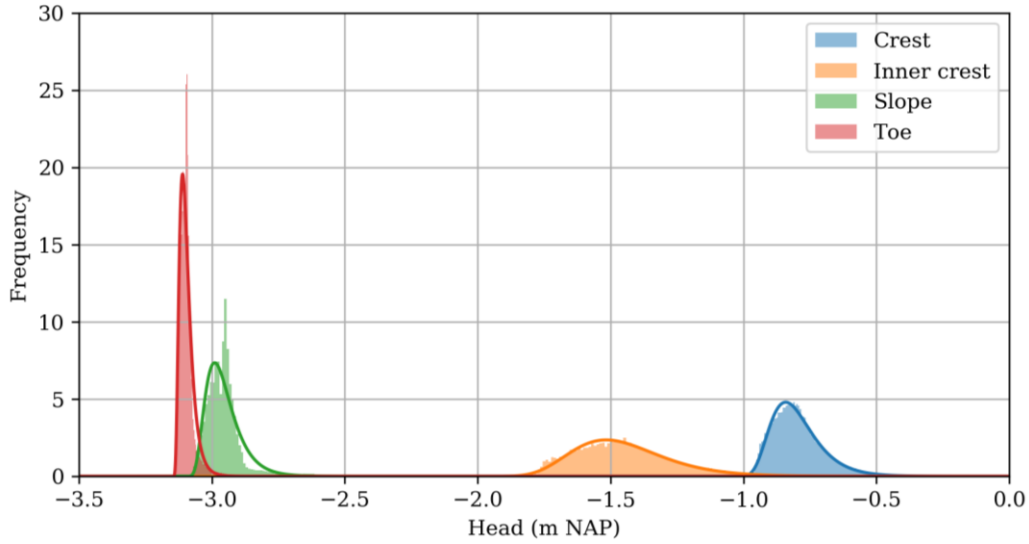

Figure 6.22: Lognormal distribution fitted to model results

The means and standard deviations for the fitted distributions are displayed in table 6.13.

Table 6.13: Means and standard deviations of the fitted lognormal distributions

Location	Crest	Inner crest	Slope	Toe
Mean	-0,797	-1,451	-2,954	-3,095
Standard deviation	0,097	0,184	0,067	0,027

These distributions could be used to calculate the probability of occurrence for the head at a certain point in the cross-section. However, to calculate the probability of exceedance of a certain value per year, an extreme value analysis would have to be conducted on the data. Furthermore, a head with a certain probability at a single point in the cross-section does not necessarily coincide with a head with the same probability in other points in the cross-section. As could be observed in figure 6.20, the maximum simulated heads in the slope did not coincide with the maximum phreatic surface on average. Although the difference was small this shows that the maximum pore pressures do not occur simultaneously in the cross-section.

6.5 Uncalibrated model

During the set-up of the models, initial values were chosen for the soil parameters as a starting point for the calibration. These values were immediately adjusted to calibrate the model for a steady-state simulation, but the extreme phreatic surfaces resulting from an uncalibrated model were not analysed. In this paragraph the results from uncalibrated models using estimated parameters are compared to the results of the calibrated models. In this way the magnitude of the error caused by using an uncalibrated model can be determined, and consequently the usefulness of a model only using estimated parameters.

6.5.1 Parameters

For the soil parameters mostly the parameters used as starting point for the calibration were used again. For location 25 a choice had to be made for the soil schematisation: the first schematisation resulting in a poor fit of the model could be used, or the schematisation adjusted based on the measurements. Eventually it was chosen to use the latter, so that the only difference between the calibrated and uncalibrated model are the soil parameters. For the parameters themselves the

initially chosen Staring types were used. For location 24 the initially chosen parameters were used as well, and the schematisation was not changed. For the uncalibrated model of the Hogedijk a Staring soil type was chosen instead of the conductivity measurements. The soil borings indicate that the dike body consists of clayey peat, which corresponds to Staring type B18. This soil type is used for the entire layer, no separations were made. For the other soil layers the Staring types initially estimated for the calibration are used. Tables of the estimated Staring types in the models are included in appendix G, paragraph G.2.1. For the anisotropy ratio and the specific yield the estimates from paragraph 5.1.3 are used.

6.5.2 Results

For all three models a transient simulation using the estimated parameters was performed. The results for location 25 are displayed in figure 6.23, the results for the other locations are included in appendix G.

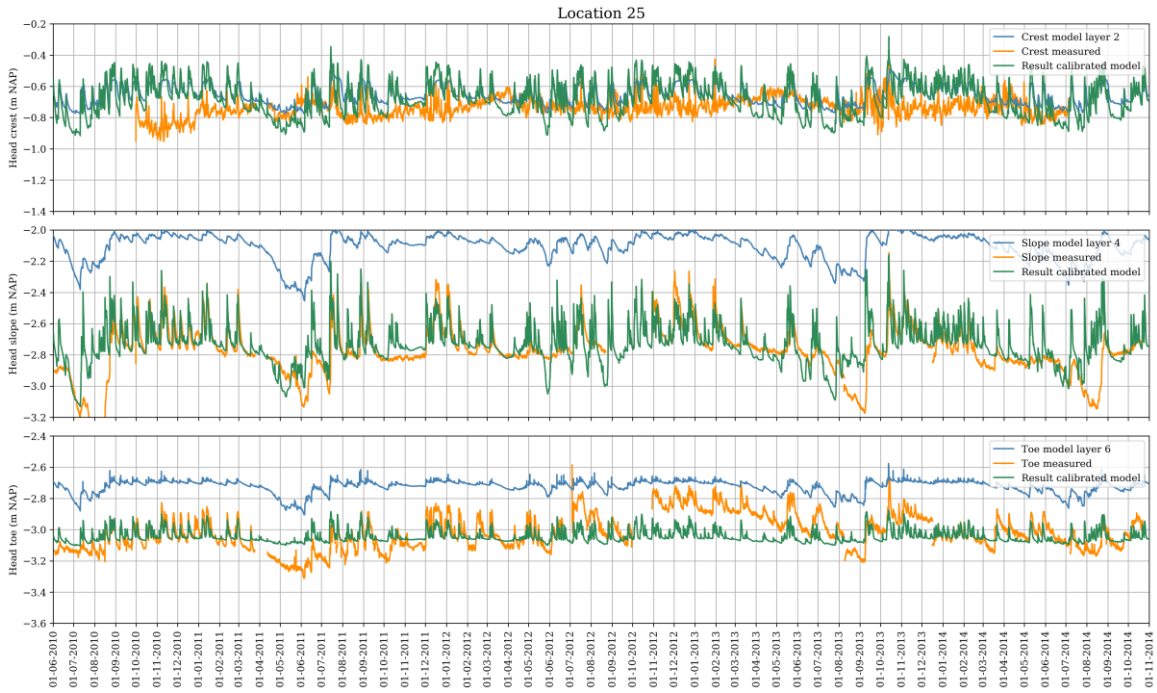

Figure 6.23: Model results location 25 for calibrated (green line) and uncalibrated model (blue line)

For the crest the fit of the uncalibrated and the calibrated model is almost the same, and at some points the fit of the uncalibrated model is actually better that of the calibrated model. However, in the slope and the toe the heads in the uncalibrated model are consistently much higher than the measurements and the calibrated model. The fluctuations caused by precipitation are smaller than in the measurements. The evapotranspiration dips are similar in size to those in the measurements.

For location 24 the heads in the crest and the slope are also consistently about 30 cm higher than the measurements and the calibrated model. In the toe the difference is smaller, but the heads are also consistently higher than in the calibrated model. The head fluctuations are smaller than in the measurements.

For the Hogedijk the difference between the calibrated and uncalibrated model is variable per monitoring well. Near the crest (HGD 1-1) the uncalibrated heads are around 25 cm too low compared to the measurements. For monitoring well HGD 1-2 the heads for calibrated and uncalibrated model are almost the same, but for the other two locations the heads are too high. For monitoring well 4 the heads in the calibrated model were much higher than the measurements, and in the uncalibrated model the heads are even higher. The modelled fluctuations are very small, smaller than those in the measurements. The reason is the high

specific yield of 0,44 estimated for peat; during the calibration this parameter was set to a much lower value.

6.5.3 Extreme simulated phreatic surfaces

Using the same method as in paragraph 6.2, the highest and lowest simulated phreatic surfaces were determined and plotted. In the plots the highest and lowest phreatic surface from the calibrated model were included as well for comparison. The highest phreatic surface for location 25 are displayed in figure 6.24.

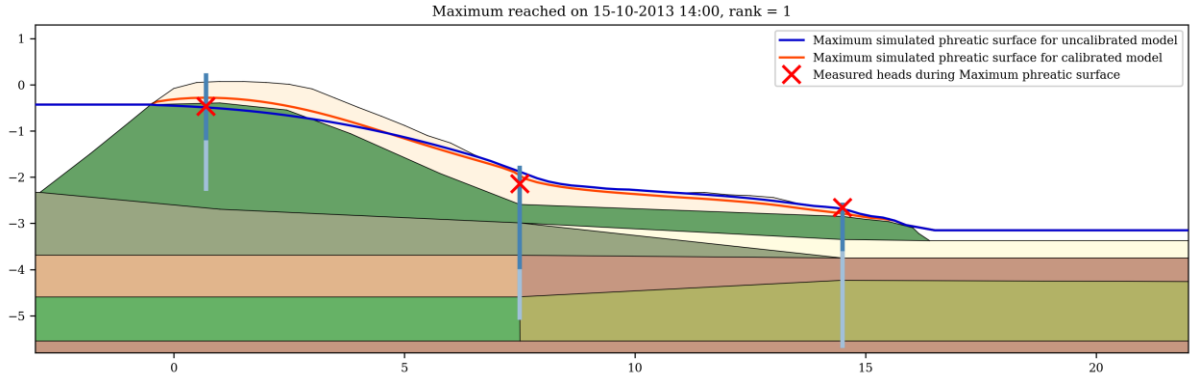

Figure 6.24: Highest phreatic surface of location 25 for the uncalibrated model (in blue) and the calibrated model (in red). The red crosses represent the measured head at the moment the extreme in the uncalibrated model was reached.

The moment at which the maximum or minimum was reached was not always the same as in the calibrated model. For location 25 the maximum in the uncalibrated model occurred 2 days later than in the calibrated model. In the crest, the maximum phreatic surface in the uncalibrated model is lower than in the calibrated model, but in the slope and toe it is higher. The uncalibrated model fits the measurements quite well for the maximum, but this is mainly because the phreatic surface is very close to the ground surface. For the minimum phreatic surface the uncalibrated phreatic surface is almost 0,5 m higher than both the model and the measurements.

For location 24 the differences between the highest phreatic surface in the calibrated and uncalibrated model are small. Both are very close to the ground surface, which is probably the reason why the difference for this maximum is small, whereas the uncalibrated model results in higher heads during normal conditions.

The fluctuations in the uncalibrated model of the Hogedijk are very small, which has the result that the difference between the maximum and the minimum phreatic surface is also small. The use of a homogeneous layer has the result that the phreatic surface is an almost straight line from the outer crest to the drainage ditch. In the crest this leads to a lower maximum phreatic surface than in the calibrated model, and in the crest to a slightly higher phreatic surface. For the minimum phreatic surface the situation is similar, but the differences are larger.

The results show that for the three research cases calibration was absolutely necessary to model the head fluctuations. For the extreme phreatic surfaces the difference between the calibrated and uncalibrated models is smaller, but this is mainly because the phreatic surface is closer to the equilibrium height in these conditions, which is close to the ground surface in both situations.

6.6 Relation to macro-stability

In order to get a picture of the relation between the phreatic surface and the macro-stability of the flood defence, several stability calculations were performed. For these calculations location 25 was used, since the long-term analysis was also performed on this case.

The parameters for the strength of the soil are taken from a stability calculation of the same flood defence, which was provided by Delfland. These were included in the form of stress tables, which relate the shear resistance to the effective stress. These stress tables are included in appendix E, paragraph E.6. The calculations were carried out using the program D-Geo Stability (Deltares, 2017). This program includes several methods to model the slip plane. The most commonly used methods in the Netherlands are the Bishop, Uplift-Van, and Spencer- van der Meij methods. When there is a risk that the soil layers behind the flood defence are pushed up by the water pressure, or when thin, weak soil layers are present, it is preferable to use Uplift-Van or Spencer- van der Meij (STOWA, 2015). Considering a thin peat layer is present at location 25, one of these two models should be used. The choice was made to use Uplift-Van, because it is easier to define the slip planes in this model, which makes it easier to keep the slip planes consistent between the calculations. Theoretically Spencer- van der Meij provides a better approximation of reality, but this analysis is aimed at determining the influence of a different phreatic surface. The actual calculated stability factor is of less importance. In the Uplift-Van model the slip plane consists of two semi-circles, connected by a horizontal segment. The pore pressures are modelled by so-called PL-lines, which indicate the course of the piezometric level over the cross-section. Multiple PL-lines can be added and assigned to the soil layers.

For reference, first a calculation was performed in which the schematised phreatic surface was used. For the schematisation of the soil layers the same schematisation as in the Modflow model was used. Two PL-lines were used: one representing the schematised phreatic surface, and another representing the head in the Pleistocene sand layer. The phreatic surface was used to model the pore pressures in the top layers, including the intermediate sand layer and the clay layer below the outside water. In the other layers, the pore pressures were linearly interpolated between the phreatic surface and the head of the Pleistocene sand layer.

Using this schematisation a stability factor of 1,15 was calculated. The model and the normative slip plane are displayed in figure 6.25.

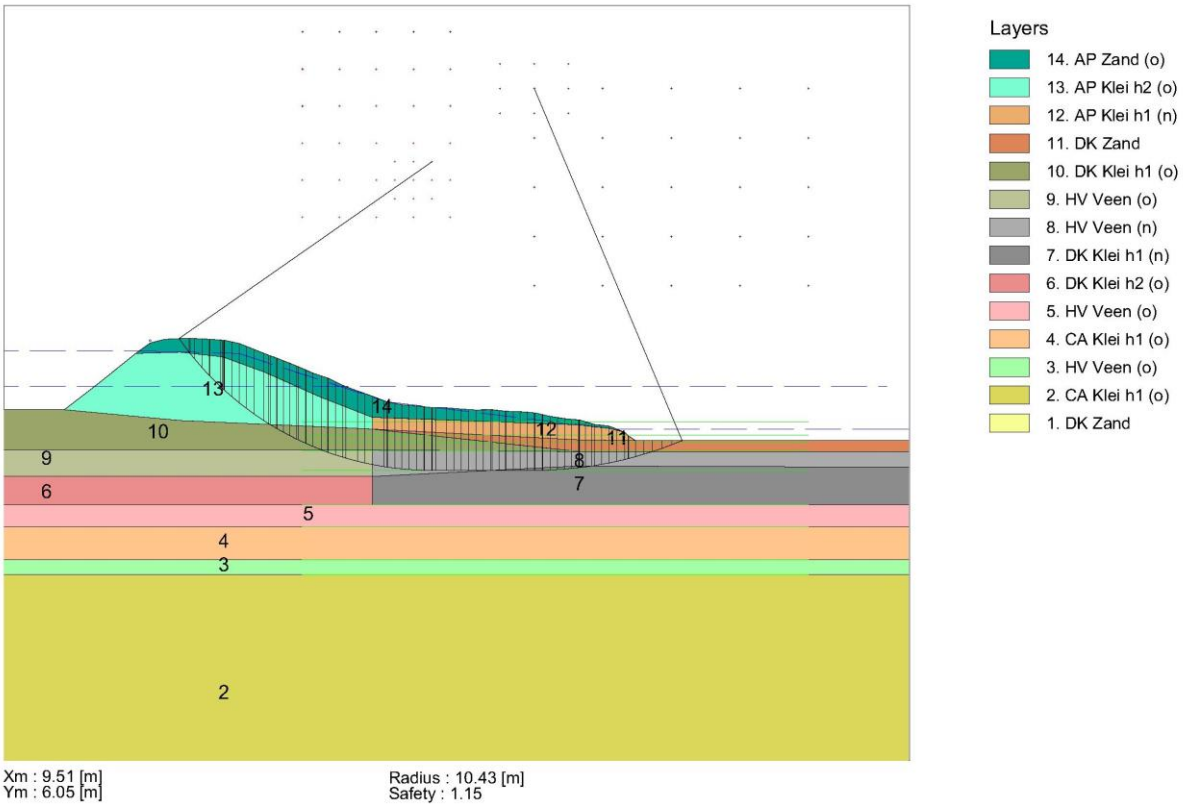

Figure 6.25: Stability calculation Delfland location 25

6.6.1 Variation characteristic points schematisation

To obtain some comprehension on where in the cross-section fluctuations have the largest influence on the stability, each of the characteristic points of the schematised phreatic surface was shifted downwards and upwards if possible. The stability was then calculated again to assess the change in stability factor.

The left- and rightmost points of the schematisation are placed at the fixed water levels, and can therefore not be shifted. Instead, two extra points were added to the schematisation which were variated. One point was added below the outer crest, about a meter removed from the entry point, and another point was added about 1,5 m removed from the drainage ditch. The four variated points are displayed in figure 6.26.

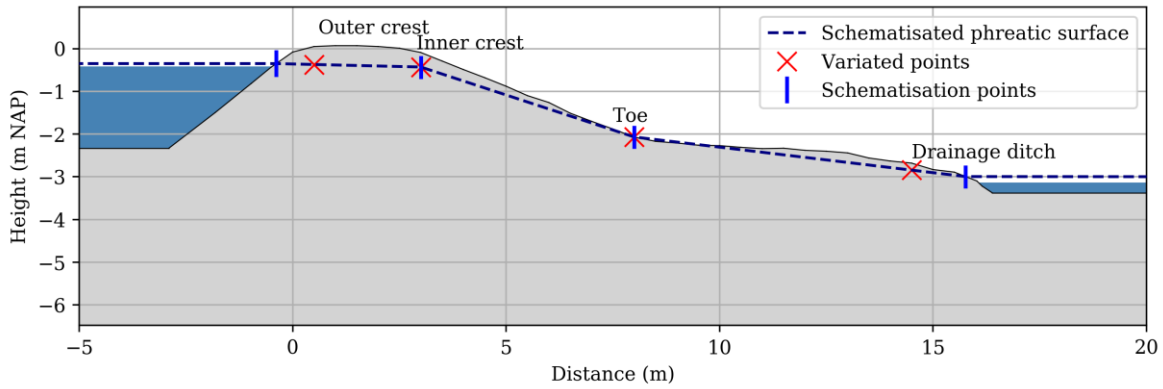

Figure 6.26: Variated points of the schematised phreatic surface

In table 6.14 the stability factors resulting from the changed schematisation points are displayed. The point near the drainage ditch could not be shifted 0,25 m upwards, since that would place the point above ground level. When all points were shifted, the individual points were shifted in the range for which this was possible.

Table 6.14: Stability factors resulting from variation of four points in the schematised phreatic surface

Point/Shift	-0,25 m	-0,1 m	0 m	+0,1 m	+0,25 m
Outer crest	1,15	1,15	1,15	1,14	1,13
Inner crest	1,20	1,17	1,15	1,13	1,10
Toe	1,21	1,17	1,15	-	-
Drainage ditch	1,18	1,16	1,15	1,13	-
All	1,30	1,21	1,15	1,11	1,05

From the resulting stability factors it can be observed that these changes of a single point have a limited effect on the stability. The lowest stability factor is 1,10 and the highest is 1,20, so the variation is relatively small. In the outer crest the effect of a variation is smallest: this is not surprising, since in figure 6.25 it can be observed that the slip plane starts about halfway in the crest. The largest influence is observed for the inner crest and the toe. In paragraph 6.4.2 it was found that the inner crest also exhibits the largest variation of the phreatic surface, which means that the inner crest is the most important location in the cross-section when regarding the influence of precipitation on the macro-stability.

When all points are shifted, a change in the phreatic surface has a more significant influence on the stability. For this flood defence the stability remains above 1, but for a flood defence with a lower initial stability such a shift of the phreatic surface could cause instability.

6.6.2 Application of model results

As a second part of the stability analysis, some phreatic surfaces obtained from the simulations are applied to the stability calculation. For these calculations, the following phreatic surfaces were used:

- The highest phreatic surface from the main simulation of 4,5 years, on 13-10-2013;
- The heads from each separate layer applied as a PL-line for each layer, again for 13-10-2013;
- The highest phreatic surface for the normative precipitation event with a return period of 100 years;
- The highest phreatic surface obtained from the uncalibrated model.

The highest simulated phreatic surface of 13-10-2013 is thus applied to the model in two ways. In the first calculation, this phreatic surface simply replaces the schematised phreatic surface. In the second calculation the heads calculated in Modflow are taken for each layer, and applied in D-Geo Stability as a separate PL-line. This replaces the linear schematisation of the pore pressures between the Pleistocene layer and the phreatic surface by the pore pressures calculated in the model, which might lead to different results. In the third calculation the simulation of a 100 year return period precipitation event is used. For this the normative duration and pattern are used, which are a duration of 192 hours and the 'High' pattern. The highest average phreatic surface was extracted from the simulation and applied as the phreatic line in the stability calculation.

The stability factors for these three calculations are displayed in table 6.15.

Table 6.15: Results of stability calculations using different phreatic surfaces

Situation	Stability factor
Schematised phreatic surface	1,15
Phreatic surface 13-10-2013	1,17
PL line for every layer for 13-10-2013	1,18
100 year return period precipitation	1,17
Uncalibrated model	1,14

Again, the difference compared to the initial calculation is small. However, the calculation using the highest simulated phreatic surface results in a slightly higher stability factor, even though the schematisation is exceeded at some points in the cross-section. Taking into account that the phreatic surface in question was the result of a precipitation event with a return period of about 250 years, this indicates that the schematisation is not necessarily unsafe, even though it is exceeded in the simulations at some points.

Using the simulated heads for each soil layer resulted in a slightly higher stability factor than when only the phreatic surface is used. This small difference indicates that a linear gradient between the Pleistocene sand layer and the phreatic surface is a good enough approximation of the pore pressure distribution. However, it should be noted that the slip plane only traverses through the upper regions of the area for which the gradient applies, so for deeper slip planes the difference could be of more importance.

The stability when using the 100 year return period precipitation is equal to the stability using the phreatic surface of 13-10-2013. The phreatic surfaces for those situations are very similar, and therefore lead to the same stability factor.

Using the highest phreatic surface simulated in the uncalibrated model results in a stability lower than when using the schematisation. The heads at the toe and near the inner slope are at the ground surface, which is higher than in the schematisation and the maximum phreatic surface of the calibrated model. Even though the phreatic surface of the uncalibrated model is lower in the crest, this results in a lower stability.

7 Conclusions

This chapter presents the conclusions from this thesis and answers the research questions. Following the conclusions are the discussion and recommendations for further research.

The objective of this thesis, as presented in chapter 1 is to extend the knowledge of modelling the phreatic surface in regional flood defences with the use of a numerical model.

The basis of the research consisted of the construction of numerical models for three regional flood defences for which pore pressure measurements from monitoring wells were available. The numerical models were calibrated to simulate the measured response of the phreatic surface to precipitation and evapotranspiration.

7.1 Conclusions

The conclusions of this research are discussed based on the research questions presented in chapter 1 . Each of the sub-questions is discussed, followed by the main research question.

1. *What are the main influencing factors on the phreatic surface?*

The main external influencing factors of influence are precipitation, evapotranspiration and water levels. Precipitation is an important influence on the phreatic surface, as it can cause large head rises of several tens of centimetres up to a metre. Various durations, volumes and patterns of precipitation may lead to different reactions. Evapotranspiration can be a factor of influence, but not in all situations. The three research cases suggest that a larger conductivity of the dike core leads to a smaller influence of evapotranspiration. The mean in- and outside water level determine the entry and exit point of the phreatic surface, and therefore are an important factor for the phreatic surface. The fluctuations of these water levels were mostly omitted in this research. For regional flood defences water levels on both sides are regulated which means the fluctuations are relatively small compared to fluctuations due to precipitation. Only the mean water levels are an important factor for the phreatic surface; the fluctuations are of smaller importance.

The internal influencing factors on the phreatic surface are the soil characteristics. This includes both the schematisation of the different soil types in the cross-section and the characteristics of these soil types. The soil composition of the cross-section has a large influence on the baseline position of the phreatic surface, especially when permeable layers are present. If the soil is relatively homogeneous in the longitudinal direction of the dike, it is sufficient to know the soil composition in the cross-section under consideration. However, when there are large variations in this direction, information on the soil composition along the longitudinal direction is required as well.

Regarding the soil types themselves, the conductivity is the most important parameter. It is often anisotropic: the conductivity in vertical direction is different than in horizontal direction. The flow from the outside towards the inside water is mainly horizontal, and therefore the horizontal conductivity is mostly important for the baseline position of the phreatic surface. The vertical conductivity has an influence on this baseline position as well, since flow also occurs to and from the Pleistocene sand layer. The vertical conductivity is also an important influence on the reaction of the phreatic surface to precipitation. A larger vertical conductivity leads to a quicker and larger response. The response is also largely dependent on the specific yield, which determines the storage capacity of the soil. A lower specific yield means less storage capacity and therefore also

leads to a larger and quicker response. The vertical conductivity and the specific yield jointly determine the reaction of the phreatic surface to precipitation.

2. *How is the phreatic surface currently schematised in regional flood defences?*

For stability analyses, the phreatic surface is usually schematised based on several points determined by the geometry of the flood defence, and the water levels. Usually raised inside and outside water levels are used, and it is assumed that seepage occurs at the toe.

In all three research cases, the schematisation was exceeded at some point during the simulation. The exceedances were mainly observed between the toe and the drainage ditch, where the modelled phreatic surface reached closer to the ground surface than the schematisation. Additionally, the model result in the crest reached levels higher than the outside water level. Since the schematisation uses a raised outside water level while the model did not, the schematisation was usually not exceeded at this location. If a raised water level was taken into account, the schematisation in the outer crest would be exceeded more often.

The fact that the simulated phreatic surface exceeded the schematisation at some points does not necessarily mean that the schematisation overall is not sufficiently conservative. The schematisation is exceeded near the toe and slightly at the outer crest, but at the inner crest the schematisation is higher than the model results. Potential improvements to the schematisation could thus be made by using a higher level at the outer crest, a lower level at the inner crest, and placing the schematisation at ground level between the toe and the drainage ditch.

The model shows that the pore pressures do not increase hydrostatically with depth, which is caused by vertical flow to and from the Pleistocene sand layer. When this non-hydrostatic gradient was taken into account in the stability calculation, the difference in stability was small. This indicates that using a linear gradient of the pore pressures between the phreatic surface and the Pleistocene sand layer is a good schematisation.

3. *What are the requirements for a numerical model to model the phreatic surface in a regional flood defences?*

In the literature study several requirements for a numerical model were listed. Based on the experiences with the Modflow model the list of requirements to a numerical model can be extended:

- The model needs to be able to simulate transient groundwater flow;
- Precipitation has to be included as a boundary condition;
- When simulating dry periods or calibrating using data from a dry period, evapotranspiration should be included as a boundary condition;
- A boundary condition to allow seepage is necessary;
- The model needs to be able to model the sometimes complex geometry of the subsoil of regional flood defences.

4. *How accurately can a numerical model simulate measured pore pressures in a regional flood defence?*

The research models have shown that it is possible to model the phreatic surface with some accuracy. The baseline position of the phreatic surface could be matched for all three models, sometimes after adjusting the soil schematisation. The accuracy of the simulated fluctuations of the phreatic surface varies between the research cases and between the locations in the cross-section. In general, monitoring wells closer to the outside water were not simulated as accurately as the monitoring wells further inward in the cross-section. A possible explanation for this could be the influence of fluctuations of the outside water level, which were omitted in the models.

However, for the locations more inward in the cross-section not all peaks were matched correctly either. The magnitude of the peaks was sometimes correct while the baseline phreatic surface was higher or lower than the measurements. In part these differences may be explained by errors in the measurements, but this does not explain all the differences. The other main causes are the simplified geometry of the cross-section, the simplified method using which the infiltration is modelled, using a non-variable water level, modelling the cross-section in 2 dimensions, and errors in the measurement set. A certain degree of simplification is always required in a model study, to keep the model manageable and because the available information is limited. Despite all these simplifications it was possible to model the fluctuations quite well for most of the measurement locations.

On average, the difference for each time step of one hour was around 10 cm. Analysis of the highest simulated phreatic surfaces has shown that the deviation of the model for these extreme events is smaller, being only several centimetres. Whether this accuracy is sufficient is open to interpretation. An indication of the significance of the error can be obtained by assessing the influence on the stability. A 10 cm raise of the entire phreatic surface leads to a small stability decrease of 0,04 for research location 25, which does not lead to instability. For this research location the average difference was smaller than for the other research locations, which means that for research location 25 the error with regard to the macro-stability is sufficiently small.

For flood defences with a smaller initial stability the effect of rise of the phreatic surface can be larger, possibly leading to instability. It can therefore not be concluded that the model is sufficiently accurate for all situations. However, research location 25 has shown that it is at least possible to construct a sufficiently accurate model, despite the necessary simplifications and limited information. For models with a less good fit improvements can likely be made when more information is available, for example with more monitoring wells for research location 24, and with a longer calibration period without a dry period for the Hogedijk. It is therefore concluded that a numerical model can simulate the measured pore pressure with sufficient accuracy with regards the macro-stability, on the condition that sufficient information is available to construct the model. The answer to research question 6 discusses what information is required.

5. How does the phreatic surface in the numerical model respond to an extreme event?

The fit of the three models for the highest occurring phreatic surfaces in the measurement set is similar to the fit under normal conditions. For the lowest phreatic surface the models exhibits heads about 10 cm lower than the measurements. This means the model performs similarly well for extreme high conditions as for normal conditions, but slightly worse for extreme low conditions.

More insight in the response to precipitation events was gained by adding various fictitious precipitation events to the models. It was found that as a general rule, events with a longer duration and lower intensity lead to larger head rises. After a certain duration a maximum head rise is reached, after which the phreatic surface rises no further. At this point an equilibrium situation is reached, in which the amount of infiltrated precipitation is equal to the outflow towards the inside water and by seepage at the toe. The duration after which this equilibrium was reached was different between the models, but for all models it was reached after at most 96 hours. The height of this equilibrium phreatic surface is dependent on the infiltration characteristics and the conductivity of the soil.

The patterns determining the distribution of the precipitation over the duration of the events also resulted in different responses. The pattern resulting in the largest head rise was different between the various durations, but it could be observed that for shorter durations the pattern with a mostly uniform distribution was normative, while for longer durations the patterns including a single peak resulted in larger head rises. The reason for this is that for long durations the equilibrium situation is reached for all patterns, while the peak results in an extra head rise

above this for a short amount of time. Precipitation events with a duration longer than 96 hours and including a single large peak therefore cause the highest phreatic surface in a regional flood defence.

6. *What parameters and data are at least required for an accurate determination of the phreatic surface using a numerical model?*

Comparison of the calibrated models and the uncalibrated models has shown that calibration is required to accurately simulate the fluctuations of the phreatic surface. For extreme high phreatic surfaces the fit of the uncalibrated model was comparable to that of the calibrated model. However, when the normal fluctuations are not modelled properly it is uncertain that the reaction to extreme events is always correct. To obtain reliable results calibration of the model is necessary, and therefore pore pressure measurements are required to set up and calibrate a geohydrological model of a regional flood defence.

The analyses have shown that the head variations in the inner crest are the largest. A measurement point at the inner crest can therefore provide the most insight in the fluctuations of the phreatic surface. To determine the course of the phreatic surface over the cross-section measurement points near the outer crest and the toe are necessary as well, meaning a minimum of three measurement points is required to calibrate the model. The required measurement time is dependent on the situation. One of the models was calibrated using only two months of measurement data, which was not sufficiently long. The calibration period was preceded by a dry period, which influenced the calibration. Although two months was too short for this model, two months of measurements conducted during more normal conditions is probably sufficiently long to calibrate the model.

Precipitation data is also required for the calibration, even if the model is used to only model the response to fictitious precipitation. The monitoring wells show the response to actual precipitation, so to calibrate the response of the model the precipitation data has to be applied to it. For two of the three models evapotranspiration had a noticeable effect on the fit of the model to the measurements. When dry periods are included, or when the response to a dry period needs to be modelled, evapotranspiration data is therefore required as well.

The models of locations 24 and 25 in Delfland have shown that measured conductivities are not strictly necessary to construct a fitting model. However, the same head fluctuations could also be modelled when using slightly different parameters. Only the hydraulic heads are considered for the phreatic surface. This means several calibrations sets resulting in the same head fluctuations may exist, but these different sets could result in different flow rates through the soil. Measurements of the conductivity can provide an ‘anchor’ to the real values of the parameters. In this way the values of the calibration parameters have more correspondence to their magnitude in the real world, which gives more confidence that the model is accurate. Measured conductivities can also provide a better understanding of the variation in the flood defence.

Perhaps the most important information required is the soil composition, especially the location of permeable and less permeable layers in the cross-section. The conductivities can be adjusted during the calibration, but if the soil schematisation is incorrect it is not possible to construct a well-fitting model. This means sufficient knowledge of the subsoil from soil borings and cone penetration tests is required. To obtain knowledge of the soil composition and the measuring points, at least three soil borings at the locations of the monitoring wells are required. The research cases have shown that this sometimes not even sufficient.

Main research question
The research sub-questions served to answer the main research question, which was defined as follows:

Can a numerical model contribute to a more accurate estimation of the phreatic surface in a regional flood defence during extreme conditions?

The research cases have shown that is possible to simulate the phreatic surface in a regional flood defence using a numerical model with sufficient accuracy. Such model could theoretically be used to estimate the phreatic surface during extreme conditions for usage in a stability calculation. Provided sufficient information on the flood defence is available, a model can therefore contribute to a more accurate estimation of the phreatic surface in a regional flood defence . However, the sufficiently good fit of the models was only reached after extensive calibration of the model to the measurement set. Pore pressure measurements are necessary to construct and calibrate an accurate model. The calibration itself can be a long-drawn process, due to the large amount of parameters that can be adjusted. The large amount of required data and the difficult calibration process make it questionable whether it is always worthwhile to construct a numerical model to determine the position of the phreatic surface. For stability assessments, construction of such a model for every flood defence is not realistic. For these situations it is more reasonable to continue improvement of the existing schematisations.

Numerical models could aid in further research regarding the pore pressures in flood defences. A model provides insight in the height of the phreatic surface over the entire cross-section, whereas pore pressure measurement only give information for a single point. The model can also be used to estimate the phreatic surface in extreme conditions, even if the measurements only include normal precipitation events. These characteristics make a numerical model useful for research regarding the phreatic surface, for example to construct new schematisations.

Further conclusions and observations
The three models have shown that modelling the unsaturated zone is not strictly necessary to model the phreatic surface. This makes setting up a geohydrological model for a flood defence simpler, since no unsaturated soil parameters are required. Calibration of the boundary conditions is necessary to construct a correct model, but this would also be necessary for the unsaturated parameters. It is however possible that if the unsaturated zone were to be modelled with correct parameters, some peaks would be matched better than in the models of this thesis. The models also show that a 2-dimensional model is sufficient in many cases, but when large variations exist in the longitudinal directions a 3-dimensional model might be required.

An extreme phreatic surface is not necessarily directly related to an extreme event. When the phreatic surface is higher than normal due to precipitation, a relatively small precipitation event can lead to an extreme phreatic surface. Conversely, an extreme event does not always lead to an extreme phreatic surface. If the phreatic surface is lowered due to drought, and the event has a short duration with a high intensity, the resulting height of the phreatic surface can be lower than when a small event occurs during a wet period. This shows that a certain rise of the phreatic surface is not only related to the event directly causing it, but also by the events of the preceding weeks.

Performing a long-term simulation using one of the models has shown that the height of the phreatic surface at a certain point in the cross-section can be described by a lognormal distribution. The standard deviation of this distribution is variable over the cross-section, and is largest at the inner crest.

Comparing the results of this long-term simulation to the schematisation, it was found that the schematisation is exceeded regularly near the toe and the inside drainage ditch. In the other simulations a slight exceedance in the outer crest was found as well, while in the inner crest the schematisation remained well above the modelled phreatic surface. This suggests that the

schematisation can potentially be improved. These potential improvements are using a higher elevation at the inner crest, a lower elevation at the inner crest, and a higher elevation in the area near the toe and the drainage ditch. More research is required to confirm this.

The results of an uncalibrated model show that for the three research cases calibration was absolutely necessary to model the head fluctuations. For the extreme phreatic surfaces the difference between the calibrated and uncalibrated models is smaller, but this is mainly because the phreatic surface is closer to the equilibrium height in these conditions, which is close to the ground surface in both situations.

7.2 Discussion

There are several assumptions and simplifications used in this research that have to be considered when interpreting the results. This paragraph discusses the validity of the most important of these assumptions.

7.2.1 Input data

First of all, it was assumed that the monitoring well measurements give a good representation of the fluctuations of the pore pressure over time at a certain point in the cross-section. However, all three measurement sets show discrepancies, shifts of a part of the set, or inexplicable peaks. It is also not clear how accurate the measurements of monitoring wells are in general. The filter of a monitoring well spans a certain vertical distance, and the head in the well is thus determined by an equilibrium of the pore pressures over this distance. It seem likely that the highest pore pressure over the filter determines the head, but this is not certain. Flow may occur through the monitoring well to deeper parts of the soil, reducing the head in the well. Additionally, monitoring wells provide storage of water. To measure a head rise, first water has to flow into the monitoring well. This storage capacity can have an influence on the pore pressures around the well, and thus distort the measurements. A further potential source of errors is the presence of cracks in the dike. If such a crack is connected to a monitoring well, runoff water can flow via the crack directly into the well. This loads to head fluctuations that do not correspond to the phreatic surface. Since the models were calibrated on the measurements, a structural error in the measurements would mean that the calibration is incorrect.

A potential problem not necessarily limited to monitoring wells, is the small number of measurement points in the cross-section. For practical reasons, the number of monitoring wells that can be placed in a flood defence is limited. It is also unknown whether the pore pressures deeper in the soil are modelled correctly or not. If a model is calibrated to match the measurement points, it can be assumed that the other points in the cross-section are correct too, but unexpected variations in the soil composition and conductivity can lead to differences. The location of the measurement points is also important: for example, at research location 24 not monitoring well was placed at the inner crest of the berm, which means there is no measurement to verify the phreatic surface in the berm.

7.2.2 Simplifications and schematisations

The soil structure in the top layers of the dikes had to be modelled in a simplified, unrealistic manner. A higher conductivity was applied to the topmost layer in the model, and a larger anisotropy ratio was used since cracks mainly increase the conductivity in vertical direction. With this approach, only the average increase of conductivity caused by the soil structure is modelled. In reality the pores and cracks form a network which forms preferential flow paths for the precipitation to infiltrate. Cracks can intercept runoff water and transport it deeper into the dike. This leads to a faster response of the phreatic surface compared to when the water has to travel through the soil. Cracks can therefore cause different infiltration characteristics at different locations in the dike, which are also variable in time due to formation and closing of cracks. The soil structure might also have an influence on the specific yield and therefore the phreatic storage

capacity. All these processes cannot be simulated in the model. Some of the observed differences between the model results might be explained by the exclusion of the soil structure.

Another simplification made to make the construction of the model manageable, was to model the a cross-section as 2-dimensional. A 2-dimensional model was able to simulate the phreatic surface sufficiently well for the three research cases, although for research location 25 it appeared that flow in the third dimension had an influence on the results. This shows that schematising the flow in the cross-section as 2-dimensional is not in all cases a valid assumption.

7.2.3 Calibration

The calibration of the model is a manual process and therefore prone to human error. Multiple sets of calibration values can lead to similar results, which makes it unclear which is the best calibration set. These different calibration sets can also lead to different pore pressures in the parts of the cross-section for which there are no measurements. Although the differences are small, this makes determination of the best calibration parameters difficult. Additionally, the model was only aimed at determining the heads in the cross-section. The flow rate through the dike was not calibrated, since this magnitude of the flow rate in reality is unknown. It is therefore unclear whether the actual flow through the dikes was modelled correctly.

Extra information could help to make the calibration process easier. For the Hogedijk the soil composition was less uncertain than for the other research locations, which reduced the number of calibration variables. Measured conductivities can provide information on the variations in the cross-section, which can also reduce the number of calibration variables.

7.3 Recommendations

Most information regarding the position of the phreatic surface in flood defences is obtained by measurements using monitoring wells or pressure sensors. As mentioned in the discussion, the validity of these measurements can be disputed. More research regarding the relation between monitoring well measurements and the actual pore pressures in flood defences might provide valuable insights on the validity of measurements, and thus indirectly on the validity of the current schematisations and this research. For example, placing monitoring wells and a pressure sensor in the single cross-section could provide more knowledge about the differences between the measurement methods.

Another recommendation is to investigate different methods to determine the pore pressures in flood defences than monitoring wells or pressure sensors. These methods only provide information on the measurement location. If a measurement method existed that could provide data of the pore pressures over the entire cross-section, a much more complete image of the phreatic surface could be obtained. An interesting possibility could be the use of fibre optic cables. These can be used to measure the temperature and therefore the presence of water. Several cables on different elevations might be used to detect the position of the phreatic surface with a finer resolution than when using separate sensors.

When measurements of the phreatic surface are being conducted, it is recommended to measure at a sufficient number of locations. At least three measurement points are required to determine the course of the phreatic surface. It is important that one of these points is placed at the inner crest, since at that location the fluctuations of the phreatic surface caused by precipitation are the largest. When the measurements are conducted with the aim to perform a model study, pore pressure measurements at various depths can be useful to chart the gradient of the hydraulic head. This makes it possible to calibrate the deeper soil layers more accurately. Conductivity measurements can be useful to provide a reference value for the calibration, and to obtain insight in the variation of the conductivity. It is preferable to use in-situ tests for these measurement, to prevent disturbance of the soil. When monitoring wells are used to measure the pore pressures, these can be also be used for in-situ conductivity tests. A disadvantage of these tests is that only

a single conductivity is measured without direction. Laboratory tests are needed to determine the anisotropy ratio. Laboratory research on samples taken at different depths and locations from various flood defences can be useful to obtain a better comprehension of typical values of the anisotropy ratio.

It was the intention to also analyse the differences between flood defences with different geometry. For this reason a dike with a road on the crest and a dike without a road were chosen. However, the soil compositions of the research cases were so different that no good comparison regarding the mentioned characteristics could be made. It is therefore recommended to conduct more research on the influence of the geometry of the dike on the phreatic surface. This concerns differences in actual geometry, like the height, the angle of the slope or the presence of a berm, but also the influence of a road on the crest.

As discussed in the conclusions, potential improvements to the currently used schematisation of the phreatic surface could be made. The number of research cases in this thesis is too small to conclude that this improvement could apply as a general rule. It is therefore recommended to execute more research whether these changes could actually provide a more accurate and safe schematisation.

References

Allen, R., Pereira, L., Raes, D., & Smith, M. (1998). *Crop evapotranspiration - Guidelines for computing crop water requirements.* Rome: Food and Agriculture Organisation of the United Nations.

Alterra. (2013). *Effecten van beregening op het verloop van het freatisch vlak in veenkades.* Wageningen.

Akker, J. van den. (2001). *Een inventarisatie van bodemfysische materiaalmodellen zoals toegepast in het landbouwkundig onderzoek.* Wageningen: Alterra.

Bakker, M., Post, V., Langevin, C., Hughes, J., White, J., Starn, J., & Fienen, M. (2018). FloPy v3.2.9:. *U.S. Geological Survey Software Release*.

Bokkel Huinink, J. ten. (2016). *Probability density distribution of the phreatic surface in a regional flood defence.*

COMSOL. (2013). *Subsurface Flow Module User's Guide.*

Delfland. (2008). *Toetsing 5 boezemkades Midden-Delfland, resultaten 2e expert workshop 17 juni 2008.*

Delfland. (2010). *Projectmap Peilbuizen meetnet droogtegevoeligheid kaden.*

Delfland. (2016). *Waterspanningen in regionale en overige keringen.*

Delfland. (2018, 10 26). *Het juiste waterpeil*. Opgehaald van Hoogheemraadschap van Delfland: https://www.hhdelfland.nl/inwoner/juiste-waterpeil/waterpeil-bepalen

Delfland. (2018, 29 10). *Legger*. Opgehaald van Hoogheemraadschap van Delfland: https://www.hhdelfland.nl/overheid/beleid-en-regelgeving/leggers

Deltares. (2017). D-Geo Stability User Manual.

Deltares. (2018). *D-Geo Flow User Manual.*

Expertisenetwerk waterveiligheid. (2009). *Technisch Rapport Actuele sterkte van dijken.*

Genuchten, M. van. (1980). *A closed-form equation for predicting the hydraulic conductivity of unsaturated soils.*

GeoDelft. (2005). *Veenkadenonderzoek; rekenmodel grondwaterstroming.*

GeoDelft. (2007). *Veenkadenonderzoek; neerslag en verdamping.*

Hollands Noorderkwartier. (2014). *Scopebepaling dijkverbetering.*

Hoogheemraadschap van Rijnland. (2018, 12 20). *Legger oppervlaktewateren*. Opgehaald van Hoogheemraadschap van Rijnland: https://www.rijnland.net/regels/legger/legger-oppervlaktewateren

Hoven, A. van. (2016). *POVM Beter benutten actuele sterkte KIJK - Schematisering waterspanningen.*

Inpijn-Blokpoel. (2010). Kade 4, Vlaardingsekade te Delfland. *Resultaten geotechnisch onderzoek*.

Iv-Infra. (2018). *Kadeverbetering Nieuwkoop Hogedijk.*

KNMI. (2018, 10 9). *Dagwaarden Neerslagstations*. Opgehaald van Koninklijk Nederlands Meteorologisch Instituut: www.knmi.nl

KNMI. (2019). *Uurgegevens van het weer in Nederland*. Opgeroepen op 01 25, 2019, van KNMI: https://projects.knmi.nl/klimatologie/uurgegevens/selectie.cg

Langevin, C., Hughes, J., Banta, E., Niswonger, R., Panday, S., & Provost, A. (2017). *Documentation for the MODFLOW 6 Groundwater Flow Model.* U.S. Geological Survey .

Loor, D. de. (2018). *An Analysis of the Phreatic Surface of Primary Flood Defences.*

Ministerie van Infrastructuur en Milieu. (2016). WBI 2017. *Schematiseringshandleiding macrostabiliteit*. Ministerie van Infrastructuur en Milieu.

Morris, D., & Johnson, A. (1967). Summary of Hydrologic and Physical Properties of Rock and Soil Materials, as Analyzed by the Hydrologic Laboratory of the U.S. Geological Survey 1948-60.

Nash, J., & Sutcliffe, J. (1970). *River flow forecasting through conceptual models part I.*

Nectaerra. (2018). Rapportage hydrologisch veldonderzoek. *Ter ondersteuning van onderzoek freatisch vlak en schematisatie voor het DIRK-programma, hoogheemraadschap van Rijnland*.

Oosterbaan, R., & Nijland, H. (1994). Determining the Saturated Hydraulic Conductivity.

PLAXIS. (2018). *PLAXIS 2D Reference Manual 2018.*

RPS & Witteveen+Bos. (2016). *Toetsing meest risicovolle kaden - traject 2: Oude Leeder Zuid.*

RPS BCC B.V. & Witteveen + Bos. (2010). *Gedetailleerde toetsing regionale keringen. Kade 4: Vlaardingsekade.*

Schuurman, J., & Droogers, P. (2010). *Penman-Monteith referentieverdamping.* STOWA.

Šimůnek, J., Van Genuchten, M., & Šejna, M. (2018). The HYDRUS Software Package for Simulating the Two- and Three-Dimensional Movement of Water, Heat, and Multiple Solutes in Variably-Saturated Porous Media. *Technical Manual*.

Sman, H. (2014). Modellering verdroging veenkaden. Deltares.

STOWA. (2004). *Statistiek van extreme neerslag in Nederland.*

STOWA. (2013). Meteobase. *Online archief van neerslag- en verdampingsgegevens voor het waterbeheer*.

STOWA. (2015). *Actualisatie meteogegevens voor waterbeheer 2015.*

STOWA. (2015). *Leidraad Toetsen op Veiligheid Regionale Waterkeringen .*

STOWA. (2018). *Neerslagstatistieken voor korte duren.*

Tauw. (2009). *Resultaat en advies nadere toetsing boezemkades Midden-Delfland.*

TAW. (1996). *Technisch rapport klei voor dijken.*

TAW. (2001). *Technisch Rapport Waterkerende Grondconstructies.* Technische Adviescommissie voor de Waterkeringen.

TAW. (2004). *Technisch Rapport Waterspanningen bij dijken.* Technische Adviescommissie voor de Waterkeringen.

TNO Geologische Dienst Nederland. (2018). Opgehaald van DINOloket: https://www.dinoloket.nl

Todd, D., & Mays, L. (2005). *Groundwater Hydrology.*

USGS. (2018). *MODFLOW and Related Programs*. Opgehaald van United States Geological Survey: https://water.usgs.gov/ogw/modflow/

Verruijt, A., & Broere, W. (2011). *Grondmechanica.* Delft: VSSD.

Wong, L., Hashim, R., & Ali, F. (2009). A Review on Hydraulic Conductivity and Compressibility of Peat.

Wösten, J., Veerman, G., De Groot, W., & Stolte, J. (2001). *Waterretentie- en doorlatendheidskarakteristieken van boven- en ondergronden in Nederland: de Staringreeks.* Wageningen: Alterra.

Appendices

A Glossary

Boezem	Network of regional canals which stores and transports excess water from polders to the outside water.
Cunet	Foundation of a road.
Evapotranspiration	Combined flux of evaporation and plant transpiration from the soil to the atmosphere.
Extinction depth	MODFLOW parameter to model evapotranspiration. The maximum depth from which evapotranspiration can take place.
Legger	Document containing waterways, structures and other objects in the management area of a water board and the properties of these objects.
KNMI	Koninklijk Nederlands Meteorologisch Instituut. Dutch meteorological institute.
MW	Monitoring well
NAP	Normaal Amsterdams Peil. Vertical reference level used in the Netherlands.
Polder	Low-lying area of land surrounded by dikes, in which a lower water level is maintained than in the surrounding areas.
Recharge	Downwards water flux from the ground surface to the groundwater table.
Runoff	Flow of precipitation water over the ground surface, which does not infiltrate in the subsoil.
STOWA	Stichting Toegepast Onderzoek waterbeheer. Foundation for applied water research.
Stress period	Time subdivision in MODFLOW between which boundary conditions can change.
TAW	Technische Adviescommissie voor de Waterkeringen. Technical advisory committee for flood defences.
Vertical staggering	Distortion of a regular grid in MODFLOW due to steep layer separations.
Water board	(Dutch: waterschap) Regional government responsible for the management of flood defences, waterways, water levels and water quality.

B List of symbols

General parameters

a	Hydraulic conductivity anisotropy ratio	[-]
A	Area	m^2
b	Riverbed thickness	m
C_{riv}	Conductance of riverbed	m^2/day
drow	Width of cell in model grid	m
g	Gravitational acceleration	m/s^2
h	Hydraulic head	m
h^t_m	Modelled head for timestep t	m NAP
h^t_o	Observed (measured) head for timestep t	m NAP
$\overline{\overline{h_o}}$	Mean of observed heads	m NAP
k	Intrinsic permeability	m/s
K	Hydraulic conductivity	m/day
m_s	Recharge multiplier for section s	[-]
m_{tot}	Recharge multiplier for entire model	[-]
m_v	Compressibility of the soil	m^2/N
n	Soil porosity	[-]
N	Net infiltration due to precipitation	m/s
NSE	Nash-Sutcliffe model efficiency coefficient	-
p_s	Precipitation rate for section s	mm/hour
q	Specific discharge	m/s
R_{cap}	Recharge capacity of the soil	mm/hour
R_{min}	Recharge threshold	mm/hour
R_s	Recharge rate for section s	m/day
S_s	Specific storage	m^{-1}
S_y	Specific yield	v
T	Number of timesteps	-
w	Width of a recharge section	m
β	Compressibility of water	m^2/N
ρ	Density	kg/m^3
ϕ	Hydraulic head	m
μ	Dynamic viscosity	$N\ s/m^2$

Van Genuchten

k_r	Relative permeability	[-]
S_{eff}	Effective saturation	[-]
θ	Water content	[-]
$θ_{res}$	Residual water content	[-]
$θ_{sat}$	Saturated water content	[-]
n	Parameter related to pore size distribution	[-]
m	1 – (1/n)	[-]
p_c	Capillary suction pressure	kN/m^2
α	Parameter related to air entry suction	m^{-1}

Penman-Monteith

d_r	Inverse relative distance earth-sun	[-]
ET_{ref}	Potential evapotranspiration rate	mm/d
e_s	Saturation vapour pressure	kPa
e_a	Daily average vapour pressure	kPa
G	Soil heat flux density	$MJ/m^2/d$
G_{sc}	Solar constant (= 118,08)	$MJ/m^2/d$
$K^{\downarrow}$	Incoming short-wave radiation	$MJ/m^2/d$
J	Day number of the year	[-]
$K^{\uparrow}$	Outgoing short-wave radiation	$MJ/m^2/d$
$K^{0\downarrow}$	Solar radiation	$MJ/m^2/d$
K_{ext}	Extra-terrestrial solar radiation	$MJ/m^2/d$
$L^{\downarrow}$	Incoming long-wave radiation	$MJ/m^2/d$
$L^{\uparrow}$	Outgoing long -wave radiation	$MJ/m^2/d$
Q_{net}	Net radiation	$MJ/m^2/d$
RH	Relative humidity	[-]
T_{mean}	Mean daily air temperature at 2 m height	°C
u_z	Daily average wind speed at z m height	m/s
z	Height of weather station above sea level	m
α	Albedo	[-]
γ	Psychrometric constant	kPa/°C
δ	Solar declination	radians
φ	Latitude	radians
ω_s	Solar time angle	radians
σ	Stefan-Boltzman constant (= $4,903*10^{-9}$)	$MJ/K^4/m^2/d$

C Meteorological data

C.1 Delfland

In this appendix it is described how the precipitation and evapotranspiration data used in the model are attained from the online archive Meteobase.nl. The data was downloaded in grid format. For this an area has to be selected on a map, which is displayed in Figure C.1. The locations of the cases are displayed on this map as red squares. For this area both the hourly precipitation data and daily evopotranspiration calculated using Penman-Monteith are downloaded for the period 2010-2014.

Figure C.1: Selected area in Meteobase

For this area the data for several grid points was delivered. The nearest of these grid points is displayed as a blue cross. The data for this grid point is used for the simulations.

The grid data from Meteobase is delivered in ASCII format, which means that every hourly or daily data point is provided as a separate file. This file contains the number of selected grid points, the coordinates of these points and the data for these points. Because of the large amount of files (43801 for the total period) the data can only be requested for a period of 2 years at once, which meant the data had to be downloaded in three parts. For the purposes of this research, the ASCII format is not very useful to work with. For this reason a Python script was written, which reads every file, extracts the data for the correct grid point, and writes this value along with the date and time in a csv file which can be opened in Excel. In Excel the data was plotted to detect any anomalies. One anomaly was found: The ASCII file for 1-1-2014 0:00 included a precipitation of 967 mm. This value is replaced with 0.1 mm, which is the average of the measurements of the nearest KNMI weather stations at Hoek van Holland and Rotterdam for this hour.

To verify the precipitation data, the data from Meteobase was compared to precipitation data from some weather stations nearby. This data was downloaded from the website of the Royal Netherlands Meteorological Institute (KNMI, 2018). Data from the following weather stations was used:

- Hoek van Holland (hourly data)
- Rotterdam (hourly data)
- Delft (daily data)
- Honselersdijk (daily data)
- Maasland (daily data)

The total precipitation over the research period from 01-06-2010 to 18-10-2014 for these stations is compared for the total precipitation from this period in the Meteobase data. This is displayed in Table C.1.

Table C.1: Comparison of Meteobase data and weather stations

Station	Distance to cases (km)	Cumulative precipitation (mm)
Hoek van Holland	11,6	3984,1
Rotterdam	8,9	3991,3
Delft	5,8	4432,0
Honselersdijk	5,9	4314,9
Maasland	4,1	4028,3
Meteobase	-	4214,2

The cumulative precipitation for the weather stations and the Meteobase data is plotted in figure D.2.

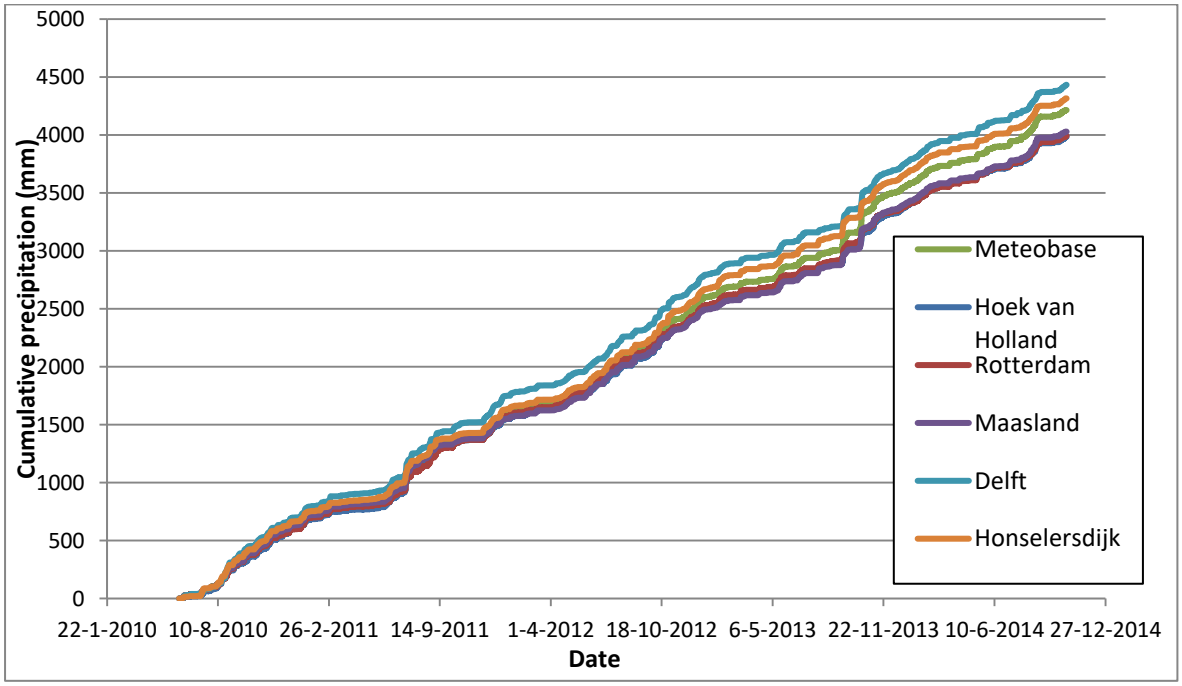

Figure D.2: Cumulative precipitation for Meteobase and weather station data.

It can be observed that there is some variance in the total precipitation over de considered period. The stations at Hoek van Holland, Rotterdam and Maasland show very similar amounts of about 4000 mm. The stations at Delft and Honselersdijk show significantly larger amounts of respectively 4432 and 4315 mm. The Meteobase data shows a value in between those values of 4214 mm. This is not surprising, considering that this data is partially based on the weather station data. However, by making this comparison it can be seen that the Meteobase data shows anomalies caused by the processing. The Meteobase data is therefore considered realistic enough to use for the simulations.

C.2 Hogedijk

To calculate the Penman-Monteith potential evapotranspiration rate from KNMI weather station data, the method described in Schuurman & Droogers (2010) was used. This method was largely based on a report from the Food and Agriculture Organisation of the United Nations (Allen, Pereira, Raes, & Smith, 1998). Since the KNMI stations do not measure al variables required for the Penman-Monteith formulations, some of the variables have to be estimated. Said reports provide a method for this.

The Penman-Monteith expression for the potential evapotranspiration rate is defined as:

$$ET_{ref} = \frac{0{,}408 * s * (Q_{net} - G) + \gamma * \frac{900}{T} * u_2 * [e_s - e_a]}{s + \gamma(1 + 0{,}34 * u_2)} \tag{D.1}$$

Where:

ET_{ref}	=	potential evapotranspiration rate	(mm/d)
Q_{net}	=	net radiation	(MJ/m²/d)
G	=	soil heat flux density	(MJ/m²/d)
γ	=	psychrometric constant	(kPa/°C)
T	=	mean daily air temperature at 2 m height	(°C)
u_2	=	daily average wind speed at 2 m height	(m/s)
e_s	=	saturation vapour pressure	(kPa)
e_a	=	daily average vapour pressure	(kPa)
$e_s - e_a$	=	saturation vapour pressure deficit	(kPa)

Slope of the vapour pressure curve (s)

The slope of the vapour pressure curve is calculated from the mean daily temperature using the following expression (Allen, Pereira, Raes, & Smith, 1998):

$$s = \frac{4098 * \left[0{,}6108 * \exp\left(\frac{17{,}27 * T_{mean}}{T_{mean} + 237{,}3}\right)\right]}{(T_{mean} + 237.3)^2} \tag{D.2}$$

For standardization purposes the daily mean temperature T_{mean} is calculated as follows:

$$T_{mean} = \frac{T_{max} - T_{min}}{2} \tag{D.3}$$

Where:

T_{mean}	=	daily mean temperature	(°C)
T_{max}	=	daily maximum temperature	(°C)
T_{min}	=	daily minimum temperature	(°C)

Net radiation (Q_{net})

The net radiation consists of two components: the net short-wave and net long-wave radiation:

$$Q_{net} = K^{\downarrow} - K^{\uparrow} + L^{\downarrow} - L^{\uparrow} \tag{D.4}$$

Where:

$K^{\downarrow}$	=	incoming short-wave radiation	(MJ/m²/d)
$K^{\uparrow}$	=	outgoing short-wave radiation	(MJ/m²/d)
$L^{\downarrow}$	=	incoming long-wave radiation	(MJ/m²/d)
$L^{\uparrow}$	=	outgoing long-wave radiation	(MJ/m²/d)

The incoming short-wave radiation is a quantity measured at the KNMI-stations. The outgoing short-wave radiation can be estimated from this quantity using the albedo. The albedo is a dimensionless number representing the ratio between the absorbed and reflected radiation. Thus, the outgoing short-wave radiation is calculated as follows (Schuurman & Droogers, 2010):

$$K^{\downarrow} = \alpha * K^{\uparrow} \tag{D.5}$$

α	=	albedo	(-)

For the Penman-Monteith formulation a fixed value of 0,23 is used for the albedo.

For the long-wave radiation no measurements are available. It has to be estimated from other meteorological measurements using the following empirical formulation (Allen, Pereira, Raes, & Smith, 1998):

$$L^{\downarrow} - L^{\uparrow} = \sigma \left[\frac{{T_{max}}^4 + {T_{min}}^4}{2}\right] (0{,}34 - 0{,}14 * \sqrt{e_a}) \left(1{,}35 * \frac{K^{\downarrow}}{{K_0}^{\downarrow}} - 0{,}35\right) \tag{D.6}$$

Where:

$L^{\downarrow}$ - $L^{\uparrow}$	=	net outgoing long-wave radiation	(MJ/m²/d)
σ	=	Stefan-Boltzman constant (= 4,903*10^{-9})	(MJ/K⁴/m²/d)
T_{max}	=	daily maximum temperature	(°C)
T_{min}	=	daily minimum temperature	(°C)
e_a	=	daily average vapour pressure	(kPa)
$K^{\downarrow}$	=	incoming short-wave radiation	(MJ/m²/d)
$K^{0\downarrow}$	=	solar radiation	(MJ/m²/d)

The daily average vapour pressure is a quantity that is also directly required in the Penman-Monteith equation, and will be discussed later. The solar radiation $K^{0\downarrow}$ is the radiation the earth would receive without clouds. Based on the ratio between this value and the measured incoming radiation the long-wave radiation is estimated. To calculate the solar radiation, the extra-terrestrial radiation K_{ext} is required, which is dependent on the time of year and the geographical location on earth. The solar radiation is calculated using the following expressions (Allen, Pereira, Raes, & Smith, 1998):

$${K_0}^{\downarrow} = (0{,}75 + 2 * 10^{-5} * z) * K_{ext} \tag{D.7}$$

$$K_{ext} = \frac{G_{sc} * d_r}{\pi} [\omega_s * \sin(\varphi) * \sin(\delta) + \cos(\varphi) * \sin(\omega_s)] \tag{D.8}$$

$$d_r = 1 + 0{,}033 * \cos\left(\frac{2\pi}{365} * J\right)$$

$$\delta = 0{,}409 * \sin\left(\frac{2\pi}{365} * J - 1{,}39\right) \quad \text{(D.9)}$$

$$\omega_s = \arccos(-\tan(\varphi)\tan(\delta)) \quad \text{(D.10)}$$

(D.11)

Where:

$K^{0\downarrow}$	=	solar radiation	(MJ/m²/d)
z	=	height of weather station above sea level	(m)
K_{ext}	=	extra-terrestrial solar radiation	(MJ/m²/d)
G_{sc}	=	solar constant (= 118,08)	(MJ/m²/d)
d_r	=	inverse relative distance earth-sun	(-)
δ	=	solar declination	(rad)
φ	=	latitude	(rad)
ω_s	=	solar time angle	(rad)
J	=	day number of the year	(-)

The height of the weather station is -2 m. The latitude is 52 degrees, or 0,911 radians.

Soil heat flux density (G)

The soil heat flux density is the energy required to heat up the soil. It can be negative when the soil cools down. When calculating the evapotranspiration over an entire day, the soil heat flux density is often set to zero, which is also done for this calculation.

Psychrometric constant (γ)

The psychrometric constant describes the relation between the partial pressure of the water in air the air temperature. It is dependent on the air pressure and therefore height. This relation between the constant and the height is small, and therefore usually a fixed value of 0,06 kPa/°C is used.

Daily mean air temperature (T)

The air temperature is measured directly for every hour. For each day the mean of these measurements is taken.

Daily average wind speed at 2 m height (u_2)

The wind speed is also a quantity directly measured; however, these measurements are taken at a height of 10 m. The wind speed close the ground surface increases logarithmically with height, and therefore the wind speed at 10 m height can be approximated using the following equation (Allen, Pereira, Raes, & Smith, 1998):

$$u_2 = u_z \frac{4{,}87}{\ln(67{,}8 * z - 5{,}42)} \quad \text{(D.12)}$$

Where:

u_2	=	wind speed at 2 m height	(m/s)
u_z	=	wind speed at z m height	(m/s)
z	=	height of the wind speed measurement (= 10 m)	(m)

Saturation vapour pressure deficit ($e_s - e_a$)

This quantity is the difference between the actual and the saturated vapour pressure, and indicates the amount of water the air can absorb. A larger saturation vapour pressure deficit means a larger evapotranspiration flux.

The actual vapour pressure e_a cannot be measured directly, and is derived from the relative humidty (RH), which is a measured quantity. The relative humidity is the ratio between the actual and the saturated vapour pressure:

$$RH = \frac{e_a}{e_s} \tag{D.13}$$

Where:

RH	=	relative humidity	(-)
e_s	=	saturation vapour pressure	(kPa)
e_a	=	daily average vapour pressure	(kPa)

The saturation vapour pressure is dependent on the air temperature. It is calculated using the following expressions (Allen, Pereira, Raes, & Smith, 1998):

$$e°(T) = 0{,}6108 * \exp\left[\frac{17{,}27\,T}{T + 237{,}3}\right] \tag{D.14}$$

$$e_a = \frac{e_s(0), T_{max} + e_s(0), T_{min}}{2} \tag{D.15}$$

Where:

$e^{\circ}(T)$	=	saturation vapour pressure at the air temperature T	(kPa)
T	=	air temperature	(°C)
T_{max}	=	daily maximum air temperature	(°C)
T_{min}	=	daily minimum air temperature	(°C)
e_a	=	daily average vapour pressure	(kPa)

The saturation vapour pressure is calculated for the daily maximum and minimum temperature, and the average is taken to obtain the mean saturation vapour pressure. Using equation D.13, the daily average vapour pressure can then be calculated using the relative humidty.
Using the equations D.2 –D.15 the input variables for the Penman-Monteith equation can be calculated from the following measured parameters:

- Temperature: measured hourly, daily maximum, minimum and mean are taken;
- Incoming short-wave radiation;
- Relative humidity;
- Wind speed at 10 m height.

These quantities are available for the KNMI weather stations Schiphol, Valkenburg and Cabauw, and were downloaded from the KNMI website (KNMI, 2018). For each station the Penman-Monteith evapotransporation was calculated for each day with the use of an Excel sheet. From these daily values the average of the three weather stations was taken, weighted by the distance to the Hogedijk.

D Measurement data

D.1 Delfland location 24

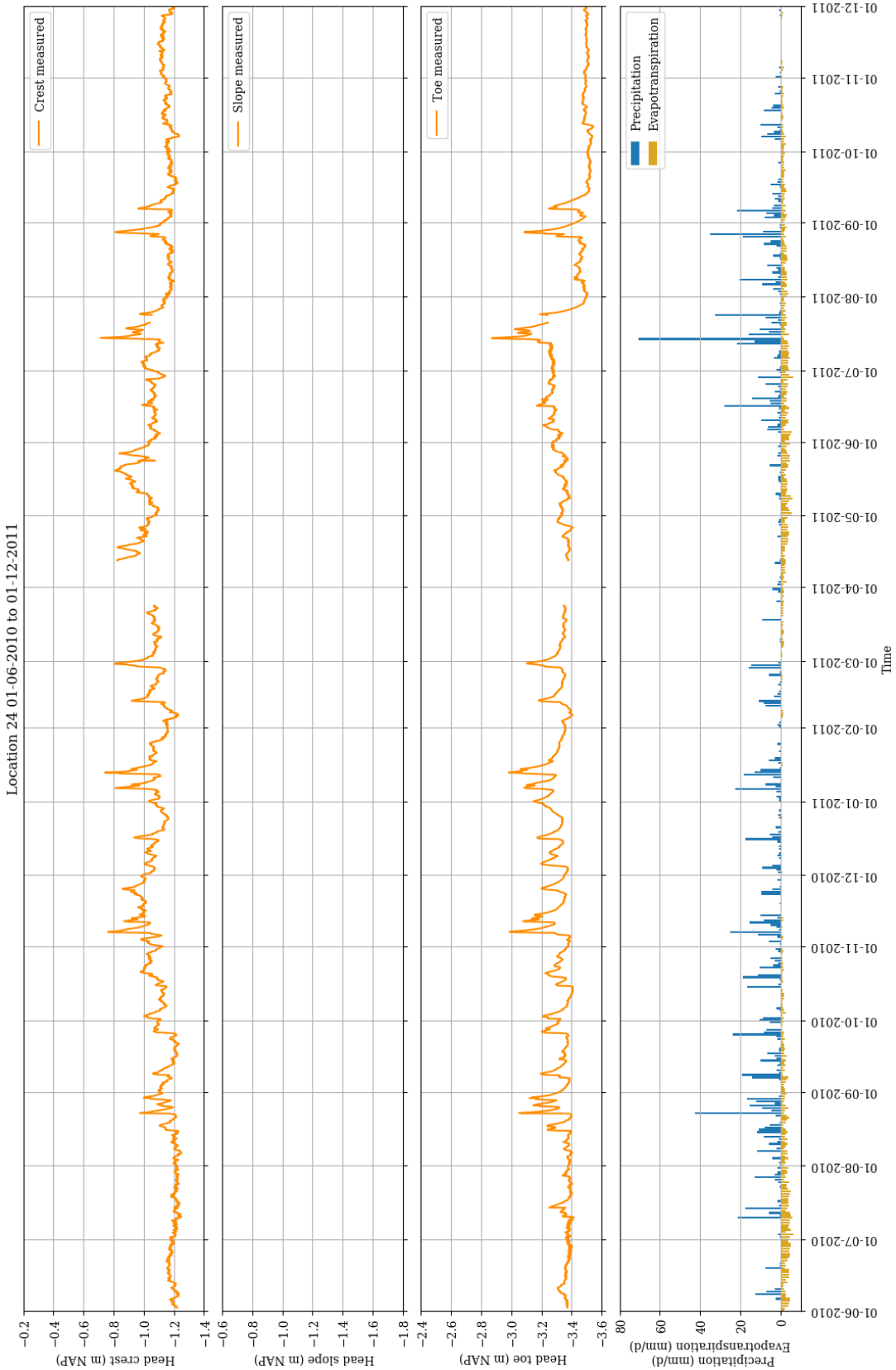

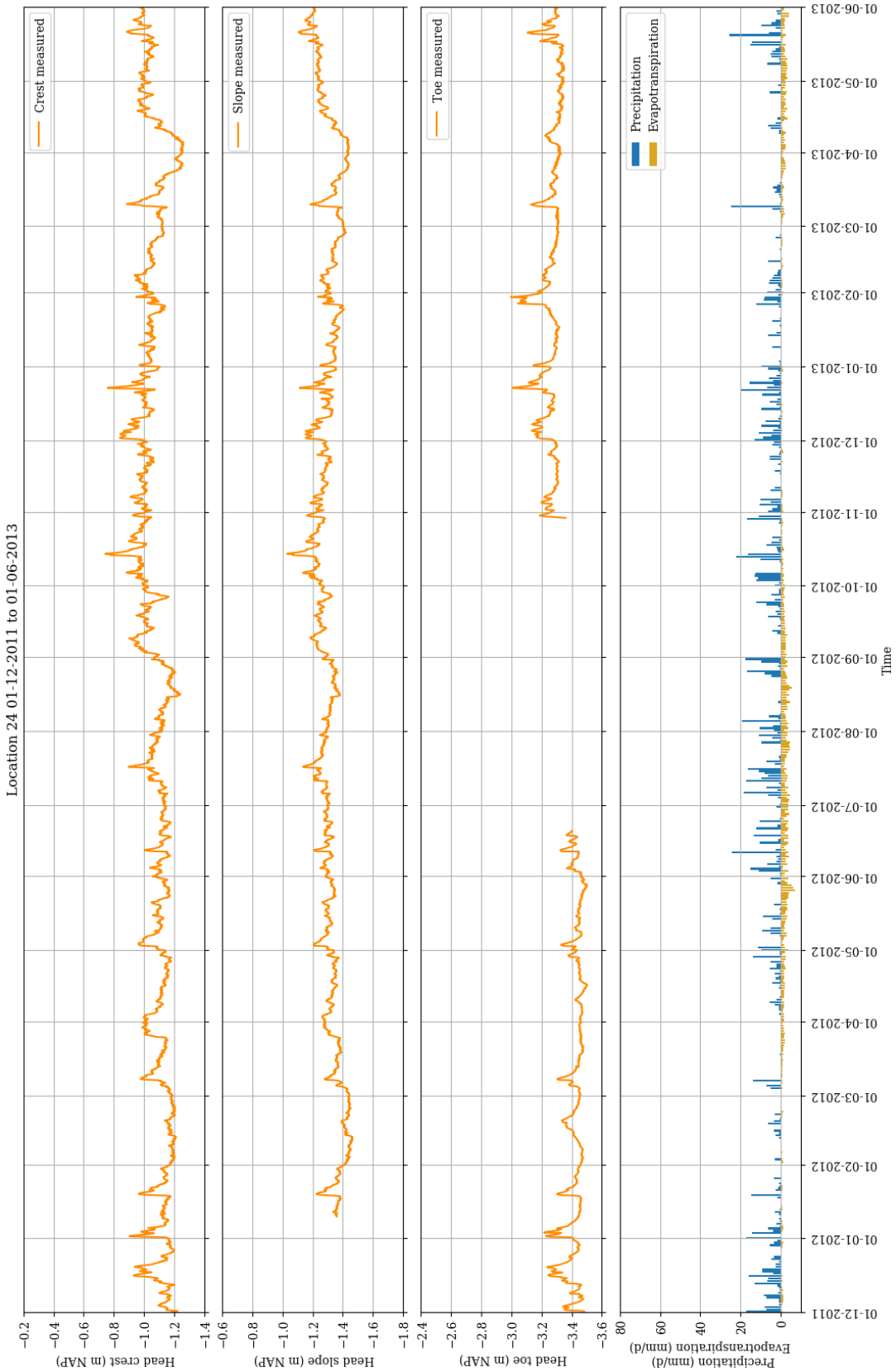
Location 24 01-12-2011 to 01-06-2013
Crest measured
Head crest (m NAP)
Slope measured
Head slope (m NAP)
Toe measured
Head toe (m NAP)
Precipitation
Evapotranspiration
Precipitation (mm/d)
Evapotranspiration (mm/d)
Time
01-12-2011
01-01-2012
01-02-2012
01-03-2012
01-04-2012
01-05-2012
01-06-2012
01-07-2012
01-08-2012
01-09-2012
01-10-2012
01-11-2012
01-12-2012
01-01-2013
01-02-2013
01-03-2013
01-04-2013
01-05-2013
01-06-2013

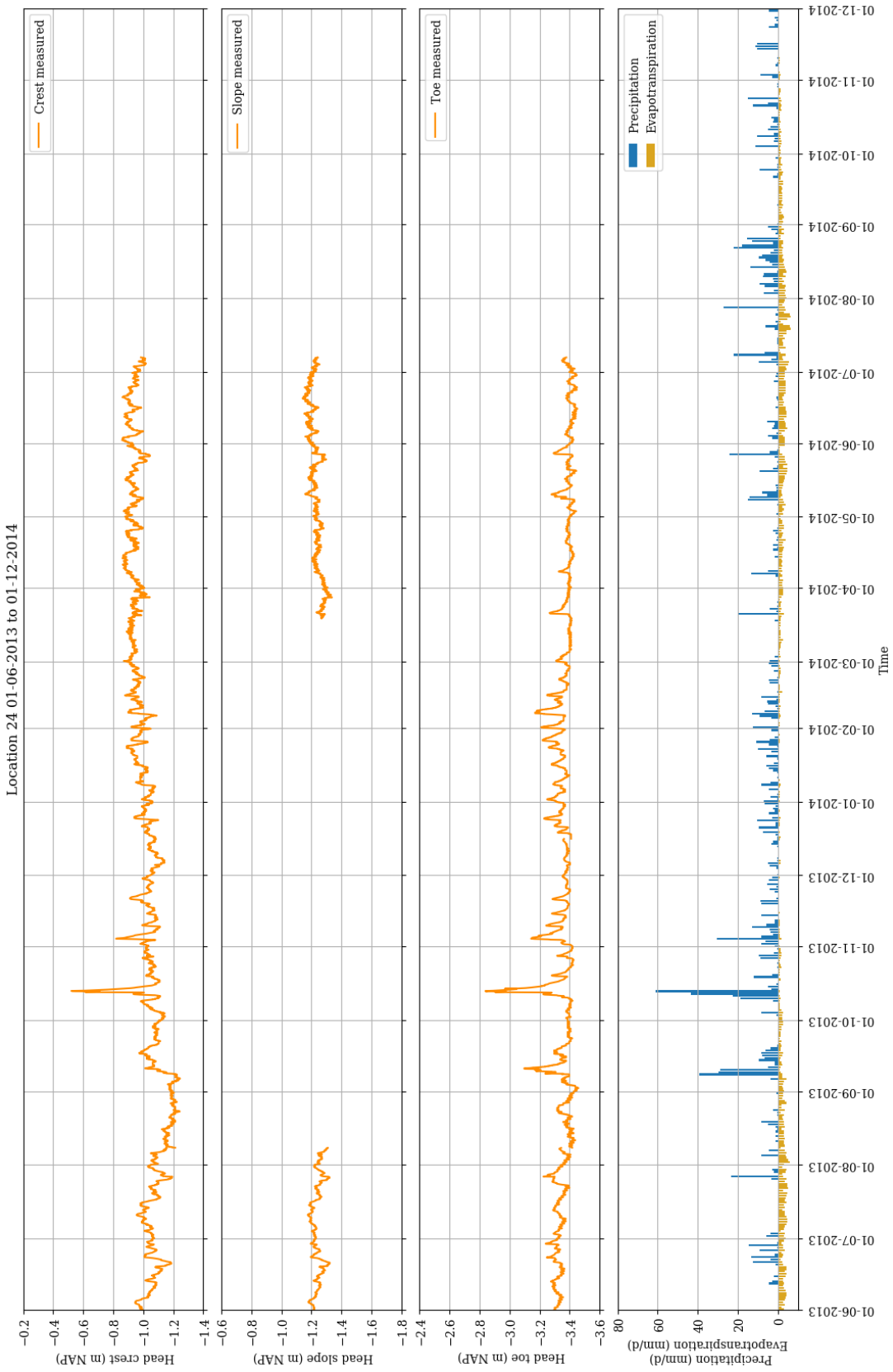
Location 24 01-06-2013 to 01-12-2014
Crest measured
Head crest (m NAP)
Slope measured
Head slope (m NAP)
Toe measured
Head toe (m NAP)
Precipitation
Evapotranspiration
Precipitation (mm/d)
Evapotranspiration (mm/d)
Time

D.2 Delfland location 25

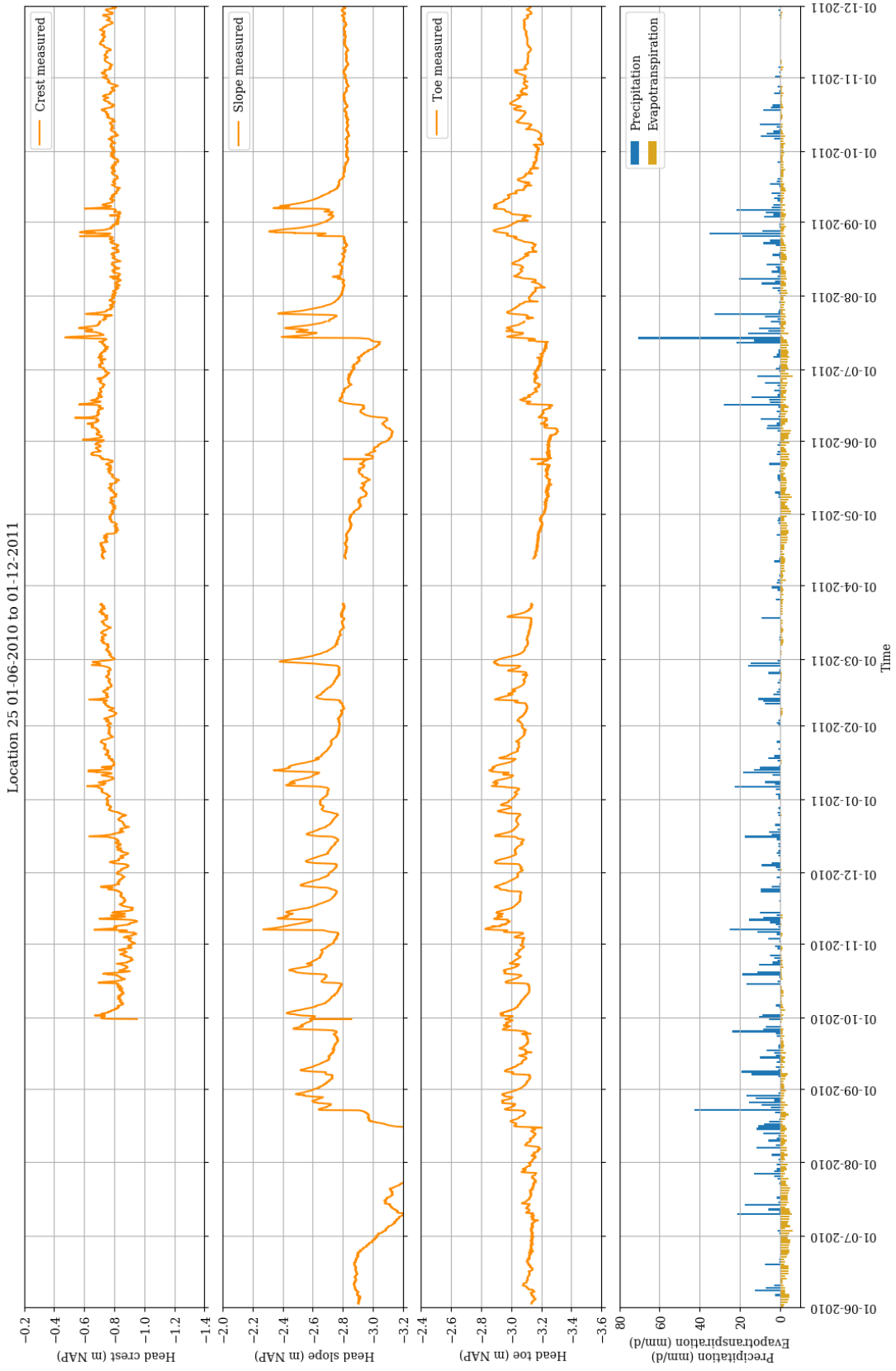

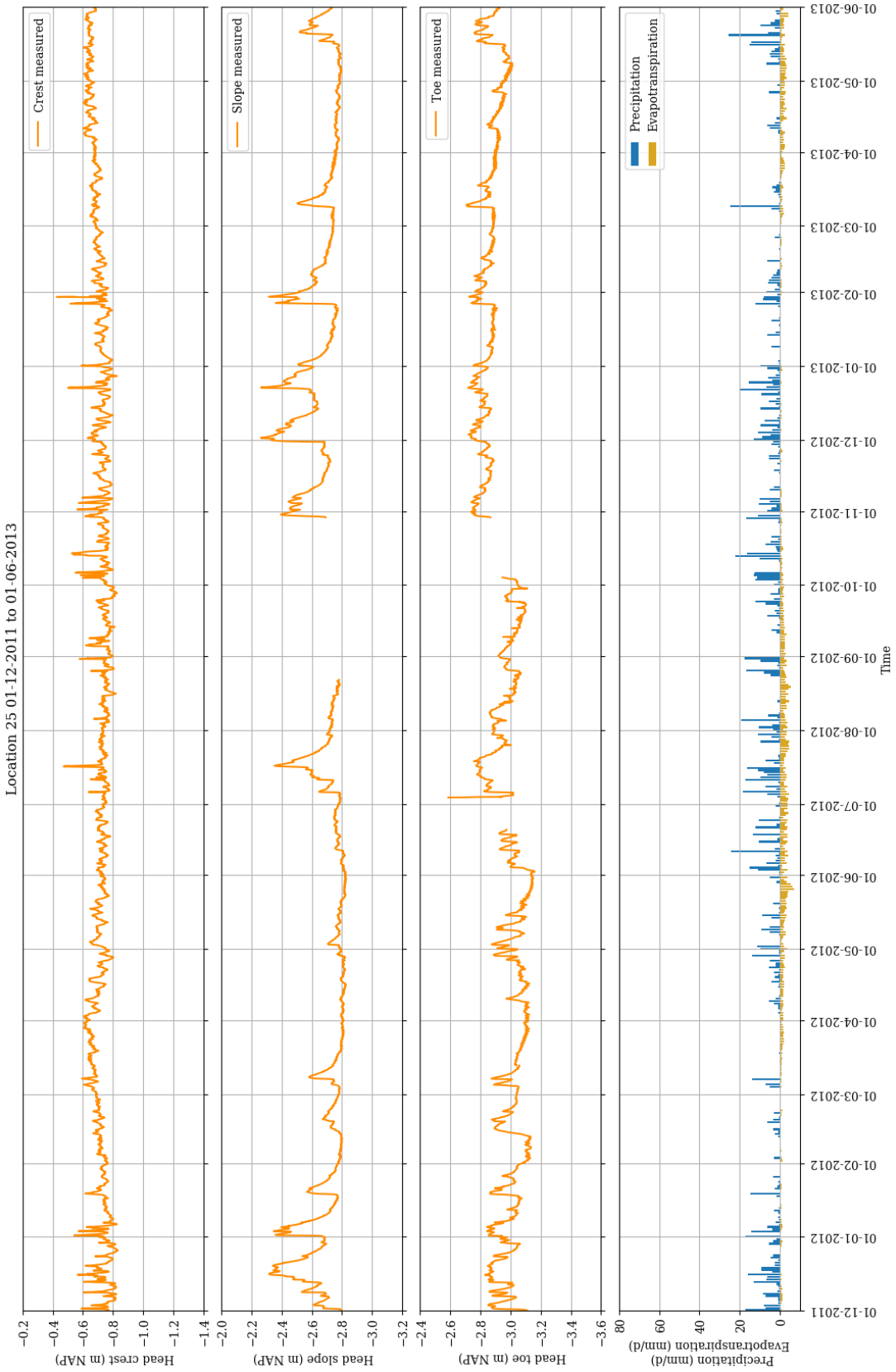
Location 25 01-12-2011 to 01-06-2013
Crest measured
Slope measured
Toe measured
Precipitation
Evapotranspiration
Head crest (m NAP)
Head slope (m NAP)
Head toe (m NAP)
Precipitation (mm/d)
Evapotranspiration (mm/d)
Time

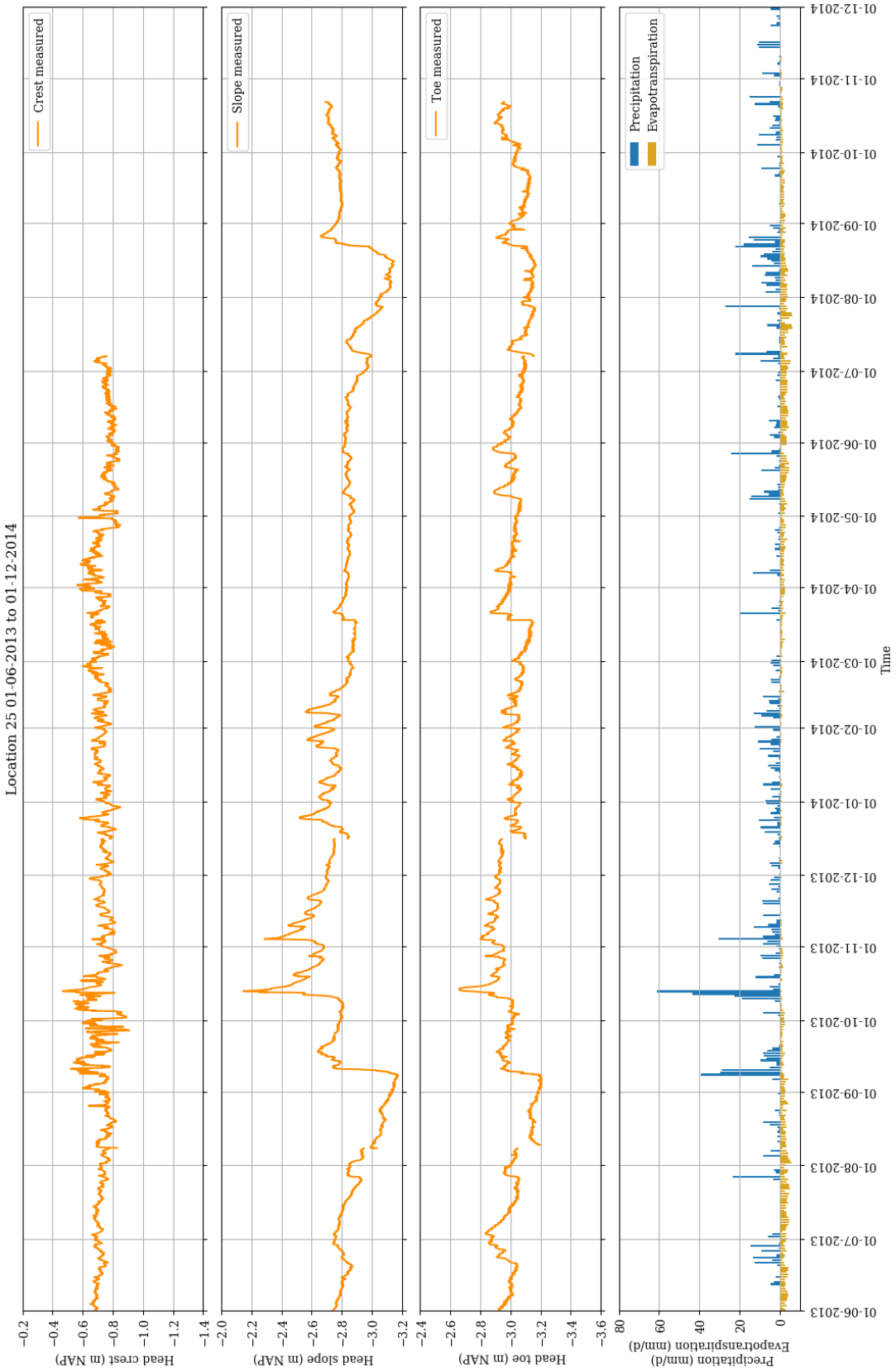
Location 25 01-06-2013 to 01-12-2014
Crest measured
Slope measured
Toe measured
Precipitation
Evapotranspiration
Head crest (m NAP)
Head slope (m NAP)
Head toe (m NAP)
Precipitation (mm/d)
Evapotranspiration (mm/d)
Time

D.3 Hogedijk

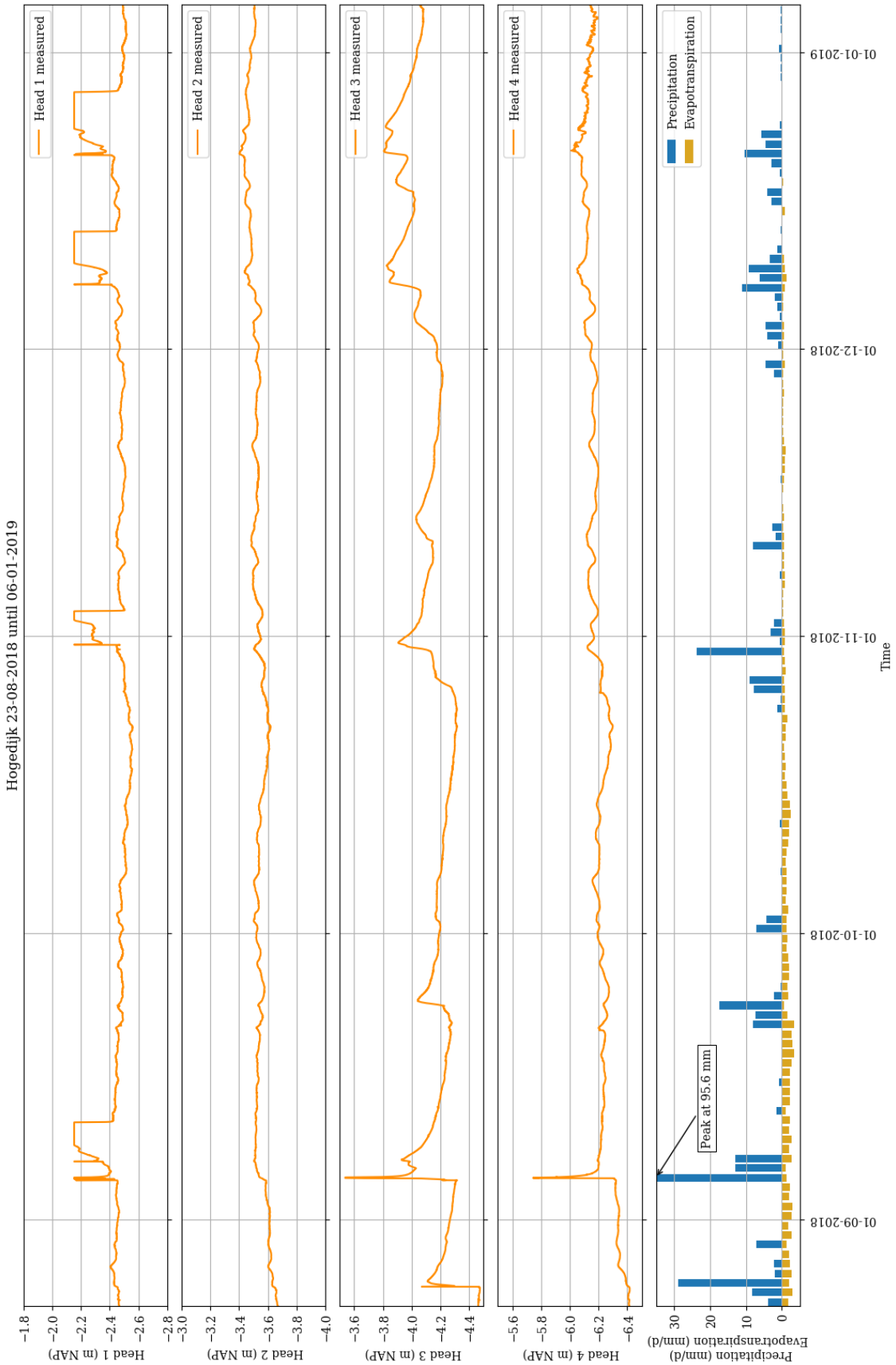
Hogedijk 23-08-2018 until 06-01-2019
Head 1 measured
Head 2 measured
Head 3 measured
Head 4 measured
Precipitation
Evapotranspiration
Peak at 95.6 mm
Head 1 (m NAP)
Head 2 (m NAP)
Head 3 (m NAP)
Head 4 (m NAP)
Precipitation (mm/d)
Evapotranspiration (mm/d)
Time
01-09-2018
01-10-2018
01-11-2018
01-12-2018
01-01-2019

D.4 Discrepancies in the measurements

D.4.1 Delfland 24

The following holes and discrepancies were found in the measurements of location 24:

- Measurements at the slope start later, on 11-01-2012. This is due to several reasons: the filter of the monitoring well was changed, for some time the settings of the data loggers were wrong and later the monitoring well was damaged.
- There are no measurements for the crest and toe from 24-03-2011 until 12-04-2011 due to an error in the settings of the data loggers.
- The crest shows a strange dip on 24-05-2015.
- There is a small gap in the data from 21-7-2011 until 24-7-2011 for the crest and toe.
- From 20-6-2012 until 29-10-2012 there are no measurements for the toe; no explanation is reported for this.
- From 8-8-2013 until 16-03-2014 the measurements for the slope are removed due to unrealistic fluctuations. On 8-8-2013 also a jump can be seen for the crest and slope, which indicates a correction. However, no manual measurement is reported for this date.
- On 16-12-2013 the data for the slope is slightly shifted based on a manual measurement. The crest is unchanged because the manual measurement is the same as the data logger.
- On 18-3-2014 another manual measurement was done, but the data is not changed based on this measurement.
- The measurements ceased on 7-7-2014. A final manual measurement has taken place on this day.

D.4.2 Delfland 25

The following remarks can be made on the measurements of location 25:

- The monitoring well at the crest was placed in an intermediate sand layer. Therefore an additional monitoring well was placed for which measurements started on 30-09-2010. The measurements at the slope show a strange peak downwards on the same date.
- There is a gap in the data from 24-03-2011 until 12-04-2011 caused by an error in the settings of the data loggers.
- The toe and slope show a strange peak downwards on 24-05-2015.
- Around 21-07-2011 there is a small gap in the data for the toe and crest.
- From 20-6-2012 until 04-07-2012 there is a gap in the data for the toe. The data for the first few hours when the measurements start again is not very meaningful. No explanation is given for this gap.
- On 22-08-2012 the measurements for the slope stop, and at 04-10-2012 for the toe as well. For both points the measurements restart on 19-10-2012. No explanation has been found for this gap.
- The measurements for the intermediate sand layer cease on 13-09-2012. The data from 08-08-2013 until 07-11-2014 is removed due to unrealistic fluctuations. It is unclear why the rest of the data is not present.
- On 08-08-2013 there is a small gap and a strange jump in the measurements for crest, slope and toe. Probably the measurements before or after are shifted higher or lower. No manual measurement is reported for this date.
- Another jump occurs on 16-12-2013. This corresponds to a manual measurement on this date, so probably the data has been shifted to fit this.
- Another jump occurs on 18-03-2014. This corresponds to another manual measurement.
- A small jump occurs on 07-07-2014 at the toe, on the same day measurements for the crest cease. This corresponds to a manual measurement.
- On 01-08-2014 measurements for the intermediate sand layer are restarted.
- On 22-10-2014 the measurements are stopped; a final manual measurement has taken place on this date.

E Cross-sections and soil data

E.1 Cross-sections

Location 24, Delfland

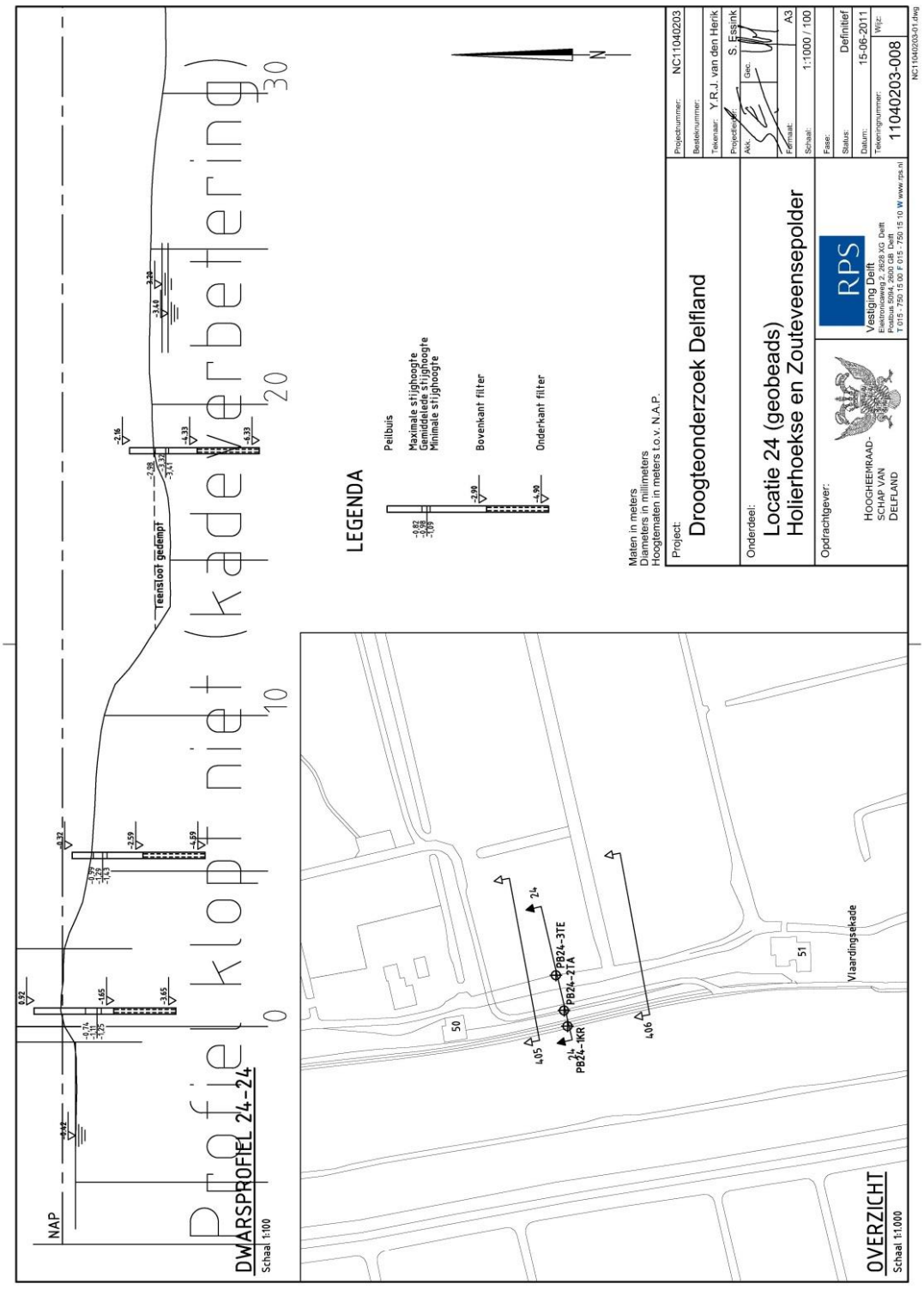

Location 25, Delfland

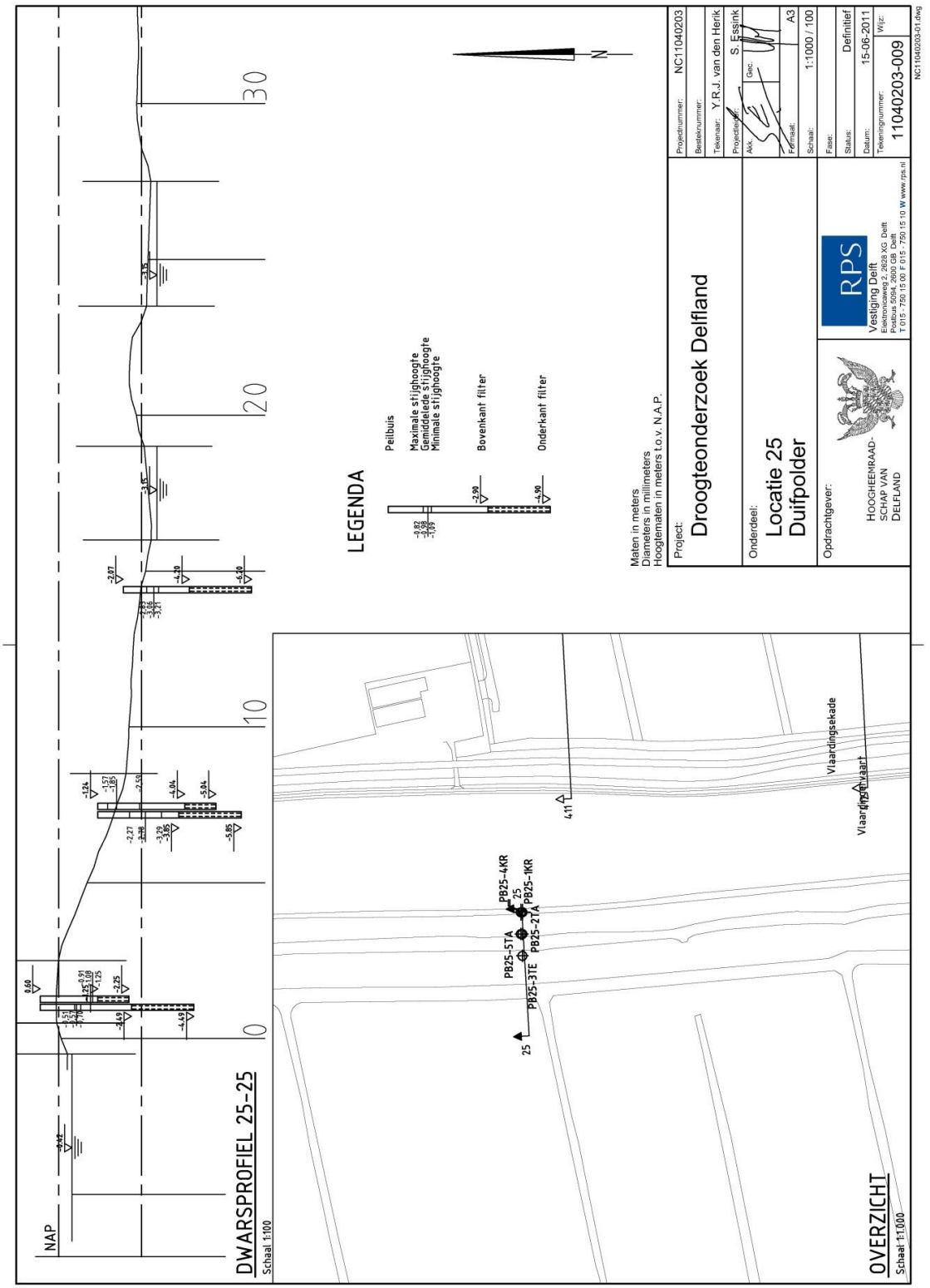

Location Hogedijk, Rijnland

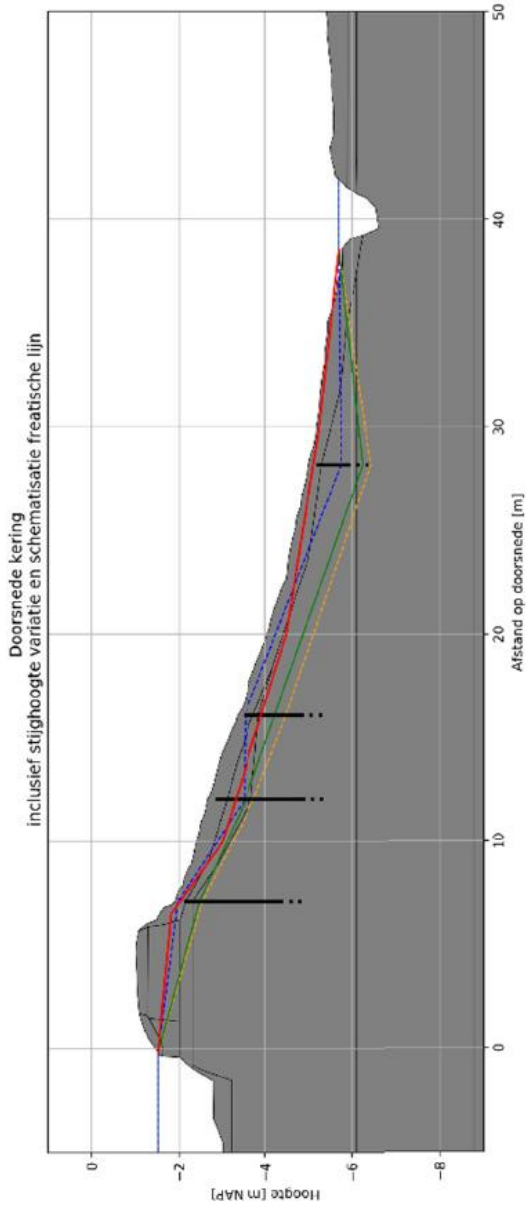

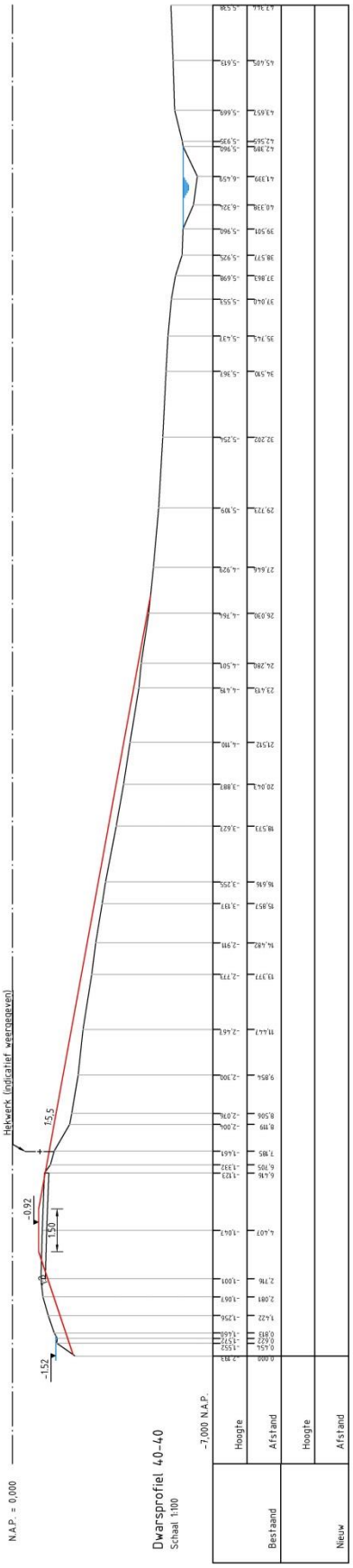

E.2 Soil borings Delfland location 24

Soil borings taken at the research location
These soil borings were taken at the locations of the monitoring wells. The initial positions of the filters of the monitoring wells also are displayed. The depths are indicated with respect to the ground surface. The elevation of the ground surface for the three locations is as follows:

Crest: NAP +0,35 m
Slope: NAP -0,94 m
Toe: NAP -2,73 m

Crest **Slope** **Toe**

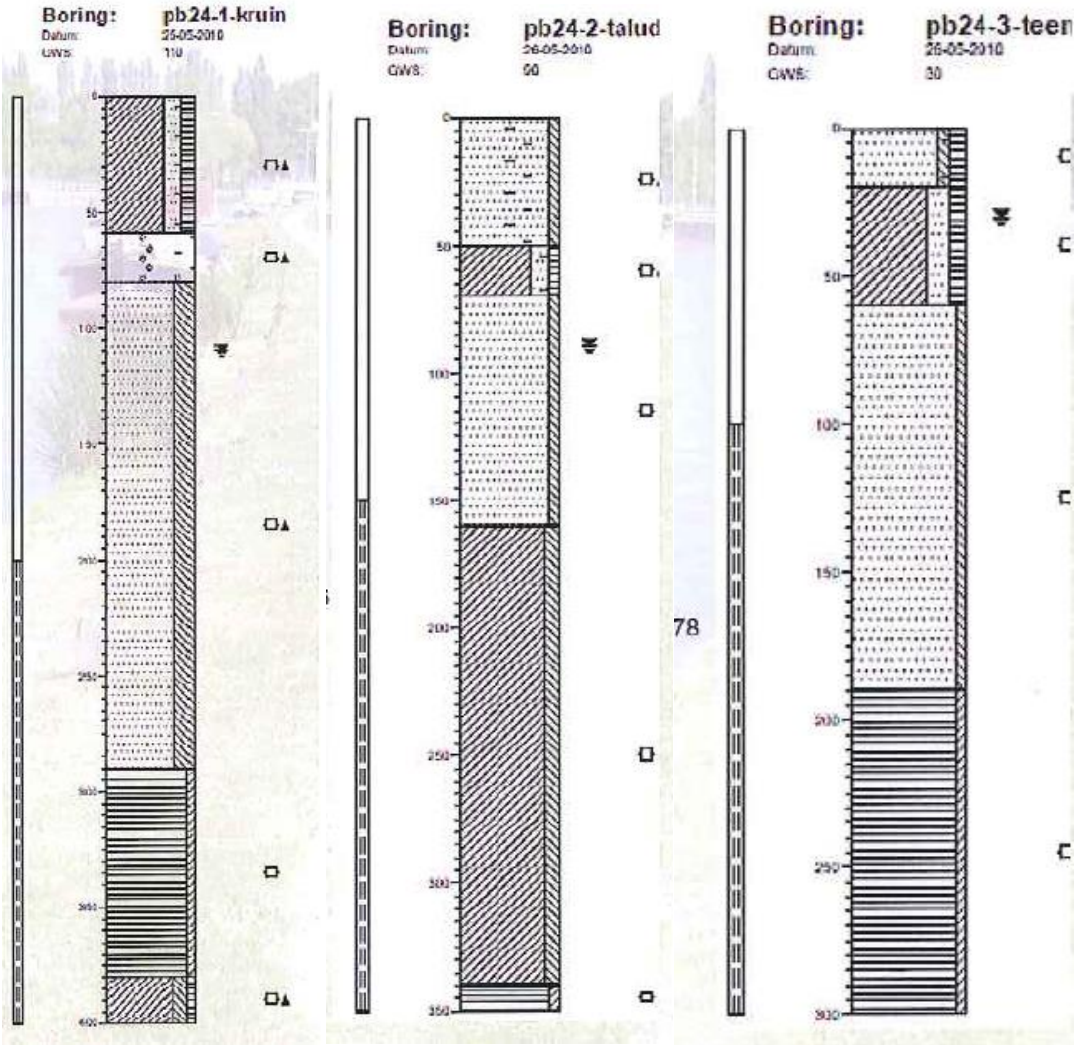

Source: (Delfland, 2010)

Other soil borings

The following borings were taken about 15 m to the south of the research cross-section, as a part of a reinforcement program for the flood defence. Due to the proximity and similarity of this cross-section these borings are considered relevant for the research location. The borings were performed on two locations, comparable to the locations of the monitoring wells in the crest and the slope in the research cross-section. Two manual borings and one mechanical boring are available.

Manual boring crest

Boring: **Hb-4.6kr.a**
Actuele GWS: 95 cm - mv
Datum: 21-10-2009
Maaiveldhoogte: 0,19 m t.o.v. N.A.P.
2e poging

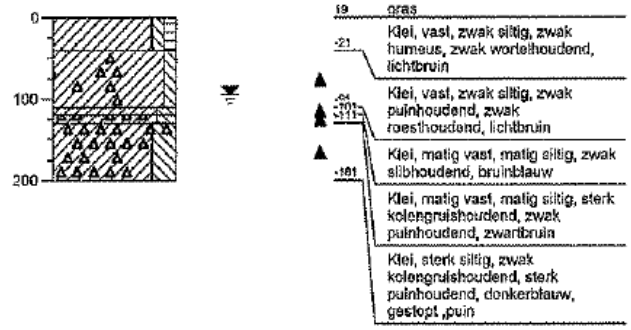

Manual boring toe

Boring: **Hb-4.6te**
Actuele GWS: 100 cm - mv
Datum: 21-10-2009
Maaiveldhoogte: -2,63 m t.o.v. N.A.P.

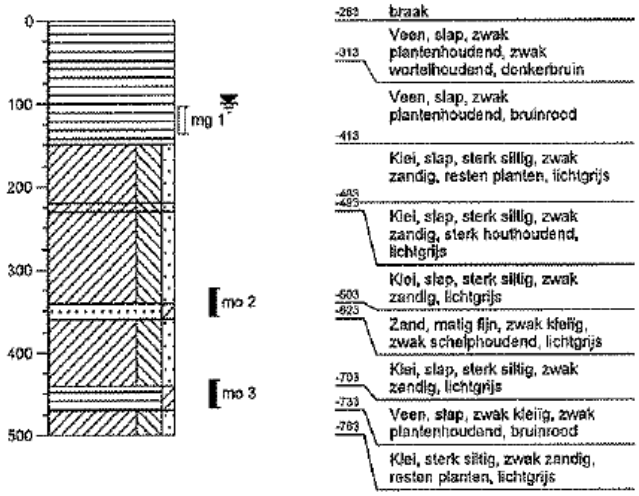

Mechanical boring crest

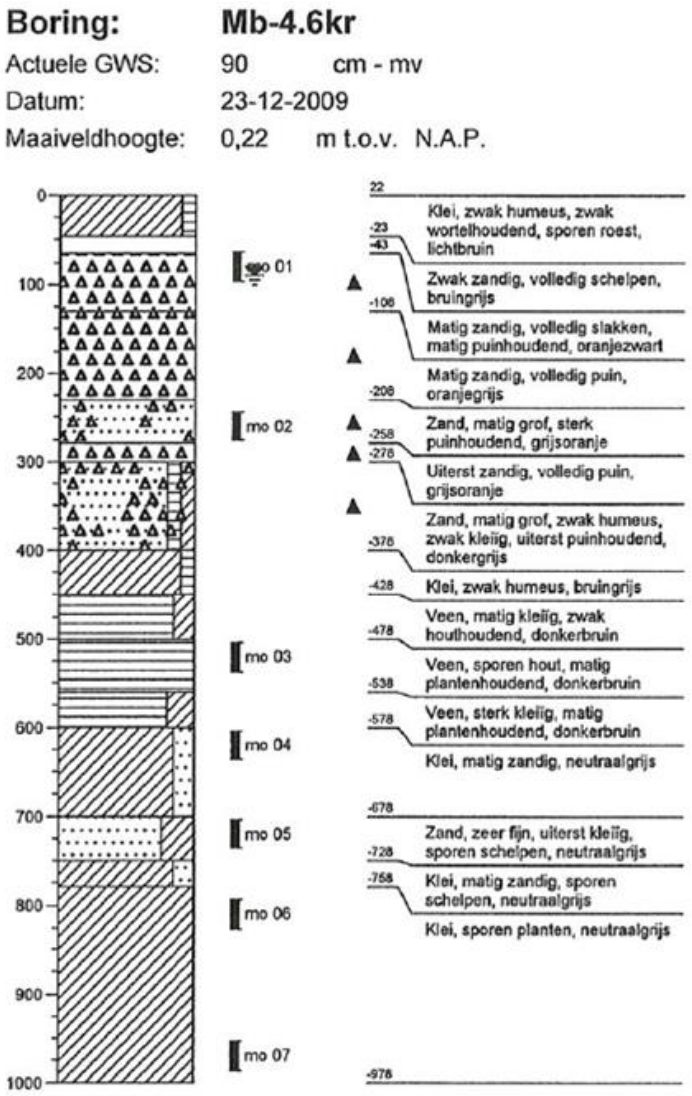

Source: (RPS BCC B.V. & Witteveen + Bos, 2010)

E.3 Soil borings Delfland location 25

Soil borings taken at the research location
These soil borings were taken at the locations of the monitoring wells. The initial positions of the filters of the monitoring wells also are displayed. The depths are indicated with respect to the ground surface. The elevation of the ground surface for the three locations is as follows:

Crest: NAP +0,006 m
Slope: NAP -1,79 m
Toe: NAP -2,65 m

Crest **Slope** **Toe**

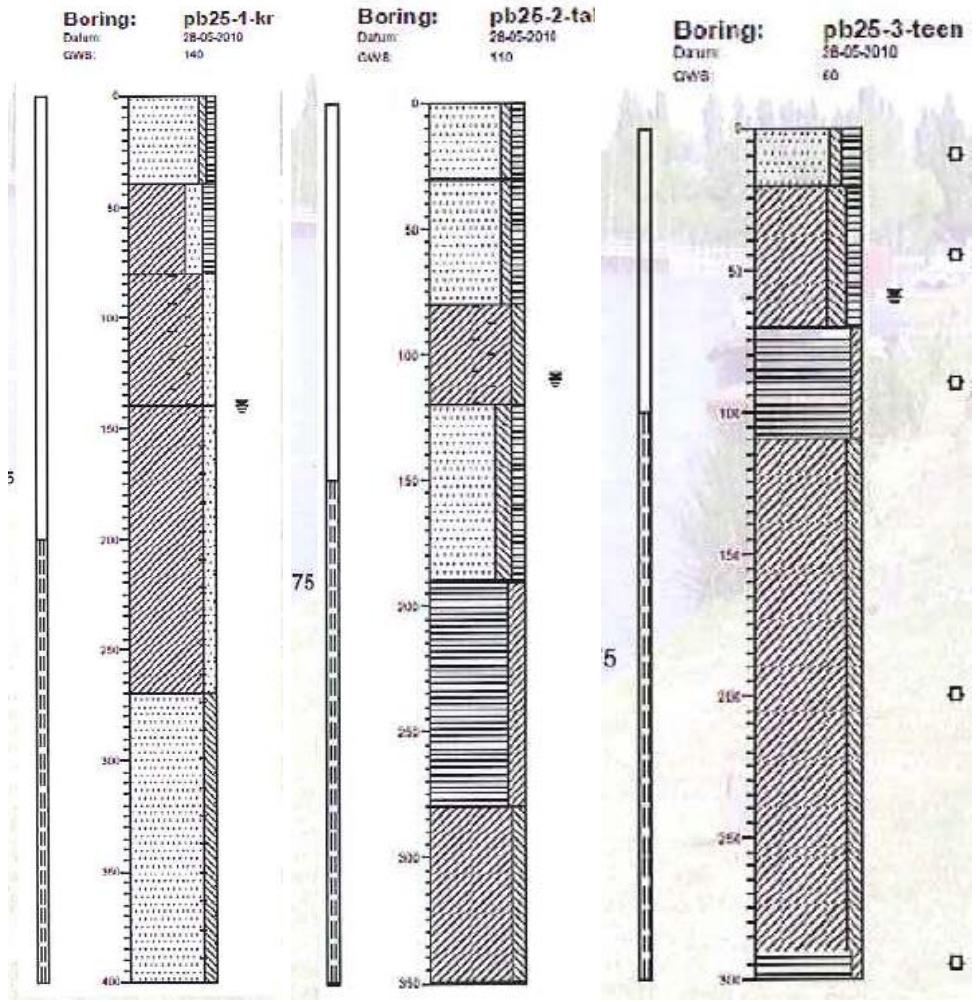

Source: (Delfland, 2010)

Subsoil

The available soil borings only reach to a depth of about 5 m below the ground surface. To determine the composition of the deeper soil layers two soil borings from the DINOloket (TNO Geologische Dienst Nederland, 2018) were used, which are displayed below.

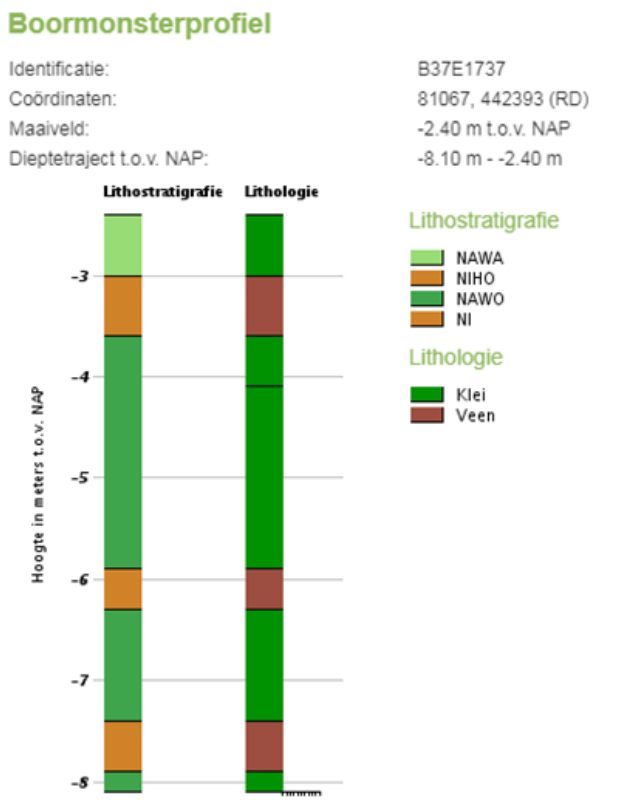

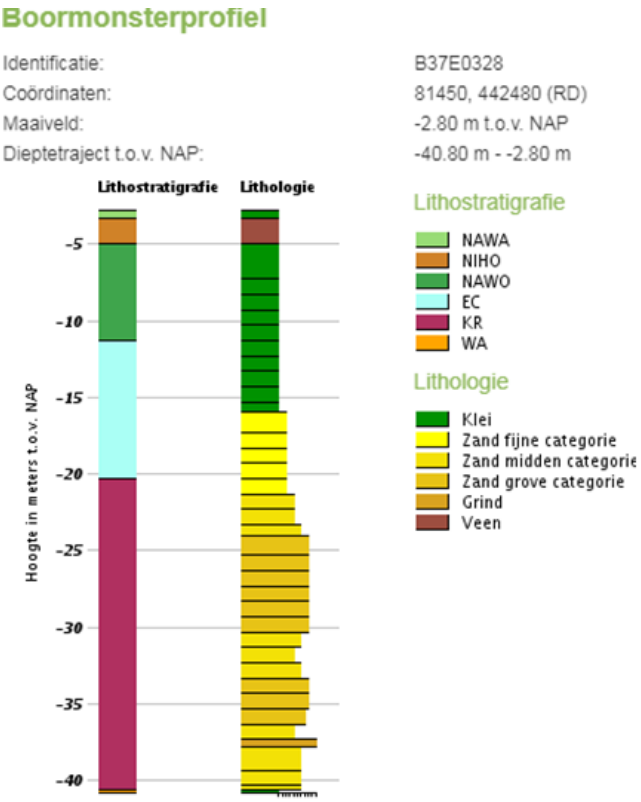

E.4 Soil borings Hogedijk

Soil borings taken at the research location
These soil borings were taken at the locations of the monitoring wells. The depths are displayed with respect to NAP. The borings (and monitoring wells) are numbered 1 to 4 from the crest towards the toe.

Boring 1

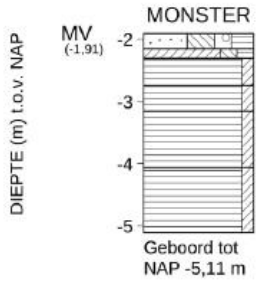

DIEPTE NAP [m]

LAAG	VAN	TOT	BESCHRIJVING
1	-1,91	-2,16	zand, uiterst siltig, matig grindig, sterk humeus Teeltlaag (bruin/grijzig) met puin van wegcunet
2	-2,16	-2,31	klei, matig siltig, matig humeus donker bruin met matige grove zandfractie
3	-2,31	-2,74	veen, zwak kleiig donkerbruin/zwart (veraard)
4	-2,74	-3,16	veen, zwak kleiig donkerbruin, matige rietresten zeer siltig
5	-3,16	-4,06	veen, zwak kleiig donkerbruin, enkele houtresten, siltig
6	-4,06	-5,11	veen, zwak kleiig bruin, met grove houtresten

Boring 2

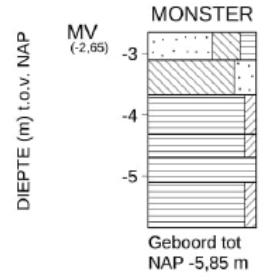

DIEPTE NAP [m]

LAAG	VAN	TOT	BESCHRIJVING
1	-2,65	-3,10	zand, uiterst siltig, matig humeus bruinig, met enkele puin en glas resten
2	-3,10	-3,68	leem, sterk zandig met enkele wortel resten (droogte scheur tot -70 cm)
3	-3,68	-4,32	veen, zwak kleiig donkerbruin, siltig met veel houtresten
4	-4,32	-4,70	veen, zwak kleiig lichtbruin, zeer siltig, gedomineerd door houtresten
5	-4,70	-5,11	veen, mineraalarm bruin, siltig, gedomineerd door rietresten
6	-5,11	-5,85	veen, zwak kleiig bruin, met rietresten

Boring 3

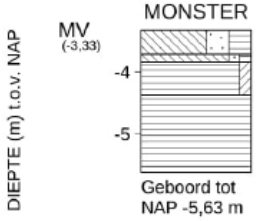

DIEPTE NAP [m]

LAAG	VAN	TOT	BESCHRIJVING
1	-3,33	-3,72	leem, sterk zandig, sterk humeus grijs/bruin (Teeltlaag)
2	-3,72	-3,85	leem, zwak zandig, zwak humeus
3	-3,85	-4,38	veen, zwak kleiig veel houtresten
4	-4,38	-5,63	veen, mineraalarm met riet en houtresten

Boring 4

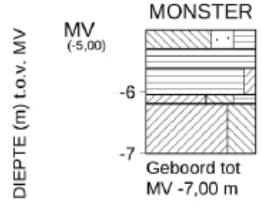

DIEPTE MV [m]

LAAG	VAN	TOT	BESCHRIJVING
1	-5,00	-5,30	leem, sterk zandig, sterk humeus bruin/grijzig (teeltlaag)
2	-5,30	-5,62	veen, mineraalarm donkerbruin met houtresten
3	-5,62	-6,05	veen, zwak kleiig lichtbruin, veel rietresten
4	-6,05	-6,20	klei, uiterst siltig, sterk humeus gemengd met veen, overvang naar klei
5	-6,20	-7,00	klei, uiterst siltig licht grijs, zeer slap

Source: (Nectaerra, 2018)

Other soil borings

About 50 m to the south two soil borings and a cone penetration test were conducted as a part of the reinforcement project of the Hogedijk.

Soil borings

BORING : HB10

Datum	: 28-06-2018	X	: 109893.520	Boormethode	: Hand
GWS	: NAP -3.97 m	Y	: 462471.170	Boormeester	: GD
Maaiveld	: NAP -2.47 m			Beschrijver	: GD
Opmerking	: Definitieve boorstaat.			MOS ref.nr.	: HB10

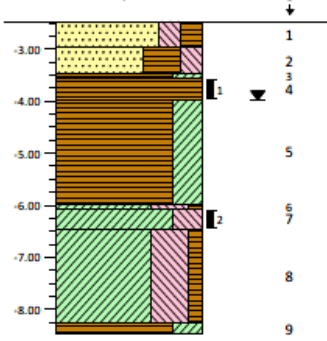

Laag nr.	Diepte [m t.o.v. NAP] van	tot	Omschrijving grondlaag gras	Kleur
1	-2.47	-2.97	Zand, zeer grof, matig siltig, matig humeus	neutraalbruin
2	-2.97	-3.47	Zand, matig fijn, uiterst humeus, matig siltig	donkerbruin
3	-3.47	-3.57	Veen, sterk kleiig, sterk houthoudend, matig plantenhoudend	neutraalbruin
4	-3.57	-3.97	Monster nr. 1	bruin
5	-3.97	-5.97	Veen, sterk kleiig, sterk houthoudend, matig plantenhoudend	neutraalbruin
6	-5.97	-6.07	Klei, uiterst siltig, zwak humeus	neutraalgrijs
7	-6.07	-6.45	Monster nr. 2	grijs
8	-6.45	-8.27	Klei, uiterst siltig, zwak humeus	neutraalgrijs
9	-8.27	-8.47	Veen, sterk kleiig, sterk houthoudend	neutraalbruin

BORING : HB110

Datum	: 28-06-2018	X	: 109906.680	Boormethode	: Hand
GWS	: NAP -4.69 m	Y	: 462472.680	Boormeester	: GD
Maaiveld	: NAP -3.99 m			Beschrijver	: GD
Opmerking	: Definitieve boorstaat.			MOS ref.nr.	: HB110

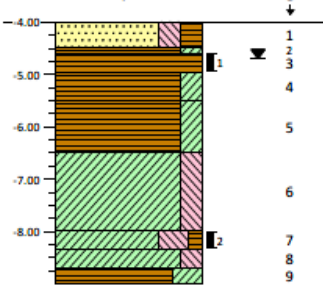

Laag nr.	Diepte [m t.o.v. NAP] van	tot	Omschrijving grondlaag gras	Kleur
1	-3.99	-4.49	Zand, matig fijn, matig siltig, matig humeus	donker
2	-4.49	-4.59	Veen, mineraalarm, matig kleiig, matig houthoudend, zwak plantenhoudend	neutraalbruin
3	-4.59	-4.96	Monster nr. 1	bruin
4	-4.96	-5.49	Veen, mineraalarm, matig kleiig, matig houthoudend, zwak plantenhoudend	neutraalbruin
5	-5.49	-6.49	Veen, mineraalarm, matig kleiig, matig houthoudend, zwak plantenhoudend	neutraalbruin
6	-6.49	-7.99	Klei, matig siltig	neutraalgrijs
7	-7.99	-8.34	Monster nr. 2	grijs
8	-8.34	-8.69	Klei, matig siltig	neutraalgrijs
9	-8.69	-8.99	Veen, sterk kleiig, matig houthoudend, zwak plantenhoudend	neutraalbruin

Cone penetration test

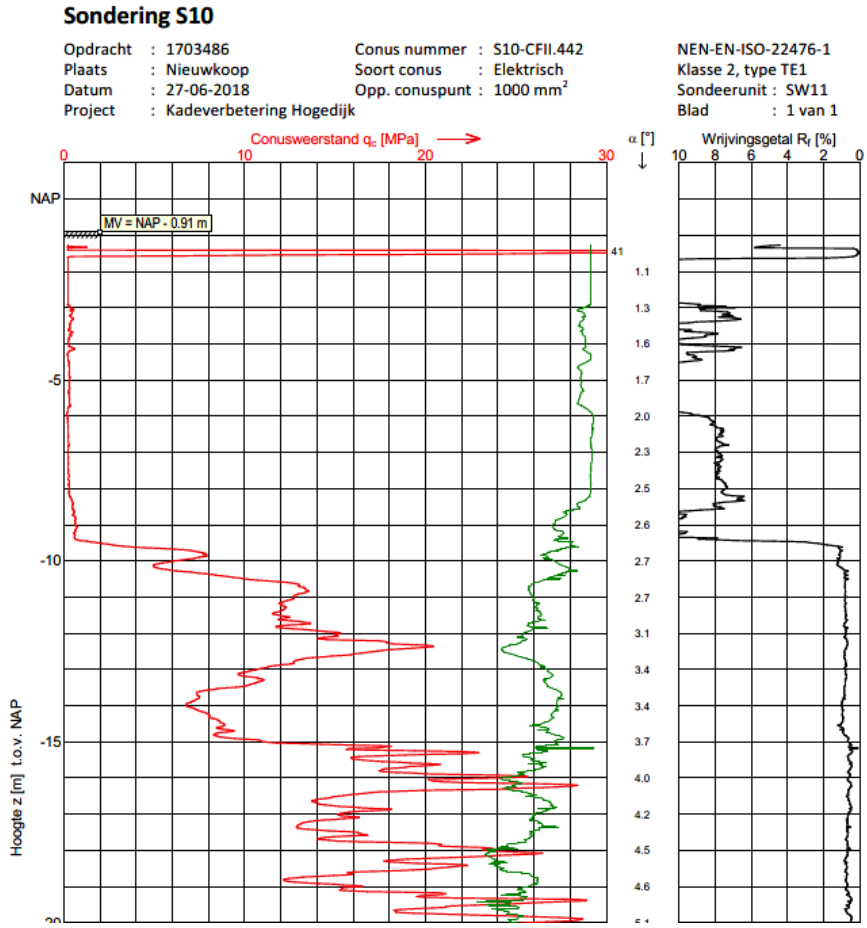

E.5 Conductivity measurements Nectaerra

Measured conductivity values Rijnland (Nectaerra, 2018)

The conductivity measured were performed at several depths and using several methods. The measurements for which a depth is specified in Table E.1 were carried out using either Amoozemeter or double-ring infiltration test. The double-ring test is used to measure the infiltration of the soil, and is therefore only used for the top 10 cm of the soil. The amoozemeter test were used up to a depth of about 70 cm. The remaining measurements were performed using Slug tests. In this test the water level in a monitoring well is temporarily raised or lowered. Then the time it takes to return to the initial water level is measured, and with this information the hydraulic conductivity around the well can be calculated. It can be observed that the measurements close the ground surface show a large conductivity, which is probably the result of the soil structure. The measurements using the Slug test were all taken in peat, and show a variation of about two orders of magnitude.

Table E.1: Conductivity measurements Nectaerra

Location	Location in dike profile	Depth	Soil type	Conductivity (m/day)
HGD-1-1	Crest	Monitoring well	Peat	0.004
HGD-1-2	Slope	Monitoring well	Peat	0.01
HGD-1-3	Slope	Monitoring well	Peat	0.005
HGD-1-4	Toe	Monitoring well	Peat	0.04
HGD-2-1	Crest	Monitoring well	Peat	0.001
HGD-2-2	Slope	Monitoring well	Peat	0.082
HGD-2-3	Slope	Monitoring well	Peat	0.022
HGD-2-4	Toe	Monitoring well	Peat	0.064
SKP-1-1	Crest	Monitoring well	Peat	0.0004
SKP-2-1	Slope	Monitoring well	Peat	0.0007
SKP-3-1	Toe	Monitoring well	Peat	0.0002
VEE-2-1	Crest	0 - 0.1	Sandy clay	8.64
VEE-2-2	Slope	0 - 0.1	Sandy clay	9
VEE-2-3	Toe	0 - 0.1	Sandy clay	11.52
VBK-2-1.5	Slope	0 - 0.1	Sandy clay	22.8
VBK-2-3	Slope	0 - 0.1	Sandy clay	31.2
VEE-2-1	Crest	0.26 - 0.46	Sandy clay	0.48
VEE-2-2	Slope	0.23 - 0.71	Sandy clay	0.22
VBK-2-4	Toe	0.2 - 0.4	Sandy clay	0.36
VEE-1-1	Crest	0.25 - 0.54	Silty clay	3.84
VEE-2-3	Toe	0.19 - 0.48	Organic clay	0.02
VBK-2-3	Slope	0.1 - 0.3	Sandy loam	3
VEE-1-1	Crest	0 - 0.1	Silty sand	1.25

E.6 Stress tables stability analysis

Three types of clay are present: anthropogenic clay (AP), Duinkerke clay (DK), and Calais clay (CA). Sand is present as anthropogenic sand and Duinkerke sand. A single type of peat is used, which is Hollandveen (HV). All the soil types are subdivided by location in the dike profile. Below the dike is indicated as 'o', and adjacent to the dike as 'n'. In the stress tables the effective stress is indicated as sigma (σ), the shear stress as tau (τ). For the clay types, the same stress tables are used multiple soil types with different volumetric weights. For example DK klei h1 and DK klei h2 use the same stress table, but have a different volumetric weight.

These values are taken from a stability calculation provided by Delfland.

Table E.2: Stress tables for clay (klei). All values are in kN/m^2.

AP Klei (o)		AP Klei (n)		DK Klei (o)		DK Klei (n)		CA Klei (o)	
σ	τ	σ	τ	σ	τ	σ	τ	σ	τ
0	1,12	0	1,03	0	1,03	0	1,95	0	0,95
12	6,6	15,56	7,89	15,56	7,89	14,39	6,96	13,71	6,75
24	12,08	25,6	12,32	25,6	12,32	21,93	9,58	21,66	10,11
36	17,34	35,64	16,41	35,64	16,41	29,47	12,99	29,61	12,34
48	21,83	45,68	20,47	45,68	20,47	37	15,33	37,56	14,57
60	25,65	55,72	24,53	55,72	24,53	44,54	17,94	45,51	16,61
72	31,37	65,76	27,83	65,76	27,83	52,08	19,24	53,46	19,56
84	35,42	75,8	30,96	75,8	30,96	59,62	20,97	61,41	21,02
96	39,91	85,84	33,76	85,84	33,76	67,16	22,25	69,36	23,33
108	42,11	95,88	34,92	95,88	34,92			77,31	24.14

Table E.3: Stress tables for sand (zand) and peat (veen). All values are in kN/m2.

AP Zand (o)		DK Zand		HV Veen (o)		HV Veen (n)	
σ	τ	σ	τ	σ	τ	σ	τ
0	0	0	0,12	0	0	0	0
7,69	3,33	18,77	8,52	9,18	5,62	7,38	3,87
15,39	7,71	25,65	11,59	13,77	8,44	11,06	5,87
23,08	10,99	32,52	14,55	18,36	10,85	14,75	7,72
30,77	14,41	39,39	17,12	22,95	12,49	18,44	9,42
38,46	17,41	46,26	19,44	27,54	14,9	22,13	11,31
46,15	19,86	53,14	21,51	32,13	15,59	25,81	13,24
53,85	22,76	60,01	23,93				
61,54	27,48	66,88	25,26				
69,23	29,4	73,76	27,85				

Table_Apx E.4: Volumetric weight of the soil type used in the stability calculation

Soil type	Volumetric weight dry (kN/m^3)	Volumetric weight wet (kN/m^3)
AP Klei h2 (o)	14,10	14,10
AP Klei h1 (n)	16,20	16,20
DK Klei h1 (o)	16,20	16,20
DK Klei h2 (o)	14,10	14,10
DK Klei h1 (n)	16,20	16,20
CA Klei h1 (o)	14,90	14,90
AP Zand (o)	18,00	20,00
DK Zand	18,00	18,30
HV Veen (o)	10,00	10,50
HV Veen (n)	10,00	10,50

F Calibration of the models

This appendix describes the calibration of the models in more detail.

F.1 Initial values

As a starting point for the calibration process, assumptions were made for the conductivity of the different soil types. For this the Staring set was used. Based on the composition of the soils found in the borings a Staring type was assumed. The motivation for these chosen types is discussed for each research case.

F.1.1 Delfland location 25

From the soil borings in appendix E a schematisation of the cross-section was constructed, which is displayed in Figure F.1. In the soil borings the fractions of the different present soil types are also indicated. Based on this information a soil type from the Staring set is chosen for each model layer. The upper sand layer contains loam and peat fractions according to the soil borings, and based on this Staring type B2 is chosen. Because the layer is on the surface, a top soil type is chosen. The clay core of the dike is also considered to be close enough to the surface to be a top soil type. For this layer B11 is chosen, which has an average permeability for clay. Layer 3, the intermediate sand layer, contains more loam than the top sand layer and is located deeper. For this reason the subsoil type O3 is assigned. The peat of layer 4 contains some clay, but no subsoil peat types containing clay are included in the Staring set. Instead the top soil type B18 is used. Since only the conductivity is used and not the unsaturated parameters, use of a topsoil type for deeper layers is unlikely to lead to problems. Layer 5 is a clay layer containing loam. For this reason the medium heavy clay subsoil type O12 is chosen.

For the layers 6 to 10 only the soil type is known, without any indication of fractions of different soil types. Because no other information is available, the same Staring set types are used as for the higher layers. The chosen soil types and motivation for the simulation are displayed in Table F.1. These soil types will be adjusted later during the calibration of the model.

Table F.1: Assigned Staring soil types location 25 for each layer

Layer	Soil type	Staring set number	Conductivity (m/day)
1	Sand	B2	0,1252
2	Clay core	B11	0,0453
3	Intermediate sand layer	O3	0,1087
4	Peat	B18	0,0667
5	Clay	O12	0,0102
6	Peat	B18	0,0667
7	Clay	O12	0,0102
8	Peat	B18	0,0667
9	Clay	O12	0,0102
10	Pleistocene sand layer	O1	0,1522

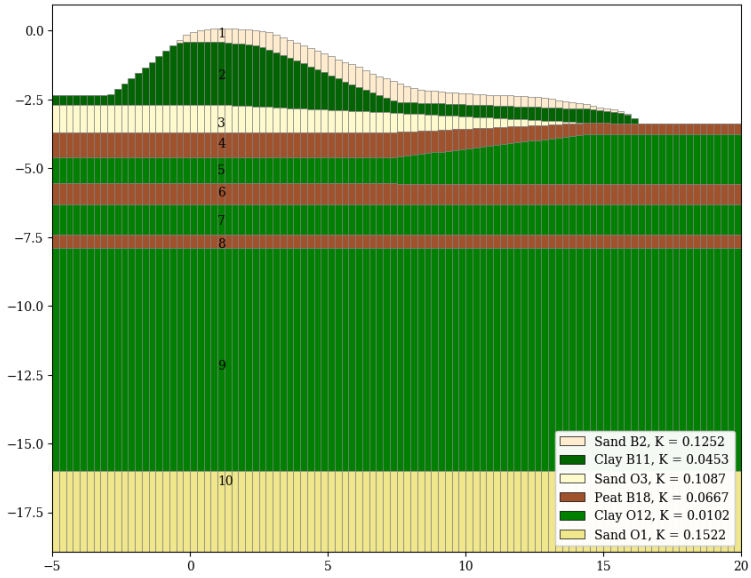

Figure F.1: Schematisation location 25

Soil scenarios

The soil schematisation is based on soil borings in the crest, slope and toe of the dike. Between these borings the layers separations are interpolated linearly. In reality the soil composition could differ from this schematisation. There is no way to determine this, and therefore soil scenarios were constructed to assess the effect of variations on the model. Eight soil composition scenarios were set up. Six of these scenarios are based on different interpretations of the soil borings. In the scenarios the same Staring soil types were used as in the basis schematisation.

The following scenarios were constructed:

- Scenario 1: The constructed soil schematisation as described in this paragraph. This scenario is used as a basis for the other scenarios. The layers between the borings were linearly interpolated, and from the leftmost and rightmost borings to the model edges the layers are assumed to be horizontal.
- Scenario 2: The intermediate sand layer is placed in direct contact to the outside water.
- Scenario 3: In scenario 1 the legger depth of the boezem was used for the bottom elevation of the outside water. In scenario 3 the minimum depth is used instead.
- Scenario 4: In the soil boring located at the toe the intermediate sand layer cannot be observed. In scenario 1 the thickness of this sand layer is assumed to linearly decrease between the slope and toe, meaning the sand layer ends at the toe. However, the sand layer could end anywhere between the two borings. In scenario 4 the sand layer is assumed to end at about a third of the distance between the slope and the crest.
- Scenario 5: Left of the soil boring in the crest the intermediate sand layer is assumed to continue with the same thickness towards the edge of the model, because it is unknown where the layer ends. In scenario 5 it is assumed that the sand layer ends below the outer toe of the dike.
- Scenario 6: The first peat layer is observed in the soil borings at the slope and the toe, but since the soil boring at the crest ends in the intermediate sand layer the soil composition below the sand layer is unknown. In scenario 1 it is assumed that the peat layer has the same thickness below the crest as below the slope and continues with this thickness towards the model edge. Scenario 6 assumes this peat layer ends at the soil boring in the crest.
- Scenario 7: From preliminary runs of the model it became clear that the simulated phreatic surface was too high at the slope and the toe. It appeared that a possible reason for this was a too limited flow of the groundwater towards the inside water. In an attempt

to increase this, the peat layer below the inside water was given a greater thickness in scenario 7. This scenario contradicts the soil boring at the toe.

- Scenario 8: In this scenario the intermediate sand layer is removed, in order to assess the influence of this layer.

The drawings of these scenarios are included in paragraph F.3.1. During the calibration each of these scenarios is tested, and based on this the most likely scenario will be chosen for use in further analyses.

F.1.2 Delfland location 24

In Figure F.2 the constructed schematisation for location 24 is displayed. Several vertical layer separations are used in this schematisation, which was necessary to prevent vertical staggering of the model grid.

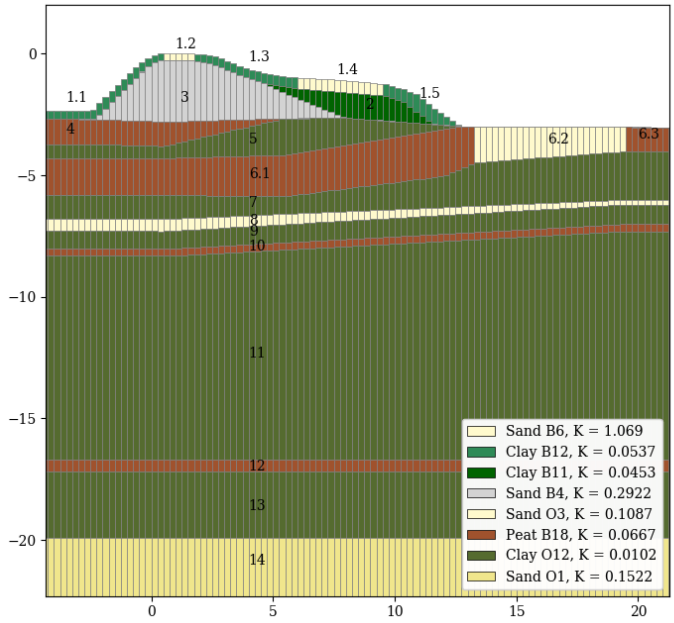

Figure F.2: Schematisation location 24

The top layer was cut in 5 parts, to model the cunets of the paths on the crest and the berm. For the clay parts of this top layer Staring soil type B12 is chosen as an initial estimate, because it has the largest permeability of the top soil types. The clay is the top soil and is therefore likely to exhibit a soil structure, increasing the permeability. For the sand of the cunets Staring type B6 is used.

One of the main problems in the schematisation is the core of the dike. At some point in the past the dike was reinforced with rubble. This rubble is mixed with clay and sand, making it is difficult to define the boundaries of the rubble layer. It can be identified in the soil borings in the crest and in the slope. In the soil boring performed near the monitoring well in the crest, the rubble is indicated as loamy sand, extending to a depth of 2,5 m below the surface (Delfland, 2010). Several meters removed from this location another soil boring was performed in the crest. This soil boring shows a rubble layer up to a depth of 4 m (Inpijn-Blokpoel, 2010). Apparently the core of the dike is very inhomogeneous, containing rubble, sand , loam and clay. Because of this it is difficult to assign a Staring soil type to the layer. Rubble by itself has a large conductivity, but the conductivity is likely to be reduced due to the mixing with sand and clay. Staring type B4 is used as an initial estimate, which corresponds to loamy sand.

The layer below the rubble core is subject to large uncertainties. The boring at the research location shows a peat layer starting 2,5 m below the surface, but the other boring several meters removed shows that the rubble extends to a depth of 4 m. Initially, it was assumed that the peat

layer below the rubble is the same layer as the peat layer found in the boring in the slope. This would mean that the peat layer is located higher below the dike than it is next to the dike. This is contrary to what would be expected: normally soil layers below the dike are located deeper due to settlement. A second possibility is that the peat layer below the rubble is a separate, extra peat layer. Whether this is truly the case cannot be verified, since the boring depth at the research location is limited and does not show any deeper layers. For the initial schematisation the choice is made to use the second option and model the peat as a separate layer. This separate layer also extends below the outside water. For this layer the same peat type as for location 25 is chosen, which is Staring B18.

Layer 2, the core of the berm, has an angled boundary with the rubble. The angle of this boundary is considered gentle enough to model the soils as separate model layers. Staring type B11 is used for this layer, since it is relatively close to the surface. This type has a slightly lower conductivity than type B12 which was used for the top layer.

The clay layer 5 and the peat layer 6 are probably similar to the layers found at location 25; therefore respectively Staring types O12 and B18 are chosen for these layers.

Layer 6 includes a section in which the peat is replaced by sand. This sand part (layer 6.2) intends to model the sand fill of the former drainage ditch. The soil boring for the monitoring well at the toe indicates that this sand fill has a thickness of more than a meter, which is much more than the former depth of the ditch. This means that the peat below the ditch has settled due the weight of the sand fill. Again, the edges of this sand fill should be sloped, but to prevent vertical staggering the separation is modelled vertically.

For the remaining soil layers the soil borings and cone penetration test taken from a soil survey (Inpijn-Blokpoel, 2010) are used. For the deeper layers the same soil types as for location 25 are used. The chosen soil types and their conductivities are displayed in Table F.2.

Table F.2: Assigned Staring soil types location 25 for each layer

Layer	Soil type	Staring set number	Conductivity (m/day)
1.1	Clay	B12	0,0537
1.2	Sand	B6	1,069
1.3	Clay	B12	0,0537
1.4	Sand	B6	1,069
1.5	Clay	B12	0,0537
2	Clay	B11	0,0453
3	Rubble	B4	0,2922
4	Peat	B18	0,0667
5	Clay	O12	0,0102
6.1	Peat	B18	0,0667
6.2	Sand fill of drainage ditch	O3	0,1087
6.3	Peat hinterland	B18	0,0667
7	Clay	O12	0,0102
8	Intermediate sand layer	O3	0,1087
9	Clay	O12	0,0102
10	Peat	B18	0,0667
11	Clay	O12	0,0102
12	Peat	B18	0,0667
13	Clay	O12	0,0102
14	Pleistocene sand layer	O1	0,1522

Soil scenarios
Similar to location 25, a number of soil scenarios was constructed for location 24. In the scenarios for which new layers were added to the basis schematisation, the same Staring soil types were used as in the basis schematisation.

- Scenario 1: The basis schematisation as displayed in figure 5.1.
- Scenario 2: As described earlier, there are some uncertainties regarding peat layer 4. In scenario 2 this peat layer is removed and instead the rubble core is extended to a greater depth, which corresponds to the soil boring several meters removed from the research location. The peat below the water is replaced by clay.
- Scenario 3: In soil borings close to location a second intermediate sand layer can be observed. This sand layer does not show up in the borings at location 24, but it may have an effect on the research cross-section. Since the model is set-up in two dimensions this cannot be modelled. Instead a scenario including the second sand layer is added.
- Scenario 4: Apart from soil borings, stability calculations of the dike were provided by Delfland. In the schematisations for these calculations the clay cover of the rubble core is only included on the crest. Because it was considered unlikely that the rubble directly borders the outside water the clay cover was extended on the outer slope in the basis schematisation. To analyse the effect of this choice scenario 4 was added, in which the clay cover on the outer slope is removed.
- Scenario 5: Clay layer 4 slowly pinches out towards the toe in the basis schematisation. In the mentioned schematisation provided by Delfland the clay layer ends below the berm. This different schematisation is included in scenario 5.
- Scenario 6: In the basis schematisation the layers 1, 2, and 4 all pinch out towards the toe of the dike. This could lead to inaccuracies near the toe. To analyse whether this is the case, a scenario is added in which clay layer 4 ends in a vertical separation with the sand fill of the drainage ditch. Because this sand fill now borders two layers, the sand fill layer and the peat layer behind it had to be split in two parts.

Drawings of these scenarios are included in paragraph F.3.2.

F.1.3 Hogedijk
The modelling of the Hogedijk is approached in a different way than the other two research cases. Not only are measurements of the conductivity available, the composition of the soil is less ambiguous than for the other two locations. Therefore no soil scenarios are constructed. The constructed soil schematisation is displayed in Figure F.3.

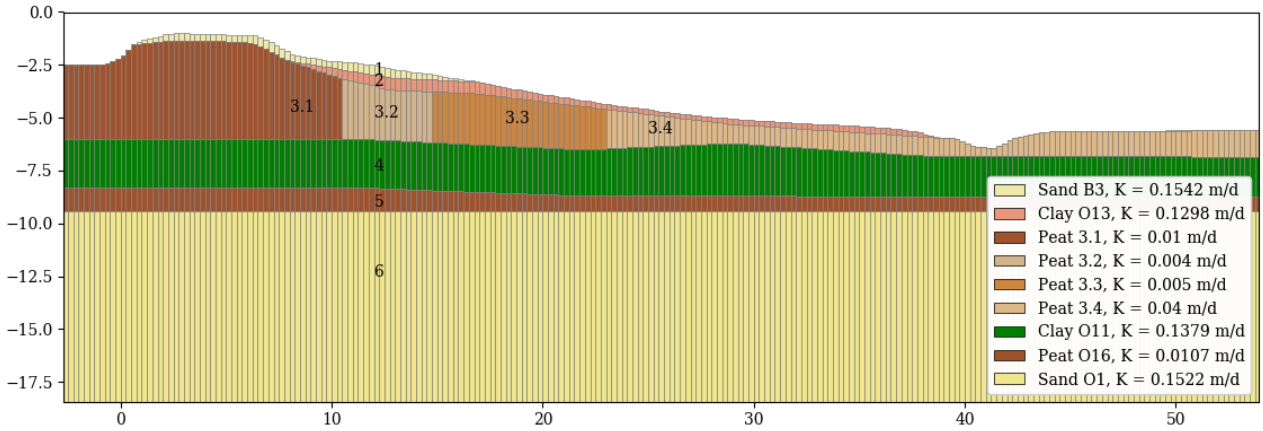

Figure F.3: Soil schematisation Hogedijk

Layer 3, the peat layer, is divided into four parts in order to apply the measured conductivities. For the other layers no measurements are available, and therefore Staring types used again to

make an estimate. According to the soil borings, the sand top layer is moderately silty, and coarse to moderately fine. Staring type B3 fits best to this description. Below the sand and at the surface from halfway on the slope to the toe onwards a sandy loam layer is present. This corresponds best to Staring type B13. For the peat layer the field measurements are used. For the silty clay layer below the peat Staring type O11 is chosen, which is light clay. Below the clay is another peat layer, which is rich in clay. Staring type O16 is assigned to this layer. For the Pleistocene sand layer type O1 is used, which is the same as for the research cases in Delfland.

The assigned conductivities are summarised in Table F.3.

Table F.3: Assigned conductivity values for each soil layer Hogedijk

Layer	Soil type	Staring set number	Conductivity (m/day)
1	Sand	B3	0,1542
2	Loam	B13	0,1298
3.1	Peat	(Measured)	0,004
3.2	Peat	(Measured)	0,01
3.3	Peat	(Measured)	0,005
3.4	Peat	(Measured)	0,04
4	Clay	O11	0,1379
5	Peat	O16	0,0107
6	Pleistocene sand layer	O1	0,1522

F.2 Calibration

The calibration process was performed in two steps: first the models were calibrated using a steady-state simulation to match the average position of the phreatic surface, and then the models were calibrated in a transient simulation to calibrate the response to precipitation and evapotranspiration.

F.2.1 Delfland location 25

Using the initially assumed soil composition and a steady state calculation was performed, for which the resulting heads are displayed in Figure F.4. The heads are calculated for each cell. To visualise this , the heads are displayed as a line for each model layer. To avoid clutter, only the heads in the topmost five layers are plotted. The monitoring wells are displayed as well, with the filter represented by a lighter colour. Furthermore the average head of the measurements is indicated by a white bar for each monitoring well. The average of the monitoring well in the intermediate sand layer is displayed as a yellow bar to the left of the monitoring well in the crest.

When comparing the heads to the average of the measurements it becomes clear that the calculated head near the crest correspond quite well to the measurements, but the heads near the slope and the toe deviate considerably. At these points the phreatic surface is so high that it exits at the slope, meaning seepage occurs. In the deeper layers the head is even higher than the ground surface.

Several attempts have been made to calibrate the model using this soil composition, but no set of hydraulic conductivities could be found for which the model matched all three measurement points. The cause of this lies with the subsoil, especially the topmost peat layer and the clay layer below it. As is visible in Figure F.4, the head in these layers varies linearly from a high level below the outside water to a lower level below the inside water. The monitoring wells at the toe and slope are placed in these layers, and show that the heads at those points are close to the inside water level. This means the linear variation as shown in the model is not correct. Changing the conductivity of these layers has no influence on the heads: the heads at the boundaries of the layers are constant, and therefore the conductivity has no influence on the variation of the heads

over the width of the layer; it only influences the flow rate through the layer. Therefore it must be concluded that the conductivity of these layers varies along the width of the dike.

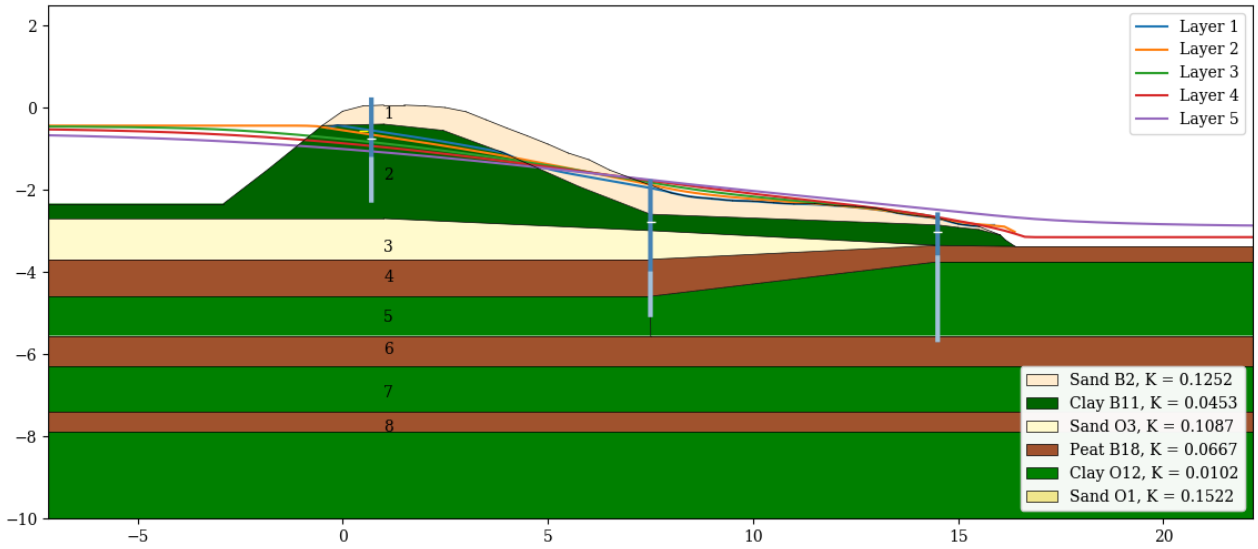

Figure F.4: Steady-state results location 25

A physical explanation for this could be that in the subsoil below the dike settlement has taken place due to the weight. The settled soil below the dike is more compacted than adjacent to the dike, meaning the conductivity is lower.

To include this difference in conductivity, layers 4 and 5 are divided in two parts, with the separation near the monitoring well in the slope. For the peat below the dike Staring type O17 is applied, and for the clay below the dike Staring type O12 is used, which is the same as the initially assumed type. The clay adjacent to the dike is changed to Staring type O11. These soil types are chosen such that the conductivity below the dike is lower than adjacent to the dike.

Using this updated schematisation another steady-state simulation was performed. The results are shown in Figure F.5. The differences compared to the first simulation are not directly obvious. Upon closer inspection it can be seen that the heads show a kink at the slope, resulting in lower heads. There is still some deviation from the measurements, but it is expected that this can be solved by tweaking the conductivities below the dike and the berm.

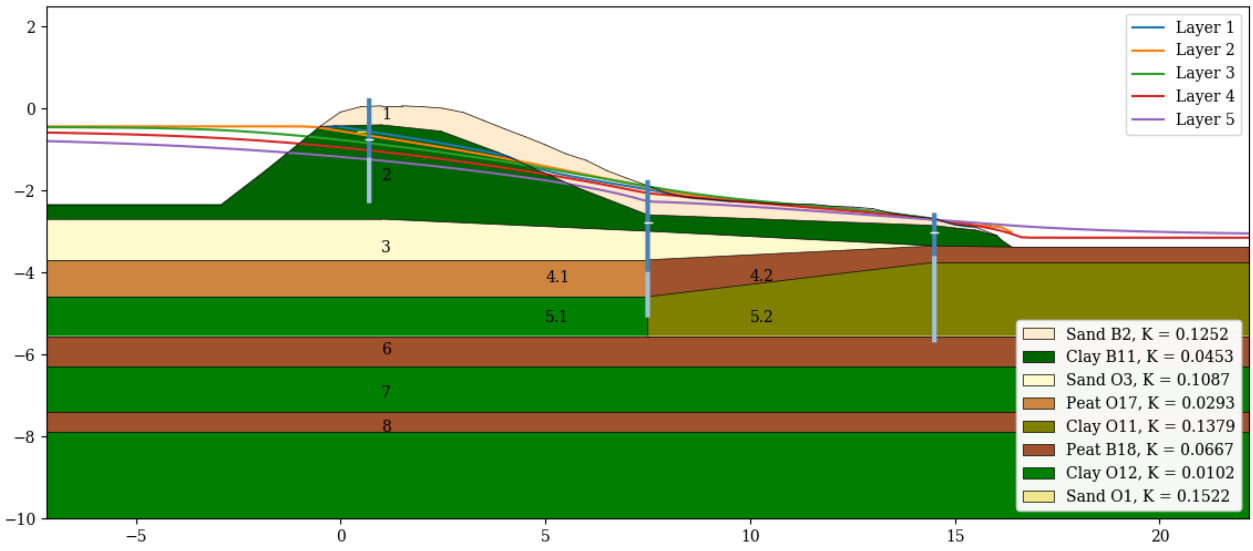

Figure F.5: Steady-state results location 25 after splitting the subsoil layers

Calibration steady state

Earlier, several soil scenarios have been set up. These scenarios initially did not contain the layer separation of layers 4 and 5, and were therefore altered to include this separation. A steady state calculation was performed for each scenario, and the difference between the calculated and the average of the measured heads was taken to compare the scenarios.

From this analysis it was observed that the difference between model and measurements is quite large at the slope and the toe for all scenarios. This indicates that the conductivities of the subsoil layers have to be adjusted. The difference between the different scenarios was small. At the slope and at the toe the simulated heads are close to or on the ground surface, which means seepage occurs. These heads therefore cannot rise higher than a certain height that is reached for all scenarios. Since the heads are too high for all scenarios, a good comparison between the scenarios is not possible for the used set of conductivities.

Since no optimum scenario could be identified, the model was calibrated for scenario 1. The conductivities in the various layers were variated until an optimum was found. This was done for each layer individually, which means this optimum does not necessarily yield the best possible result for the entire model. Therefore the process was repeated several times: after a conductivity was adjusted, the other layers were variated again. It was not possible to exactly fit the model to the average of all of the measurements simultaneously. Therefore values were chosen such that on average the difference was minimised. Using these values, the different scenarios were analysed again. In Figure F.6 the difference between the model results and the measurements are displayed for each scenario.

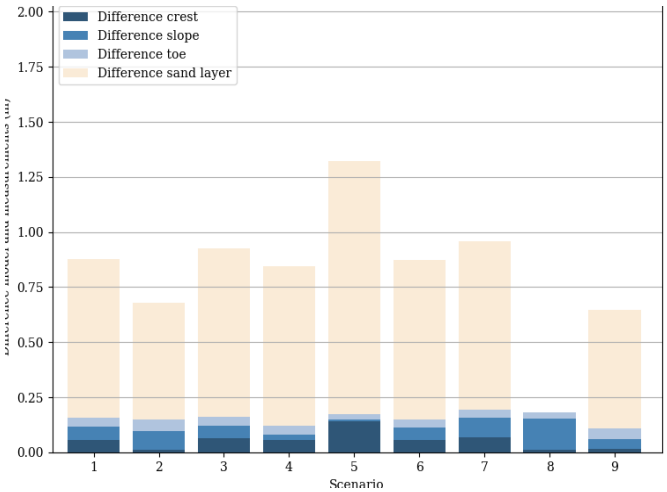

Figure F.6: Differences between model results and measurements using calibrated conductivities

The differences between the scenarios have become larger. The large differences for the intermediate sand layer stand out. However, it should be noted that the monitoring well in this layer was not specifically set up to measure the head in the sand layer; the filter also extended into the clay core of the dike. In the model, the heads in the clay core are higher than in the sand layer, which means that if the model is correct, the monitoring well would indicate the head in the clay core rather than the head in the sand layer. It is therefore best to base the choice for a scenario on the three other measurements.

Observing the total differences for each scenario, it appears that the scenarios 2 and 4 yield the best results, but for different reasons: scenario 2 minimises the difference for the crest and the sand layer, while scenario 4 minimises the difference for the slope and toe. Both scenarios involve changes in the intermediate sand layer: scenario 2 directly connects the sand layer to the outside water, while in scenario 4 the sand layer extends less far below the dike. Due to these differences it is expected that a combination of the two scenarios leads to an even better fit of the model. This combined scenario (scenario 9) is also included in Figure F.6. This scenario indeed further

minimises the difference between the model and the measurements. Since scenario 9 does not contradict the available soil information, this scenario will be used for further analyses.

The conductivity values have been calibrated for scenario 1, which means that these values are not necessarily the best values for scenario 9 as well. Therefore the model was calibrated again. For most of the layers no better values could be found than those from the first calibration, except for the clay core for which a conductivity of 0,02 m/day yielded the best results. Since the deviation for the three relevant monitoring wells is less than 10 cm no further calibration will be done for the steady-state simulation. The calibrated conductivity values, along with the initially assumed conductivities based on the Staring set, are displayed in Table F.4.

Table F.4: Original and calibrated conductivities Delfland location 25

Layer	Soil type	Initially assumed conductivity (m/day)	Conductivity after calibration (m/day)	Anisotropy ratio after calibration
1	Sand	0,1252	0,5	0,66
2	Clay	0,0453	0,02	2
3	Sand	0,1087	0,10	0,66
4.1	Peat dike	0,0293	0,01	0,01
4.2	Peat berm	0,0667	0,80	0,1
5.1	Clay dike	0,0102	0,005	0,33
5.2	Clay berm	0,1379	0,02	0,33
6	Peat	0,0667	0,01	0,1
7	Clay	0,0102	0,01	0,33
8	Peat	0,0667	0,01	0,1
9	Clay	0,0102	0,01	0,33
10	Sand	0,1522	0,15	1

For the deeper layers the difference between the original and calibrated values are relatively small. The main differences are found for layers 2, 4 and 5; the conductivity for layer 2 is much smaller than the assumed value, whereas the conductivity for layers 4 and 5 is an order of magnitude higher. The conductivities for layers 4 and 5 are within the range of the Staring set, but the conductivity of layer 2 is about 10 times smaller than the lowest value for clay in the Staring set (B10). In Figure F.7 the results of a steady state simulation using these values are displayed.

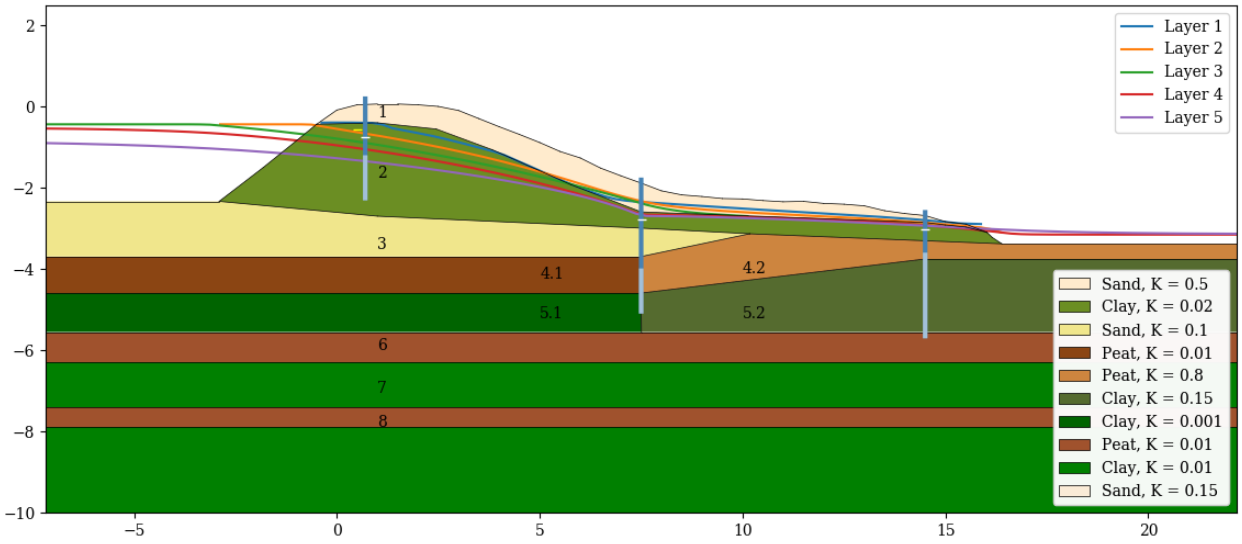

Figure F.7: Delfland location 25, results steady state simulation using calibrated values

Intermediate sand layer

In Figure F.7 it can be seen that the heads make a sharp bend at the division between the soil below the dike and below the berm. The explanation for this is found in the conductivity values. Peat layer 4.2 has a very large conductivity: 80 times larger than part 4.1, which is the same layer, and 8 times larger than the intermediate sand layer. This calibration is therefore not realistic. The conductivities may fall within the range of possibility for the soil types, but the relative values are not realistic. Since the conductivity is the only defining characteristic of a soil type in this model, these conductivities basically imply that layer 3 is peat instead of sand, and that layer 4.2 is a sand layer instead.

Attempts were made to calibrate the model such that the intermediate sand layer has a larger conductivity than the peat layer, but no satisfactory result were obtained. The same was true for the other scenarios, even if the intermediate sand layer was not directly connected to the outside water. The measurement from the middle monitoring well could only be matched when peat layer 4.2 had a larger conductivity than the intermediate sand layer.

There appears to be a contradiction between the soil borings and the measurements. The soil borings show that the sand layer is present below the crest, but not below the toe. On the other hand, the measurements in the slope and the toe are very close, while the difference between the slope and the crest is large. This implies that the conductivity between the toe and slope is large, while the conductivity between the slope and the crest is small. This points towards a sand layer that extends from below the slope towards the polder.

More information regarding this sand layer was found in a report provided by Delfland, regarding a safety assessment of the Duifkade, the flood defence location 25 is on (Tauw, 2009). For the cross-sections along the flood defence, an assessment was made of the locations the sand layer was present. This assessment is displayed in Table F.5. This was based on soil borings different than those executed for the monitoring well research. Cross-section 4.1.36 corresponds to location 25.

Table F.5: Locations along the Duifkade where the intermediate sand layer is present. o: sand layer present, x: sand layer not present. Source: Tauw (2009)

Cross-section	Crest	Slope	Toe
4.1.32	o	x	o
4.1.33	x	o	o
4.1.34	o		o
4.1.35	x		o
4.1.36a	x		x
4.1.36	x	x	o
4.1.36b	o		o
4.1.37	x		o
4.1.38	o		o

According to the report, the sand layer below location 25 is only present below the toe, which contradicts the soil borings from the monitoring wells. Extra borings were performed 50 m to the south and to the north of location 25 (4.1.36a and 4.1.36b). The borings to the north show a sand layer present below the crest and the toe, while the borings to the south show no sand layer at all. In the other cross-sections the presence of the sand layer varies as well. This information therefore provides no clarity whether the sand layer at location 25 can be present below the toe. On the other hand, it does show that there is a large variation in the longitudinal direction of the

flood defence. This could lead to flow in the longitudinal, which is not simulated since the model is two dimensional.

Summarising, two possible causes can be identified for the contradiction between the model calibration and the soil borings:

- Information uncertainty regarding the soil composition: available soil borings are in contradiction to each other, and provide no information for locations between the two borings.
- Flow in the longitudinal direction occurs in the sand layer, which cannot be modelled using the two-dimensional model.

Eventually the choice was made to use a model with the intermediate sand layer below the toe. This was the only soil composition for which the measurements could be matched, and for which the conductivities had realistic values. Another soil composition was tested in which the sand layer extended from the polder to below the crest without being in contact with the boezem, but this resulted in a head that was too low at the crest. The position of the sand layer can be considered a simplification of the variation in longitudinal direction, which is not modelled. This soil composition including the heads after steady-state calibration is displayed in Figure F.8.

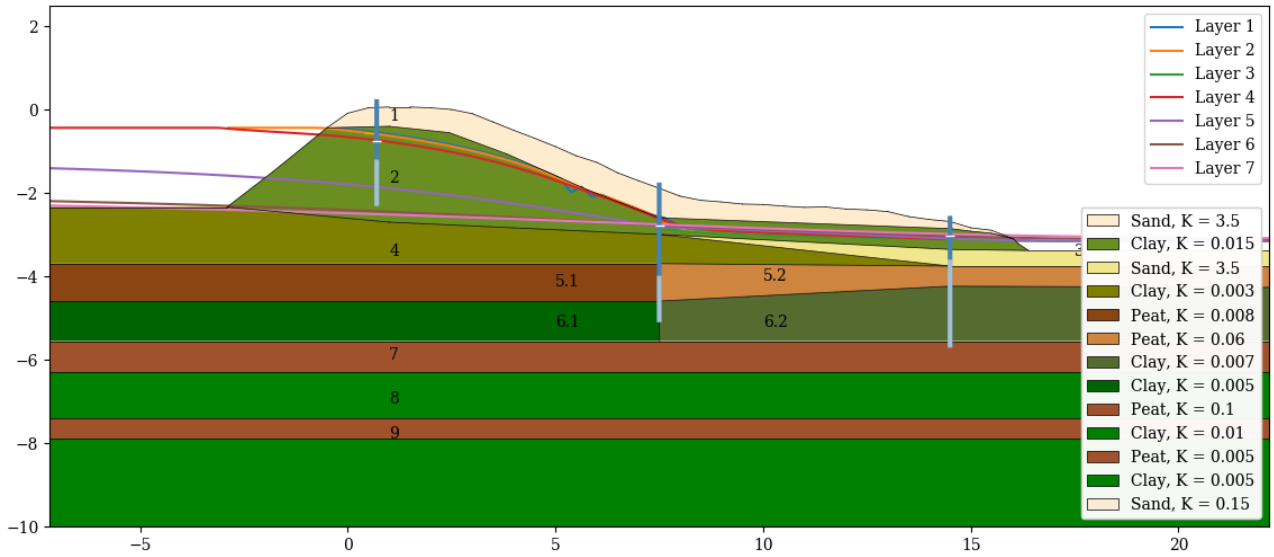

Figure F.8: Delfland location 25, results calibrated steady state simulation using the adjusted soil schematisation

The intermediate sand layer below the crest was replaced by clay. To make room for the new sand layer, peat layer 5 was shifted downwards at the expense of clay layer 6. The geometry of the other layers has not been changed.

Calibration transient

Conductivity
First the simulation was run using the values from the steady-state calibration. On average, the simulated heads matched the measured heads quite well. However, the magnitude of the fluctuations due to precipitation in the simulation is too small for the toe and slope, and too large for the crest. Variation of the conductivities shows that a larger conductivity of the clay core leads to more pronounced peaks of the heads in the slope and toe. However, this larger conductivity also leads to a higher average level of the heads. This probably cannot be solved by varying the other conductivities, since the used values are the optimum values from the steady-state calibration. However, when only the vertical conductivity is changed, the magnitude of the fluctuations increases without raising the average heads. Changing the vertical conductivity is

done by changing the anisotropy ratio of the soil type. To obtain fluctuations close to what is observed in the measurements an anisotropy ratio larger than 1 is required, meaning the vertical conductivity is larger than the horizontal conductivity. This is uncommon, in most soils the opposite is the case. However, De Loor (2018) also uses a larger vertical than horizontal conductivity for the top part of clay layers in his research. The explanation for this is that the cracks and pores in the clay mainly enlarge the vertical conductivity.

Increasing the conductivity of the topmost sand layer also has a positive effect on the fluctuation of the heads. This conductivity has a small influence on the steady-state simulation, and was therefore assumed to be 0,50 m/day, based on the Staring set. This conductivity is changed to 3,5 m/day.

Specific yield
The specific yield only influences the partially submerged layers, which are in this case the sand top layer and the clay core. For the clay core a change in the specific yield has a small influence. The assumed value of 0,03 is relatively low and leaves small room for variation. Decreasing the value to 0,015 has no significant effect on the peaks of the heads. Increasing the specific yield has a negative effect on the size of the peaks. Because of its small influence, the specific yield of the clay core is not changed.

For the sand top layer the effect of the specific yield is more prominent. Lowering the assumed value of 0,23 again results in a larger response of the heads to precipitation. A value of 0,05 results in the best approximation of the peaks in the model.

Recharge parameters
The initially assumed recharge parameters resulted in a reasonably well-fitting model. Only slight adjustments were made to the assumed values. The difference between the largest peaks was too small, and therefore the recharge capacity was increased. In general this resulted in more differentiation between the larger peaks, but there were also peaks that actually decreased when increasing the recharge capacity. The influence of the phreatic surface at the start of a precipitation event can result in expected reactions in the model. A recharge capacity of 15 mm/h resulted in the best approximation for most peaks. The recharge threshold was decreased to 0,1, because this resulted in a slightly better fit of the smallest peaks. This means there is no actually no threshold, since the precipitation data is supplied with an accuracy of 0,1 mm. The section multipliers had a very small influence on the model, and were not changed from the original value. The cause for this small influence is probably that the top sand layer, which has relatively large conductivity compared to the clay below, redistributes the recharge over the cross-section. The overall multiplier was decreased to 0,85, since overall the peaks were slightly too high. In Table F.6 the original and the calibrated recharge parameters are summarised.

Table F.6: Recharge parameters location 25

Parameter	Original value	Calibrated value
Rcap	5 mm/h	15 mm/h
Rmin	0,2 mm/h	0,1 mm/h
$\mathbf{m_1}$	0,5	0,5
$\mathbf{m_2}$	0,7	0,7
$\mathbf{m_3}$	0,5	0,5
$\mathbf{m_4}$	1	1
$\mathbf{m_{tot}}$	1	0,85

The soil parameters resulting from the calibration are displayed in Table F.7.

Table F.7: Calibrated parameters Delfland location 25

Layer	Soil type	Conductivity (m/day)	Anisotropy ratio	Specific yield (-)
1	Sand	3,5	0,66	0,05
2	Clay	0,015	2,5	0,02
3	Sand	3,5	0,66	0,23
4	Clay	0,003	0,33	0,03
5.1	Peat dike	0,008	0,01	0,03
5.2	Peat berm	0,06	0,5	0,03
6.1	Clay dike	0,007	0,1	0,03
6.2	Clay berm	0,005	0,66	0,03
7	Peat	0,1	0,3	0,03
8	Clay	0,01	0,1	0,03
9	Peat	0,005	0,02	0,03
10	Clay	0,005	0,1	0,03
11	Sand	0,15	1	0,23

F.2.2 Delfland location 24

Based on the experiences with location 25 the earlier soil schematisation of location 24 was adjusted. The clay layer and the peat layer below it are divided in two parts: below the dike and below the berm. The soil below the berm is probably less compacted and therefore has a higher conductivity than the soil below the dike. Staring types O12 and O13 are used for the clay below the dike and berm respectively, and for the peat the types O16 and B18. The other soil types and the boundary conditions were applied to the model as described in chapter 5 . The results of the steady-state simulation using these input parameters are displayed in Figure F.9.

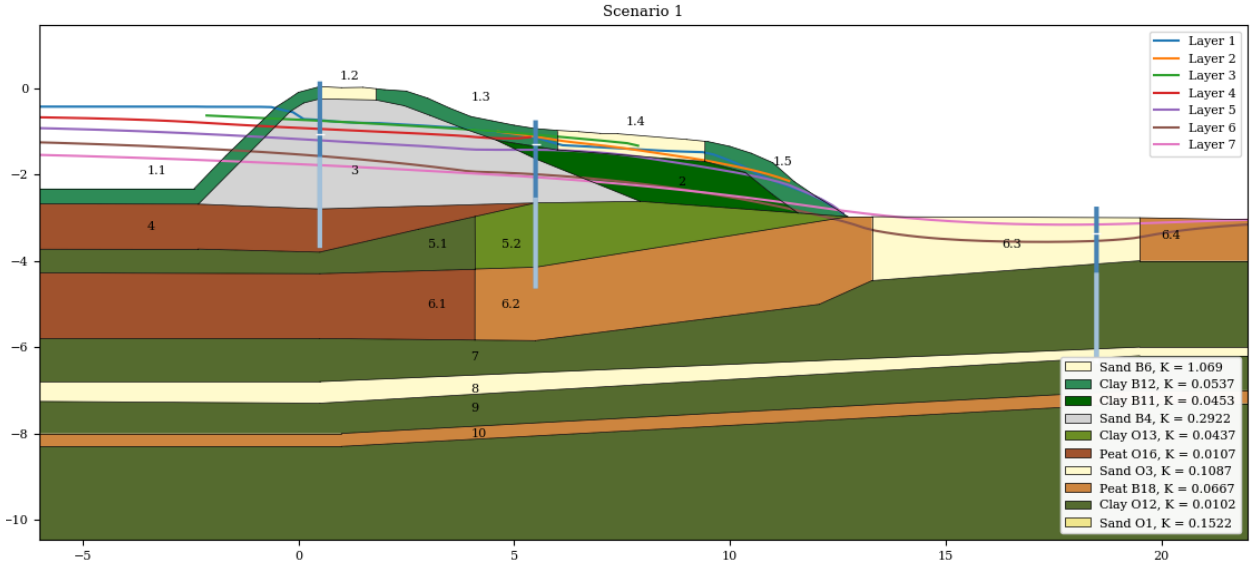

Figure F.9: Steady-state results location 24

From these results it stands out that the heads nearly horizontal over the rubble core of the dike, and only start to significantly decline in the clay berm. This is also observed in the measurements: the average head in the slope is almost as high as the average head in the crest. However, the simulated heads are about 20 cm higher than the measured values. Furthermore, the phreatic

surface exits the ground surface near the toe, and the simulated head in the sand fill of the drainage ditch does not correspond to the measurements.

Calibration steady state
The fit of the model to the measurement in the steady state simulation is evaluated in the same way as for location 25. The difference between the model and the measurements at the locations of the monitoring wells is calculated for each scenario. For the model result at the crest and slope the head in the rubble core (layer 3) is used. The filter of the monitoring well in the slope is mostly located in clay layer 5.2, but a small part extends into the rubble core. Since the heads in the rubble are much higher than in the clay, and the measurements show that the head is in fact relatively high, the choice is made to use the head in the rubble. For the head in the monitoring well near the sand fill the clay layer 7 is used. This monitoring well does not provide any information regarding the phreatic surface in the dike, but still provides useful information regarding the groundwater table in the polder.

The results of this analysis are displayed in Figure F.10.

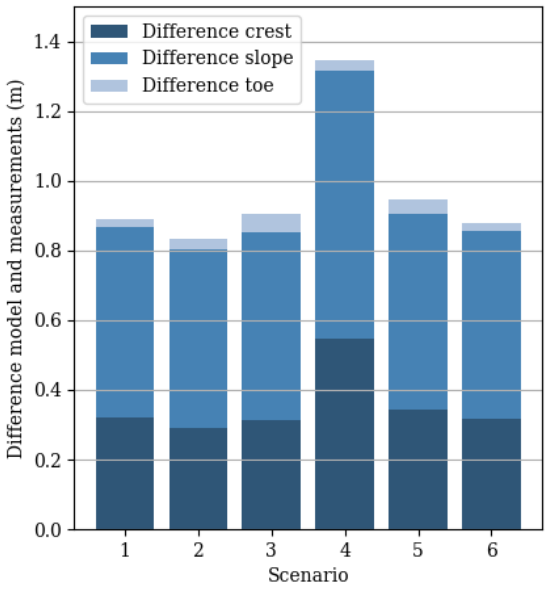

Figure F.10: Difference between steady-state model results and measurements for 7 soil scenarios

In this analysis scenario 2 yields the best results. Compared to scenario 1, the heads in the rubble core are higher because the soil below the outside water has a higher conductivity. However, it should be noted that the same result could be reached by using a lower conductivity for the clay cover. Scenario 3, which contains a second intermediate sand layer, gives slightly better results than the basis scenario. This is probably also caused by the lowering of the heads in the rubble core. Scenario 4, which excludes the clay cover, unsurprisingly shows unrealistically high heads in the core. Therefore it can be concluded that a clay cover must be present, even though no evidence was available for this at the moment of calibration. A later visual inspection has confirmed this. Scenarios 5 concerns small changes in the geometry based on schematisations provided by Delfland. It gives a slightly larger deviation compared to the measurements than scenario 1, and it is therefore not considered in further analyses. Scenario 6 was aimed at improving the model grid near the toe of the dike, since at this point three of the soil layers pinched out. However, the difference compared to scenario 1 are small. Near the toe a small difference can be observed in the heads compared to scenario 1. Therefore it is concluded that the pinching out of the three layers has a negligible effect on the results.

Even though the results found in scenario 2 showed a slightly better fit to the measurements, scenario 1 was chosen for the soil schematisation used for the further analyses. By changing the

conductivity of the clay cover, similar results to scenario 2 could be reached. The difference between the scenarios was therefore too small to prefer one over the other based on the model results. Scenario 1 is based on soil borings directly at the measurement location, whereas scenario 2 is based on soil borings further away. Scenario 1 is therefore preferable, and is used in the further calibration.

The steady-state calibration process was started by matching the measurements at the monitoring well near the sand-filled drainage ditch. This was mainly done by varying the conductance of the general head boundary package. Increasing this conductance results in more flow from the sand layer to the boundary condition, which results in a lower head and a smaller head rise due to precipitation. However, the model could not be fitted well to the measurements due to the high head in the lower soil layers. The monitoring well was placed in clay layer 7 and this layer showed a higher head in the model than the sand layer above it, as can be observed in Figure F.9. The cause of this is the influence of the head in the Pleistocene sand layer, which is about 2 m higher than the polder water level. This means a head decline must occur from the sand layer head towards the polder water level. The conductivities of the lower soil layers were such that this resulted in heads that were too high in the layers closer to the surface. This was solved by changing the conductivities of the deeper layers; the conductivity of the deepest clay layer was decreased and the conductivity of the higher layers was slightly increased. The results of this change was that the largest part of the decline of the heads over the depth occurred in the deeper soil layers, resulting in a lower head near the surface. After this change the conductance of the boundary could be changed such that a relatively good fit of the measurements could be reached.

Next, the heads at the other two monitoring wells were calibrated. Merely reducing the conductivity of the clay cover at the outside water (layer 1.1) to 0,02 m/day was sufficient to match the measurements. However, even when no recharge was applied to the model seepage occurred. Under normal circumstances it is not desirable for a dike to show seepage at the toe, so it is assumed that this does not occur in reality. Therefore an attempt was made to calibrate the model such that no seepage occurs, but without contradicting the measurements. Changing the conductivity of the clay berm, clay layer 5, and peat layer 6 yielded the desired results, which are displayed in Figure F.11. The conductivities resulting from the calibration are displayed in Table F.8.

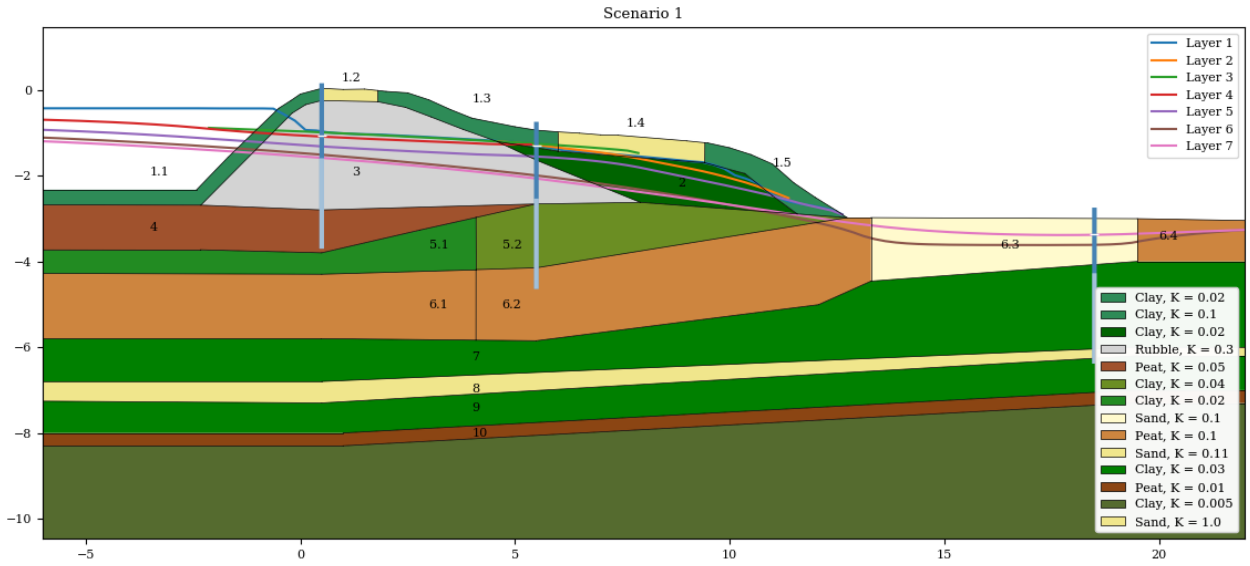

Figure F.11: Delfland location 24, results steady state simulation using calibrated values

Table F.8: Original and calibrated conductivities Delfland location 25

Layer	Soil type	Estimated conductivity (m/day)	Steady state calibrated conductivity (m/day)
1.1	Clay	0,0537	0,012
1.2	Sand	1,069	1,0
1.3	Clay	0,0537	0,1
1.4	Sand	1,069	1,0
1.5	Clay	0,0537	0,1
2	Clay	0,0453	0,02
3	Rubble	0,2922	0,3
4	Peat	0,0667	0,05
5.1	Clay below dike	0,0102	0,02
5.2	Clay below berm	0,0437	0,04
6.1	Peat below dike	0,0446	0,1
6.2	Peat below berm	0,0667	0,1
6.3	Sand fill of drainage ditch	0,1087	1,0
6.4	Peat hinterland	0,0667	0,1
7	Clay	0,0102	0,03
8	Intermediate sand layer	0,1087	0,11
9	Clay	0,0102	0,03
10	Peat	0,0667	0,05
11	Clay	0,0102	0,005
12	Peat	0,0667	0,05
13	Clay	0,0102	0,005
14	Pleistocene sand layer	0,1522	1,0

Calibration transient

Performing a transient simulation using the values from the steady-state calibrated showed that on average the measurements are matched relatively well. The magnitude of the fluctuations due to precipitation at the crest and slope is approximately the same as in the measurements. At the sand filled drainage ditch the simulated fluctuations are much smaller than in the measurements.

When observing longer term variations, it appears that the applied evapotranspiration rate is too high. The simulated head in the slope is too high in the winter months and too low in the summer months. This might be a result of the road on the berm and the footpath of the crest. These may locally reduce or even prevent the occurrence of evapotranspiration. To model this the evapotranspiration rate was set to zero for the locations of the footpath and the road. This gave a better result, but the evapotranspiration influence was still too large. Therefore the evapotranspiration multiplier was reduced to 0,5.

Similar to location 25, the vertical conductivity of the clay top layer was increased to increase the magnitude of the head fluctuations due to precipitation. The anisotropy ratio was set to 2. This was only done for the parts to which precipitation is applied, for the part of the top layer bordering the outside water the conductivity was actually decreased slightly. Furthermore, the conductivity of the peat in the hinterland was increased, which lead to more flow towards the sand fill. In this way the magnitude of the head fluctuations in this sand was increased, which matches the measurements better. The specific yield of the rubble core, the clay of the berm, and of the sand fill in the drainage ditch were decreased, also to increase the magnitude of the head fluctuations.

Several changes were made in the recharge parameters. The section multipliers had a more noticeable influence for this model than for the model of location 25. These multipliers were

slightly adjusted to increase the precipitation peaks near the toe. Like location 25, the recharge threshold was set to 0,1 mm/h to obtain more detail in the smallest peaks. The recharge capacity was kept at 5 mm/h; increasing the value did not lead to a better fit of the model. Finally, the overall multiplier was decreased to 0,9 to fit the peaks better.

Table F.9: Changes in recharge parameters location 24

Parameter	Initial value	Calibrated value
Rcap	5 mm/h	5 mm/h
Rmin	0,2 mm/h	0,1 mm/h
m_1	0,5	0,5
m_2	2	1,5
m_3	0,5	0,5
m_4	2	1,5
m_5	0,5	0,5
m_6	0,7	0,8
m_{tot}	1	0,9

The soil parameters resulting from the transient calibration are displayed in Table F.10.

Table F.10: Transient calibrated conductivities Delfland location 24

Layer	Soil type	Transient calibrated conductivity (m/day)	Hydraulic anisotropy ratio (-)	Specific yield (-)
1.1	Clay	0,012	0,33	0,03
1.2	Sand	1,0	0,66	0,23
1.3	Clay	0,1	2	0,03
1.4	Sand	1,0	0,66	0,23
1.5	Clay	0,1	2	0,03
2	Clay	0,02	0,5	0,03
3	Rubble	0,3	0,66	0,06
4	Peat	0,05	0,1	0,44
5.1	Clay below dike	0,02	0,33	0,03
5.2	Clay below berm	0,04	0,33	0,03
6.1	Peat below dike	0,1	0,1	0,44
6.2	Peat below berm	0,1	0,1	0,44
6.3	Sand fill of drainage ditch	1,0	0,66	0,1
6.4	Peat hinterland	0,2	0,1	0,44
7	Clay	0,01	0,33	0,03
8	Intermediate sand layer	0,11	0,66	0,23
9	Clay	0,01	0,33	0,03
10	Peat	0,05	0,1	0,44
11	Clay	0,005	0,33	0,03
12	Peat	0,05	0,1	0,44
13	Clay	0,005	0,33	0,03
14	Pleistocene sand layer	1,0	0,66	0,23

F.2.3 Hogedijk

Since the measurement period was too short to calibrate the model to the average of the measurements, the model for the Hogedijk was calibrated in a transient simulation directly. The initial condition of this simulation was still calculated using a steady state simulation, with the assumed average recharge rate of 525 mm/year. To include the influence of the dry summer months, the starting date of the transient simulation was set at 01-01-2018.

In Figure F.12 the results of the transient simulation using the initially assigned values are displayed. Only the part of the simulation for which measurements are available is displayed.

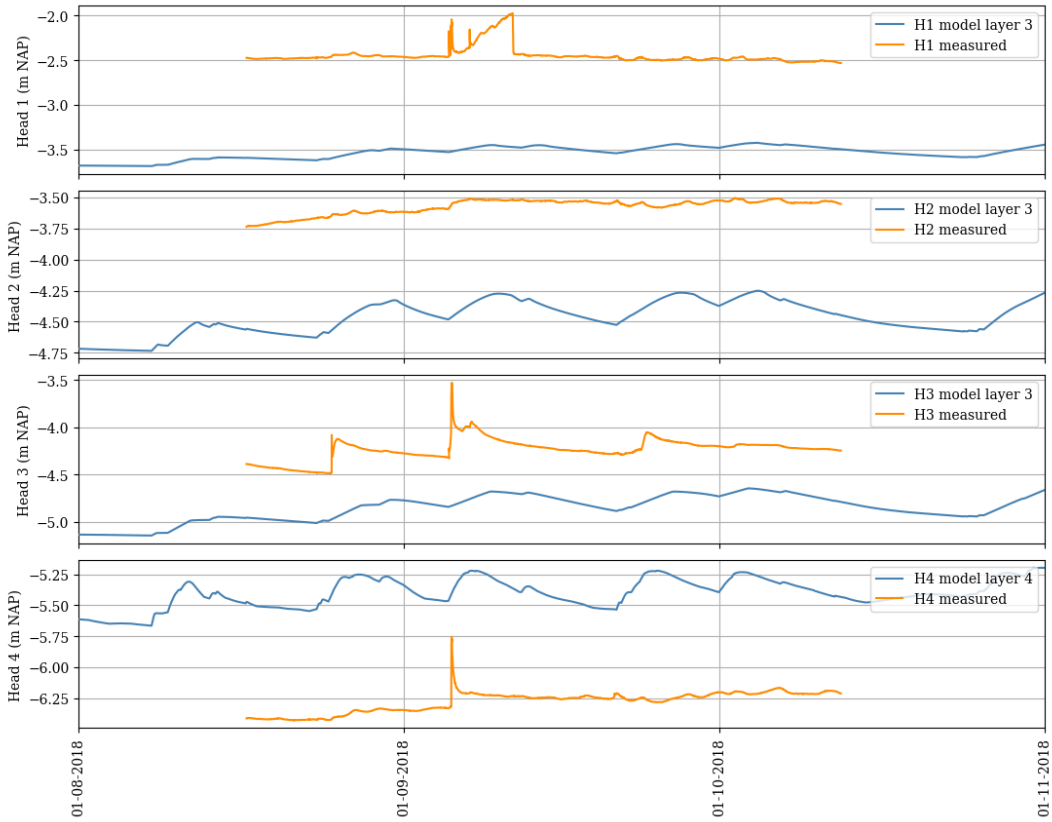

Figure F.12: Model results Hogedijk using initial uncalibrated values

It appears that the simulated heads for monitoring wells 1, 2, and 3 are too low, whereas for monitoring well 4 the head is too high. However, when looking at the heads of monitoring well 4 something strange can be observed: the head is almost continuously lower than the polder water level, except for one peak caused by a precipitation event, The polder water level appears to be correct, so possibly something is wrong with the measurements. Therefore the calibration was mostly aimed at matching the model to the other three measurement points.

Even considering the low measured values for monitoring well 4, the head at this point in the simulation is still quite high. Based on the experiences with the preceding models, a possible solution could be to adjust the conductivities of the deeper soil layers, to diminish the influence of the head in the Pleistocene sand layer. This head is between the inside and outside water level, and thus lowers the phreatic surface in the crest and upper slope, while it raises the phreatic surface at the lower slope and the toe of the dike. This change had some effect: heads 2 and 3 became higher and thus closer to the measurements, but head 1, while also becoming higher, did not reach the level of the measurements. The effect on head 4 was small.

Another change that was made was the extinction depth of the evapotranspiration package. This depth was set at 2 m, resulting in a low phreatic surface due to the dry summer months. By

changing this depth to 1 m, the phreatic surface became higher in this period and in the measurement period. However, it is unknown whether this change is correct. It is unknown how low the phreatic surface was during june and july 2018, and therefore it is unknown whether the model is more correct using and extinction depth of 1 or 2 m. Using 1 m results in a better fit for the measurement period, but might not result in as good a fit for later measurements.

Since changing the conductivities of the deeper layers did not result in a good enough fit of the model, the conductivity of the peat layer has to be changed. Initially it was tried to keep the horizontal conductivity constant on the measured values, while changing the anisotropy ratio and thus the vertical conductivity. This had some effect, but still nog head could be reached at point 1 that approached the measured value. Lowering the horizontal conductivity of part 1 of the peat layer resulted in a higher head, but this always raised the head at monitoring well 2.

This problem is probably a result of the chosen division of the peat layer, with divisions in the middle between the monitoring wells. Disregarding precipitation, evapotranspiration and the influence of the deeper soil layer, the head gradient in each part of the peat layer is approximately linear. Calibrating one of these parts to a monitoring well means that the head in the middle of the part is correct, but might be unrealistic near the separation. For example, lowering the conductivity in part 1 to match the monitoring well results in a head close to the surface at the layer separation.

There are two possible solutions for this:

- Place the layer separations at the monitoring wells. Between the wells the soil then becomes homogeneous, resulting in a more linear course of the phreatic surface. A disadvantage is that the separations are placed at the point where the head is evaluated, meaning inaccuracies caused by the layer separation influence the model results.
- Varying the conductivities between the monitoring wells. This will result in a smoother phreatic surface because the change in conductivity over the width is more gradual.

The choice was made to use the second option. The conductivity between the monitoring wells was interpolated linearly. Using the measured values for the conductivity this resulted in a reasonably good fit of monitoring wells 2 and 3, but still the measurements of monitoring well 1 were not matched. Changing the conductivity such that monitoring well 1 was matched resulted in a deviation from monitoring wells 2 and 3. This could only be solved by making another cut in the peat layer in the crest. The new section in the peat layer between the outside water and this cut was assigned a higher conductivity, and in this way monitoring well 1 could be matched as well. This higher conductivity zone could be present in reality as well, since this zone is located below the road on the crest. Sand and rubble from the road cunet could result in a higher conductivity.

After this modification the general height of the phreatic surface was in accordance to the measurements, but the shape and magnitude of the precipitation peaks was not. One of the parameters that was of influence for this was the conductivity of layer 2, the loam top layer. Assigning this layer a lower conductivity resulted in higher peaks near the crest. This is contrary to the observations made in the other two models: a larger (vertical) conductivity of the top layer resulted in higher peaks. The explanation for this is seepage. During precipitation events seepage occurs near the toe through the loam layer, so a low conductivity of this layer provides more resistance to seepage. Since the water cannot flow away as easily, the head ‘upstream’ in the cross-section will rise more. Since the loam layer does not extend fully towards the crest, the lower conductivity has no influence on the resistance to recharge in the crest.

A strange phenomenon that could not be modelled properly was the difference in reaction between monitoring wells 2 and 3. In the measurements, monitoring well 2 shows a damped response to precipitation, whereas monitoring well 3 shows a much more peaked response. This is strange, since these wells are located close to each other, and both are placed in the slope of the

dike. In the model this different response could not be reached. It was possible to approximately match the damped response or the peaked response for both points simultaneously, but not for each point individually. Changing recharge multipliers slightly increased the difference between the two points, but not enough to match the measurements.

Eventually the model was calibrated by changing the specific yields such that both monitoring wells 2 and 3 are matched approximately. At neither location the peaks could be matched exactly. The fast, almost direct response of monitoring well 3 to the precipitation event in early September could not be modelled. The model responds more slowly, and reaches the peak after a few days. The height of the peak could be matched, but if this was done the phreatic surface remained too high for weeks after the precipitation. The choice was made to calibrate so that the model result is close to the measurements most of the time, even though the peak height is not matched.

The result of this calibration is displayed in Figure F.13.

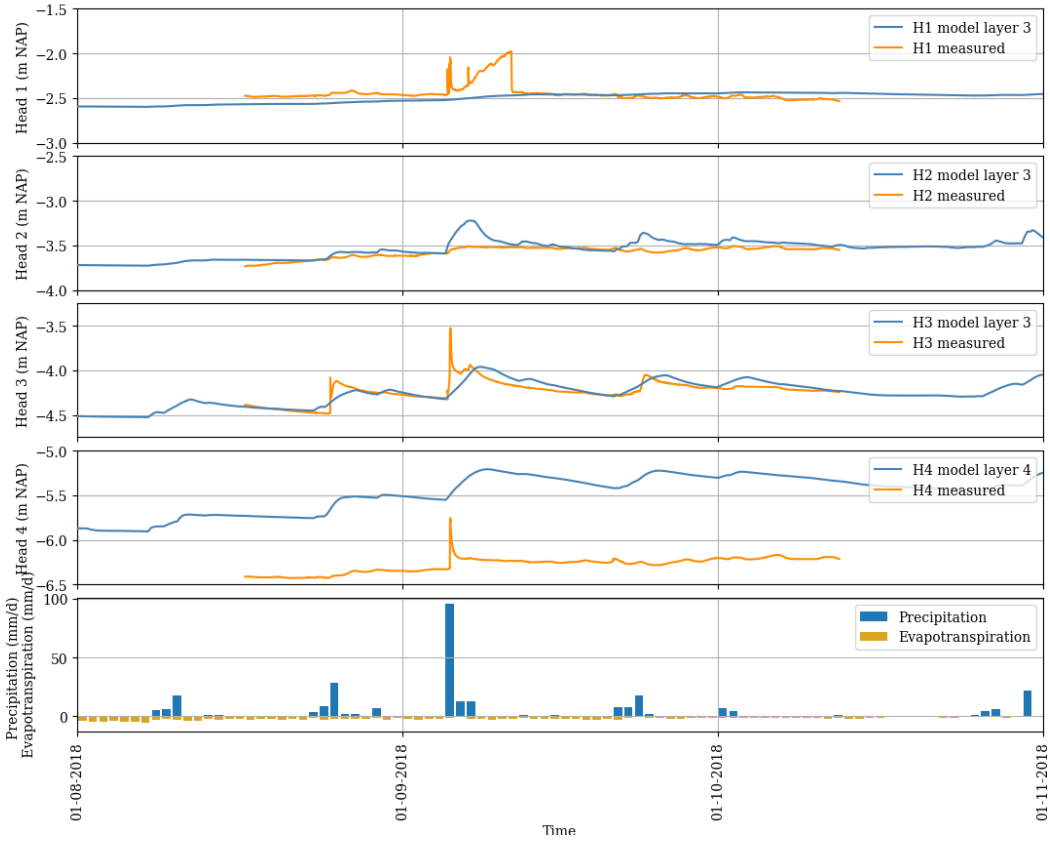

Figure F.13: Calibration Hogedijk

It can be observed that excepting the peaks, the model fits the measurements of monitoring wells 1,2, and 3 quite well. As discussed earlier, monitoring well 1 shows a gradual rise of the head and a sudden jump back to the original level. This is probably an error in the measurements, and it could not be reproduced in the model. For monitoring well 2 the peaks in the model are too high compared to the measurements. It was possible to calibrate the model such that the measurements were matched, but this resulted in a less good fit for monitoring well 3. For that well the fit is quite good, except for the peaks: the head rises much slower. The fast response as observed in the measurements could not be reproduced.

The calibrated parameters are displayed in Table F.11. The measured conductivities in the peat layer did not need to be changed. Altering the conductivities of the other layers and the anisotropy ratio and specific yield was sufficient to calibrate the model.

Table F.11: Calibrated parameters Hogedijk

Layer	Soil type	Conductivity (m/day)	Anisotropy ratio (-)	Specific yield (-)
1.1	Top layer	2,5	2	0,1
1.2	Rubble/sand from road	2,5	2	0,1
2	Loam	1	3	0,01
3.0	Peat	0,012	0,2	0,05
3.1	Peat	0,004	0,2	0,05
3.2	Peat	0,01	0,3	0,05
3.3	Peat	0,005	0,2	0,006
3.4	Peat	0,04	0,2	0,05
4	Clay	0,001	0,2	0,01
5	Peat	0,002	0,01	0,03
6	Pleistocene sand layer	10	0,66	0,23

F.3 Scenarios

F.3.1 Delfland location 25

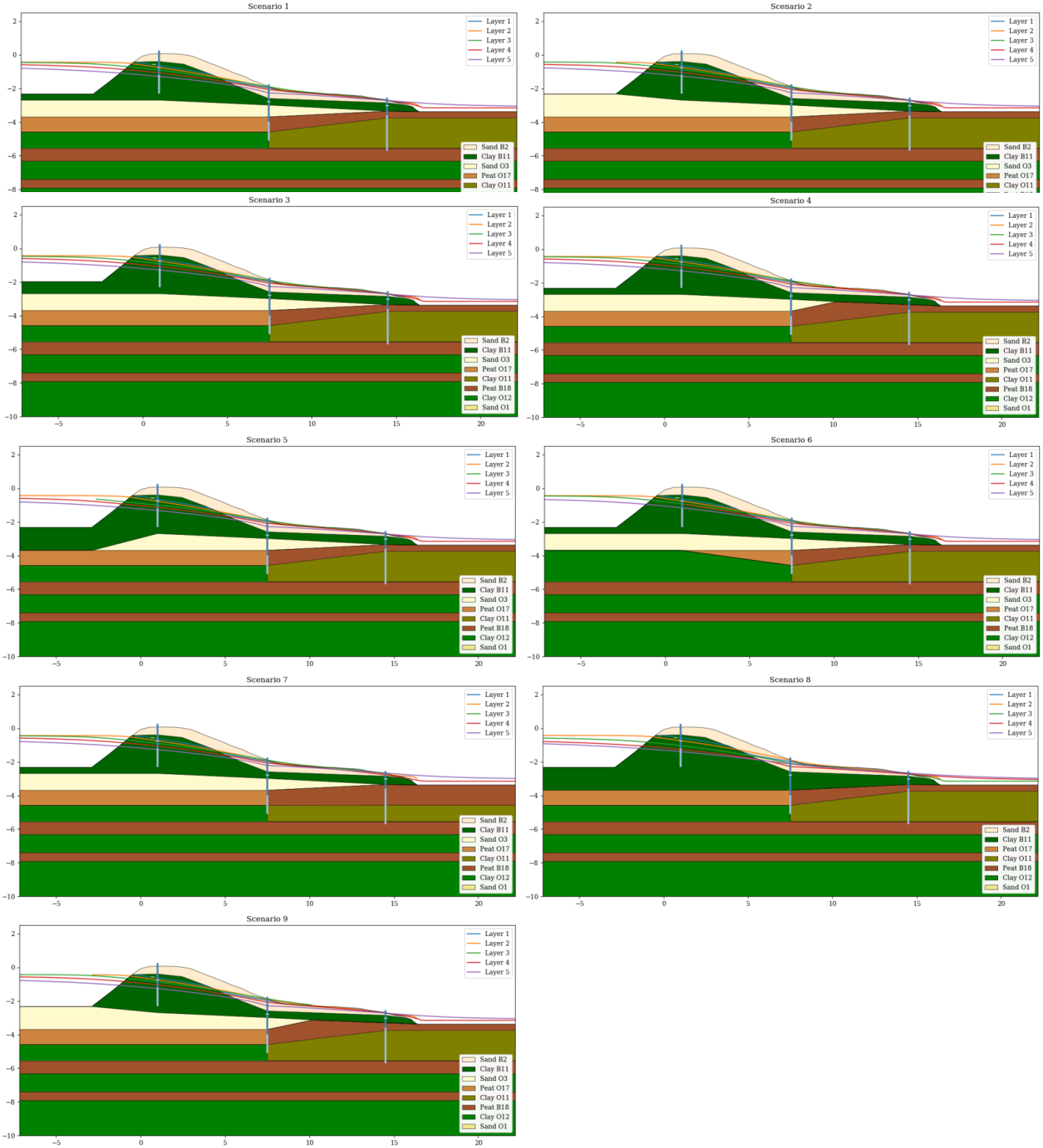

F.3.2 Delfland location 24

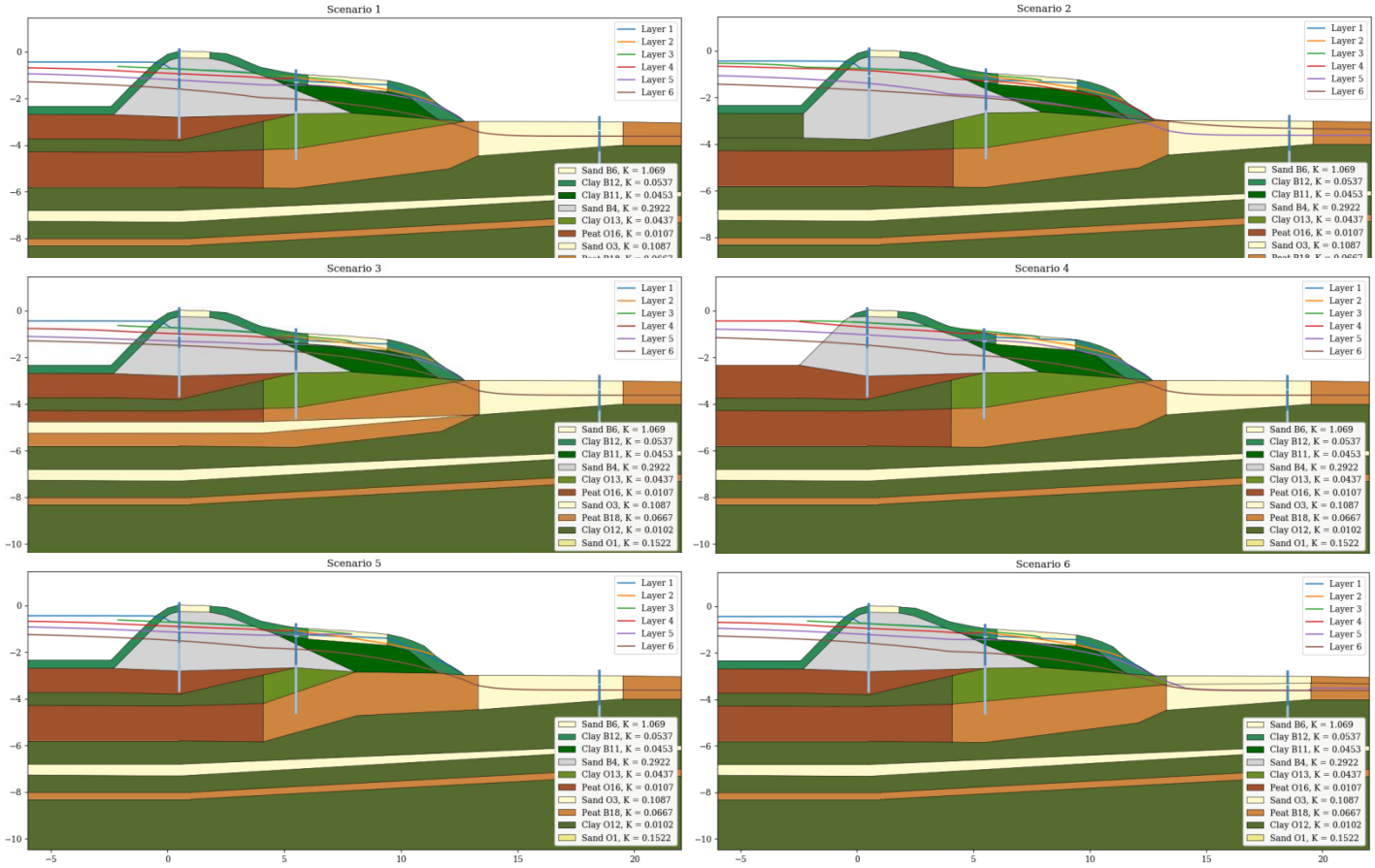

G Model results

G.1 Calibrated models

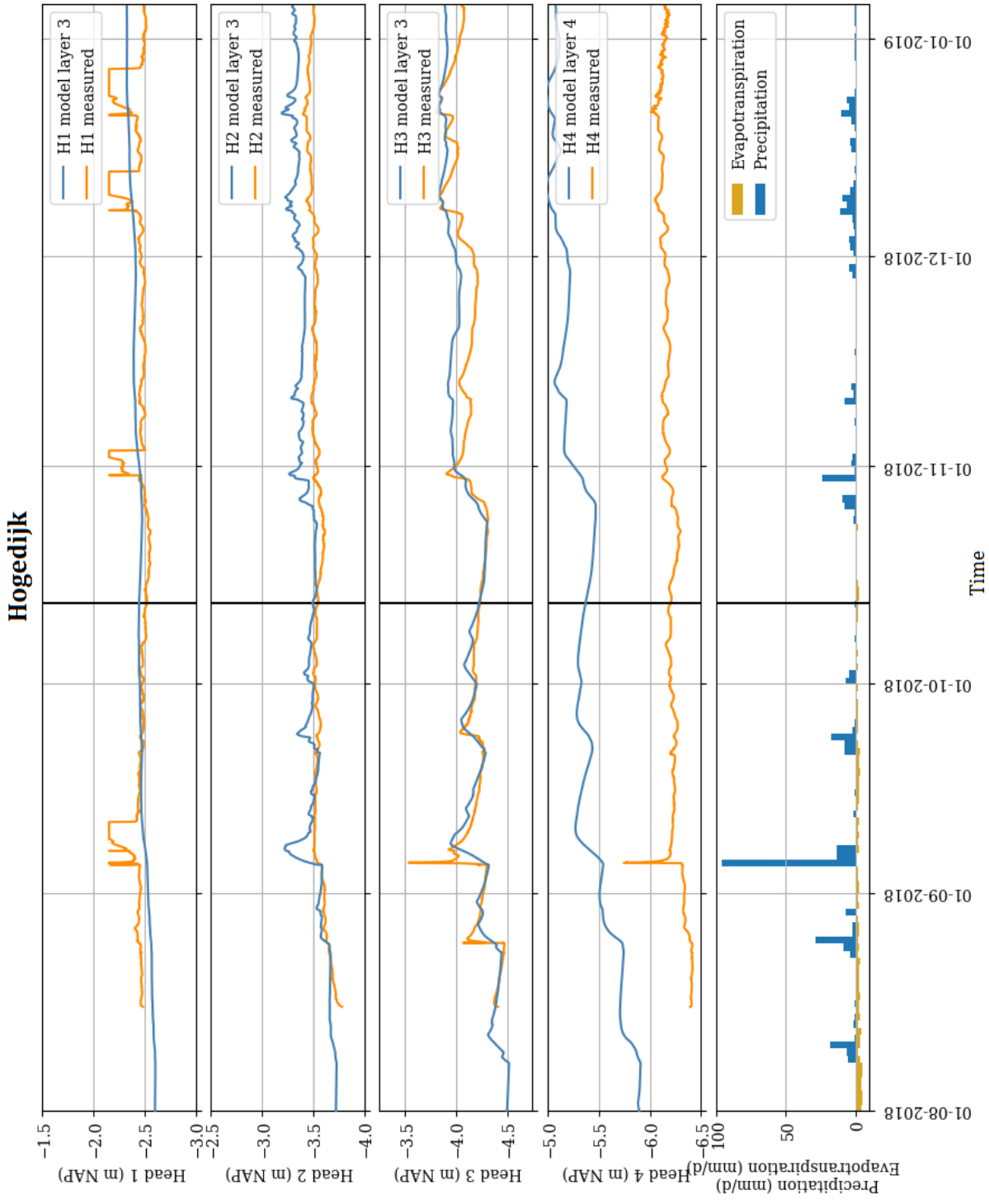

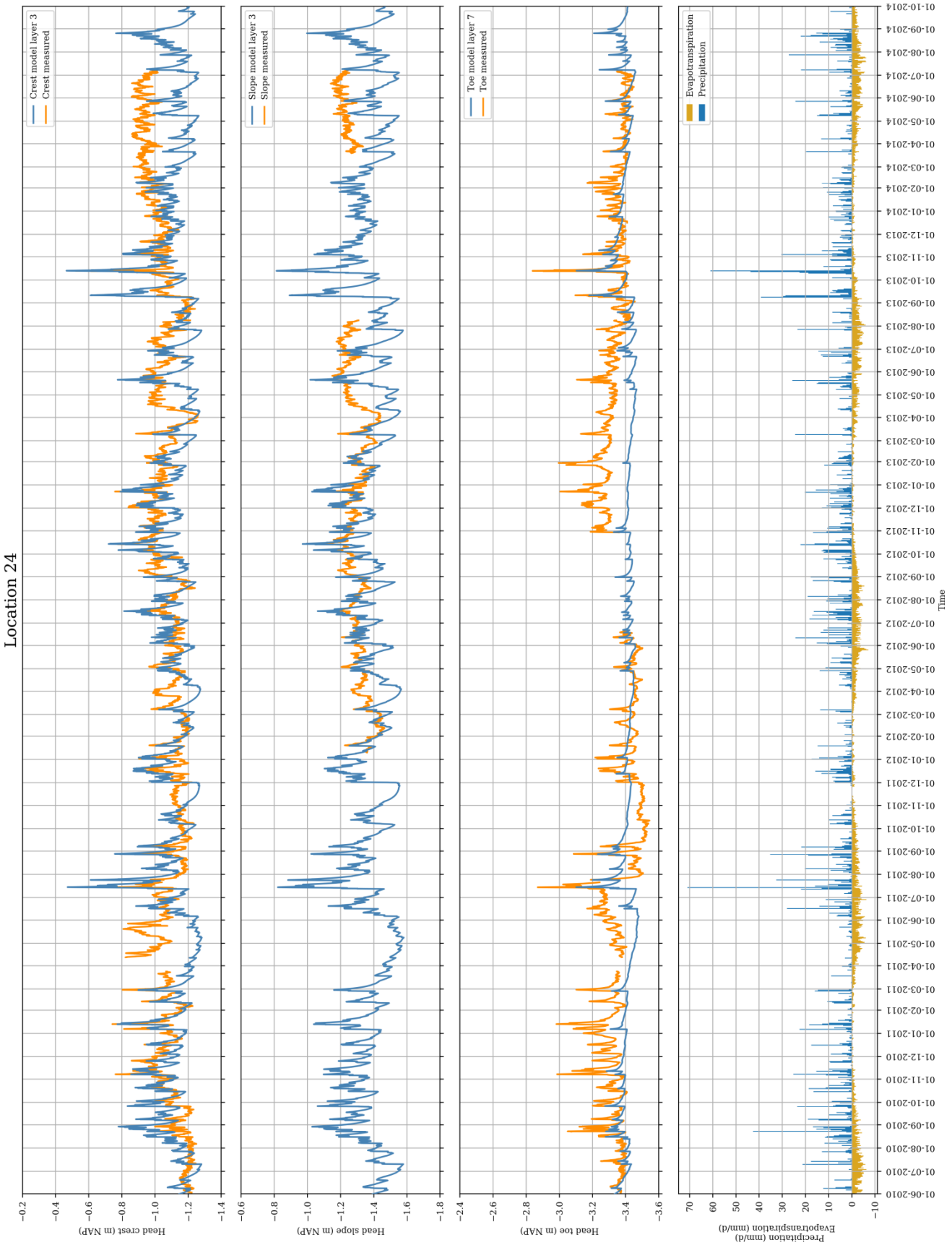
Location 24
Crest model layer 3
Crest measured
Head crest (m NAP)
Slope model layer 3
Slope measured
Head slope (m NAP)
Toe model layer 7
Toe measured
Head toe (m NAP)
Evapotranspiration
Precipitation
Precipitation (mm/d)
Evapotranspiration (mm/d)
Time

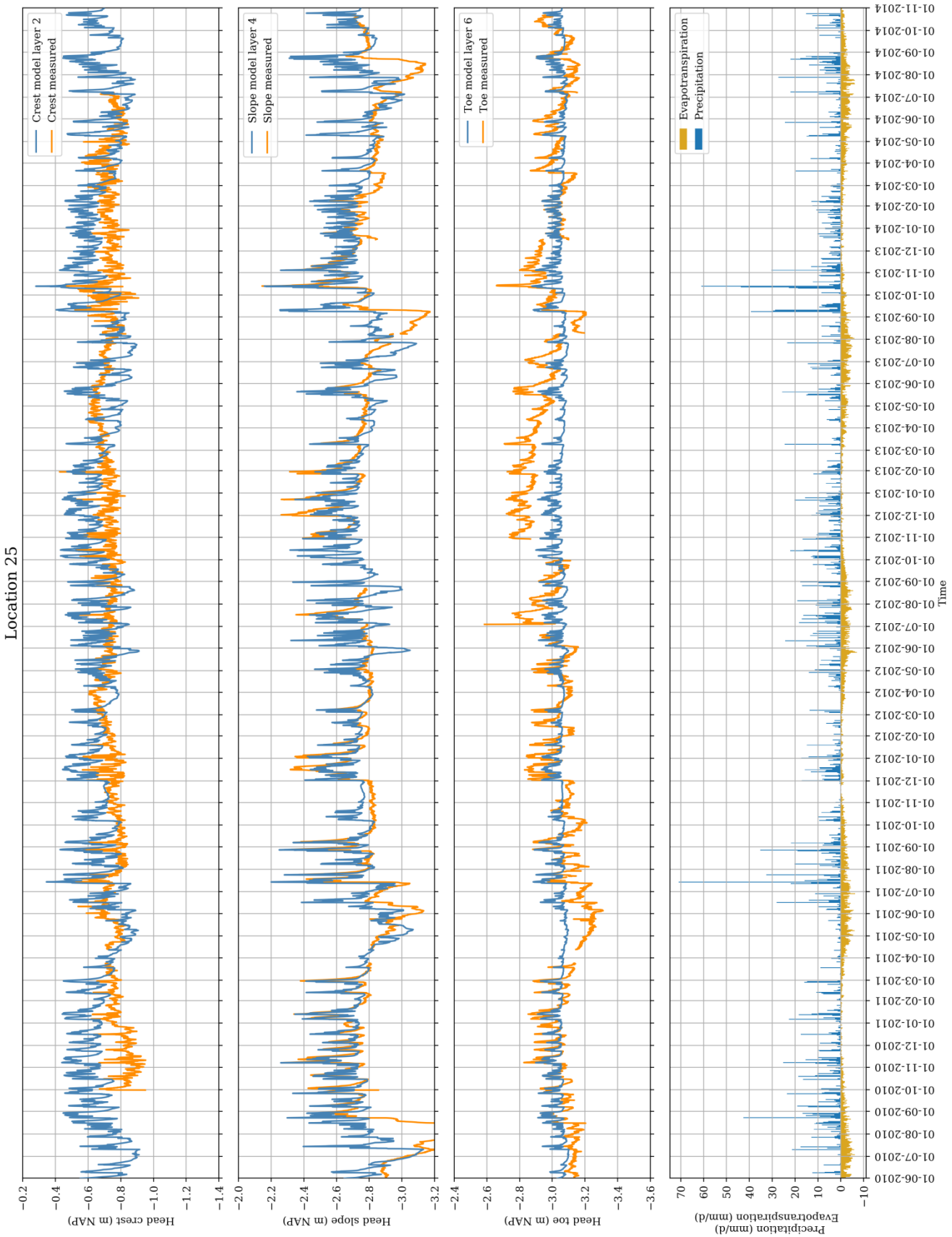
Location 25
Crest model layer 2
Crest measured
Head crest (m NAP)
Slope model layer 4
Slope measured
Head slope (m NAP)
Toe model layer 6
Toe measured
Head toe (m NAP)
Evapotranspiration
Precipitation
Precipitation (mm/d)
Evapotranspiration (mm/d)
Time

G.2 Uncalibrated models

G.2.1 Parameters

Table G.1: Parameters for the uncalibrated model of location 25

Layer	Soil type	Staring type	Conductivity (m/day)	Anisotropy ratio (-)	Specific yield (-)
1	Sand	B2	0,1252	0,66	0,23
2	Clay	B11	0,0453	0,33	0,03
3	Sand	O3	0,1087	0,66	0,23
4	Clay	B10	0,0070	0,33	0,03
5.1	Peat dike	O17	0,0102	0,1	0,44
5.2	Peat berm	B18	0,0667	0,1	0,44
6.1	Clay dike	O12	0,0102	0,33	0,03
6.2	Clay berm	O11	0,0667	0,33	0,03
7	Peat	B18	0,0667	0,1	0,44
8	Clay	O12	0,0102	0,33	0,03
9	Peat	B18	0,0667	0,1	0,44
10	Clay	O12	0,0102	0,33	0,03
11	Sand	O1	0,1522	0,66	0,23

Table G.2: Parameters for the uncalibrated model of location 24

Layer	Soil type	Staring type	Conductivity (m/day)	Anisotropy ratio (-)	Specific yield (-)
1.1	Clay	B12	0,0537	0,33	0,03
1.2	Sand	B6	1,069	0,66	0,23
1.3	Clay	B12	0,0537	0,33	0,03
1.4	Sand	B6	1,069	0,66	0,23
1.5	Clay	B12	0,0537	0,33	0,03
2	Clay	B11	0,0453	0,33	0,03
3	Rubble	B4	0,2922	0,66	0,23
4	Peat	O16	0,0107	0,1	0,44
5.1	Clay	O12	0,0102	0,33	0,03
5.2	Clay	O13	0,0437	0,33	0,03
6.1	Peat	O16	0,0107	0,1	0,44
6.2	Peat	B18	0,0667	0,1	0,44
6.3	Sand fill of drainage ditch	O3	0,1087	0,66	0,23
6.4	Peat hinterland	B18	0,0667	0,1	0,44
7	Clay	O12	0,0102	0,33	0,03
8	Intermediate sand layer	O3	0,1087	0,66	0,23
9	Clay	O12	0,0102	0,33	0,03
10	Peat	B18	0,0667	0,1	0,44
11	Clay	O12	0,0102	0,33	0,03
12	Peat	B18	0,0667	0,1	0,44
13	Clay	O12	0,0102	0,33	0,03
14	Pleistocene sand layer	O1	0,1522	0,66	0,23

Table G.3: Parameters for the uncalibrated model of the Hogedijk

Layer	Soil type	Staring type	Conductivity (m/day)	Anisotropy ratio (-)	Specific yield (-)
1	Sand	B3	0,1542	0,66	0,23
2	Loam	B13	0,1298	0,33	0,03
3.1	Peat	B18	0,0667	0,1	0,44
3.2	Peat	B18	0,0667	0,1	0,44
3.3	Peat	B18	0,0667	0,1	0,44
3.4	Peat	B18	0,0667	0,1	0,44
4	Clay	O11	0,1379	0,33	0,03
5	Peat	O16	0,0107	0,1	0,44
6	Pleistocene sand layer	O1	0,1522	0,66	0,23

G.2.2 Results

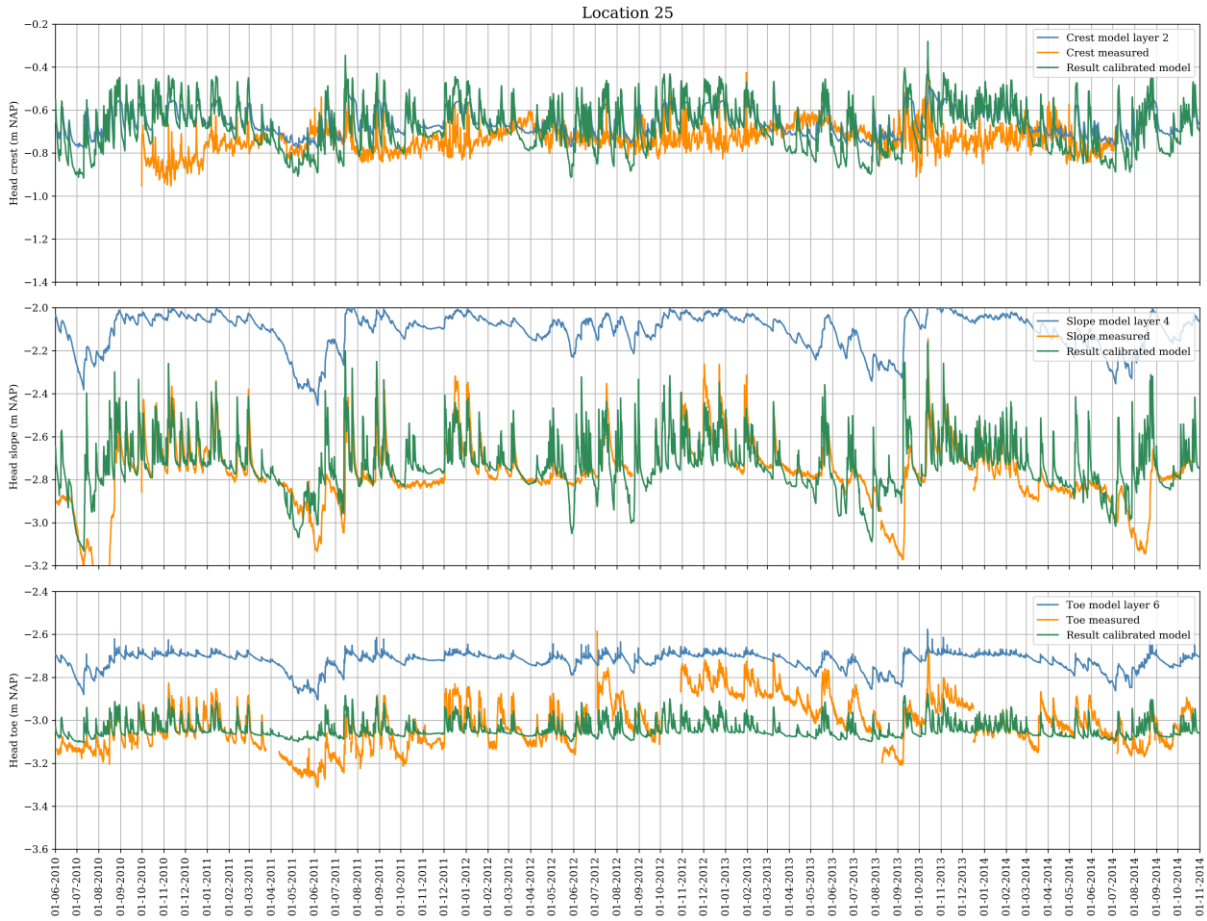

Figure G.1: Heads calibrated and uncalibrated model location 25

Figure G.2: Heads calibrated and uncalibrated model location 24

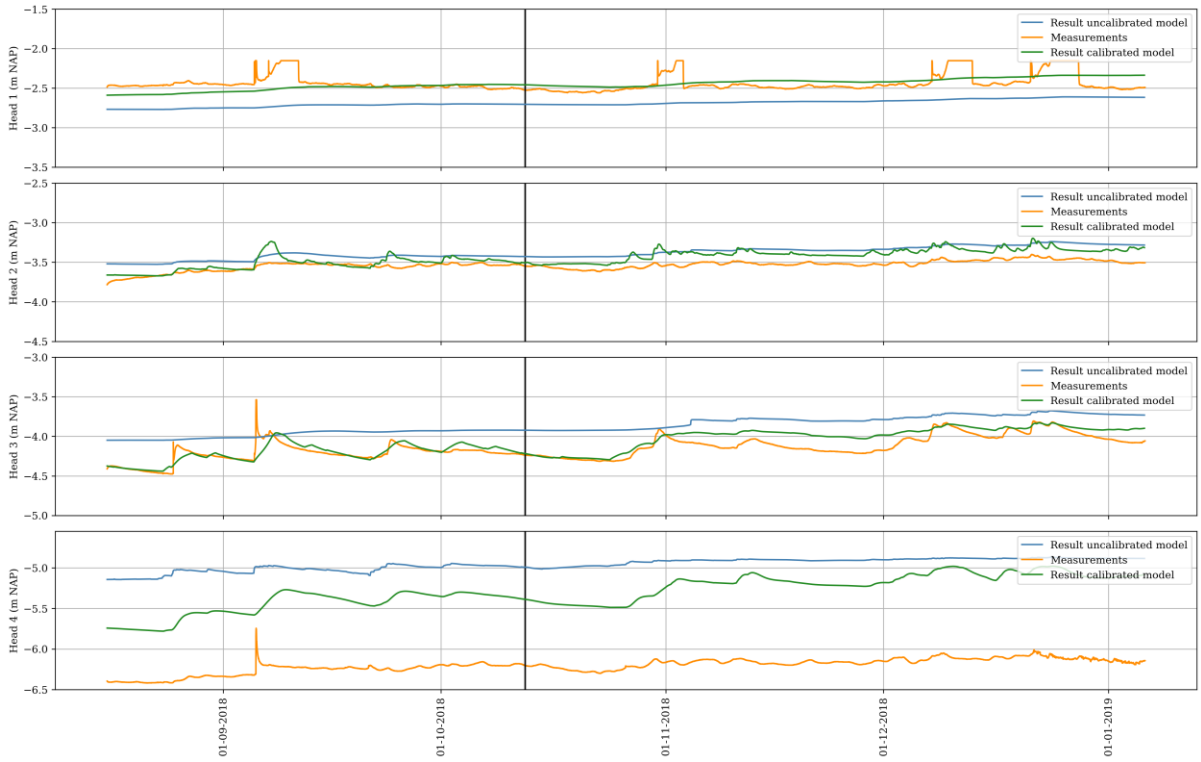

Figure G.3: Heads calibrated and uncalibrated model Hogedijk

G.2.3 Highest and lowest simulated phreatic surfaces

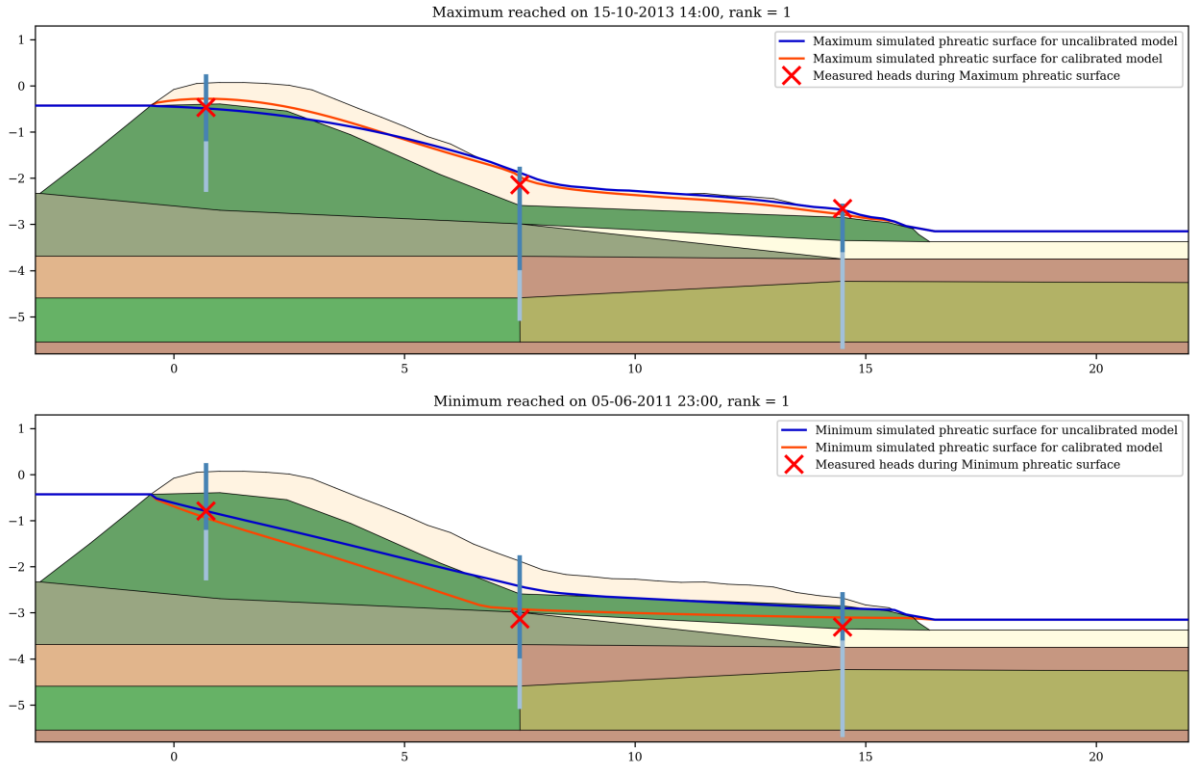

Figure G.4: Highest and lowest phreatic surface for the uncalibrated model (in blue) and the calibrated model (in red) of location 25.

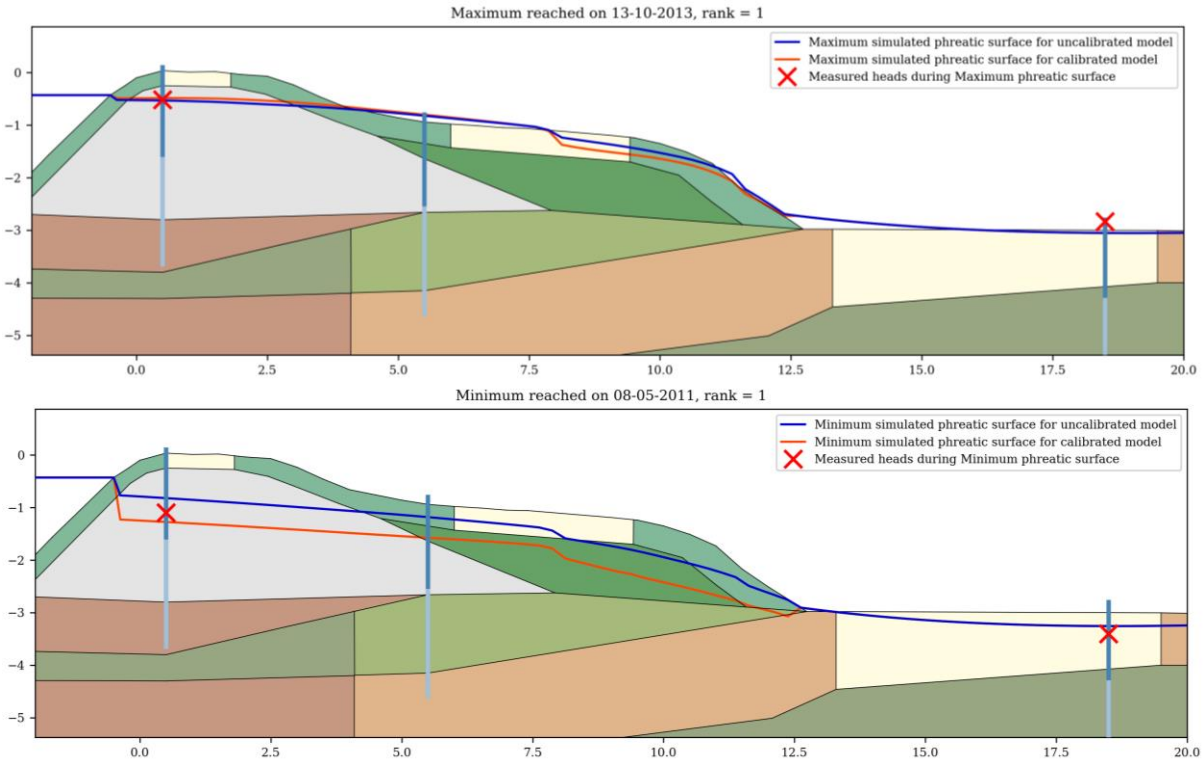

Figure G.5: Highest and lowest phreatic surface for the uncalibrated model (in blue) and the calibrated model (in red) of location 25.

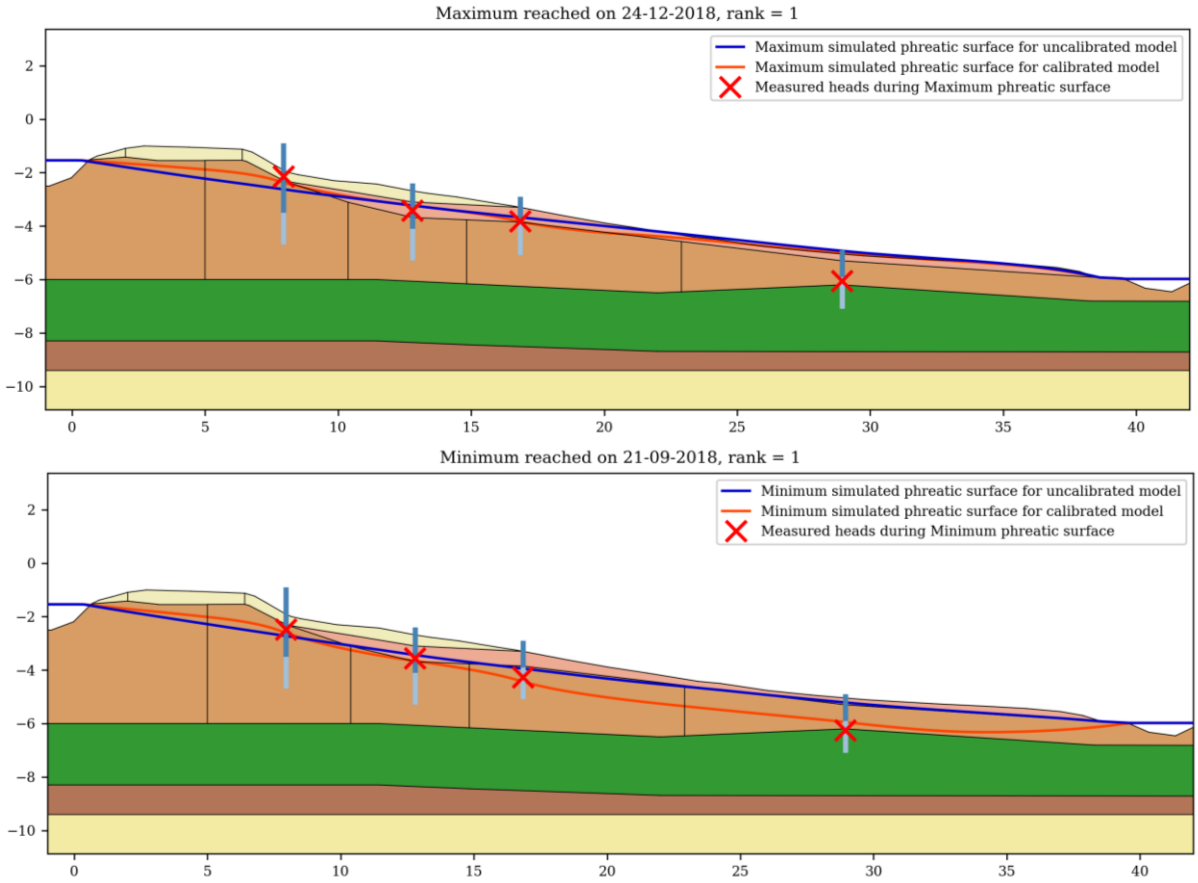

Figure G.6: Highest and lowest phreatic surface for the uncalibrated model (in blue) and the calibrated model (in red) of location Hogedijk

H Extreme events

H.1 Delfland 25 (Duifkade)

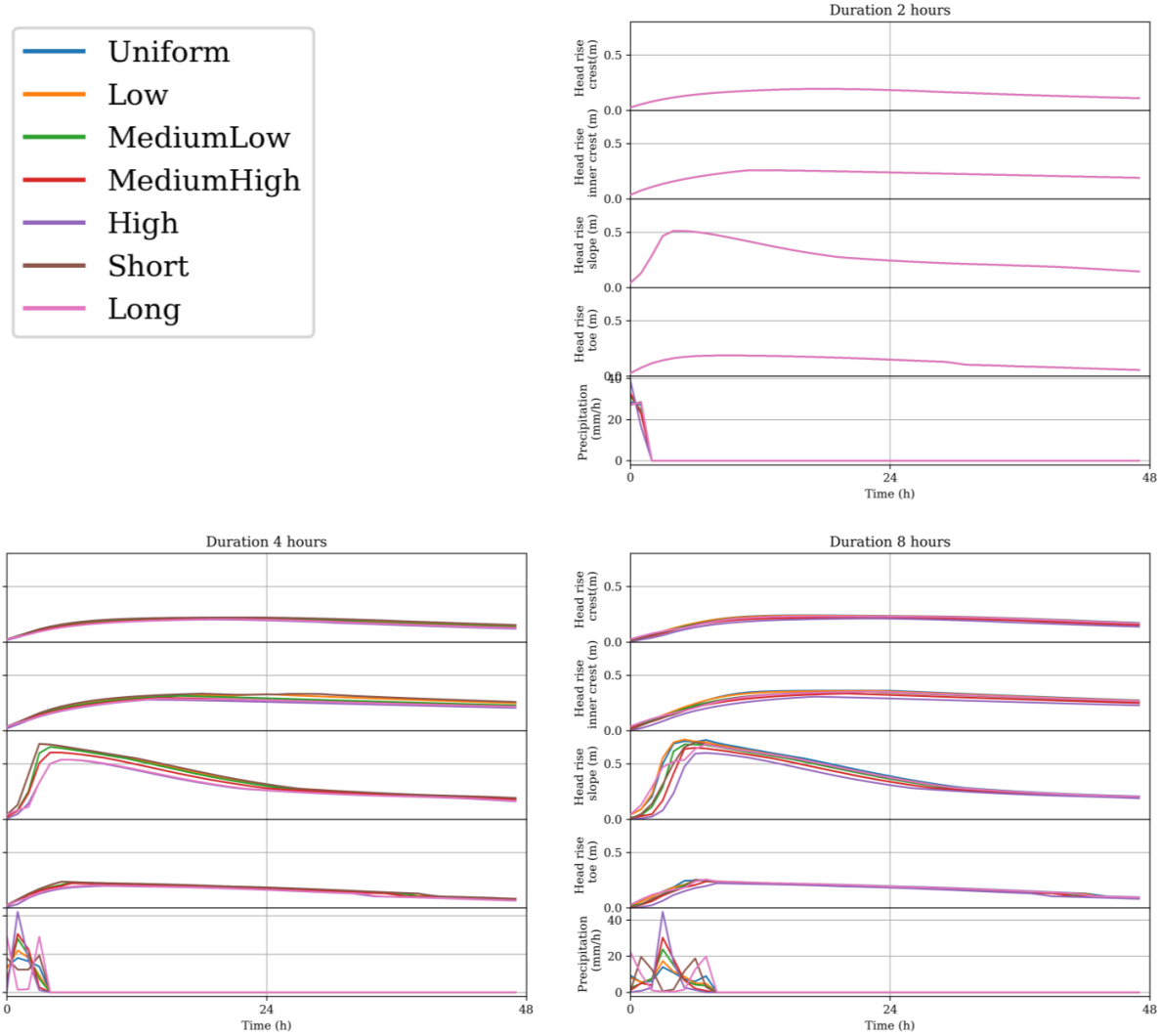

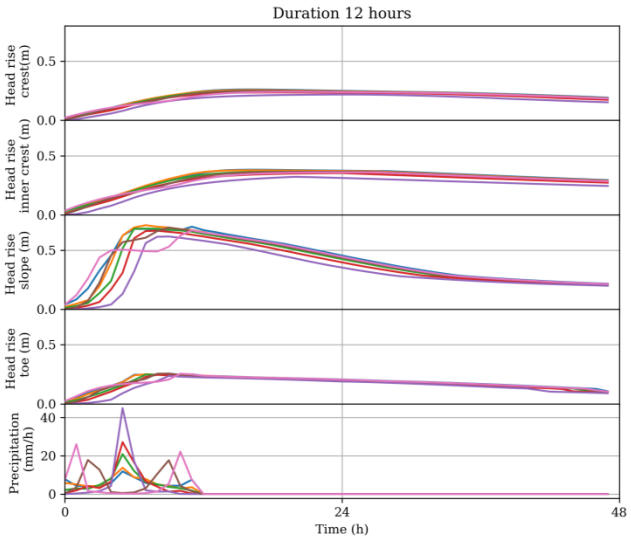
Duration 12 hours
Head rise crest(m)
Head rise inner crest (m)
Head rise slope (m)
Head rise toe (m)
Precipitation (mm/h)
Time (h)

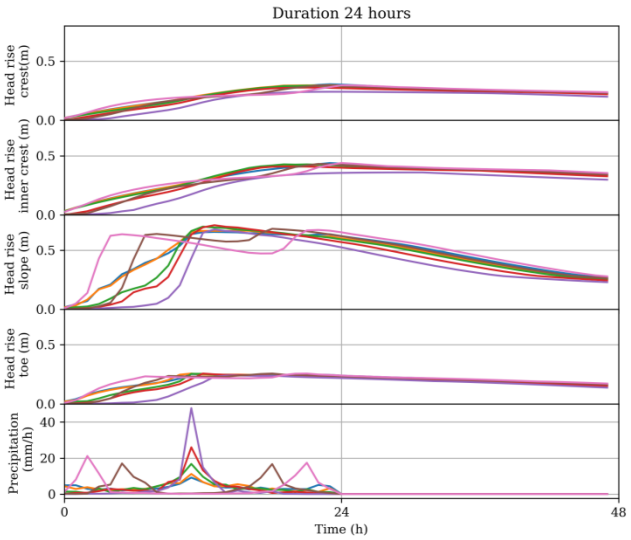
Duration 24 hours
Head rise crest(m)
Head rise inner crest (m)
Head rise slope (m)
Head rise toe (m)
Precipitation (mm/h)
Time (h)

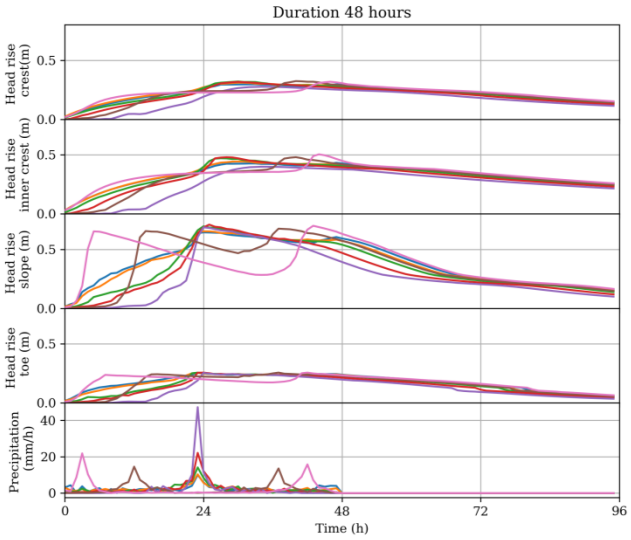
Duration 48 hours
Head rise crest(m)
Head rise inner crest (m)
Head rise slope (m)
Head rise toe (m)
Precipitation (mm/h)
Time (h)

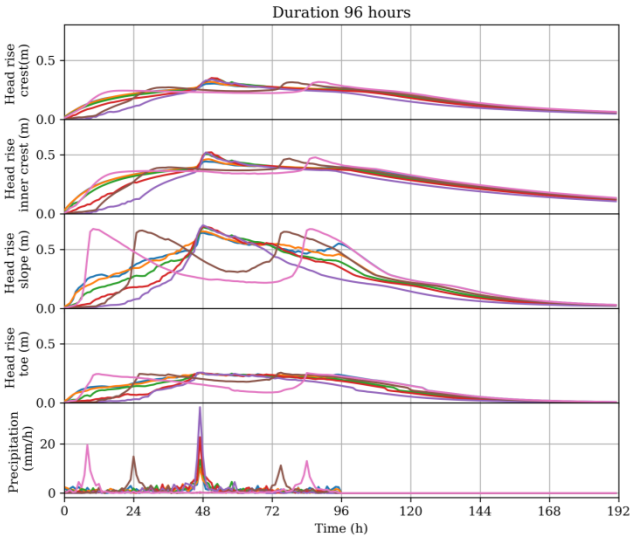
Duration 96 hours
Head rise crest(m)
Head rise inner crest (m)
Head rise slope (m)
Head rise toe (m)
Precipitation (mm/h)
Time (h)

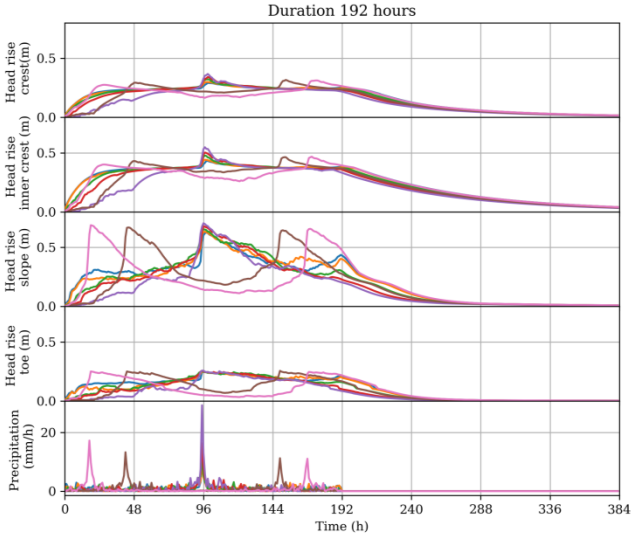
Duration 192 hours
Head rise crest(m)
Head rise inner crest (m)
Head rise slope (m)
Head rise toe (m)
Precipitation (mm/h)
Time (h)

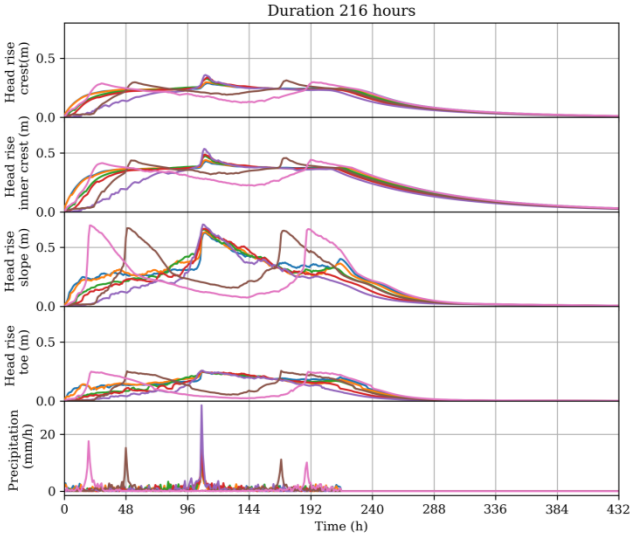
Duration 216 hours
Head rise crest(m)
Head rise inner crest (m)
Head rise slope (m)
Head rise toe (m)
Precipitation (mm/h)
Time (h)

H.2 Delfland 24 (Vlaardingsekade)

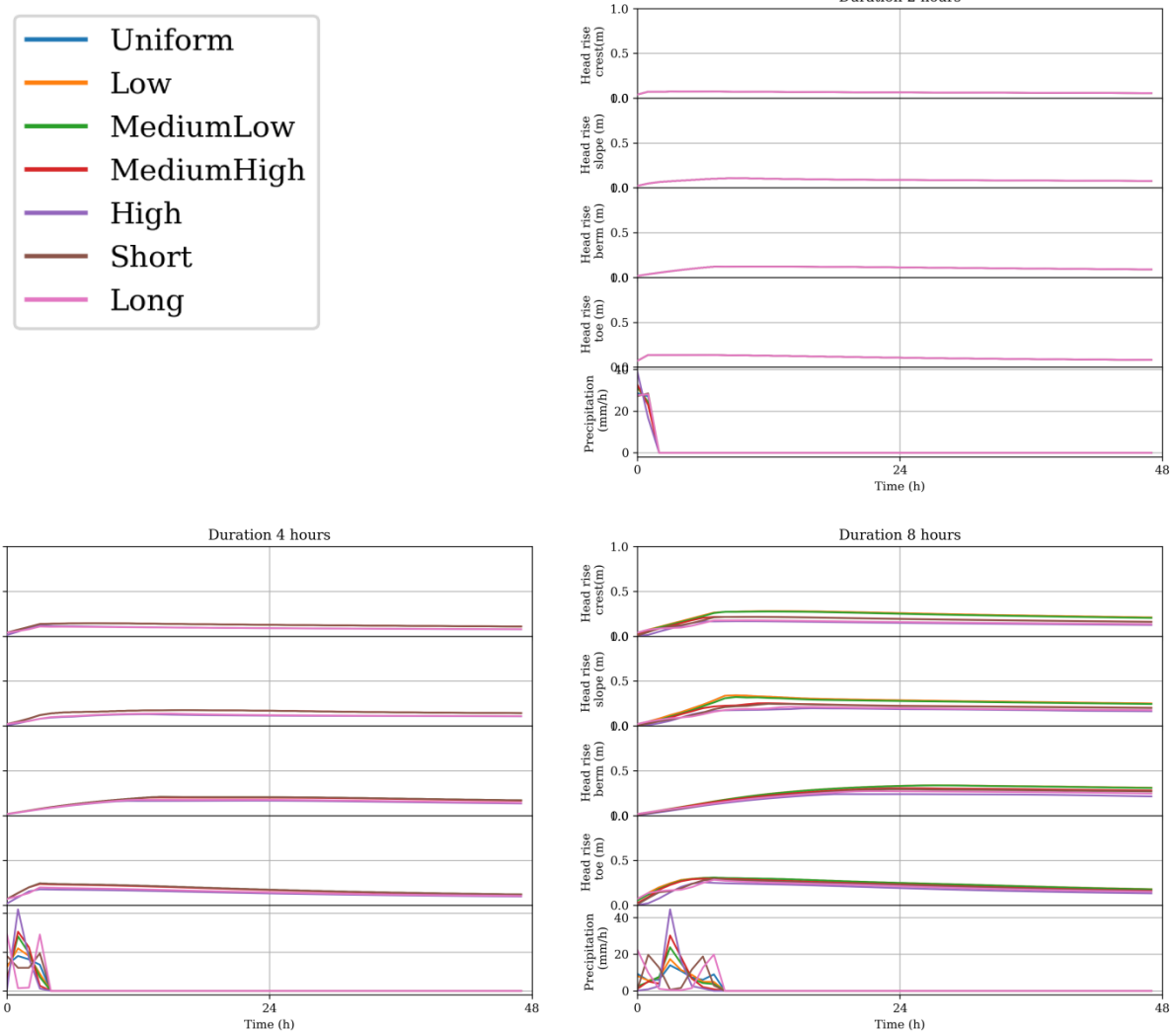

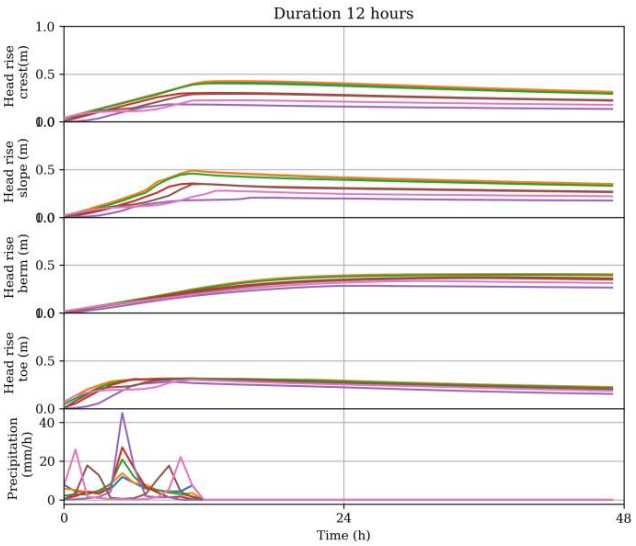
Duration 12 hours
Head rise crest(m)
Head rise slope (m)
Head rise berm (m)
Head rise toe (m)
Precipitation (mm/h)
Time (h)

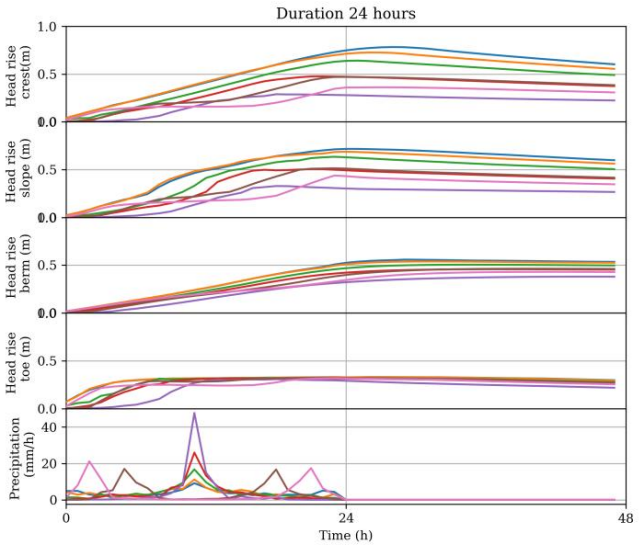
Duration 24 hours
Head rise crest(m)
Head rise slope (m)
Head rise berm (m)
Head rise toe (m)
Precipitation (mm/h)
Time (h)

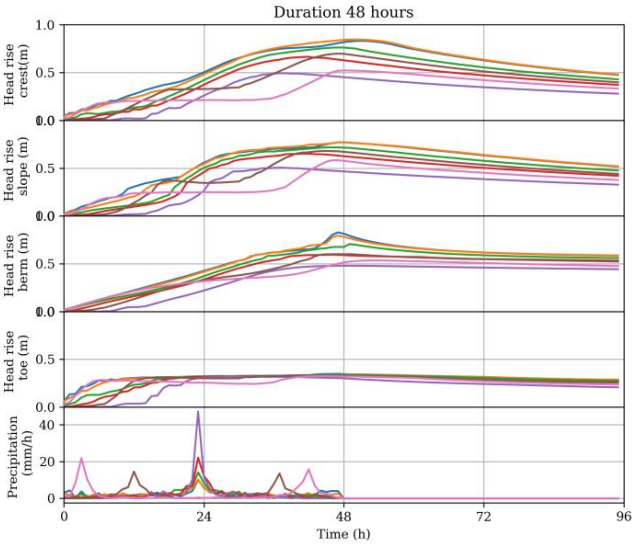
Duration 48 hours
Head rise crest(m)
Head rise slope (m)
Head rise berm (m)
Head rise toe (m)
Precipitation (mm/h)
Time (h)

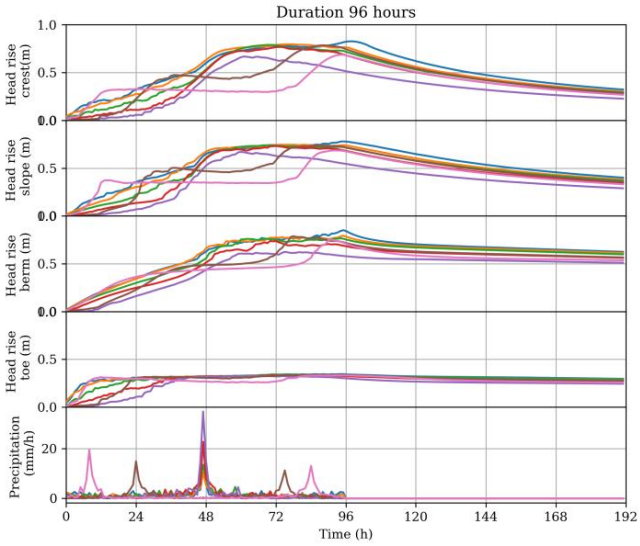
Duration 96 hours
Head rise crest(m)
Head rise slope (m)
Head rise berm (m)
Head rise toe (m)
Precipitation (mm/h)
Time (h)

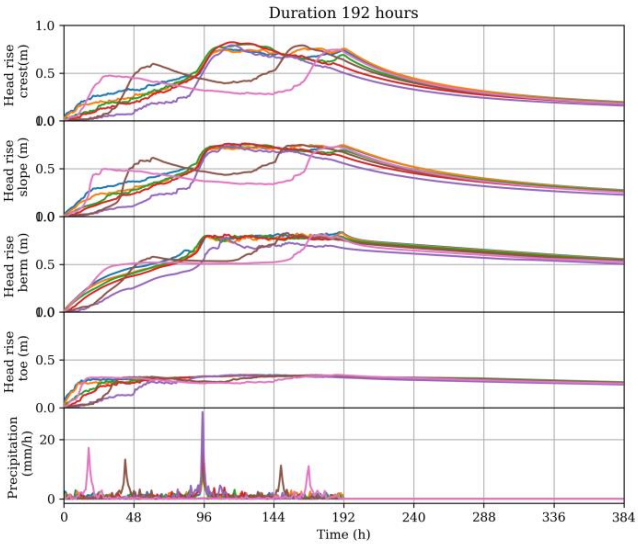
Duration 192 hours
Head rise crest(m)
Head rise slope (m)
Head rise berm (m)
Head rise toe (m)
Precipitation (mm/h)
Time (h)

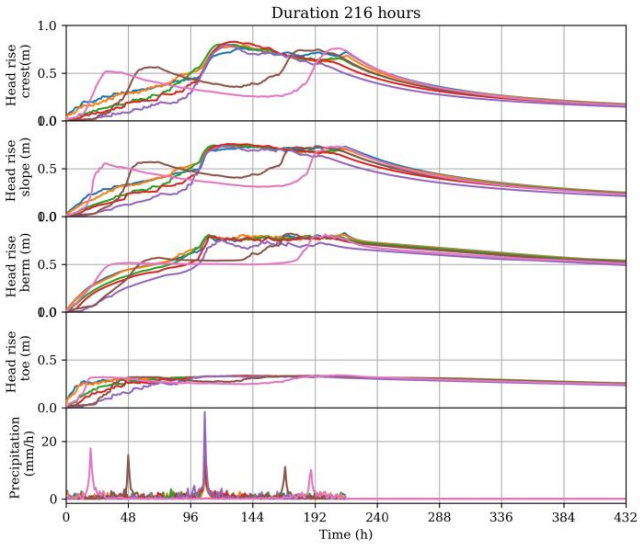
Duration 216 hours
Head rise crest(m)
Head rise slope (m)
Head rise berm (m)
Head rise toe (m)
Precipitation (mm/h)
Time (h)

H.3 Hogedijk


Uniform
Low
MediumLow
MediumHigh
High
Short
Long

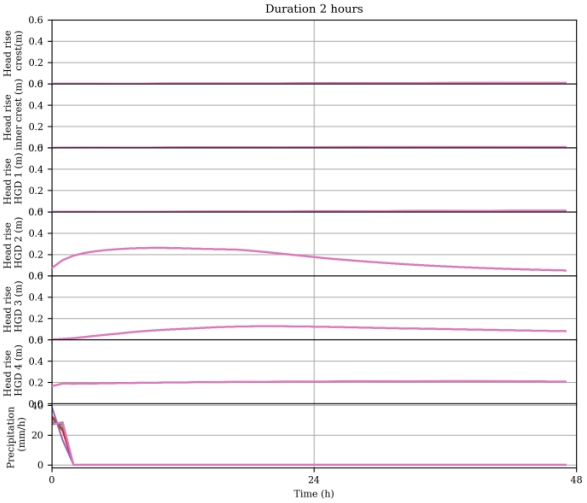
Duration 2 hours
Head rise crest(m)
Head rise inner crest (m)
Head rise HGD 1 (m)
Head rise HGD 2 (m)
Head rise HGD 3 (m)
Head rise HGD 4 (m)
Precipitation (mm/h)
Time (h)

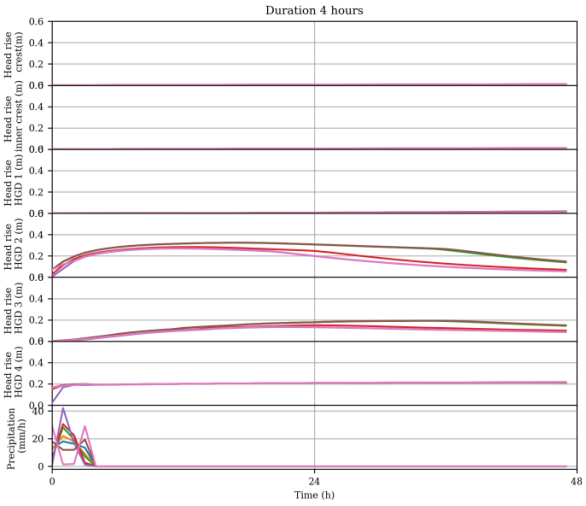
Duration 4 hours
Head rise crest(m)
Head rise inner crest (m)
Head rise HGD 1 (m)
Head rise HGD 2 (m)
Head rise HGD 3 (m)
Head rise HGD 4 (m)
Precipitation (mm/h)
Time (h)

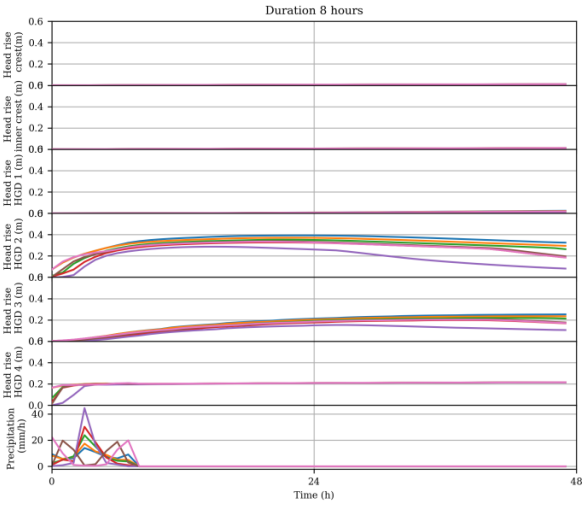
Duration 8 hours
Head rise crest(m)
Head rise inner crest (m)
Head rise HGD 1 (m)
Head rise HGD 2 (m)
Head rise HGD 3 (m)
Head rise HGD 4 (m)
Precipitation (mm/h)
Time (h)

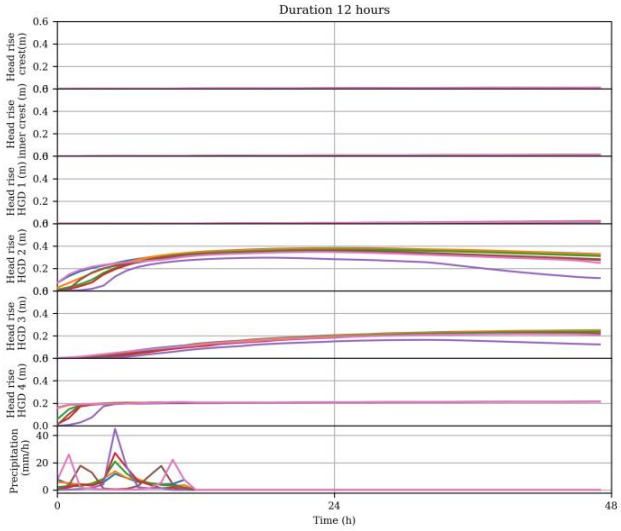
Duration 12 hours
Head rise crest(m)
Head rise inner crest (m)
Head rise HGD 1 (m)
Head rise HGD 2 (m)
Head rise HGD 3 (m)
Head rise HGD 4 (m)
Precipitation (mm/h)
Time (h)

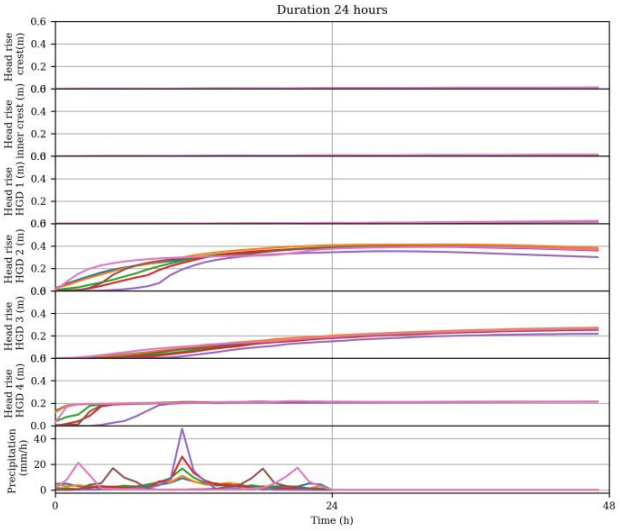
Duration 24 hours
Head rise crest(m)
Head rise inner crest (m)
Head rise HGD 1 (m)
Head rise HGD 2 (m)
Head rise HGD 3 (m)
Head rise HGD 4 (m)
Precipitation (mm/h)
Time (h)

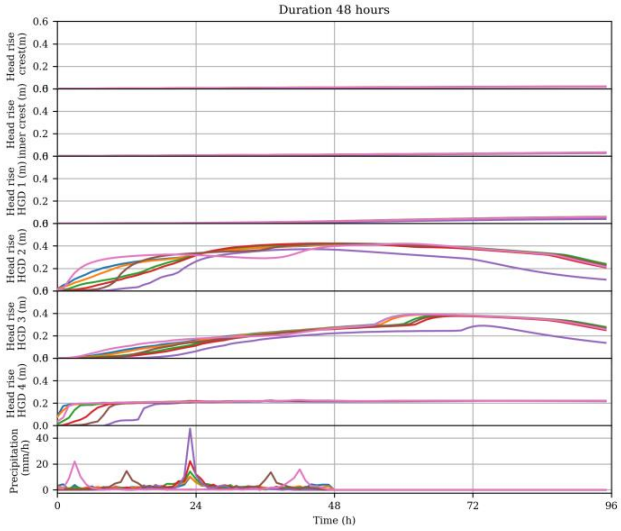
Duration 48 hours
Head rise crest(m)
Head rise inner crest (m)
Head rise HGD 1 (m)
Head rise HGD 2 (m)
Head rise HGD 3 (m)
Head rise HGD 4 (m)
Precipitation (mm/h)
Time (h)

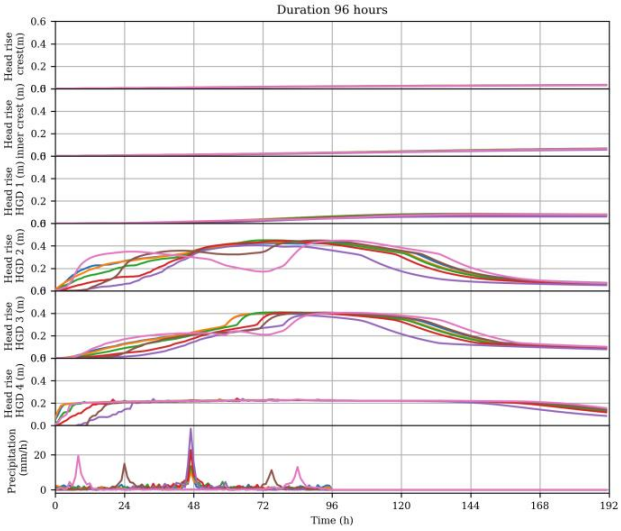
Duration 96 hours
Head rise crest(m)
Head rise inner crest (m)
Head rise HGD 1 (m)
Head rise HGD 2 (m)
Head rise HGD 3 (m)
Head rise HGD 4 (m)
Precipitation (mm/h)
Time (h)

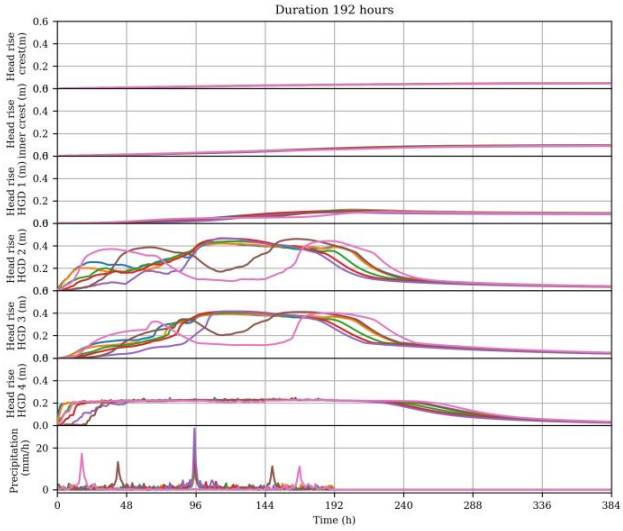
Duration 192 hours
Head rise crest(m)
Head rise inner crest (m)
Head rise HGD 1 (m)
Head rise HGD 2 (m)
Head rise HGD 3 (m)
Head rise HGD 4 (m)
Precipitation (mm/h)
Time (h)

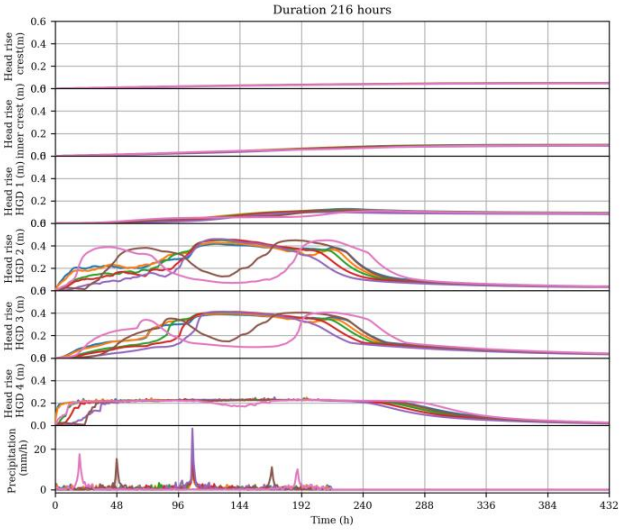
Duration 216 hours
Head rise crest(m)
Head rise inner crest (m)
Head rise HGD 1 (m)
Head rise HGD 2 (m)
Head rise HGD 3 (m)
Head rise HGD 4 (m)
Precipitation (mm/h)
Time (h)